Porosity and effective stress relationships in mudrocks

Harrold, Toby Winston Dominic

Porosity and effective stress relationships in mudrocks

By

Toby Winston Dominic Harrold

This thesis was submitted as partial fulfilment of the requirements for the degree of

Doctor of Philosophy

Abstract

It has generally been assumed that porosity reduction during mechanical compaction of a sediment is controlled by the increase in vertical effective stress. But the theory of mechanical compaction shows that it is the mean effective stress which controls porosity reduction. According to published data, horizontal stresses increase with overpressure, as well as with depth, so mean stress and vertical stress profiles are poorly correlated in overpressured sections.

In this study, a new methodology was developed whereby mudrock pore pressures were estimated principally by comparison of void ratios calculated from wireline log response with hydrostatic mean effective stress (the mean effective stress assuming the pore pressure is hydrostatic). These pressure estimates in the low permeability units were compared to the direct measurements in the aquifer units and an interpretation is made as to the origin of the excess pressure.

The results of analysis of seven wells from SE Asia are presented including one study where seismic velocity analysis and basin modelling were performed to assess the pore pressure.

The main conclusions of the study are:

- The proposed new methodology for estimating shale pore pressure from void ratio and mean effective stress analysis appears to be more consistent with the data and represents an improvement on previous methodologies using porosity and vertical effective stress or depth.
- Analysis of the mudrocks in this study indicates that the shales often appear to have significantly higher pressures than the adjacent aquifer units.
- The results of using mean (as opposed to vertical) effective stress analysis indicates that the pressure profiles in the wells studied, the profiles disequilibrium compaction can account for all or nearly all of the encountered overpressures.
- Evidence has been found for significant overpressure generated by fluid expansion in one of the seven wells studied.
- Further work to refine the Breckels and Van Eekelen (1982) relationship between overpressure and horizontal stress is proposed to improve the accuracy of the methodology used in this study.

Acknowledgements

I must firstly thank my supervisors, Dick Swarbrick and Neil Goulty. Dick, for his conception, creation and constraint of the project. From day one, he organised and delivered an excellent dataset and provided opportunities to extend my project via his encouragement for me to present my results and establish links with industry. Neil Goulty for his help and support throughout the study with his constant focus on the clarity of my presentation (written or spoken) and relevance of any of my observations to the finished product you are currently reading.

Working with these two has been an enormously rewarding experience for me and I hope that this work goes some way towards justifying the amount of support and advice they have given me.

From outside the department, my project benefited enormously from having the opportunity to discuss ideas and results with people within industry. Many thanks to the companies who supplied the data for the project: ARCO, Elf, Enterprise Oil, Petronas and Total.

My main thanks have to go to the folks at ARCO who showed a lot of interest in the project and paid me during the summer of 1997 when I worked with them in Plano: To Keith Katahara for his initial interest and constant willing to exchange ideas; to Bill Kilsdonk for mentoring me, to Fred Dula for making it all possible; to Alton Brown for valuable insights; to TK Kan and Ray Wydrinski for their help with the seismic analysis and to Zhiong He and Steve Crews for their help with the basin modelling.

Thanks also to Dominique Grauls, Yves Grosjean, Martin Traugott, Rick Lahann and Phil Holbrook for discussion and help throughout.

Thanks go to all those from GeoPOP who were there to help and exchange ideas, in particular, Daniel, Paul, Grouter, Gareth Yardley, Andy Aplin and Yunlai Yang.

To all the other staff and friends from the department and who helped me through the nadir that was year three. In particular I would like to thank Sue, Jonny, Ziad, Alun, Simon and Wayne.

To my family who have supported me emotionally and financially for what must seem like decades to them, I couldn't have made it without you.

And finally I would like to thank Christina for her love and help through three long, hard years, I wouldn't have made it without you.

Table of Contents

List of Tables

Table of Figures

Declaration

The content of this thesis is the original work of the author (other people's work, where included, is acknowleged by reference). It has not been previously submitted for a degree at this or any other university.

T.W.D.Harrold
Durham
October 1999

Copyright

Chapter 1: Introduction

"I studied out the landmarks of the gloom
To find my bearings there, as best I could"
Dante Aligheri

1.1 Introduction to Overpressure

In sedimentary basins, **normal** or **hydrostatic** pore pressures are defined as values that lie on a pressure/depth gradient of a freestanding column of water extending to the topographic surface (Figure 1.1). For fresh water, this pressure/depth gradient is 0.979 MPa/km (0.43psi/ft) and for a saturated salt solution, the gradient is 11.9MPa/km (0.53psi.ft). Formation pressures that exceed the pressure gradient for their given fluid density are referred to as **overpressured** or geopressured; pressures lower than the pressure gradient for their given density are referred to as **underpressured** (Figure 1.1).

1.1.1 Impact of overpressure on drilling

The presence of overpressured formation fluids in sediments affects the drilling of wells in three important ways:

1. When a borehole is drilled into a permeable formation that is overpressured, the pressure exerted by the mud in the borehole must be increased to at least balance the pressure in the aquifer and prevent influx of formation fluid into the borehole. If the pore pressure increase is unexpected and too fast or high to be shut in at the well head, a "blowout" will result as formation fluid escapes, uncontrolled, to the surface.
2. Drilling into a permeable aquifer that has a formation pressure greater than the pressure required to fracture sediments shallower in the borehole can result in losses of drilling mud. If not quickly controlled, this situation can result in the rapid movement of considerable volumes of formation fluid into the shallower formation, referred to as an "internal blowout". To avoid this situation, the weaker, shallow sediments have to be isolated from the higher pressure sediments by the setting of casing.
3. When a well is drilled though low permeability sediments that are overpressured, the mudweight in the borehole will generally have to be increased to prevent influx of sediment and gas held in solution into the borehole.

It is not possible however, to simply increase the mudweight in the borehole to cover the possibility that overpressured sediments will be encountered. Drilling through sediments with mudweights that are in excess of the formation pressures (drilling overbalanced) has it's own consequences:

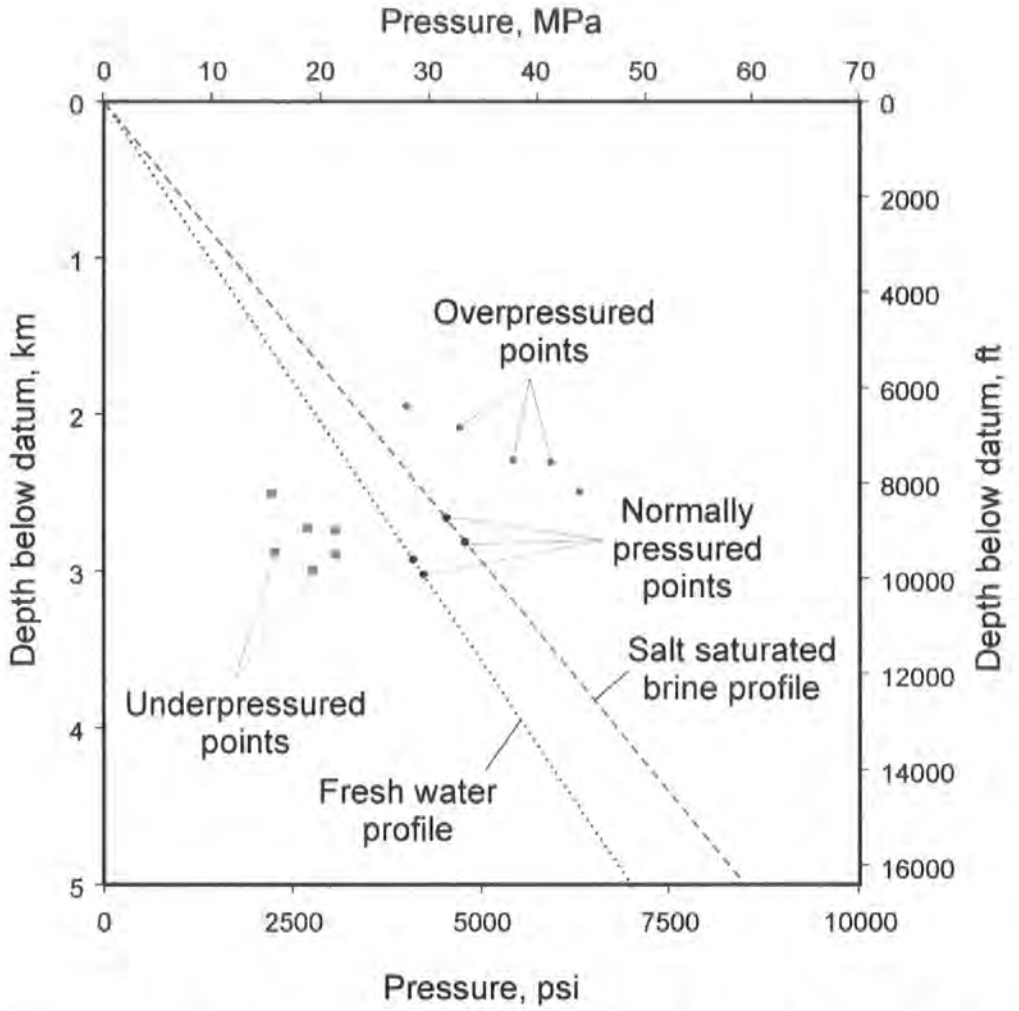

Figure 1.1 Hydrostatic pressure depth profiles for fresh and salt saturated brines together with data points representing actual formation pressures. Points that lie on the normal pressure profile for their corresponding density

1. Drilling overbalanced is, in general, slower and therefore more costly than using the correct mudweight.
2. Drilling permeable units with mudweights that are too high will result in the loss of costly drilling fluid into the formation. The injection of drilling mud into the formation can significantly reduce the permeability of the aquifer units, extremely important if they happen to be the productive reservoirs of a hydrocarbon accumulation.
3. Drilling with mudweights that are too high can fracture the formation and result in fluid losses. Setting casing shallower than expected to control the losses may prevent the well from reaching its target depth, knowing the pressure and planning the casing settings is critical to the success of the operation (e.g., Appe, 1998).

All of the consequences of drilling wells with pressures that are too high or too low have significant safety and cost implications. Any study, therefore, that aids the detection of the origin, distribution and magnitude of overpressure will aid the planning and drilling of wells.

1.1.2 Impact of overpressure on petroleum systems

When a hydrocarbon accumulation is proposed, the prospective accumulation has to be assessed in terms of hydrocarbon migration and the sealing potential of the formations that surround the hydrocarbon reservoir.

Understanding the origin, magnitude and distribution of overpressure will indicate the potential directions of fluid flow in the subsurface and allow the validity of possible migration pathways to be tested.

The amount of overpressure present in the subsurface will strongly influence the sealing capacity of the formations/faults that trap the hydrocarbons. If the pore pressures exceed the pressure required to fracture the sealing lithology (Roberts and Nunn, 1994), or to open the fault (Jev et al, 1993; Berg and Avery, 1995) then hydrocarbons may be able to escape from the structure. It is important, therefore, to assess the origin and magnitude of the overpressures relative to the strength of the sealing units prior to drilling.

1.1.3 Historical nature of overpressure

The first oil discoveries drilled at the start of the late 1800's and early 1900's penetrated shallow (<0.5km) oil accumulations and regularly experienced blowouts or "gushers" as they were then referred to. Initial drilling rigs and wooden casing were not able to control oil overpressured by buoyancy effects that often pushed formation pressures close to the values required to fracture the formation. As equipment and techniques were developed to control these initial environments, they allowed wells to be drilled deeper into the basins. Overpressure produced by connection of reservoirs to elevated water tables began to be encountered and up until the 1960's, hydrodynamics and buoyancy could account for the encountered overpressures (Hubbert, 1940; Hunt, 1980). As technology allowed wells to be drilled ever deeper, though, overpressure from disequilibrium compaction (or "undercompaction", Section 1.8.1) began to be encountered.

Techniques were developed not only to control the high pressures, but also to quantify them such that their control could be optimised. The last forty years has seen further improvements in understanding of the processes that generate overpresssure and the technology required to control it (mainly funded by peaks in oil prices). These developments have allowed wells to be economically drilled to tap hydrocarbons in ever more extreme environments, be they extreme depth, extreme pressure and/or temperature and, more recently, extreme water depth.

As the focus of hydrocarbon exploration continues to shift into areas with more extreme pressure conditions, prediction/understanding of pore pressure (prior to drilling and during the analysis of the petroleum system) becomes ever more important. In many cases identifying the mechanisms responsible for generating the overpressure are critical to solving the technical problems of developing a particular accumulation. For other environments where formation pressures approach the fracture pressure of the rock, studies are focussed on the stress regime that controls the retention of the hydrocarbons and the origin of the overpressure is of secondary importance (Gaarenstrom et al., 1993). In recent times, a large number of studies have focused on how to predict pore pressure from measurements during drilling (e.g., Holbrook, 1995), from seismic (e.g., Kan and Kilsdonk, 1999) and from basin modelling (Alberty, pers. comm.). This study proposes a new method of pore pressure analysis pertinent to all of these different approaches.

1.2 Rationale

The aim of this study is to use the compaction behaviour of mudrocks to identify mechanisms that generate overpressure in the subsurface.

It is commonly understood in the soil mechanics literature (Jones, 1994, Burland 1990) and recently proposed in the petroleum industry (Goulty, 1998) that the compaction of mudrocks depends upon two components, the mean stress applied on the sediment and the pressure of the fluid in the pore spaces. Any process which affects the pore fluid pressure, will influence the compaction of the sediment in relation to the applied stress. Studies of compaction behaviour can therefore shed insight on the processes that affect fluid pressure in the sediment.

The object of this study has been to test this compaction theory by analysing the void ratio and mean effective stress behaviour of mudrocks from seven wells in SE Asia.

In this study, mudrock porosity calculated from wireline log responses is used as the measure of compaction in the sediment. Porosity is compared against normal compaction behaviour computed for each of the wells and pressure magnitudes due to mechanical processes are calculated. These pressure values are compared against actual measurements of fluid pressure made in the borehole and interpretations are made as to the origin and evolution of the pore pressures.

In one of the wells, seismic and modelling data were also used to test theories as to the origin and redistribution of overpressure in 2D.

The relevance of the study lies in the need to:

- Understand pore pressure when drilling, important for minimising lost time and preventing accidents.
- Improve prediction of pore pressures, allowing better well planning.
- Understand the hydrocarbon system more effectively: directions of fluid flow, seal failure, porosity permeability effects.

1.3 Key terms

Four key terms are used in this study, namely porosity, void ratio, effective stress and compaction. Void ratio and effective stress, are used in this study to calculate

pore pressures in the subsurface. Compaction is the process which links void ratio and effective stress.

Porosity: a sediment can be seen as consisting of two components (Figure 1.2), a solid matrix made up of different minerals and voids/pores filled with fluid. The porosity of the sediment is the fraction of the sediment volume that is occupied by void spaces and is normally represented by a percentage value.

Void ratio: For a given sediment, the void ratio is defined as the volumetric ratio of its void and solid components.

Effective stress: when a stress is applied to a sediment (e.g., during burial), the load is distributed between the pore fluid and the solid matrix component (Figure 1.2). The normal stress acting in a particular direction that is borne by the sediment matrix is referred to as the effective stress, first defined by Terzaghi (1936). The vertical effective stress thus represents the overburden load per unit area borne by the grain-to-grain contacts of the sediment matrix.

Compaction: the mechanical response of a sediment experiencing an increase in effective stress is to undergo a reduction of volume by means of reorganisation and deformation of the matrix material and the loss of porosity. Chemical processes may also occur and contribute to the loss of porosity. This process of porosity reduction is referred to as compaction. During normal compaction, a mudrock undergoes a monotonic increase in effective stress which causes an elasto-plastic reduction in porosity (and void ratio). The resultant relationship between effective stress and void ratio is known as the normal compaction curve (Figure 1.3).

1.4 Processes of normal compaction

The conversion of very high (>80%) porosity clay deposited on the sea bed to a compact mudrock with <5% porosity at higher effective stress values is achieved by three main processes:

Mechanical Realignment: for very high porosity shales in the shallow sections (sea bed-~200m depth), porosity loss induced by effective stress increase is achieved by the grain reorganisation and alignment of the clay particles. Once the sediment has been slightly compacted, the potential for further reorganisation of the matrix material without grain fracture is reduced and the process can only account for a small fraction of subsequent porosity loss.

Mechanical compaction: the majority of porosity loss in the subsurface is achieved by elasto-plastic deformation of the grains between porosity values of 60 to less than 5%. Once the sediment grains are in close contact, the majority of porosity loss can only be achieved by plastic deformation of the matrix material; (a small component of the deformation will be produced by elastic compression of the grains).

Chemical compaction: at higher effective stresses (>30MPa) and lower porosities (<10%) an increasing component of further porosity loss is achieved by chemical compaction. Porosity loss by this process is achieved by pressure solution and reprecipitation of the grains, as well as by diagenetic changes of the minerals which result in a volume decrease (e.g., smectite to illite transition). The amount of chemical compaction is influenced by the presence of minerals which are susceptible to such changes (e.g., smectite, kerogen and carbonates) as well as by elevated temperatures and effective stresses.

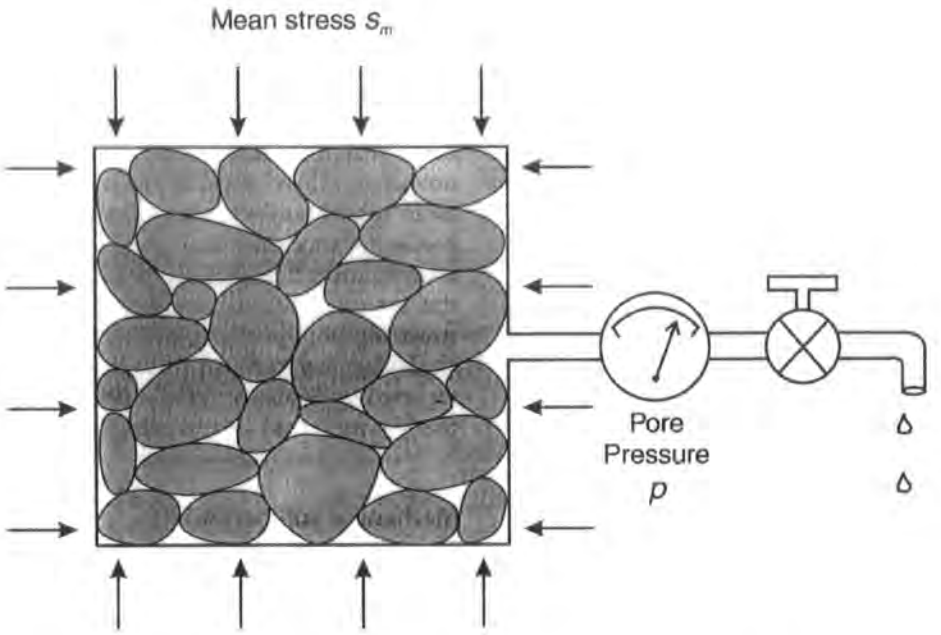

Figure 1.2 Cartoon illustrating a clastic sediment made up of matrix and pore space subject to a mean effective stress (σ_m) equal to the difference between the mean stress (s_m) and the pore pressure (p_p). (Redrawn after Goulty, 1998)

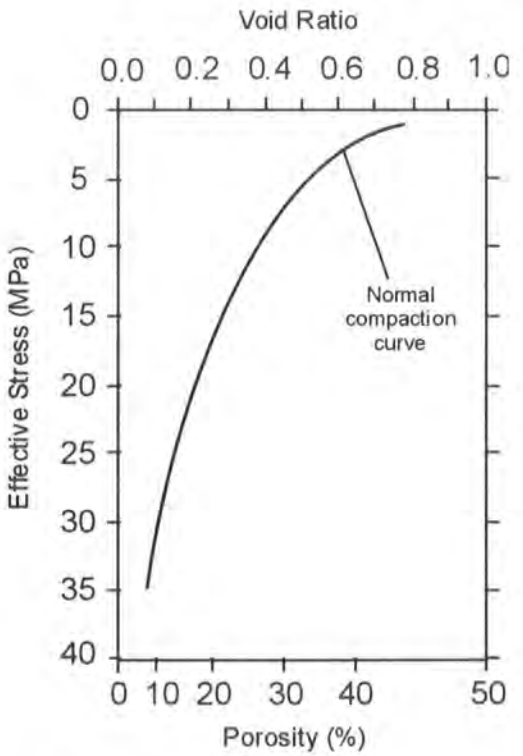

Figure 1.3 Shale normal compaction curve

1.5 Terzaghi effective stress

The process of soil and sediment compaction has been studied for a considerable amount of time in the fields of soil mechanics, engineering and more recently petroleum geology. The amount of compaction/porosity loss was first quantitatively related to the load applied by Terzaghi (*1925*). This relationship was achieved by the definition of "effective stress" (σ) as the difference between the applied normal stress (s) in a specified direction and the pore pressure (p):

$$\sigma = s - p \qquad [1]$$

This basic theory led to the development of experimental apparatus (oedometers) where porosity loss in sediments could be related to measured increases in applied stress. Design of oedometric apparatus for compression tests has mainly focussed on measuring 1D or uniaxial compaction (e.g., Burland, 1990; Skempton, 1970), although in some studies the horizontal stresses have been varied and measured (e.g., Karig and Hou, 1992). Using a uniaxial apparatus allows for easy application of loads to a sample and the accurate measurement of induced strain (compaction) in the direction of the applied stress.

The uniaxial compression tests were seen as analogous to the burial of sediments in non-compressional sedimentary basins where the vertical stress was believed to be the driving force behind compaction. Consequently, relationships were developed between void ratio $e = \phi/(1-\phi)$ and vertical effective stress (e.g., Burland, 1990):

$$\log_{10}\left(\frac{\sigma_v}{\sigma_{100}}\right) = \frac{e_{100} - e}{C_c}, \qquad [2]$$

where σ_v is the vertical effective stress in units of kilopascals; σ_{100} is some reference value of effective stress, taken here to be 100 kPa; e_{100} is the void ratio at 100 kPa effective stress; and C_c is the compaction coefficient. The values of the sediment mechanical parameters, e_{100} and C_c, depend on the lithology. Relationships of this type have been applied to study the compaction behaviour of actual sediments in basin environments (e.g., Audet 1995; Aplin et al., 1995).

In reality, however, in sedimentary environments as well as uniaxial experimental apparatus, horizontal (and therefore mean) stresses vary with burial/compression. Goulty (1998) has re-formulated the theory for the mechanical

consolidation of an isotropic sediment, given by Biot (1941), in the following terms. For a sediment which is being normally compacted during burial, increases of Δp_f in the pore pressure, Δs_m in the mean stress, and ΔT in temperature cause a dilatation of

$$\frac{\Delta V}{V} = -\frac{1}{k_s}\Delta p_f - \frac{1}{k_{nc}}\left(\Delta s_m - \Delta p_f\right) + \alpha_s \Delta T, \qquad [3]$$

where k_{nc} is the frame bulk modulus for a sediment undergoing normal compaction, k_s is the bulk modulus of the solid grains, and α_s is the volumetric thermal expansion coefficient of the solid grains. The fractional change in volume of the solid matrix material, V_s, due to increases in the same independent variables is

$$\frac{\Delta V_s}{V_s} = -\frac{1}{k_s}\Delta p_f - \frac{1}{k_s}\left(\frac{\Delta s_m - \Delta p_f}{1-\phi}\right) + \alpha_s \Delta T. \qquad [4]$$

Writing the porosity as $\phi = 1 - \frac{V_s}{V}$ and differentiating, gives

$$\Delta\phi = \frac{V_s \Delta V}{V^2} - \frac{\Delta V_s}{V} = (1-\phi)\left(\frac{\Delta V}{V} - \frac{\Delta V_s}{V_s}\right). \qquad [5]$$

Substituting expressions [3] and [4] for $\frac{\Delta V}{V}$ and $\frac{\Delta V_s}{V_s}$ into [5] yields

$$\Delta\phi = -\left(\frac{1-\phi}{k_{nc}} - \frac{1}{k_s}\right)\Delta\sigma_m, \qquad [6]$$

where $\Delta\sigma_m = \Delta s_m - \Delta p_f$. The bracket on the right-hand side contains the porosity, the frame bulk modulus during normal compaction, and the bulk modulus of the solid grains. The frame bulk modulus will itself be a function of porosity, and other factors such as the geometry of the pore distribution and the bulk moduli of the grains; but it is independent of pore pressure and mean stress. Hence porosity depends on the mean effective stress, not on the vertical effective stress.

It should be appreciated here that the frame bulk modulus during normal compaction, k_{nc}, is not an elastic modulus. Normal compaction is achieved by a process of mainly plastic, and only partly elastic, deformation of the matrix, accompanied by the loss of pore fluid such that the pore pressure is equal to the hydrostatic pressure at all depths.

Although, under conditions of zero lateral strain in oedometric tests, there may be a systematic relationship between vertical and mean effective stress allowing [2] to give accurate results. In actual sediments where there are tectonic and pore pressure influences, it is highly unlikely that the conditions will mimic those of an oedometer, and [2] cannot therefore be applied.

For this study, therefore, void ratio was related to mean stress using an empirical relationship of the same form as [2] between porosity and mean effective stress,

$$\log_{10}\left(\frac{\sigma_m}{\sigma_{100}}\right)=\frac{e_{100}-e}{C_c}, \qquad [7]$$

The values of e_{100} and C_c will, in general, be different when porosity is related to the mean effective stress instead of to the vertical effective stress (Section 6.3.2.1).

A number of other approaches have been taken to analyse compaction behaviour including relating porosity to depth (Athy, 1930; Sclater and Christie, 1980; Baldwin and Butler, 1985), sonic to effective stress (Bowers, 1994). The approach taken in this study to relate void ratio to mean effective stress was chosen as it is the closest to the established soil mechanics theory (Jones 1994; Burland, 1990) and it therefore allows comparison of the results with sediment behaviour reported in the literature (e.g., Skempton, 1970) and compression tests on sediment samples.

1.6 Lithological behaviour

The theory introduced in Section 1.5 describes the compaction behaviour of a single mineralogy mudrock with constant properties during burial. However, mudrocks in sedimentary basins are rarely homogenous, especially over significant depth intervals. Skempton (1970) published compaction curves for a number of different grain size clays Figure 1.4. These results indicated that as the clay fraction of a mudrock increased (and particle size decreased), the initial porosity and the compressibility of the sediment increased. This observation was used by Aplin et al. (1995) to identify sedimentary compaction parameters from the density log derived porosity.

For this study, the influence of lithological behaviour has been accounted for by subdividing the shales selected for analysis into groups with similar log characteristics and deriving individual compaction curves for each of the groups. Each of these curves will have slightly different values of e_{100} and C_c, as shown in Figure 1.5.

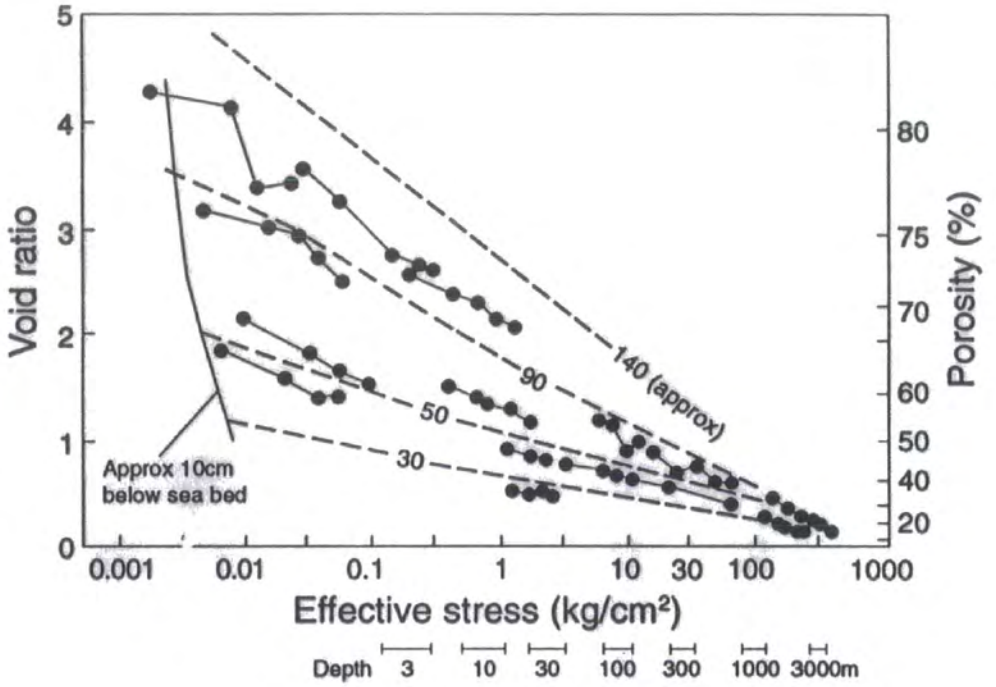

Figure 1.4 Relationship between porosity and effective stress for shales with varying liquid limit (a function of clay fraction), reproduced after Skempton (1970).

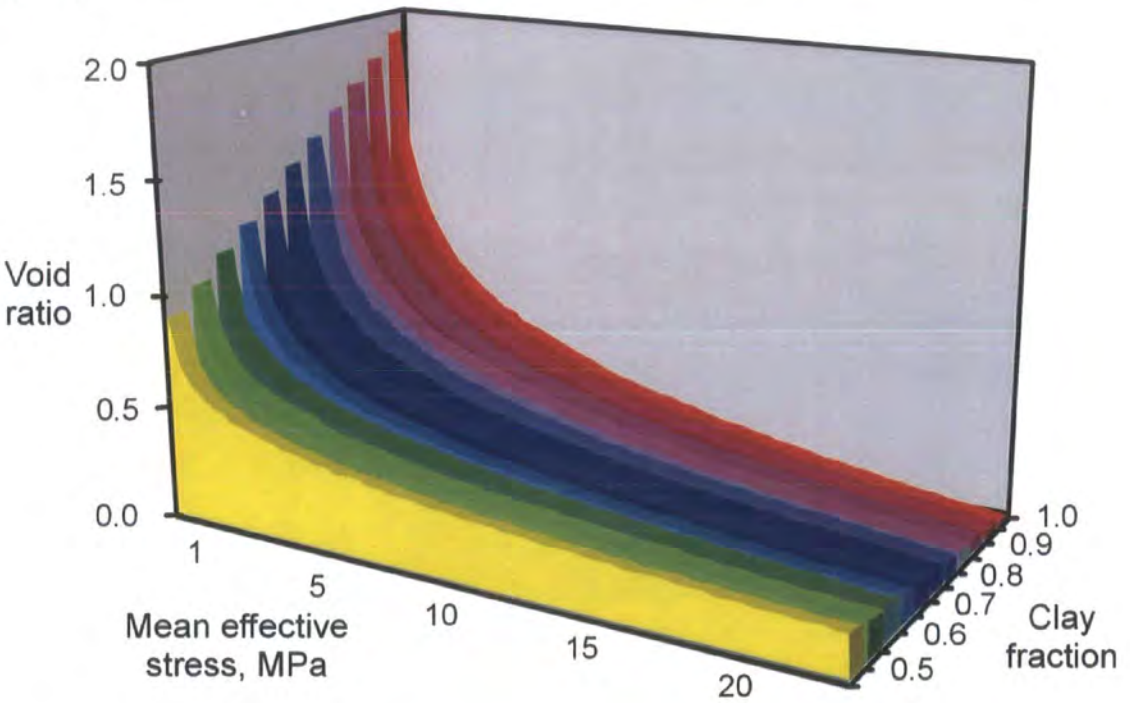

Figure 1.5 Suite of void ratio vs mean effective stress normal compaction curves for shales of varying clay fraction.

1.7 Effects of pore pressure on porosity / effective stress relationships.

Any process which affects pore pressure will affect the compaction behaviour of the mudrocks. As the process of compaction is an elasto-plastic phenomenon, a reduction in effective stress does not induce the full recovery of the porosity lost during compaction. Only the elastic components of deformation are recovered when the effective stress is reduced.

Bowers (1994) used this principle to distinguish between two groups of overpressure generating mechanisms that influence the effective stress of the sediment. The overpressure generating mechanisms were subdivided into "loading" and "unloading" mechanisms.

"Loading" refers to overpressure generated under non-decreasing effective stress states and covers disequilibrium compaction and overpressure driven by mechanical stresses (Section 1.8.1).

"Unloading" refers to overpressure mechanisms that induce decreases in the effective stress acting on the sediment. Uplift and erosion can produce reduction of effective stress; however, in the context of this study, unloading generally refers to mechanisms associated with fluid volume increase in the pore spaces (Section 1.8.2).

Bowers (1994) plotted sonic velocity (as a proxy for compaction) against effective stress calculated from measurements of pore pressure in the borehole (Figure 1.6). Where data points appeared to lie on the normal compaction curve, then the overpressure generating mechanism is interpreted as being due to loading or mechanical processes. If the data points plot to the left of the normal compaction curve, then part of the encountered overpressure is due to unloading mechanisms (Figure 1.6).

This approach taken by Bowers (1994) assumes that the effective stress in the sands, where pressure measurements are made, and the very low permeability mudrocks are equal. In this study, it was decided that the assumption of full pressure equilibrium between units is frequently not valid and a different approach was taken:

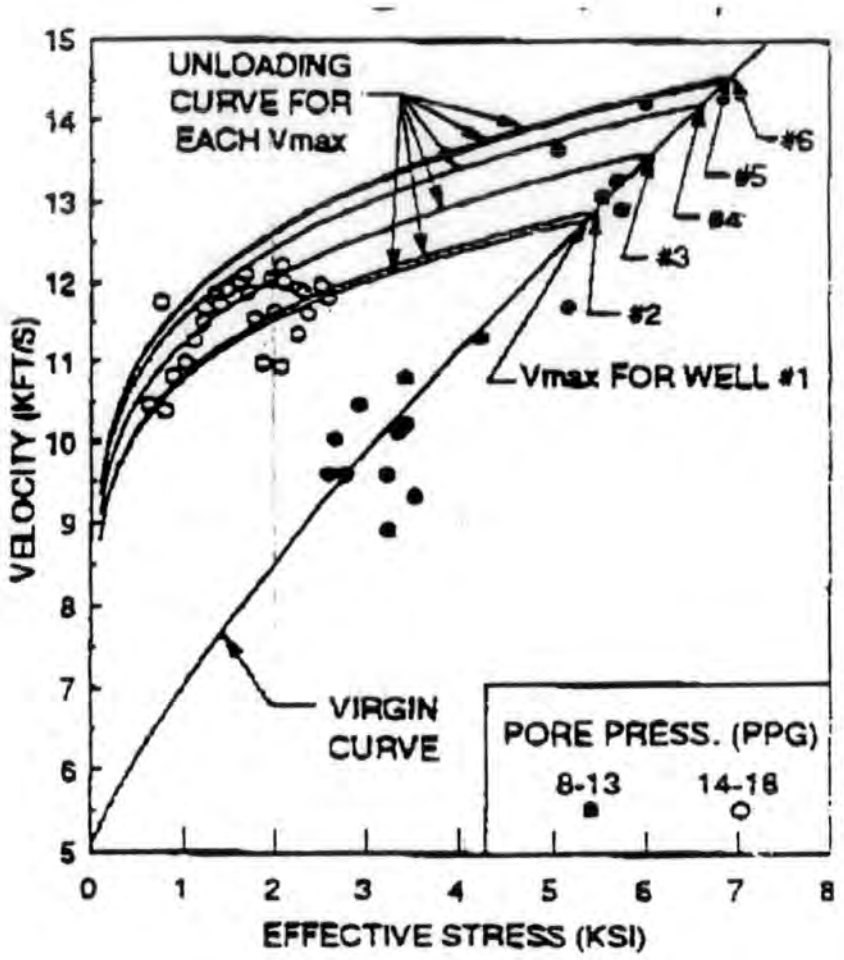

Figure 1.6 Velocity vs effective stress plot indicating the distinction between sediments that are either normally compacted or overpressured by disequilibrium compaction which lie on the loading or "virgin" curve and sediments overpressured by fluid expansion mechanisms which lie on the "unloading" curve. (Reproduced after Bowers, 1994)

1. Porosity values were plotted against values of "hydrostatic mean effective stress" (mean effective stress calculated on the assumption that the pore pressure in the sediments is hydrostatic).
2. Normal compaction curves were defined from the porosity values in the parts of the section which could reasonably be interpreted as being normally pressured.
3. Pore pressures and mean stresses were estimated from the porosity values and compared to the actual measurements of pore pressure down the borehole.
4. Differences between actual and computed pore pressures are interpreted in terms of processes.

The procedure described above represents a new methodology for pore pressure estimation developed by the author incorporating studies by Goulty (1998), Audet (1995), Aplin et al. (1995) and Bowers (1994). The approach is detailed further in Section 2.3.

1.8 Overpressure generating mechanisms

This section gives a brief description of the mechanisms that generate overpressure and their effect on the porosity / effective stress relationship. Following the approach taken by Bowers (1994), the mechanisms have been subdivided into loading and unloading processes.

1.8.1 Loading / mechanically generated overpressure.

When fluid escape from the pore spaces is restricted during burial, due to low permeability and/or rapid sedimentation, the pore pressure becomes greater than hydrostatic. Under these circumstances, compaction is reduced as the rate of increase of effective stress is slowed or stopped if no fluid can escape. This process is termed "disequilibrium compaction", and the sediment is said to be "undercompacted". Disequilibrium compaction is generally held to be the most frequent cause of most overpressure encountered in sedimentary basins (Swarbrick and Osborne, 1999) as it depends mainly upon rapid burial for its effectiveness. High sedimentation rates are a common feature of Tertiary sedimentary sequences where the majority of petroleum exploration is taking place (e.g., North Sea, Gulf Coast, SE Asia, Niger delta).

Studies of disequilibrium compaction (e.g., Mann and Mackenzie, 1990) have used relationships between porosity and depth or vertical effective stress to explain the generation of overpressure. These models limit the maximum rate of pressure increase to the rate of vertical stress increase. A plot representing the relationships

between void ratio and "hydrostatic vertical effective stress" (vertical effective stress calculated on the assumption that the pore pressure in the sediments is hydrostatic) under these assumptions is shown in Figure 1.7. At shallow depths the shale is normally compacted (points lie on the normal compaction curve). In the overpressured section where the pore fluid in the sediment has become trapped, the vertical effective stress and therefore the porosity remain constant. As the hydrostatic vertical effective stress increases with depth, the porosity values do not change from their value at the onset of overpressure. The corresponding pore pressure profile shows hydrostatic pressures for the interval where the porosity values lie on the normal compaction curve and a profile that follows the rate of increase of lithostatic stress increase in the overpressured section (Figure 1.7).

As sediment compaction actually depends upon the mean effective stress, this process of overpressure generation can also be produced when the horizontal stresses are increased in the sediment. The implication, therefore, is that, instead of following the rate of lithostatic stress increase, the maximum rate of pore pressure increase will follow the rate of increase of the mean stress (Figure 1.8) which can exceed the rate of lithostatic stress increase.

A plot representing the relationships between void ratio and hydrostatic mean effective stress and the corresponding pore pressure profile produced by disequilibrium compaction are shown in Figure 1.8. The void ratio versus hydrostatic mean effective stress diagram is almost the same as in Figure 1.9, showing a zone of normally compacted porosity values above a zone of constant porosity. The corresponding pore pressure profile, however, shows that in the overpressured section, the rate of pore pressure increase exceeds the rate of lithostatic stress increase following the rate of mean stress increase. The pressure depth plot also shows the mean stress profile calculated assuming hydrostatic pore pressure conditions.

Plotting the porosity values from Figure 1.8 against actual mean effective stress in the subsurface produces a plot where all of the data points lie on the normal compaction curve (Figure 1.9). This observation indicates that the process generating the overpressure has only slowed or stopped the compaction process, in agreement with Bowers (1994).

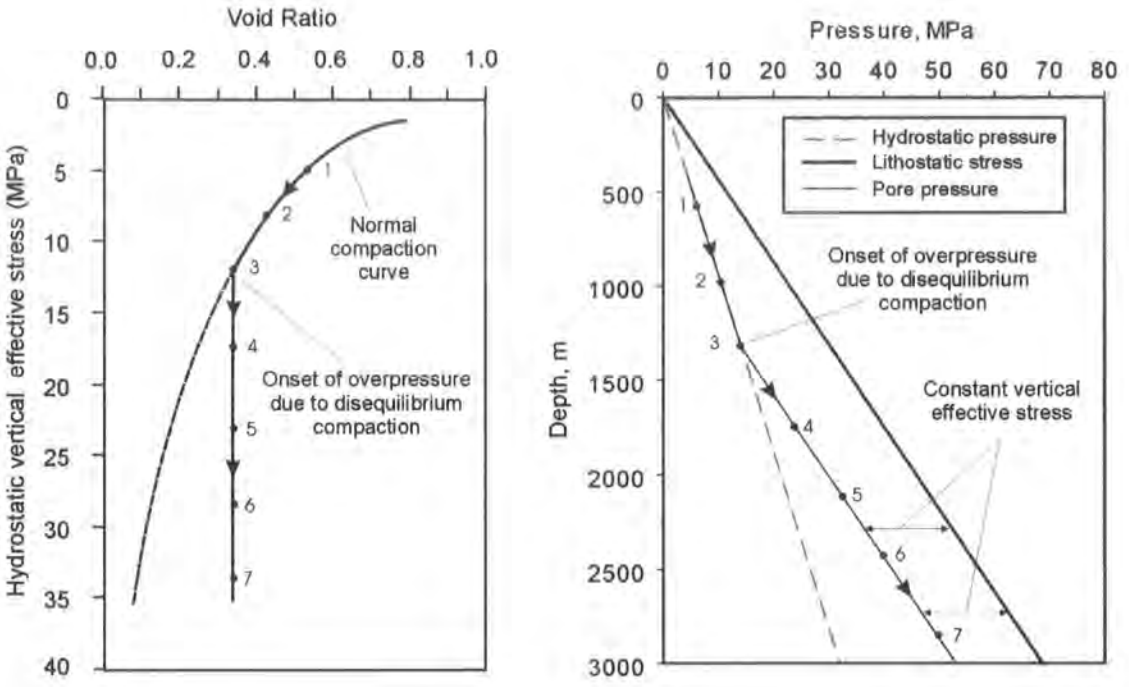

Figure 1.7 Relationship between porosity and vertical effective stress

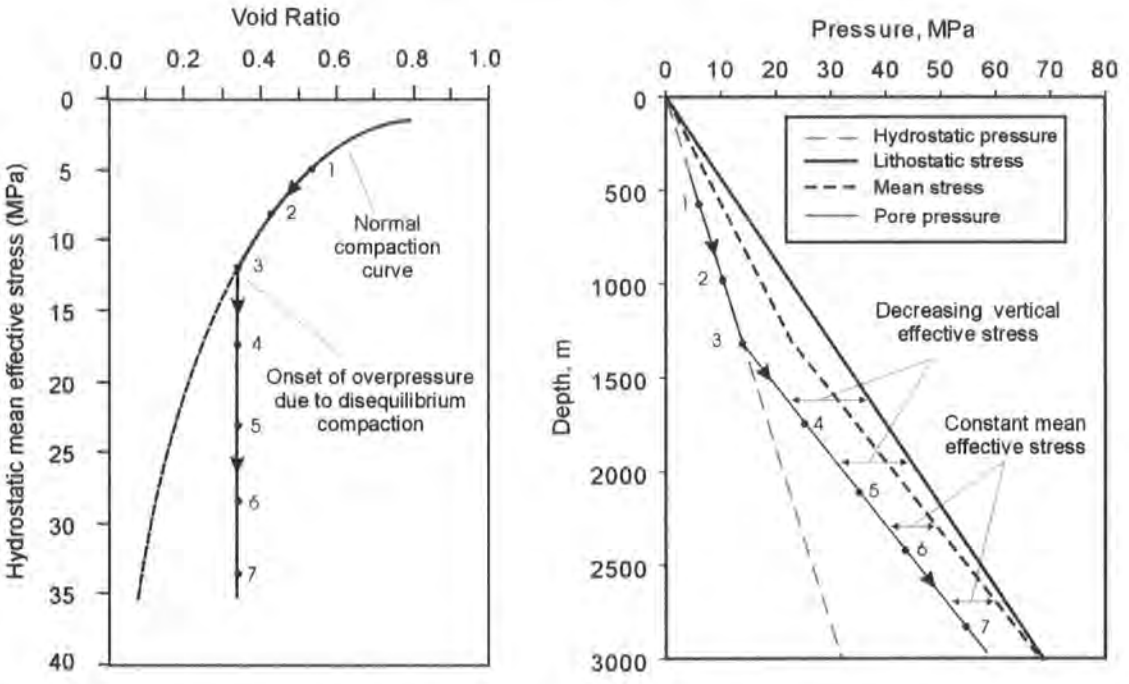

Figure 1.8 Relationship between porosity and mean effective stress

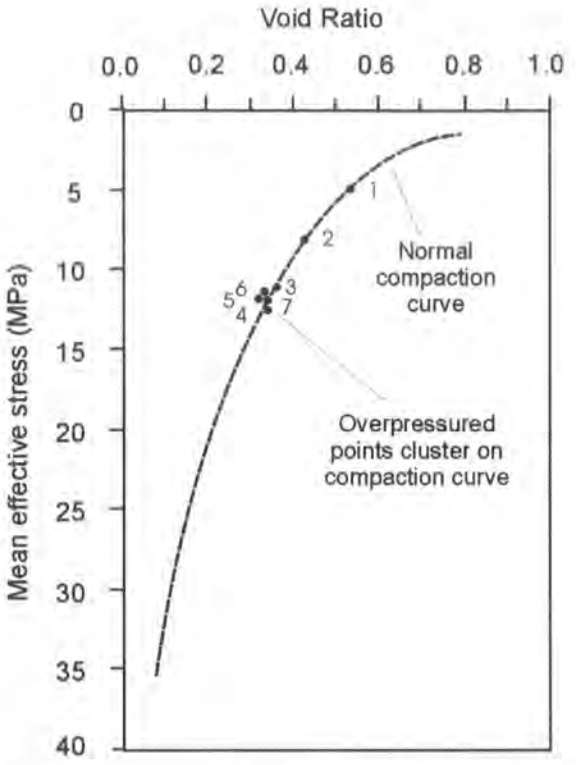

Figure 1.9 Void ratios from Figure 1.8 plotted against mean effective stress.

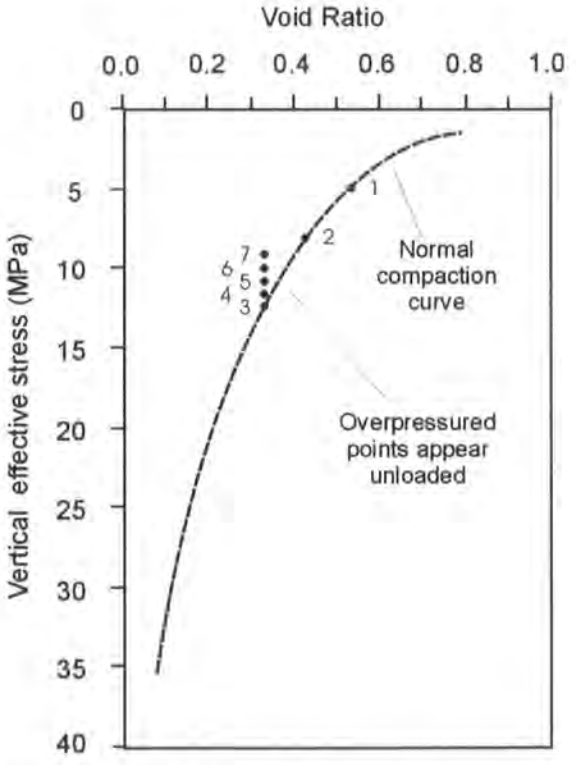

Figure 1.10 Void ratios from Figure 1.8 plotted against vertical effective stress.

If the porosity values are plotted against vertical effective stress computed from the pore pressure profile in Figure 1.8, then instead of all the overpressured points returning to the normal compaction curve, some of the data points plot above the normal compaction curve (Figure 1.10). Data plotting in this field would normally be considered as being caused by unloading processes contributing some of the encountered overpressure (Bowers, 1994). In this instance, however, the reason that the porosity values do not plot on the normal compaction curve is that vertical effective stress is not proportional to the mean effective stress.

1.8.2 Unloading mechanisms

Unloading mechanisms encompass a number of different processes which affect sediments in the subsurface. Each of these processes relies on different circumstances to be effective. By definition, they all result in a decrease in the effective stress of the sediment and are generally associated with anomalously high pore pressure for the porosity of the sediment (Swarbrick and Osborne, 1999; Bowers, 1994). This section describes the effects of unloading on the porosity - effective stress relationships in mudrocks and then describes how the different mechanisms operate.

The basic relationship between void ratio, mean effective stress and the corresponding pore pressure profile is shown in Figure 1.11. The porosity versus mean effective stress plot shows the path followed by a single packet of shale during burial and unloading. During burial, initially the pore pressures are hydrostatic and the void ratios of the compacting shale plot on the normal compaction curve. At a certain depth, the pore pressure in the shale begins to increase rapidly as overpressure is generated by an unloading mechanism. The shale experiences a decrease in effective stress and the corresponding void ratios (of the shale) plot on a different curve, above the normal compaction curve (Figure 1.11).

The unloading curve represents the elastic increase in shale porosity as the effective stress is reduced. For a given decrease in effective stress, there is only a relatively small porosity increase corresponding to the elastic part of the porosity loss during compaction. The frame bulk modulus during unloading is, therefore, an elastic modulus, and is much greater than the frame bulk modulus during normal compaction.

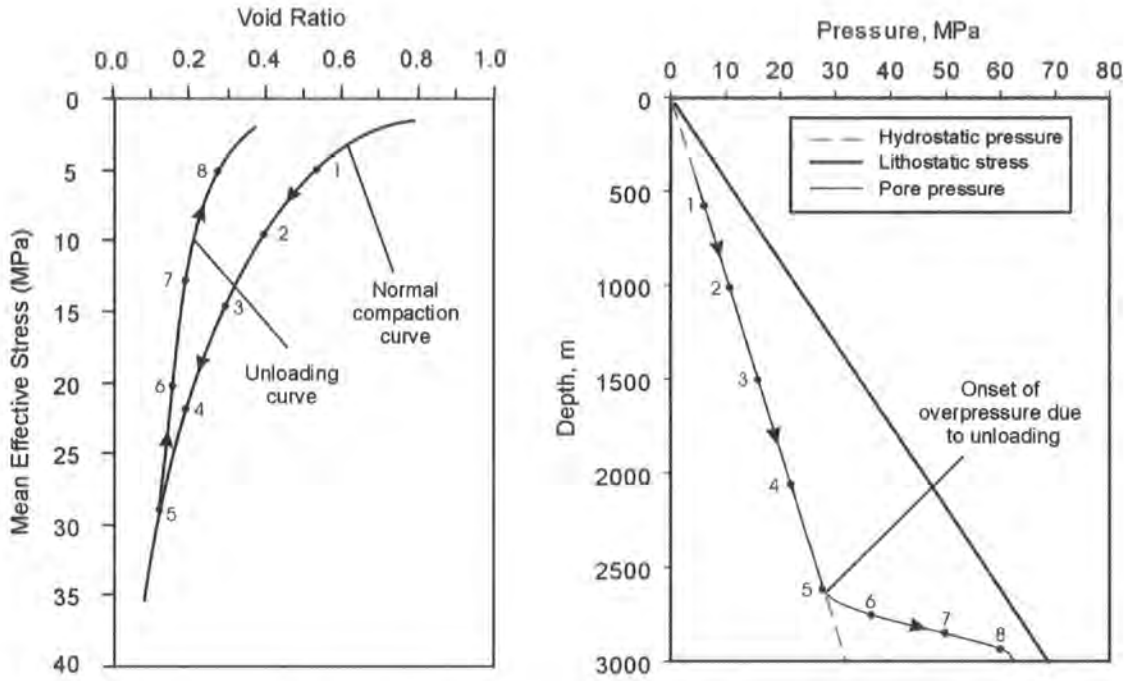

Figure 1.11 Relationship between void ratio and mean effective stress for sediment overpressured by a fluid expansion mechanism.

1.8.2.1 "Thermally" or "temperature" induced unloading

If the temperature of a sediment volume increases, the fluid volume in the pore spaces can increase by one of three mechanisms. An increase in the volume of fluid in the pore spaces will produce an increase in the pore pressure and a decrease in the effective stress.

The most obvious process which can occur when the pore fluid is heated, is that the volume will increase by thermal expansion, referred to as **aquathermal pressuring** (Barker, 1972). This process has been the subject of a number of different studies which are either in favour (Barker, 1972) or against (Luo and Vasseur, 1992) its potential to generate significant amounts of overpressure. The main argument against the effectiveness of this mechanism as with most unloading mechanisms is that they require very low permeabilities to be effective. Any escape of fluid from the pore volume will allow a significant amount of the pore pressure to escape. Swarbrick and Osborne (1999) carried out an assessment of overpressure generating mechanisms and concluded that for a package of sediment being buried at rates between 0.1-2km/My and with geothermal gradients of 20-40°c/km, the contribution from aquathermal pressuring would be less than 1MPa (even when the rate of temperature increase involved is up to 40°C/km).

A second mechanism for generating fluid volume expansion induced by temperature increases is the conversion of solid kerogen to fluid phase hydrocarbon, often referred to as **hydrocarbon generation**. This process has been studied by looking at the volume changes associated with the hydrocarbon generation and applying them to basin environments (e.g., Meissner, 1978; Ungerer et al., 1983). Swarbrick et al. (1998) report the results of recent studies which indicate that there is the potential for significant volume, and therefore, pressure increases (up to 40MPa depending upon the kinetic model chosen, and the amount of pore fluid that is allowed to escape from the system).

The final of the three thermal processes involves the cracking of liquid phase hydrocarbon in the pore spaces to form gaseous hydrocarbons, referred to as **gas generation** or **hydrocarbon cracking**. Although in theory the percentage volume increase attributable to this process is significant, Swarbrick and Osborne (1999) caution that the volume increase must be considered as a fraction of the whole volume of the sediment where the transformation is taking place. They cite an example from

the Northern North Sea where despite evidence for a large amount of hydrocarbon cracking and the presence of high overpressures (~35MPa at 4km depth), only ~4MPa of the total overpressure can be attributed to hydrocarbon cracking.

1.8.2.2 Chemical processes

In the subsurface, as well as the volume expansions associated with temperature changes, a number of chemical reactions can take place which induce a change in the volume of pore fluid and hence the pore pressure.

One of the most common transformations cited in studies is the **smectite to illite transformation** in mudrocks (Freed and Peacor, 1989; Colton-Bradley, 1987; Mello et al, 1994). A number of studies have been carried out to assess the fluid volume increase associated with the transformation (Osborne and Swarbrick, 1997; Audet, 1995a). This process is not considered as an important mechanism for the wells in this study for the simple reason that the mudrocks in each of the basins contain very little smectite.

A second way in which smectite to illite transformation can influence the pore pressure is proposed by Lahann (1998), whereby the transformation from smectite to illite is accompanied by a change in the compressibility of the sediment. If the compressibility increases (as proposed by Lahann, 1998) but the porosity remains approximately constant, then the sediment will have an anomalously high porosity for the given effective stress. Unless the sediment can compact, a greater proportion of the applied stress will be transferred to the pore fluid, the pressure of which will increase.

Although the lack of smectites in this study precludes direct comparison with Lahann's (1998) results, the mechanism may apply to other mineral transformations such as feldspar dissolution in reservoir units (Osborne and Swarbrick, 1997) or any process which causes a reduction in the strength of the matrix. Such changes are here referred to as **chemical compaction**. These processes can induce pressure changes in-situ by the transfer of the stress from the framework to the pore fluid described above, or by expelling a greater volume of fluid which has to be lost from the system before normal compaction can resume (Brown A., pers. comm.). Osborne and Swarbrick (1997) have cited the first of the two processes as being capable of generating a significant amount of overpressure (up to 7.6MPa extra pressure in a study where load-bearing kerogen was converted to liquid hydrocarbon).

Chemical compaction is not technically an unloading mechanism, as it is only responsible for changing the compressibility of the sediments. This change gives the transformed sediment an enhanced porosity relative to its normal compaction curve (the same as sediments overpressured by disequilibrium compaction). The sediment will appear unloaded, however, if the change in the compressibility is not identified from the analysis of samples or wireline log responses. Porosity values of the more compressible sediment compared against the compaction curve for the less compressible sediment will result in an underestimation of the actual pore pressure which could be interpreted as unloading.

1.8.2.3 Dynamic transfer

Dynamic transfer refers to the movement of pore fluid and transfer of overpressure from one part of a basin to another. The transfer can be achieved by one of two main processes. One is by Darcy flow along permeable units that connect less permeable sediments with differing hydraulic potential (e.g., Traugott, 1996; Yardley et al., 1998), this process is often referred to as **lateral transfer.** The second way in which overpressure can be transferred between sedimentary units, is if fluid pressures deeper in a basin become sufficiently high to fracture overlying formations, expelling fluid via hydrofractures (Roberts and Nunn, 1995) or open fault systems (Grauls, 1997).

Lateral transfer was first identified by Hubbert (1940) as a function of differential sedimentation along tilted aquifers (Figure 1.12). The plot shows a tilted aquifer unit encased in overpressured shale. The overpressure in the shale section increases with increasing burial rate, so the amount of overpressure at the base of the structure is higher than in the shales at the crest of the structure. Because the aquifer unit is permeable, it cannot sustain a significant overpressure gradient and pore pressures within the aquifer unit are reorganised to produce constant hydraulic potential. The consequence of such a reorganisation is that overpressure relative to the encasing shale decreases at the base of the structure and increases at the crest of the structure (Figure 1.12). As the process of pressure reorganisation is almost instantaneous, therefore preventing any significant overpressure differences developing, lateral transfer was not initially proposed as an effective generating mechanism.

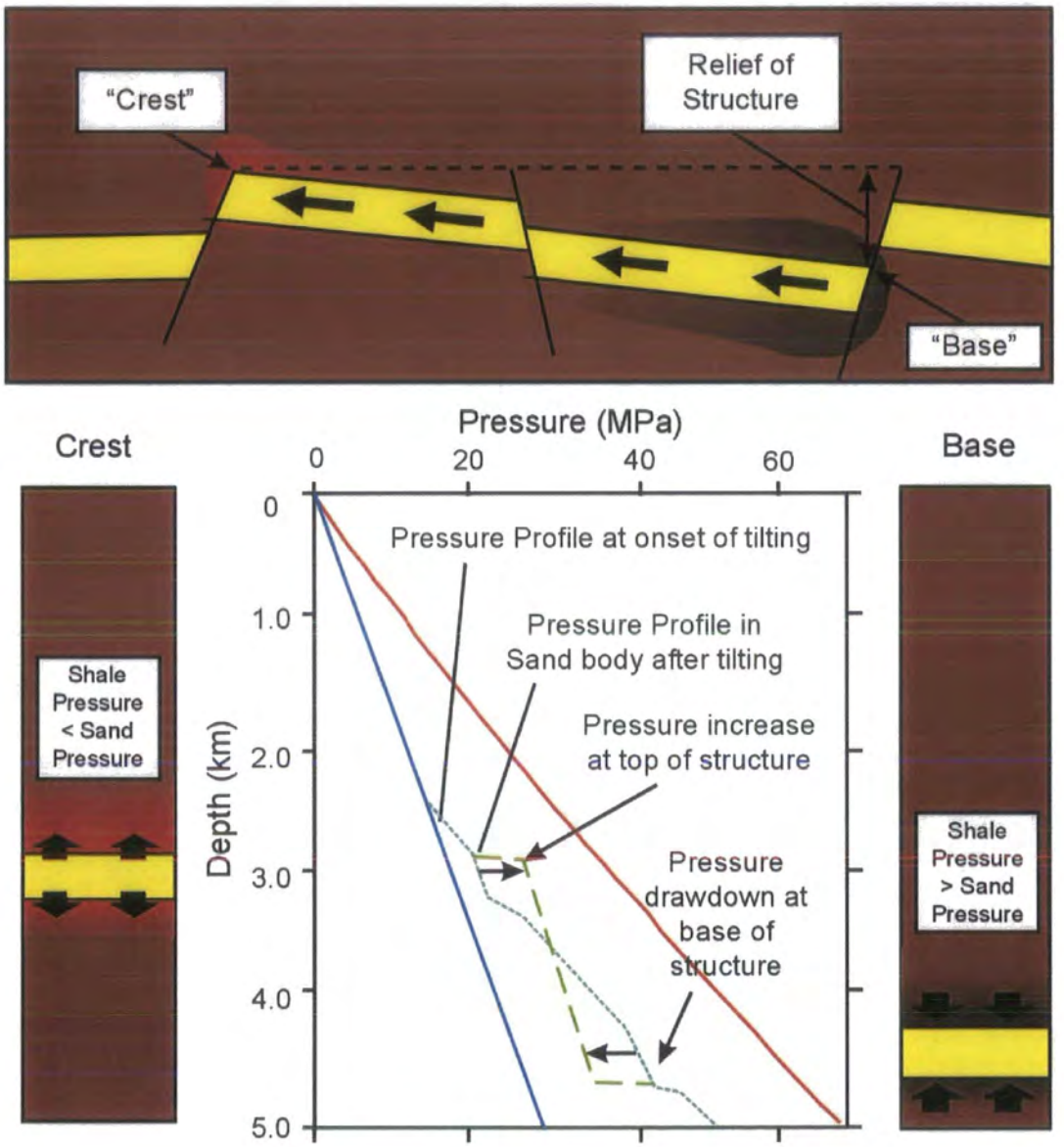

Figure 1.12 Reorganisation of overpressure in a dipping aquifer unit by lateral transfer.

More recent studies which calculated pore pressures in mudrocks from depth or vertical effective stress (Heppard and Traugott, 1999; Stump et al., 1998; Traugott, 1996) invoked unloading due to lateral transfer where computed pore pressures fell short of the encountered overpressure and other fluid expansion mechanisms had been ruled out. Kan and Kilsdonk (1998) and Kilsdonk (1996) cited evidence from seismic velocity distribution to support lateral transfer in SE Asia and the Gulf Coast. Both studies identified zones of velocity increase (porosity reduction) at the base of the structure as being due to pressure "drawdown" from the shales (Figure 1.12). A lack of corresponding velocity decrease (porosity increase) at the crest of the structure, coupled with underestimation of the pore pressures encountered at the crest of the structure, led to the conclusion that lateral transfer was responsible for some of the pore pressure. The process was also proposed to be causing unloading in the sediments at the crest of the structure (hence no discernible porosity increase here).

Results presented in this thesis using mean effective stress to compute pore pressures (Harrold et al., 1999) indicate that the vertical effective stress approach underpredicts pore pressures. Also, 1D and 2D modelling studies (Yardley et al., 1998) indicate that, except under certain extreme conditions, the effect of lateral transfer is to enhance pressures generated by disequilibrium compaction, rather than induce significant amounts of unloading.

1.8.2.4 Other mechanisms

A number of other processes that generate overpressure in the subsurface can result in a decrease in the effective stress of the sediment.

The first of these, the **artesian effect** or **hydraulic head**, can result in significant amounts of overpressure in the subsurface (~10MPa overpressure per km) when aquifer units are in hydraulic communication with highland areas where recharge is taking place. The amount of overpressure can be easily accounted for (e.g., Bachu and Underschultz, 1993). In this study, although there is considerable lateral and vertical connectivity in the reservoir units, hydraulic head is not believed to contribute to the encountered overpressures by more than 1-2MPa.

Another way in which pore pressure can be enhanced is by **hydrocarbon buoyancy** whereby overpressure is produced within the hydrocarbon column by virtue of it displacing higher density brine previously filling the pore spaces. As with hydraulic head, hydrocarbon buoyancy is simple to calculate, and is not believed to be

an important factor in the generation of overpressure in this study, due to the lack of significant hydrocarbon columns.

The final method of overpressure generation to be discussed in this study is **osmosis** which has been calculated as being capable of producing up to 4MPa overpressure in shales as long as the salinity contrasts are maintained, between formations (Osborne and Swarbrick, 1997). Due to low salinities reported throughout the wells in this study, it is not expected that osmosis is a significant contributor to the encountered overpressures.

1.9 Data

For this study, a total of seven, vertical wells were supplied for pressure analysis. Data for each of the wells comprises:

1. Pressure data including direct measurements from the permeable aquifers, well kicks and mudweights.
2. Wireline log printouts/digital values. For all the wells, caliper, gamma ray, sonic and resistivity logs were supplied as standard, with neutron and density data given for four of the wells.
3. Estimates of the minimum stresses from leakoff tests and formation integrity tests.
4. Well reports including more information as to the stratigraphy, lithology, drilling information and structural setting of the well.
5. For one of the wells, seismic velocity data and the results of basin modelling were also supplied for the analysis.

1.10 Key assumptions associated with the analysis

A number of assumptions are required for all the theory and methodology described in Chapters 1 and 2:

Lithology calculation: it has be assumed that the gamma ray and neutron-density log responses respond to variations in quartz, clay and pore fluid, all of uniform properties for each of the wells.

Porosity calculation: from the sonic response, where no information from the well is available, it has to be assumed that the shale lithology is very similar to the set of criteria proposed by Issler (1992). For density-derived porosity values, it is assumed that there is little or no variation of grain densities.

Compaction curves: it is assumed that all of the shales (other than those experiencing unloading due to fluid expansion processes) are presently at their maximum effective stress and that creep compaction and significant amounts of diagenetic changes have not taken place. It also has to be assumed that it is valid to compare the porosities of mudrocks with similar lithologies inferred from log response from different depth intervals in the wells.

The study is focused on young sediments which have not experienced very high effective stress values (>40MPa), hence diagenesis is expected to be slight rather than severe.

1.11 Synopsis

This study has been divided into seven chapters as follows

Chapter 1 introduces the aims of the study, the theory and terminology used in the study as well as some of the previous work in this field.

Chapter 2 describes the methodology used in the pressure analysis.

Chapter 3 presents the results of pressure analysis of three wells from different basins in SE Asia. Data for these three wells were supplied in paper format. This section also includes a comparison of the results of hydrostatic mean and vertical effective stress pore pressure calculation.

Chapter 4 presents the results of pressure analysis of a single well that encountered extremely high pressures and temperatures at depths greater than 5km. Seismic pore pressure analysis as well as 1D and 2D basin modelling were integrated with the porosity-effective stress analysis to draw conclusions as to the origin of the overpressures. This section also includes modelling analysis examining the effectiveness of lateral transfer in relation to the structure studied.

Chapter 5 presents the results of pressure analysis of three wells from the same basin in SE Asia. The data were supplied in digital format. This section also tests the validity of using a common approach to the subdivision of lithologies and the fitting of compaction curves.

Chapter 6 details an appraisal of the methodology used in the study and describes possible improvements that could be made but which were either unavailable or beyond the scope of the study.

Chapter 7 summarises the results of chapters 3-5 and discusses similarities between the wells. Conclusions are drawn as to the influence the results presented here have on the way different overpressure mechanisms operate. Implications for other methods of analysis such as seismic and basin modelling are also presented. A summary of suggested future work on the subject completes the study.

Chapter 2: Methodology

This chapter is subdivided into three sections.

Section 2.1 describes all the different types of data used in the analysis, from pressure data to wireline logs. For each of the data types, a brief description of the principles of measurement is given together with the limitations of the measurements and any assumptions which have been made in using the data.

Section 2.2 details how the parameters used in the analysis are calculated from the raw data values. This section focuses on the derivation of the three main properties used in pressure analysis: lithology, porosity and hydrostatic mean effective stress. Formulae for all the derivations are supplied, together with a brief description of their limitations.

Section 2.3 describes the procedure for calculating pore pressure and mean stress from the parameters described in section 2.2.

Further discussion of the methodology and assumptions is given in Chapter 6.

"watch where you go once you have entered here,
and to whom you turn!
Do not be misled by that wide and easy passage!"
Dante Aligheri

2.1 Data sources

2.1.1 Pressure data

Direct measurements of pressure taken in the wells are the most important data source used in this study. Without these data, pressure analysis from porosity data are merely estimates with no means of validification by comparison with the actual conditions. Fluid pressure data comes from a variety of different sources which vary in their accuracy and importance as shown in Table 2.1. Those that have been used in this study are marked with an asterisk.

Data Source	Hierarchy
Repeat Formation Tester (RFT*/FMT, MDT)	High
Formation Interval Tester (FIT)*	
DST (drill stem test)*	
Well or pressure kick*	
Connection gas	
Measurement/logging whilst drilling (MWD / LWD)	
Mudweight*	
Equivalent depth	Low
Drilling exponent (D, D_c)	

Table 2.1: Sources of pressure data organised by reliability (after Swarbrick, 1999). * Data sources used in this study.

2.1.1.1 Repeat Formation Tester, Formation Multi Tester (RFT/FMT)

The RFT/FMT[1] tool is used to measure formation pressure and to collect samples of formation fluids down the borehole. The tool can make an unlimited number of pressure measurements and can normally collect two samples of the borehole fluid on a single "run".

The tool operates by isolating a small area of the formation from the well bore fluids and allowing formation fluids to flow into two chambers. A pressure gauge

[1] RFT is the trademark of Schlumberger; FMT is the trademark of Dresser Atlas.

records the inflow into and the subsequent pressure build-up, the rate of which is a function primarily of formation permeability.

For this study, as well as pressure values from the tests, one of three drillers comments were supplied where the pressure measurement was not successful (Swarbrick, 1999; Schlumberger, 1996):

1. "Tight": when the formation permeability is low (<1mD) the time taken for the pressure to build up is often too long and the test is aborted to avoid drilling problems.
2. "Seal Failure": the measured pressure will remain the close to the mud pressure if the area of sediment being investigated is not effectively isolated from the borehole fluids.
3. "Supercharging": anomalously high fluid pressures are sometimes recorded during RFT tests taken in lower permeability formations when higher pressure mud filtrate is drawn into the formation whilst the filter cake seal is forming. When the pressure measurement is taken, the tool sees the higher (mud) pressure rather than the formation pressure (Schlumberger, 1996).

For this study, only the interpreted pressure values plus drilling comments were supplied for use in the analysis. The comments allowed for the reappraisal of some of the data (Well B, section 3.3.3); however, the raw logs showing the pressure build up would have been a more ideal data source for the study.

2.1.1.2 Formation Interval Tester (FIT)

The FIT is used for pressure measurements in cased-holes and works on the same principle as the RFT/FMT tools it preceded. Pressure data from this tool were supplied for the analysis of Well C (section 3.4.3). Use of the FIT was largely discontinued with the development of the RFT tool and subsequently the MDT tool (Modular Dynamic Tester) which both work in an open hole environment.

2.1.1.3 Drill stem test (DST)

In a number of the wells included in this study, as well as the RFT and FIT pressure measurements, drill stem tests were performed to assess the composition of the pore fluid, the formation pressures and the reservoir permeability.

The test is performed by isolating an interval of the borehole and allowing fluid to flow into the test apparatus and subsequently up the drill pipe to the surface for

sampling. The pressure is continuously monitored throughout the test which comprises

- an initial flow period,
- an initial pressure build up period which yields the Initial Shut In Pressure (ISIP), the best estimate of true formation pressure.
- a second period of flow.
- a final pressure build up which yields the final shut in pressure (FSIP).

For easier depth interval selection and isolation of the formations, DSTs are normally conducted through perforated casing.

For this study, only ISIP pressure values were supplied, no raw logs were supplied for further interrogation. It therefore has to be assumed that the values presented are derived from thorough analysis following the correct procedure listed above.

2.1.1.4 Well "kick"

During drilling, the volumes of mud in the system are continuously monitored. If the pore pressure in the sediments exceeds the mud pressure then fluid will flow into the borehole and displace mud at the top of the borehole, referred to as a kick. The formation pressure can be calculated knowing the volume and density of mud displaced (e.g., Swarbrick, 1999). Inaccuracies in the measurement of volume changes mean that kicks are not as accurate as direct pressure measurements. They are, however, a more reliable indicator of formation pressures than mudweight data (Table 2.1). Two well kicks are reported at the base of well A (section 3.2.3) and used as a minimum estimate of the pore pressures in the analysis.

2.1.1.5 Mud-weight

A depth interval and an equivalent density in g/cc or lb/gal describe the mudweight used to drill a well. This notation refers to depth below the drilling table (rkb) and the density of the mudweight used to control the borehole. Values of pressure are computed by using [1]:

$$p = Zg\rho \qquad [8]$$

where p is the pressure in megapascals, Z is the depth in kilometres, g is the acceleration due to gravity ($9.87 ms^{-2}$) and ρ is the mud density in g/cc. Values computed using [8] are plotted against TVDSS (true vertical depth sub-sea) for comparison with the other pressure measurements.

As seen in Table 2.1, mudweight ranks very low as a source of pressure information in terms of accuracy. One reason for the low ranking is that it is possible to drill through impermeable units with mudweights that are significantly different from the actual pore pressures. Another reason is the fact that the mudweights are planned prior to drilling, especially in production wells, so the onset of overpressure represented by the first increase in the mudweight may represent the anticipated, rather than the actual, depth of overpressure onset (Swarbrick, pers. comm.). Only when the mudweights are used to balance formation pressures in permeable units can this source be considered as anything other than an indication of the pressure conditions. An example of how pore pressure can be approximated from mudweight values in the absence of direct pressure measurements is when the mudweights used to balance a reservoir interval are very close to the fracture pressure of the interval. Significantly exceeding the formation pressure in permeable reservoir units can cause lost circulation and damage to the reservoir, exceeding the fracture pressure of the formation may result in a blowout and loss of the well, therefore, mudweights will rarely approach the fracture pressure unless driven by the need to balance high formation pressures.

2.1.1.6 Estimates of minimum stress from leak off tests (LOTs)

As well as the measurements of the pore fluid pressures in the borehole, LOTs are performed to assess the minimum stress values in the section cut by the wellbore. The use of this data in calculating horizontal and mean stresses is discussed in section 2.2.3.3.

The LOT is generally conducted after casing has been set in the well and cement has been applied to isolate the shallower sections from any higher pressure fluids that may be encountered deeper in the section.

Firstly, a short section (typically 20 feet) is drilled below the base of the cement before increasing the pressure in the borehole until mud is lost into the formation. The pressure in the mud is continuously monitored and recorded throughout the test. As long as the cement is sound, mud loss is a consequence of failure of the rock usually by the propagation of fractures in the direction of minimum stress. The LOT pressure value represents the magnitude of the minimum stress plus the tensile strength of the formation, which has to be exceeded before fractures will form (Swarbrick, 1999; Mouchet and Mitchell, 1989).

In many cases "leak off" is not reached, but a defined maximum pressure is reached without mud loss, and considered high enough to continue drilling ahead safely. This is often referred to as a formation integrity test (Swarbrick, 1999). Many of the LOT values reported for wells E-G in Chapter 5 are believed to represent formation integrity tests due to the fact that there are many values reported between casing intervals. True LOT tests are normally carried out only at the end of the casing run.

For each of the wells in this study, leak off values with corresponding depths and drillers comments were the only information reported; no raw data logs were supplied such that the data could be further appraised. It is for this reason that caution has been exercised when invoking conclusions from the LOT data.

2.1.2 Wireline logs

The majority of the data used in this study come from the openhole wireline logs. For all of the wells in the study logs were supplied in either paper or digital format. The format influences the type of analysis which could be carried out (section 2.3.1).

2.1.2.1 Caliper log

The caliper log was supplied for all wells in this study and proved important when picking data points. The tool makes measurements of the well bore diameter as it is pulled up the borehole by means of one or more spring mounted "arms".

The caliper log was important in this study for the reason that most, if not all, of the wells experienced a number of problems with overpressure during drilling. These problems often resulted in damage to the borehole and influenced the response of the other wireline tools, particularly those such as the density tool, which rely on direct contact with the borehole wall to take measurements. In standard petrophysical analysis of wireline logs, borehole corrections are applied to the different tool responses to compensate for the effects of the changing borehole diameter. For the analyses carried out in this study, rather than apply corrections, picking of data was avoided from areas identified as having borehole damage to try and ensure that all the values used in the study were representative of ideal measurement conditions.

2.1.2.2 Natural gamma ray tool.

All rocks emit natural gamma radioactivity as a function of their mineralogy where radioactive elements, chiefly potassium uranium and thorium, are present. As the radioactive elements decay, they emit alpha particles, beta particles or, of prime importance for this tool, gamma rays. A scintillation detector in the tool detects gamma rays, and the number of detected gamma rays is recorded in standard API (American Petroleum Institute) units.

The radioactive isotopes of potassium, uranium and thorium are found in a number of minerals such as illite (potassium), organic matter (uranium) and heavy minerals such as zircon and sphene (thorium). All of these minerals are normally far more abundant in mudrocks than sandstones (the dominant lithologies encountered in the wells in this study) so mudrocks have higher gamma ray API responses than sand bodies.

The importance of the gamma ray tool to this study comes from the fact that it was supplied for all the wells and is the main data source used to subdivide the lithologies and pick data points for use in the pressure analysis.

2.1.2.3 Sonic log

Along with the gamma ray, caliper and resistivity tools, the acoustic logging tool is used as standard for logging wells. For this study the sonic log was used as the key data source for the calculation of mudrock porosity.

The tool measures the interval transit time (ITT) of the formation being investigated. A compressional wave signal is emitted at one end of the tool and travels through the mud into the formation, is refracted along the borehole wall, and generates head waves which are refracted back into the borehole to be detected by the two receivers at the other end of the tool. As the spacing of the two receivers is constant, the difference in signal arrival time corresponds to the speed of sound in the formation between the two receivers and the measured interval transit time is taken to represent the velocity at the midpoint between the two (e.g., Etnyre, 1988).

Special circumstances where the first arrival is not the head wave from energy refracted along the borehole wall include cases of severe borehole damage/fractures, the presence of gas in the pore spaces and very high porosity as in the case of Well B (section 3.3.4).

The key factors that affect the speed of propagation of elastic waves are matrix velocity, pore fluid velocity (dependent upon composition and temperature), porosity and fabric (i.e., arrangement of porosity and matrix).

Effective stress may influence the speed of propagation (Hermanrud et al. 1996; Bowers, 1994). This theory has generally been restricted to areas where fluid volume expansion unloading (section 1.8.2) is implicated and the transit time shows a relative increase in excess of the response of the other logs. The increase is attributed to a change in the fabric of the mudrocks induced by unloading which has resulted in microcrack formation (Hermanrud et al., 1996).

The sonic log is not as strongly influenced by borehole conditions as some of the other logging tools such as the density log (see below). However, caving and rugosity can induce spikes on the sonic response, which have to be assessed when picking data for the analysis (section 2.3).

2.1.2.4 Resistivity and conductivity log

The resistivity and induction tools are used in almost all wells drilled to measure the electrical current carrying capacities of the formations. The resistivity tools measure the formation's resistance to the flow of electrical current (the resistivity), whilst the induction tools measure the formation's ability to conduct current (the conductivity) (e.g., Rider, 1996). The measurements are equivalent since the conductivity is the reciprocal of the resistivity.

The flow of current in the formation is controlled by a number of factors: the resistivity of the pore fluid, the resistivity of the matrix material, the resistivity of the mud-filtrate, porosity, fabric (arrangement of porosity) borehole conditions and the temperature.

For this study, the resistivity and conductivity logs were used for empirical comparison with the other log responses as well as to identify hydrocarbon bearing formations and zones of borehole damage where the caliper log is missing. The reasons for not using the tool responses for porosity calculation stem from the number of factors which influence the resisitivity response (e.g., mud properties, formation resistivity and temperature) which were not available for use in this study. Also, although resistivity has in the past been used extensively in the U.S. Gulf Coast area to identify overpressure in shales (Mouchet and Mitchell, 1989), the approach taken is an empirical one and the porosity was not generally calculated as part of the analysis

(e.g., Eaton, 1960). Recent studies which have calculated porosity from the resistivity response (e.g., Holbrook, 1995) use assumptions as to the nature of the pore fluid composition and detailed lithological information gained during drilling. In most studies, where no data restrictions apply, sonic and density logs are the preferred data source for mudrock porosity and pore pressure calculation

2.1.2.5 Density log

The importance of the density log to this study is for the calculation of shale porosity (section 2.2.2.2) and vertical stress in the wells (section 2.2.3.2) as well as for lithological analysis when combined with the neutron log response (section 2.2.1.3). Where it has been supplied for analysis, density-derived porosity is used for comparison with porosity computed from the sonic log. Such a comparison has been proposed for use in determining whether unloading had contributed to observed overpressures (Bowers, 1998). The theory here is that unloading induces a change in the fabric of the shales which effects the sonic waves more than the density log, causing a separation in the two tool responses over the interval that is unloaded.

The density tool works by bombarding the formation with medium energy, focused gamma rays and measuring the back scattered flux of gamma rays at near and far detectors. As the density of the formation increases, so the count per second of gamma rays decreases.

To accurately measure the formation density, the source and detector are kept as close to the formation as possible. This is achieved by mounting the source and detectors on a sensor pad that is pressed hard against the borehole wall by a spring mounted caliper arm. Problems arise with the measurements when the sensor pad is not in contact with the borehole wall due to caving or increased rugosity (a measure of the roughness of the borehole wall). As the separation between the sensor and the borehole wall increases, the density values become representative of the mud, which results in "spiking" of the log response or intervals of anomalously low values when large caves are encountered.

Unfortunately, the sensitivity of the density tool to borehole damage meant that it was not possible to collect density values over many intervals in the boreholes, in particular Wells E-G (Chapter 5). For the purposes of this study, data points were not selected from intervals where either the caliper log indicated damage to the borehole or intervals where the log response was spiked.

2.1.2.6 Neutron log

The neutron tool works by emitting a large number of high energy neutrons from a radioactive source and detecting the response of the formation. Energy is lost from the neutrons when they collide with atoms of similar mass, chiefly hydrogen. The flux of back scattered neutrons with reduced energies which arrive at the detectors therefore depends upon the number of hydrogen atoms in the formation (e.g., Rider, 1998). The tool is calibrated to give output values in porosity assuming the lithology is limestone with fresh water as the pore fluid. However, in addition to the water in the pore spaces, clay minerals contain surface-bound water which is detected by the tool, making the neutron porosity artificially high (the amount by which a specific mineral produces an increase in the neutron log response is referred to as its "hydrogen index"). The neutron tool therefore can be used as an indicator of clay fraction as well as porosity in the formations, and when combined with the density log response can be used to derive both lithology and porosity (section 2.2.1.3).

Although the passage of the neutrons will be affected by an increase in the borehole diameter, (the particles have to travel through more hydrogen-rich muds before encountering the formation) two detector units are used to compensate for this effect (Rider, 1996). The result is that the neutron response is less influenced by borehole conditions than the density tool. Although the tool is less susceptible to borehole damage, the relationship between the tool response and the porosity has been described as non-linear above 40% (Cannon, 1995). Values exceeding 40% require correction to derive representative porosities.

For the purposes of this study, the lack of detailed information concerning the mineralogy, and therefore the hydrogen index meant that the neutron porosity values were generally used qualitatively for comparison with the sonic derived porosity values (e.g., section 3.3.4). Where the log response was used in conjunction with the density log for lithology/porosity (section 2.2.1.3), an assumption was made for an average response of the shale matrix alone, and porosity values greater than 40% were discarded or only used for qualitative comparison. Use of this methodology in the study was restricted by borehole damage and poor quality density log data.

2.1.3 Seismic data

For some of the wells in this study, interpreted 2D seismic profiles were included with the well reports for the analysis. This data source was used to test/support

hypotheses as to the generation of the overpressure encountered in the borehole. For example, if a proposed generating mechanism requires a significant amount of structural relief to be effective, this can be tested by comparison with the seismic cross section. For confidentiality reasons, the profiles cannot be included in this study with the exception of Well D (Figure 4.2, section 4.1).

As well as the 2D seismic cross section, the velocities used for pre-stack depth migration were also supplied for the pressure analysis of Well D (section 4.5.1). This data source was used to calculate pore pressure magnitude and distribution relative to the seismic line. As this data source was only used for the analysis of one well, the description of the data and the data processing are dealt with in section 4.5.1, with a further discussion of the implications and limitations of this type of analysis in section 6.10.

2.1.4 1D and 2D basin modelling

Modelling using in-house and commercial basin modelling software was used for comparison with the mudrock analyses, and both were compared with the direct pressure measurements. Current basin modelling packages assume that porosity is related to vertical effective stress. One of the main benefits of basin modelling is that it allows the sensitivity of parameters to be investigated and uncertainty explored. The value of basin modelling is dependent on:

1. Knowing the input parameters which have been used (although there may be some uncertainty as to their validity).
2. Knowing the relationships on which the calculations are made (although the relationships themselves may not be correct for earth systems).
3. Speed of computation.
4. Insights into processes which govern pressure development in sediment.

1D modelling has the advantages that it is simple to construct and interrogate the models, and the speed of computation is much greater. Sensitivity of the system to changes in the sediment properties can therefore be more quickly assessed using 1D models. The disadvantage of using 1D models is that they may be an oversimplification of the system because they cannot include 2D and 3D components of compaction and fluid flow.

2D models have the advantages over 1D that they include components of 2D fluid flow and compaction, and that the results can be compared against spatial pressure distributions from wells. Sensitivity of the directions and magnitudes of fluid flow can be investigated by varying the parameters used to define the sediments' compaction behaviour. The disadvantage of 2D models is that they are more complicated and therefore require more time to construct, process and interrogate when compared to 1D models. Also, in common with 1D, 2D models may be an oversimplification of the 3D system.

3D modelling is the ideal solution to carry out analysis for comparison with actual subsurface conditions, as it allows the maximum amount of complexity of the system to be included and tested. The drawback is that 3D models are even more complicated to construct, process and interrogate and therefore it takes far longer to carry out analysis. Although they have advantages over 1D and 2D models, 3D models will still be an oversimplification of the actual system being modelled.

2.2 Parameters

In order to estimate pore pressures in mudrocks, three key parameters need to be derived: lithology, porosity and hydrostatic mean effective stress. These parameters are calculated by processing the raw data described in section 2.1 through a number of steps laid out in this section. For each of the parameters, there are a number of different ways of calculating the values depending upon the data sources available. This section describes all the methods applied to calculate the parameters from the raw data supplied.

2.2.1 Lithology

2.2.1.1 Information from well reports and composite logs

Although the majority of lithological information is derived from wireline log responses (descriptions to follow in sections 2.2.1.2 and 2.2.1.3), primary information as to the nature of the clays in each of the wells comes from the well report and composite logs supplied with the data sets in this study. The lithological information has been taken from analyses of the cuttings and cores during drilling.

The most detailed information comes from the results of X-ray diffraction (XRD) analysis of clay samples taken from sidewall plugs or cuttings. These data were

available only for two of the wells from a limited number of samples (Well B, section 3.3.2; Well D section 2.2.1.3). The analysis produces details of the nature and relative proportions of the different minerals (in particular clay minerals) present in the mudrocks. Clay mineralogy is important for:

a) Calculation of porosity in shales from the sonic, density and neutron logs. This requires knowledge of the matrix travel time, grain density and matrix properties for the neutron log, respectively (sections 2.2.2.1, 2.2.2.2 and 2.2.2.3).
b) Comparison of shales which have been grouped according to wireline response (section 2.2.1.1, 2.2.1.2) from different depths. It is important that their matrix composition is consistent for such a comparison to be valid.
c) Determining whether the shales have undergone diagenetic changes during burial. This is more important in certain clay minerals, in particular smectites/montmorillonites. The consequence of such changes is that comparisons of shales of similar mineralogy are restricted to smaller depth intervals (Lahann, 1998). Further discussion of this point is given in section 7.3.5.

Petrographic descriptions of cuttings produced during drilling are also provided from individual beds at intervals between 5-30m down the borehole. The descriptions supplied tend to focus on the encountered reservoir units. The nature and appearance of the mudrocks are generally described every 30m or so in the argillaceous intervals. This information is used in two ways:

1. As a discriminant to avoid picking data from zones where the mudrocks are described as cemented or having an anomalous appearance.
2. To identify formations where the high gamma ray response is due, not to high clay content, but instead to an increase in mica content of the sands. This is particularly important in wells where the neutron and density logs are not available.

As cuttings produced during drilling may take variable amounts of time to reach the surface, the descriptions cannot be accurately tied to depth in the borehole and errors of over 5m may exist. For this reason, where the cuttings descriptions indicate that the mudrocks are unsuitable for inclusion in the pressure analysis, values are not selected for the study 5-10m above or below the depth where the description was made.

For each of the wells, the lithological information was used to check that the mudrocks were of suitable composition for analysis using the methods described in this chapter and that they fitted the basic assumptions laid out in section 1.10.

2.2.1.2 Gamma ray

The gamma ray response is a key component of the lithological analysis in this study. It was used to discriminate between sands and shales in the wells and for subdivision of the shales into groups of similar properties, an important part of the pressure analysis (section 2.3.2).

The key assumption associated with the lithological analysis is that the gamma ray response in API units (Gr) for each of the units encountered is a function of a mixture of low gamma quartz (Gr_{qtz}) and high gamma clays (Gr_{cly}):

$$Gr = V_{qtz} Gr_{qtz} + V_{cly} Gr_{cly} \quad [9]$$

The parameters Gr_{qtz} and Gr_{cly} are determined empirically for each of the wells following the methodology described in Rider (1996): the average lowest values for the API response are assigned the value of a clean sand (Gr_{qtz}) and the highest average values are assigned the value of a pure clay (Gr_{cly}). Once the pure sands and shales have been identified, points for analysis are selected by virtue of having a clay fraction greater than 50%. All the data points are subsequently sorted on the basis of API response, a direct function of V_{cly}, so that a more detailed lithological analysis can be included in the calculation of pore pressures. Rider (1996) argues that, particularly for unconsolidated Tertiary sediments, the relationship between V_{cly} and Gr is not linear. For this reason, although [9] is the basis for the subdivision of lithology, API values are not converted to values of V_{cly}, as no relationship was available for the wells drilled in SE Asia. Instead the data from each well (Chapters 3-4) or groups of wells (Chapter 5) were subdivided empirically into groups of similar API response which should correspond to mudrocks of similar mineralogy and V_{cly}.

An example of how groups of similar lithology are subdivided is shown for wells E, F and G (Figure 2.1). The plot shows two histograms for each of the three wells.

The first histogram (shaded on Figure 2.1) shows the percentage that each API value makes up of the total number of values in the entire well (around 25,000 values). The second histogram (demarked by empty frames) shows the percentage that each of the API groups subdivided for the pressure analysis make up of the total number of values picked (between 250-850 values). Clear differences in the

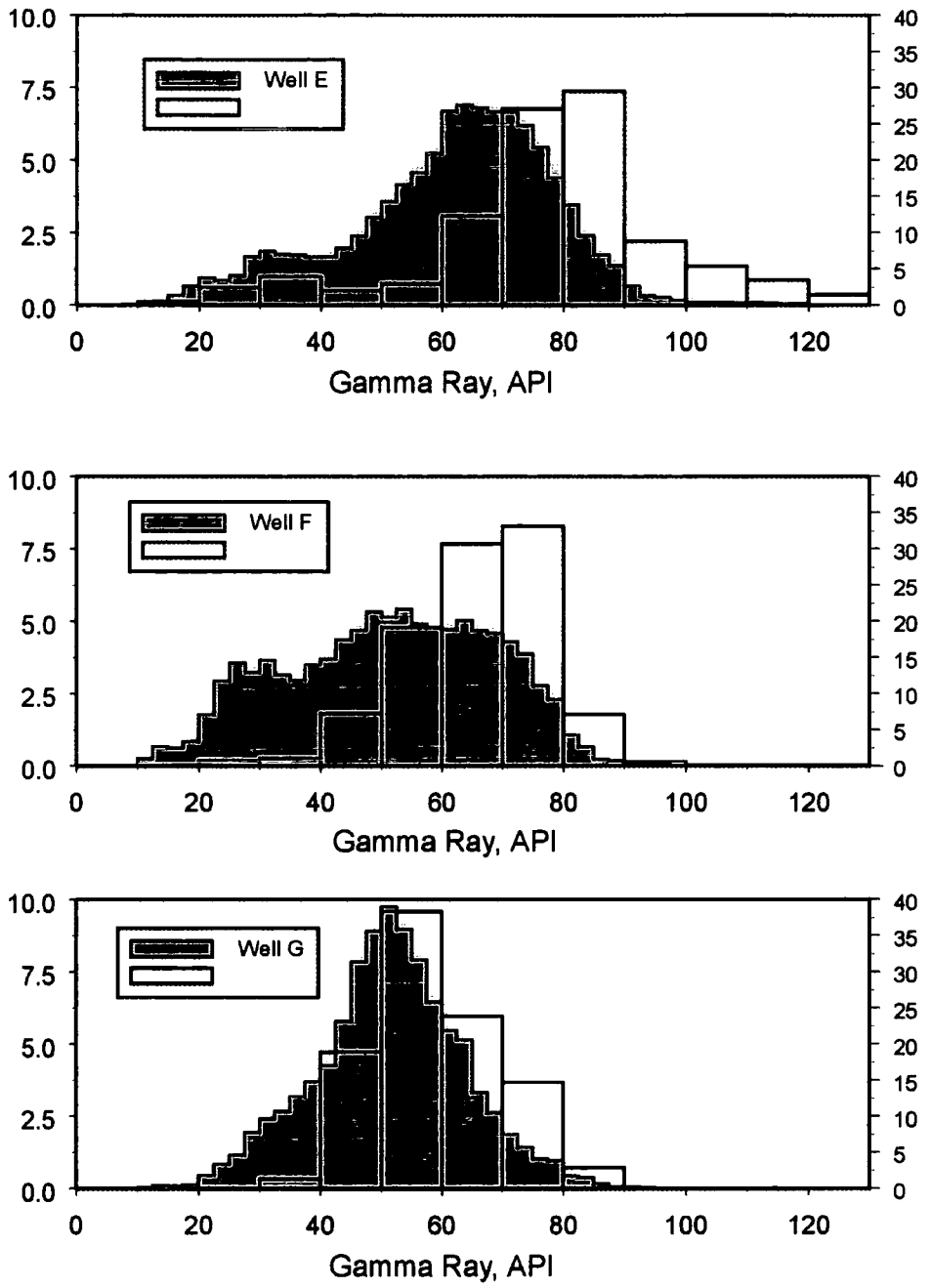

Figure 2.1: Histograms showing the percentage of data values within each range of gamma ray response for Wells E-G. Shaded area indicates inclusion of all gamma ray values from the wells. Transparent columns indicate histograms constructed from the gamma ray values of the shales selected for analysis only.

distribution of all the gamma ray values can be seen between the wells (more fully explored in Chapter 5.1.2).

As all three wells were drilled in the same basin with a common depositional source, it was decided that variation in the mudrock API values was not a function of changing clay mineralogy, but of varying abundance of quartz and clay of near constant composition. Consequently the data were subdivided into groups of API values as shown by the overlain histogram in Figure 2.1. As the subdivision of data is consistent for all three wells, then comparison of the behaviour of individual lithology groups can be made between the wells.

The main assumptions for using this methodology are:

1. There are no significant differences in mud chemistry between the wells which could affect the gamma ray response.
2. The varying API values in the mudrock units were not a function of changing clay mineralogy but simply of varying abundance of quartz and clay of near constant properties.
3. The gamma ray tools for each of the wells are responding in the same way, i.e., the tools are properly calibrated to read the correct API values.

2.2.1.3 Neutron-density cross plot

Neutron-density cross plots are regularly used in well log analysis to calculate lithology and porosity from the log responses (Rider, 1996). The approach is generally applied to the analysis of carbonate, sand and evaporite sequences (Schlumberger, 1989). For this study, the methodology has been extended to the quantitative analysis of shale porosity and lithology following the work of Katahara (pers. comm.).

The principle of calculation is that the sediment comprises three components: quartz, clay of uniform properties, and water, each of which have different neutron and density responses as shown for Well D in Figure 2.2. Knowledge of the log responses for these three components means that lithology and porosity can be calculated from actual log responses in the borehole.

Neutron and density values are assigned to each of the three components as marked in Figure 2.2. In practice it is best to calibrate these values for the three points

from analysis of samples of the well (Table 2.2). The following procedure was adopted for Well D:

1. Grain densities for sands and shales were taken from XRD analysis of actual samples from the well.
2. Neutron log responses were calibrated to measure sandstone porosity so the sand matrix has a neutron response of zero (Schlumberger, 1989).
3. The shale matrix response was derived empirically from the analysis of a number of wells.
4. Fluid density was defined by measurements in the borehole, and the neutron response of pure water was assumed to be 1.00 (porosity = 100%).

	DENSITY	NEUTRON RESPONSE (SANDSTONE MATRIX)
Clay	2.85	0.47
Quartz	2.65	0.00
Water	1.03	1.00

Table 2.2: Neutron and density values defined for Well D. Grain densities from clays are derived from XRD analysis, (Katahara 1997, pers. comm.)

Using the values defined in Table 2.2 it was then possible calculate the amount of clay, quartz and water in the sediment by solving the following three linear equations:

$$1 = cly + qtz + wat \quad [10]$$

$$\rho_b = \rho_{bcly} cly + \rho_{bqtz} qtz + \rho_{b\,wat} . wat \quad [11]$$

$$\phi_n = \phi_{ncly} . cly + \phi_{nqtz} . qtz + \phi_{nwat} . wat \quad [12]$$

where *cly* is the volume of clay, *qtz* is the volume of quartz and *wat* is the volume of water in the sediment; ρ_b is the actual density response, ρ_{bcly}, ρ_{bqtz} and ρ_{bwat} refer to the density values of pure clay, quartz and water respectively presented in Table 2.2; ϕ_n is the actual neutron response, ϕ_{ncly}, ϕ_{nqtz} and ϕ_{nwat} refer to the neutron responses of pure clay, quartz and water respectively (Table 2.2).

The three equations were solved by using a matrix inversion within Microsoft Excel software package to yield the amounts of clay, quartz and pore fluid in the sediment:

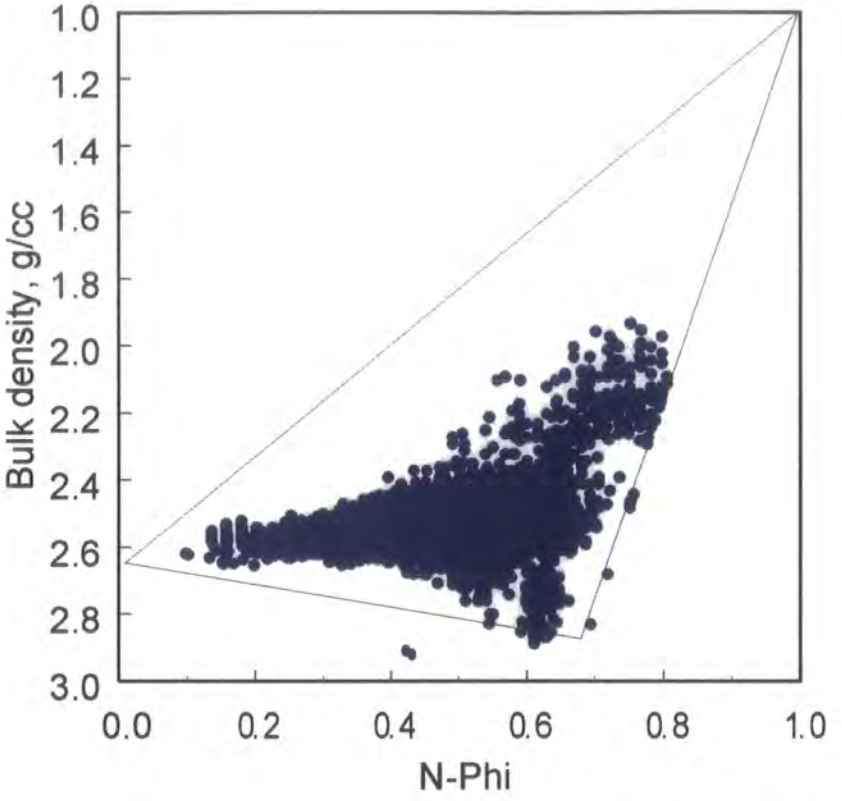

Figure 2.2: Neutron-density crossplot for sediments from Well D showing the distribution of the data points and log values for quartz, clay and water. Neutron porosity N-phi is in limestone porosity units.

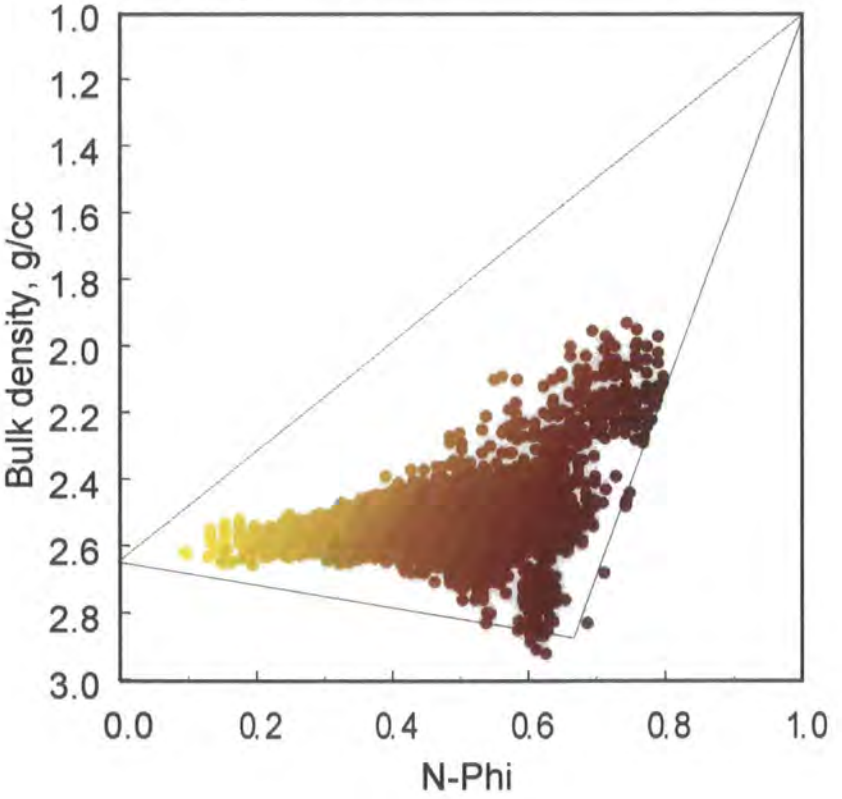

Figure 2.3: As for Figure 2.2, data points are shaded for clay fraction.

$$\begin{pmatrix} cly \\ qtz \\ wat \end{pmatrix} = \begin{pmatrix} 1 & 1 & 1 \\ \rho_{bcly} & \rho_{bqtz} & \rho_{bwat} \\ \phi_{ncly} & \phi_{nqtz} & \phi_{nwat} \end{pmatrix}^{-1} \begin{pmatrix} 1 \\ \rho_b \\ \phi_n \end{pmatrix} \quad [13]$$

To get a value of clay fraction (V_{cly}) for use in the lithological analysis the clay volume (*cly*) from [13] is divided by the total solid fraction of sediment (*cly+qtz*) as shown in [14] such that shales with differing porosity but similar mineralogy are grouped together.

$$V_{cly} = \frac{cly}{cly + qtz} \quad [14]$$

Figure 2.3 shows the same data as Figure 2.2 now with the data points shaded to represent V_{cly}. Values of other log responses/parameters can now be plotted against depth shaded for V_{cly} to see the relationship between the calculated lithology and different parameters (or vice\versa), as shown in Figure 2.4. This type of plot is useful for selecting intervals to be used in the pressure analysis (section 2.3.1)

2.2.2 Porosity / void ratio

The porosity (ϕ) of a sediment is the fraction of the sediment volume occupied by pore space, and may be expressed either as a fraction of unity or a percentage. For this study porosity values are presented in the form of percentages throughout.

The importance of porosity to this study is that it can be used as a proxy for mechanical compaction of sediment (in particular mudrocks). It is also the key parameter used in the calculation of pore pressure (section 1.3, section 2.3).

For all analysis carried out in this study, the value of mudrock porosity, calculated as described in sections 2.2.2.1-2.2.2.4, is converted to a value of void ratio, *e*, which is the ratio of voids to solids in the sediment:

$$e = \phi/(1-\phi) \quad [15]$$

Void ratio is the parameter used in soil mechanics to measure compaction, therefore using void ratio in the pressure analysis allows comparison of the results with actual tests carried out on samples (Audet, 1995).

Porosity can be measured directly from samples by the injection of either mercury, nitrogen or hydrogen into the pore space. Direct measurement of porosity was beyond the scope of this study. Porosity was calculated using data from the sonic, density and neutron log responses.

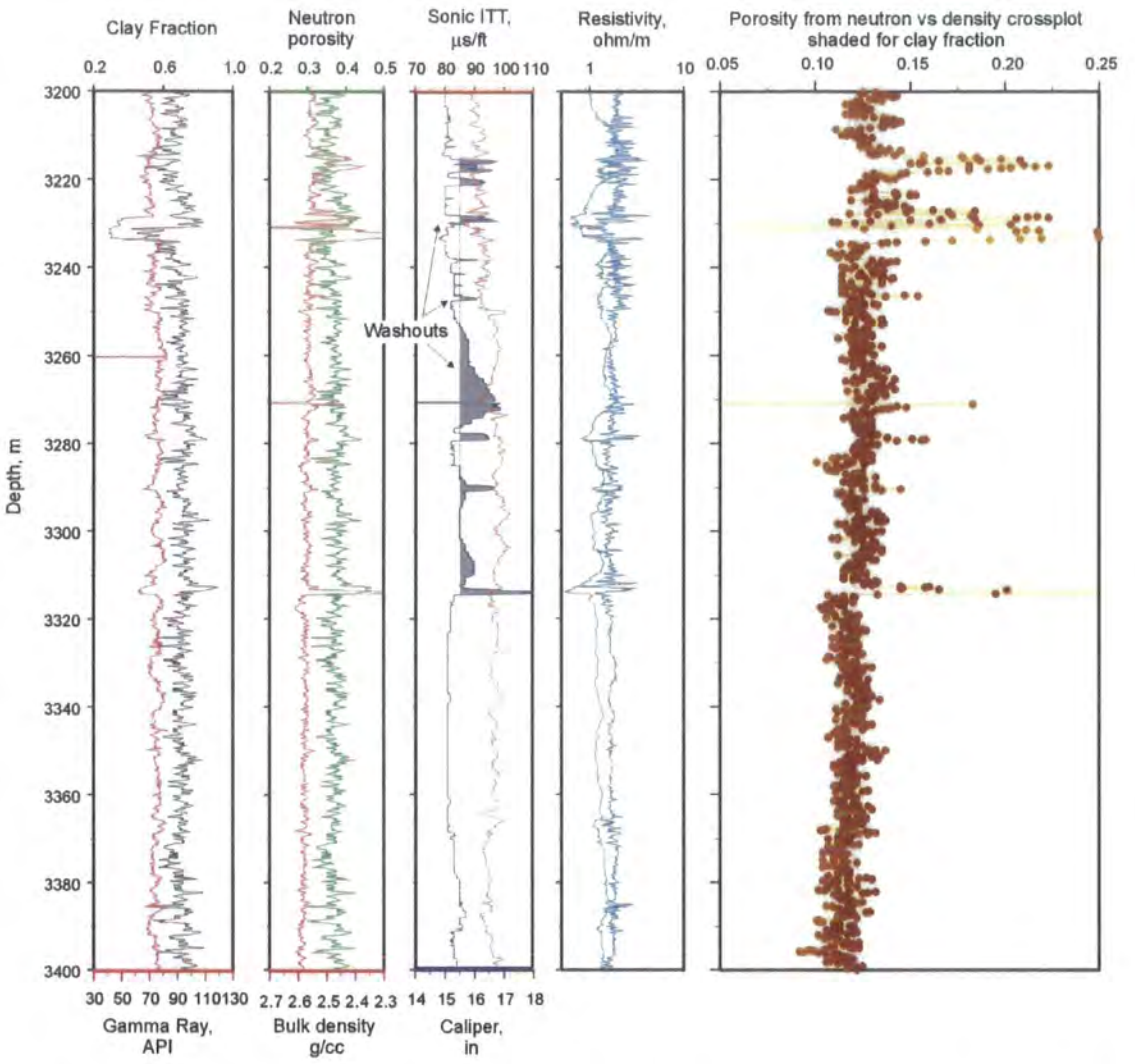

Figure 2.4: Plot showing gamma ray (red), clay fraction (black), bulk density (red), neutron porosity (blue), caliper (black) shaded grey to indicate washout zones, sonic ITT (blue) along with deep (pale blue) and shallow resistivity (dark blue) log values from Well D plotted against depth. Also plotted is the porosity computed from the neutron-density crossplot, porosity values are shaded for clay fraction (high = brown, low = yellow).

2.2 2.1 Shale porosity from sonic interval transit time.

For all of the wells in this study, the sonic log was chosen as the main source of porosity information for shales for the reasons set out in section 1.2.

The key relationship used between porosity (ϕ) and interval transit time (Δt) measured by the sonic log is taken from Issler (1992):

$$\phi = 1 - \left({}^{\Delta t_{ma}}/_{\Delta t} \right)^{1/x} \qquad [16]$$

where Δt_{ma} is the matrix transit time (equal to $220 \mu s/m$) and x is the formation acoustic factor (equal to 2.19) both these values are taken from Issler (1992). The form of this equation is referred to as the "acoustic formation factor" approach proposed by Raiga-Clemenceau (1988).

A similar relationship to [16] is proposed by Hansen (1996) to estimate the porosity of mudrocks from the Norwegian shelf. The reported values of Δt_{ma} and x differ only slightly from the values used by Issler (1992) (e.g., Δt_{ma} = $220 \mu s/m$ and x =2.19 for the Beaufort–Mackenzie basin, Δt_{ma} =$232 \mu s/m$ and x = 2.17 for the Norwegian shelf). The similarity of these results from the two different settings strengthens the argument for using the "acoustic formation factor" approach for analysis of the poorly consolidated Tertiary mudrocks in this study. Equation [16] was also used in the compaction analysis of Tertiary shales from the Gulf Coast (Audet, 1995). As no systematic analysis was made to justify the form of the equation used; only the author's comments on the consistency of the results were considered when choosing the appropriate porosity transform.

The reasons for using Issler's values of Δt_{ma} for this study when his relationship was originally derived from analysis of samples in the Beaufort-Mackenzie basin, Northern Canada are as follows:

- The mudrocks from all the wells in this study have fairly uniform mineralogy with only small amounts of carbonate (typically under 5%), total organic carbon (TOC <5%) and smectite. Issler (1992) cites the absence of these three components from the mudrocks as being important for the consistency of the results.
- The sediments were all deposited very rapidly and many have had less opportunity to be altered chemically by diagenesis/chemical compaction than might be

expected for older, more slowly deposited Mesozoic sediments such as those encountered at depth in the Central North Sea.

- In common with the study area described in Issler (1992), most of the sediments in this study were deposited in a deltaic environment with sediments being derived from a terrestrial source.

A plot showing how porosity calculated using [16] varies with interval transit time is shown in Figure 2.5. This diagram emphasises the limitations of use of the equation to Δt values between 220 and ~673$\mu s/m$ (67-205$\mu s/ft$). Below 220$\mu s/m$ the inferred porosity becomes negative, whilst above 673$\mu s/m$ the calculated porosity values exceed 40% which is outside the range of values used to derive the original relationship. For the mudrocks from the wells in this study, interval transit times only approach 673$\mu s/m$ either at very shallow depths where the porosity may actually be very high, or when the sediments are highly overpressured. Where Δt values approach 673$\mu s/m$, the values are not converted to porosities, and the origin of the very slow speed of wave propagation is discussed in the results section of the well analysis (Well B, section 3.3.4).

Shale porosity can also be calculated from the "time average equation" relating interval transit time to porosity in sandstones proposed by Wyllie et al. (1956):

$$\phi = (\Delta t - \Delta t_{ma})/(\Delta t_f - \Delta t_{ma}) \qquad [17]$$

where Δt is the measured interval transit time, Δt_f is the transit time in the interstitial fluid and Δt_{ma} is the transit time of the matrix material. Although the acoustic formation factor approach was also originally derived using sandstones, it is preferred over the time average equation which was derived over a much narrower range of porosity values in sandstones and has not been adapted for specific use with shales other than by the addition of the "compensation factor" (Schlumberger, 1989):

$$\phi = (1/C_p)(\Delta t - \Delta t_{ma})/(\Delta t_f - \Delta t_{ma}) \qquad [18]$$

where C_p is the compensation factor. This factor is invoked when the linear form of [17] overpredicts porosity in unconsolidated sediments (Raymer et al., 1980). As C_p was not provided for any of the wells in this study, the acoustic formation factor equation was chosen ahead of the time average equation to compute shale porosity (the applicability of the acoustic formation factor approach to shales had been demonstrated by previous studies, Issler, 1992; Hansen 1996).

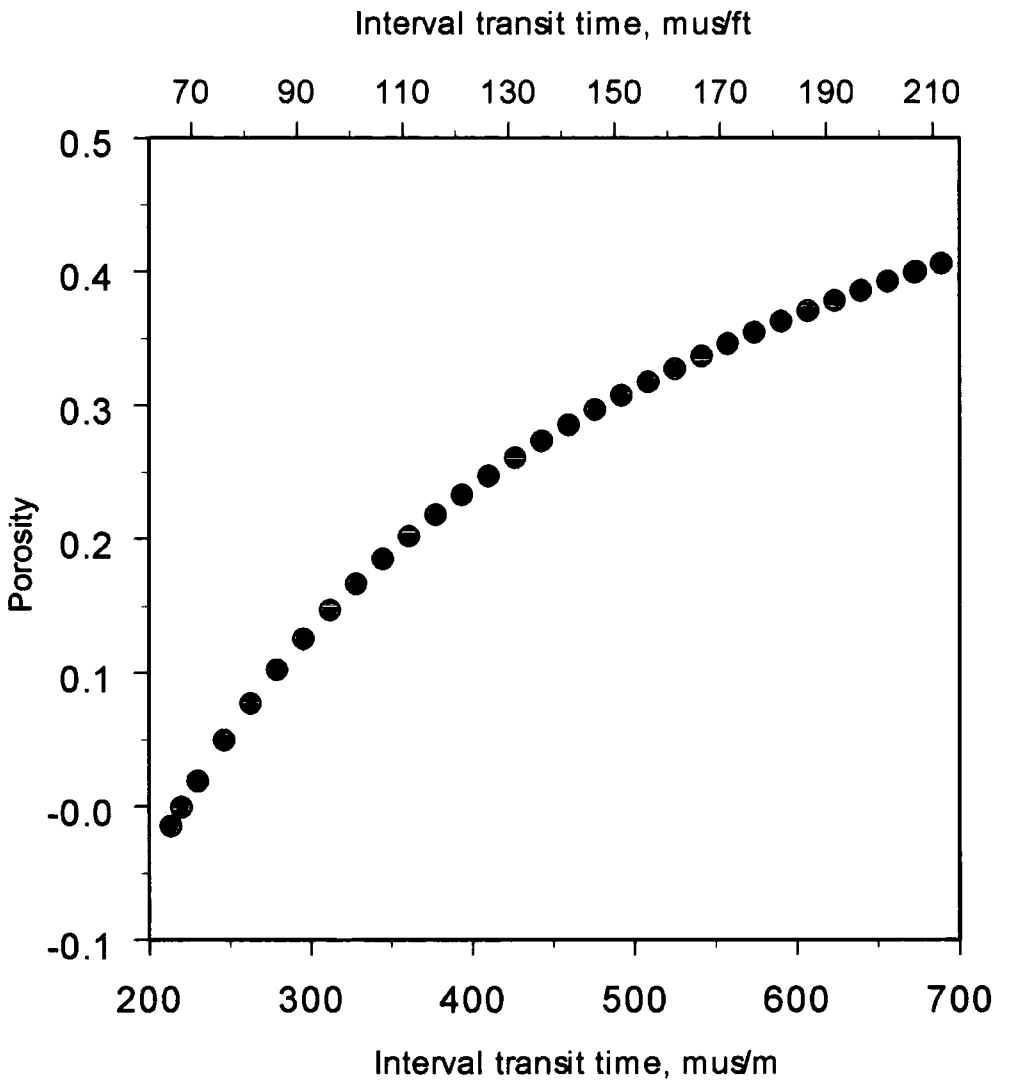

Figure 2.5: Sonic interval transit time versus porosity calculated using [16] from Issler (1992).

2.2.2.2. Shale porosity from density log values.

Porosity can be calculated from the density log using the formula:

$$\phi = (\rho_{ma} - \rho_b)/(\rho_{ma} - \rho_f) \quad [19]$$

Care has to be taken when applying this formula in formations where the mineralogy is variable (shale grain densities have been reported at anywhere between 2.45-2.9g/cc (Rider, 1996)) as this can introduce errors into the calculated porosities. Where no measurements exist, grain densities have to be assumed (as in this study). Brown (1998) has suggested using artificial neural networks to calculate the grain density and therefore porosity (section 6.10).

For this study, porosities have been calculated assuming constant grain densities derived from analysis of mudrock samples from each of the wells (e.g., Table 2.2) and fluid densities derived from RFT samples and the well reports. The computed porosity values were only used for comparison with the porosities calculated from the sonic interval transit time, due to problems with the density logs and the lack of more accurate grain density information.

2.2.2.3 Shale porosity from the neutron log response.

Neutron log data were supplied for five of the wells in this study. Since the values were given as percentage values (rather than the raw neutron log response in limestone porosity units), the data were used only for qualitative comparison with the sonic and density porosity estimates.

2.2.2.4 Shale neutron-density cross plot

As described in section 2.2.1.3, neutron and density values can be cross-plotted to derive lithology and porosity. Although there are some limitations with the use of the neutron log values (see above), cross plotting both logs reduces scatter as long as bad data are discarded.

2.2.2.5 Sand porosity calculation

Direct measurements of sand porosity from cuttings and core are the most reliable form of measurement, and are the only values used as part of the pressure analysis (Well A, Figure 3.7, and section 3.2.4). Sand porosity was used only in the calculation

of lithostatic stress. Porosity for the sands can be calculated from the sonic log using one of a number of different formulae:

1. The Wyllie time average equation [17] substituting the value of $53\mu s/ft$ for the matrix travel time through quartz,
2. The Raiga-Clemenceau form equation [16] using $53\mu s/ft$ for the matrix travel time through quartz and 1.7 for the formation factor.
3. The Hunt transform equation below:

$$\phi = 0.625\frac{(\Delta t - \Delta t_{ma})}{\Delta t_{ma}} \qquad [20]$$

where Δt is the interval transit time and Δt_{ma} is the matrix travel time for quartz ($53\mu s/ft$ was the value used in this study).

2.2.3 Hydrostatic and lithostatic pressure calculation

2.2.3.1 Hydrostatic pressure

Hydrostatic pressure is a function of the fluid density and the vertical height of the fluid column. Hydrostatic pressure can be expressed by the equation [8]. Use of this equation assumes that there is continuity of the water column from depth to the surface, that the salinity of the water column is constant and that the water column is in static equilibrium (i.e. it is moving neither in the subsurface nor at the surface).

In drilling terminology, hydrostatic pressure is used to describe the weight of the column of mud as well as the column of fluid in the pore spaces. For the purposes of this study, hydrostatic pressure is only used to describe the normal pressure exerted by the column of pore fluid. Drillers measurements of the pressure conditions due to the column of mud are referred to as "mudweights" only.

2.2.3.2 Lithostatic stress

Lithostatic stress is also known as overburden pressure or overburden stress, and is the combined weight of the overlying sediments and fluids at a specified depth.

Lithostatic pressure can be expressed by the equation:

$$s_v = \rho_b g Z \qquad [21]$$

where s_v is the lithostatic stress; ρ_b is the average bulk density and Z is the vertical depth from datum.

Where the density log is available, the vertical stress due to each sampling interval (s_{vi}) is calculated from

$$s_{vi} = \rho_{bi} g \Delta Z \quad [22]$$

where ρ_{bi} is the density of the interval and ΔZ is the depth sampling interval of the log (typically 0.25m). To calculate s_v at a depth $Z=N\Delta Z$, the values of s_{vi} for each of the intervals from the surface are summed:

$$s_v = \sum_{i=1}^{N} s_{vi} \quad [23]$$

where the density log is affected by poor borehole conditions (section 5.1.1) the density log is plotted against depth, and a curve of density versus depth is visually fitted over the data values (Figure 2.6). The curve is integrated to calculate s_v using [22] and [23].

For Wells A-C (Chapter 3) the density logs were either absent or not available for the shallower intervals. For these wells, the following steps were followed to compute the vertical stress:

1. The log is split into sections of uniform properties (typically between 10-50m).
2. The sonic responses for the sands and shales are averaged and the relative proportions of the two are estimated from the gamma ray log.
3. Average porosity values are calculated using [16] for the shales and [17] or [20] for the sands.
4. Average bulk density values are calculated using:

$$\rho_b = V_{cly}\left(\phi_{cly}\rho_{wat} + (1-\phi_{cly})\rho_{cly}\right) + V_{qtz}\left(\phi_{qtz}\rho_{wat} + (1-\phi_{qtz})\rho_{qtz}\right) \quad [24]$$

where V_{cly} is the fraction of the interval that is clay; ϕ_{cly} is the shale porosity from [16]; ρ_{bcly} is the shale grain density; V_{qtz} is the fraction of the interval that is sand; ϕ_{qtz} is the sand porosity from [17]; and ρ_{bqtz}, is the sand grain density. Note that $V_{cly} + V_{qtz} = 1$.

5. s_{vi} is calculated for each of the intervals using [22] with Δt as a variable and not a fixed value.
6. s_v is calculated by using [23] and linear interpolation is used to calculate values of s_v within individual intervals.

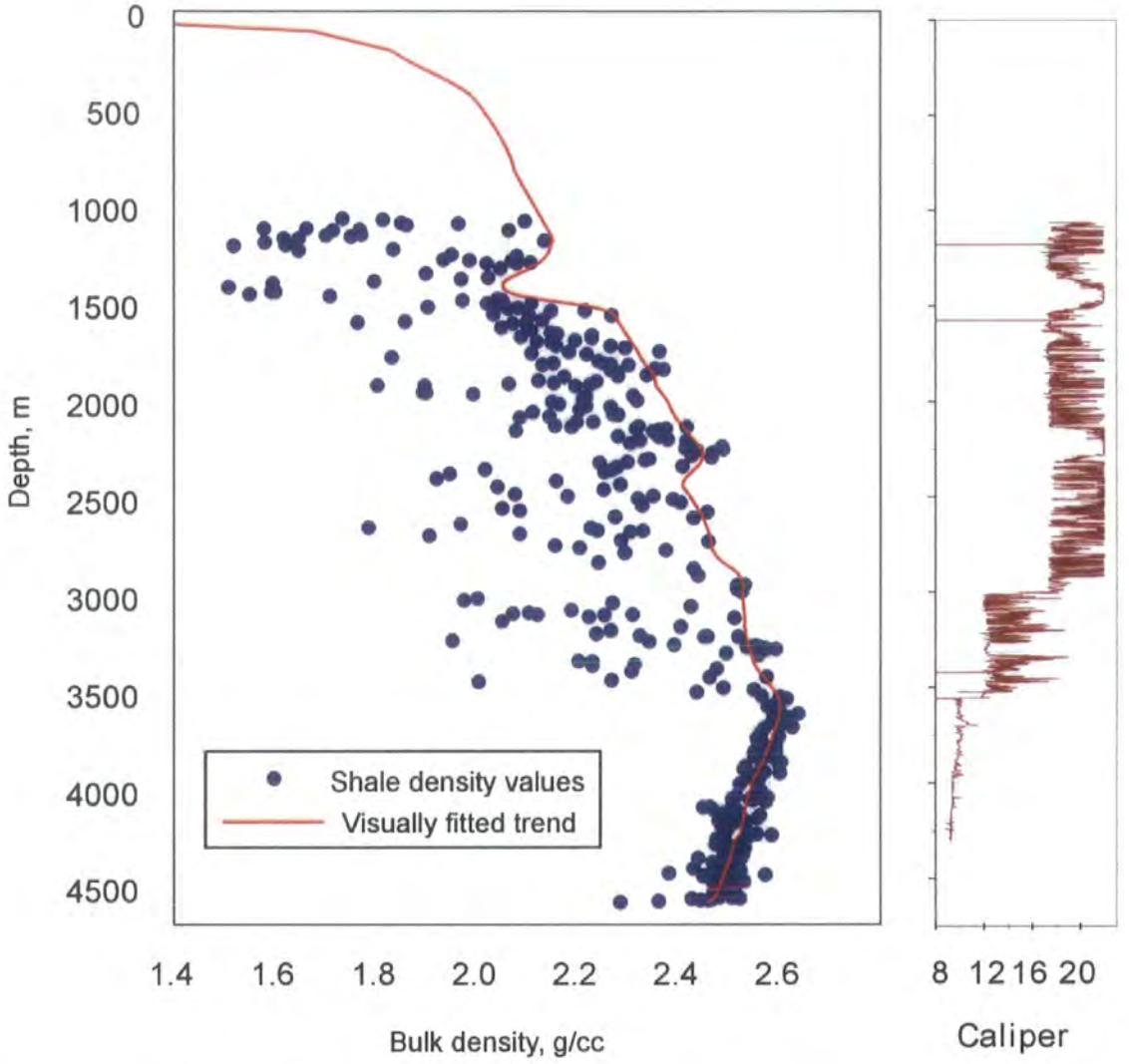

Figure 2.6: Density log and caliper log values vs depth for Well G showing the effects of borehole damage. Also shown is a curve visually fitted over the density values used to calculate the lithostatic stress values.

2.2.3.3 Horizontal and mean stress.

In the type of basins used in this study (extensional/strike-slip dominated), the minimum principal stress tends to be horizontal, at least above 2.5km. It is denoted by the symbol s_h and is the parameter measured during leak off tests (section 2.1.1.6). In most wells, LOTs are only performed when casing is set, prior to drilling deeper into the section. The result is that data are limited to casing setting depths. In this study, there are only 10 LOT values above 2.5km. There are no data in the shallow section of four of the wells. Because there are so few data points, it was decided to use a published relationship to derive s_h, rather than attempt to construct a new one with such poor constraints. Thus s_h was calculated using [25] taken from Breckels and van Eekelen (1982):

$$s_h = 16.6Z^{1.145} + 0.49\left(p_p - p_{hyd}\right), \qquad [25]$$

where the units of s_h, p_p and the hydrostatic pressure, p_{hyd}, are megapascals and Z is the depth in kilometres. The form of [25] is based upon the analysis of over 300 LOT values from the Gulf Coast by Breckels and van Eekelen (1982). In the same study, the authors adapted the Gulf Coast relationship and adapted it to fit a smaller dataset from offshore Brunei (Figure 2.7) to yield [25].

At this stage of the analysis, p_p in the shales is not known so an assumption is made that all the sediments are normally pressured, resulting in p_p- p_{hyd}= 0, and S_h is a function of depth only:

$$s_h = 16.6Z^{1.145} \qquad [26]$$

The mean stress (assuming normal pore pressures) is normally calculated using:

$$s_m = \frac{1}{3}\left(s_v + s_h + s_H\right), \qquad [27]$$

with s_h and s_H being the minimum and maximum horizontal stresses, respectively. As no data was available which could constrain the relationship between s_h and s_H in the subsurface, it was assumed, in this study, that the two horizontal stresses are of equal magnitude and could be calculated using [25] from Breckels and van Eekelen (1982). Justification for the choice of using [25] comes from the fact that in the wells studied, available leak-off test data and information from drilling reports on mud weights which appear to induce hydraulic fracture are consistent with [25], as shown in Figure 2.7.

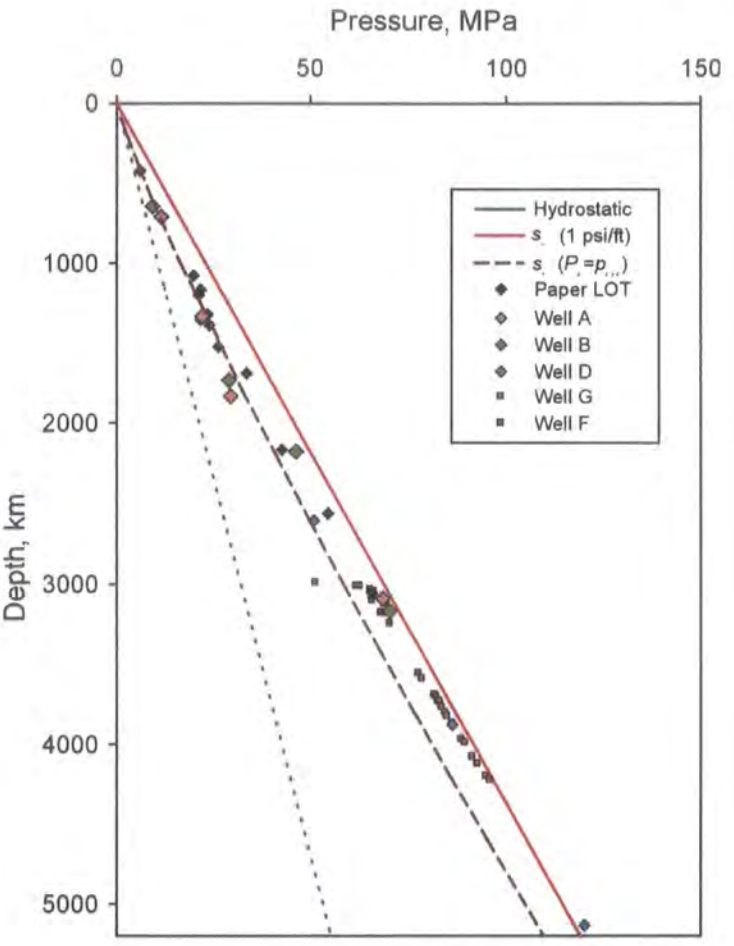

Figure 2.7 LOT values from Breckels and van Eekelen (1982) represented by solid black diamonds (paper LOT), plotted together with horizontal stress values calculated using [25] (dashed line), LOT values from wells A, B & D (shaded diamonds) and formation integrity test results from wells F and G (shaded squares). Dotted and solid lines represent hydrostatic pressure and lithostatic stress respectively.

The plot shows the LOT values from offshore Brunei (Breckels and van Eekelen, 1982, Figure 8) together with the horizontal stress values calculated using [25] and the LOT values used in this study. Hydrostatic pressure was calculated using a brine density of 1.03g/cc and lithostatic stress was calculated using a gradient of 1psi/ft. LOT values from Breckels and van Eekelen (1982) which were taken in underpressured reservoirs have been excluded from Figure 2.7.

Breckels and van Eekelen (1982) gave two other empirical relationships based on observed data for the Gulf of Mexico and Venezuela. The empirical relationship for Brunei was chosen because the tectonic regime is similar to that in the SE Asia basins where the studied wells are located. The limitations of using such a formula are discussed in section 6.2.

2.2.3.4 Hydrostatic effective stress

The effective stress is the difference between the normal stress, s, and the pore pressure, p_p, as given by [1]. Due to low permeability, it is not possible to measure the pore pressure in mudrocks. The calculation of pore pressure from mudrock porosity relies instead on plotting the porosity data against "hydrostatic effective stress" (σ_{hyd}) (section 2.3). This parameter is defined as the effective stress assuming that the pore pressures are hydrostatic:

$$\sigma_{hyd} = s_{hyd} - p_{hyd} \quad [28]$$

Previous studies have used a relationship between porosity and vertical effective stress to calculate pore pressures (section 1.5). Where a vertical effective stress approach is used section 2.4.2, the vertical hydrostatic effective stress can be calculated using:

$$\sigma_{vhyd} = s_v - p_{hyd} \quad [29]$$

where σ_{vhyd} is the vertical hydrostatic effective stress, s_v is calculated as described in section 2.2.3.2 and p_{hyd} is calculated using [1].

As Goulty (1998) and workers in the field of soil mechanics (Jones 1996; Burland 1990) have pointed out, porosity should be related to the mean effective stress, σ_m, rather than to the vertical effective stress (section 1.5). The mean effective stress is defined as the difference between the mean stress, s_m (see [27]), and the pore pressure p_p:

$$\sigma_m = s_m - p_p, \quad [30]$$

Once again, as p_p in the shales is not known, hydrostatic mean effective stress is calculated on the assumption that the pore pressures are hydrostatic:

$$\sigma_{mhyd} = s_{mhyd} - p_{hyd}, \quad [31]$$

where σ_{mhyd} is the mean hydrostatic effective stress, s_{mhyd} is calculated using [27] and p_{hyd} is calculated using [8]. Where fluid compositional data was not available, a brine density of 1.03g/cc (representative of standard marine conditions in the region, Ismail Che Mat Zin, pers. comm.) was used in the calculation of hydrostatic pressure.

2.3 Pore pressure calculation from void ratio vs. effective stress analysis

This section describes how data are selected from the wireline logs, plotted and used to calculate pore pressures. The full procedure is summarised in Figure 2.8. Although this section describes the methodology applied to porosity data derived from the wireline logs, the same procedure is carried out where a different source is used (e.g., use of seismic velocity data to calculate pore pressures in section 4.4.1.2).

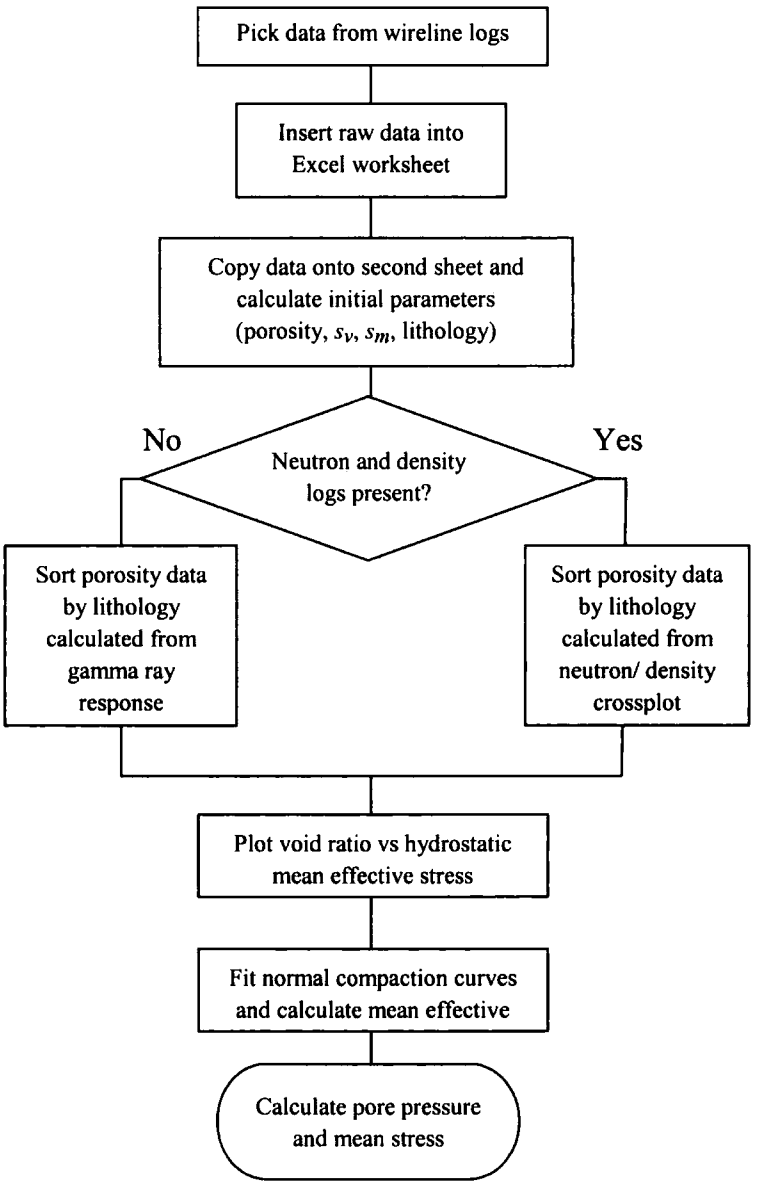

Figure 2.8: Procedure for pressure calculation from porosity data.

2.3.1 Picking data from the wireline logs

Data were supplied in two formats for analysis in this study, paper copies of composite logs where data had to be read off and typed in manually, and digital logs which can be analysed using well log analysis packages, and the raw values can be selected directly from the log file.

2.3.1.1 Picking data from paper composite logs

For wells A-C (Chapter 3) paper copies of the composite logs were supplied for the pressure analysis. The format of the log plot is shown in Figure 2.9, and generally focuses on the gamma ray, caliper, sonic and resistivity information, with lithology and stratigraphic data plotted in the margins. The example shown is representative of the log format used for the analysis of Well B, with the inclusion of neutron and density log printouts.

Points marked with an X on the log plot represent values which are selected for inclusion in the pressure analysis. Values are selected from the log where the gamma response indicates that

a) The unit is shale;
b) The values of each of the log responses conform to the limits set out in section 2.2.1, (i.e., the caliper log is not indicating caving or the neutron and density values are not anomalously high);
c) That there are no adverse comments in the well report indicating that the log response is due, for example, to the presence of a micaceous sandstone rather than shale. For example, an interval may have a gamma ray response indicative of shale lithology, the sonic and density logs show little response, but the neutron log shows a decrease in porosity which would not be expected if there were an increase in the clay fraction. This example shows the value of having the neutron and density logs for help with discrimination of data values where the elevated gamma response is not due to shales. Where these logs are not supplied, the lithological comments on the composite printout and in the well report have to be relied on more heavily.

Ideally, data are picked from intervals of the log where the responses of all the tools are constant as shown at 3039m depth (Figure 2.9). Often however, the shale beds are less than 5m thick which means that values can only be selected from peaks.

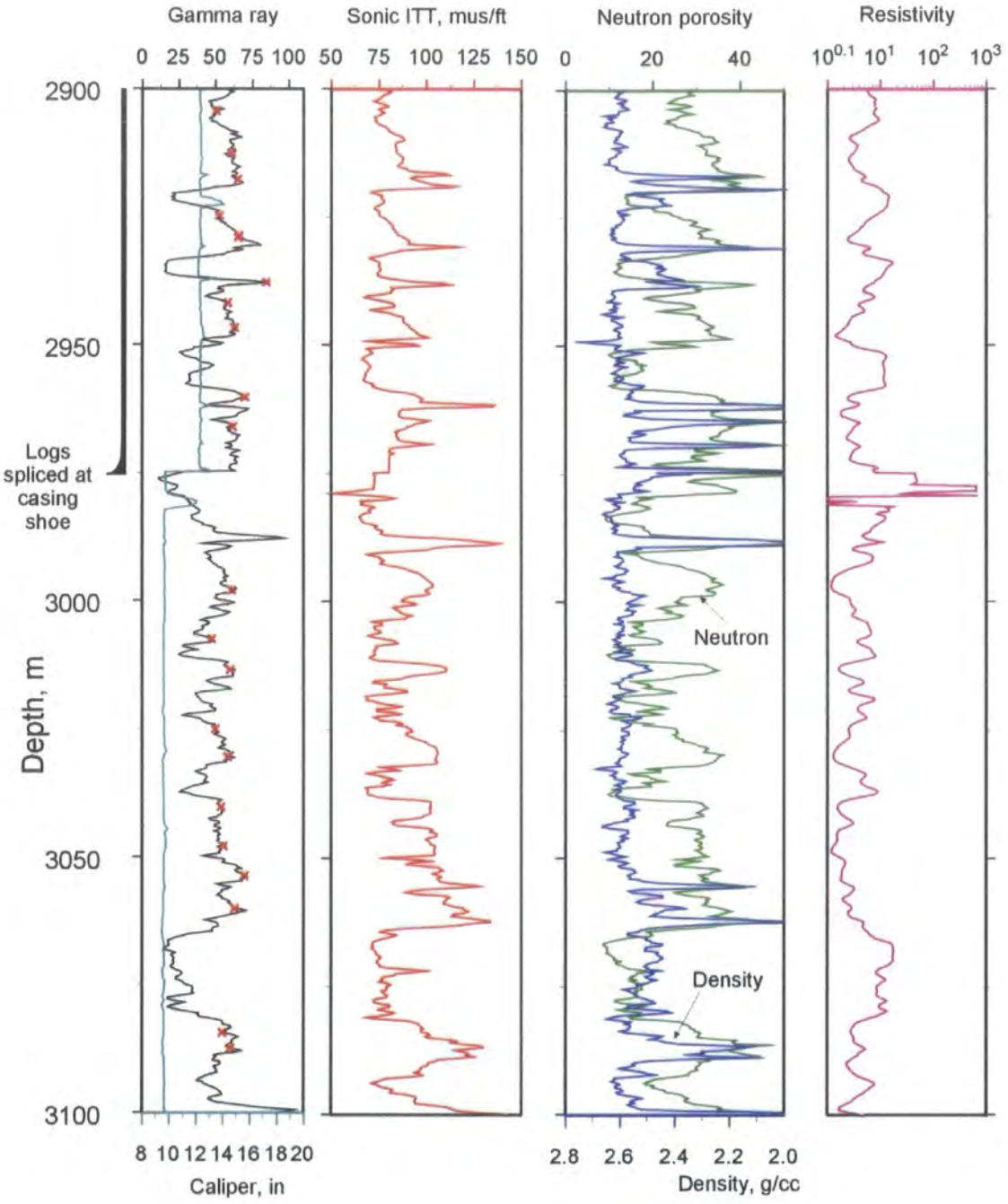

Figure 2.9: Log plot showing gamma ray, caliper, sonic, neutron, density and resistivity curves used in the pressure analysis. Points for inclusion in the analysis are marked with an X.

Where values are selected from peaks, a consistency of response between the gamma, sonic and resistivity response (gamma and neutron if available) is looked for, and very high sonic values which could be due to spiking are avoided.

It can be seen that across the interval of 200m shown, there are only 20 data points selected, even though the gamma response indicates a high proportion of shale in the section. The reason for the low picking density is generally due to the printer resolution of the composite log plots supplied. Figure 2.9 is printed out using maximum resolution of the printer to show the log values normally selected for inclusion in the analysis. In reality, the lines which represent the log values tend to be thicker and less clear than those shown. This difference in resolution limits the accuracy of visually reading values off the plot. Consequently more than one data point is seldom picked from the same 5m interval.

2.3.1.2 Picking data from digital format logs.

For wells D-G (Chapters 4-5) the wireline log data were supplied in digital format, as opposed to the paper copies of the composite logs described in the preceding section. The advantages of using this data format are:

1. The actual values recorded by the logging tool are available for analysis, as opposed to reading values off a printout, a process which can introduce errors.
2. Plots can be configured to suit the scale required for analysis rather than being restricted to the default scale of the composite log. This means that more detailed analysis can be carried out on particular zones of interest. It also means that far more data points can be accurately picked from the well compared to the method described in the preceding section.
3. Extra plots can be constructed so that different parameters can be viewed at the picking stage. For example, one parameter can be shaded by a second value as shown in Figure 2.10 where porosity and resistivity responses are shaded by the clay fraction computed using a neutron density cross plot (section 2.2.1.3). This type of plot can help visualise the effect of borehole conditions on the wireline log responses and how different parameters such as porosity and lithology interact.

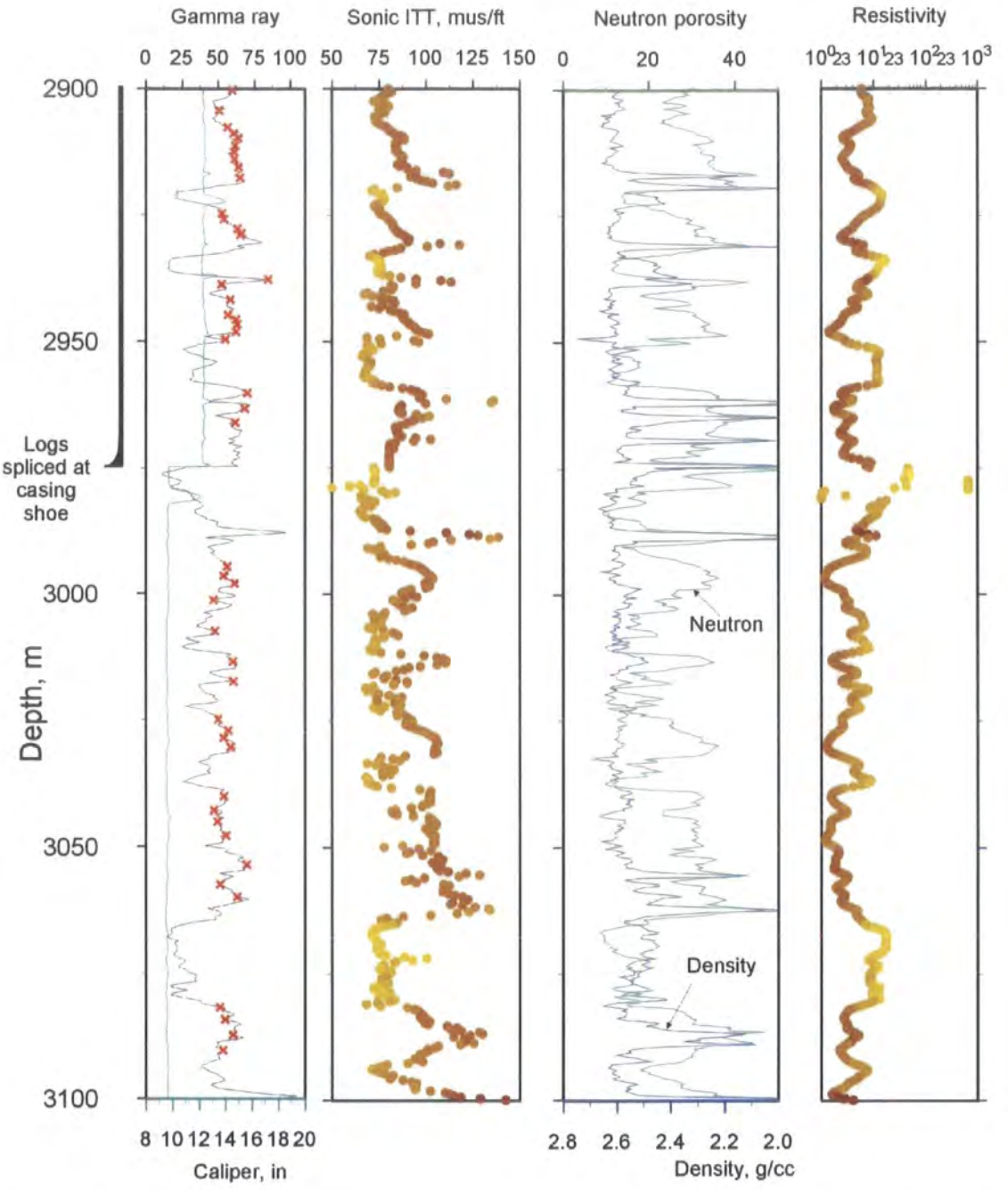

Figure 2.10: Log plot showing gamma ray, caliper, sonic, neutron, density and resistivity curves used in the pressure analysis of wells in digital format. The sonic and resistivity curves are shaded for clay fraction. Points for inclusion in the analysis are marked with an X.

4. Cross plots can be constructed using Terra Station well logging analysis package, and used to discriminate more effectively against intervals of the well dominated by unsuitable lithologies (Rider, 1999).

The key differences between the two formats is that bad data can be more effectively identified, and the number/density of data points that can be accurately picked from a well is enhanced (Wells A-C have on average 160 data points (50 points per km) whilst wells D-G average 350 points (85 per km)).

Well F is slightly different from the other wells in this study in that the caliper and resistivity logs indicate good borehole conditions for almost the entire borehole. Consequently, several data points are selected from nearly all the mudrock intervals throughout the well (Figure 2.10) with the result that there are ~850 data points picked from the well (212 points per km). The implications of higher volumes of data for pressure calculation are discussed in sections 5.3.4 and 5.5. and 6.3.1

2.3.2 Subdividing, plotting data and fitting normal compaction curves.

Once the raw values have been picked from the well log, they are sorted into groups of similar lithology and plotted to calculate values of effective stress (Figure 2.8). Manipulation of the data takes place within Microsoft Excel software package using the following steps:

1. The raw data picked from the well log are input into a worksheet.
2. For each point, the parameters used in the analysis (void ratio, s_v, lithology etc.) are calculated.
3. Data points plus parameters are copied onto a separate sheet.
4. The copied data are sorted into groups of similar lithologies:
   a) Where there is no neutron or density data, or the values have been affected by borehole conditions, data are sorted by lithology computed from the gamma ray response as detailed in section 2.2.1.2. The subdivision of shales into groups of similar gamma response is illustrated for wells E-G in Figure 2.1, (section 2.2.1.2). Subdivision was carried out in a similar way for the other wells in this study.
   b) If the neutron and density logs are available and the log quality is good, the data are sorted into groups of similar clay fraction calculated by cross

plotting the neutron and density values (section 2.2.1.3). The data are subdivided empirically into four or five groups of the form: clay =50-60%, clay =60-70% ...etc. following the same procedure for the subdivision of gamma ray groups (section 2.2.1.3).

Once the data have been sorted, void ratios for the individual lithology groups are plotted against hydrostatic mean effective stress calculated using [31] (section 2.2.3.4) Figure 2.11. The plot highlights a single group of shales with void ratios which for the first 15MPa decrease with increasing hydrostatic mean effective stress, indicative of normal compaction (section 1.6). Below 15MPa effective stress, the void ratios of the highlighted group and the other shales are seen to increase and remain elevated down to 26MPa hydrostatic mean effective stress indicating that the shales are in fact overpressured.

In order to calculate the effective stress of the shales, normal compaction curves are fitted to bound the data points where the pore pressure is judged to be hydrostatic for each class of lithology (Figure 2.11). The example shown in Figure 2.11 indicates that only two or three of the data points are normally pressured. The form of the fitted curve was guided by similar data from the other lithological groups (Figure 2.12)

The form of the compaction curves chosen in this study is derived from Burland (1990) section 1.5, where porosity, represented by void ratio, is related to mean effective stress.

$$\log_{10}\left(\frac{\sigma_m}{\sigma_{100}}\right) = \frac{e_{100} - e}{C_c}, \qquad [7]$$

where σ_m is the mean effective stress in units of kilopascals; σ_{100} is some reference value of effective stress, taken here to be 100 kPa; e_{100} is the void ratio at 100 kPa effective stress; and C_c is the compaction coefficient. The values of the sediment mechanical parameters, e_{100} and C_c, depend on the lithology. The sediment mechanical parameters are obtained from the slope and intercept of the best-fit straight line on plotting the log of mean (or vertical) effective stress against the void ratio for these data points. They define the normal compaction curves for each class of lithology through [2] or [7]. The values of e_{100} and C_c will, in general, be different

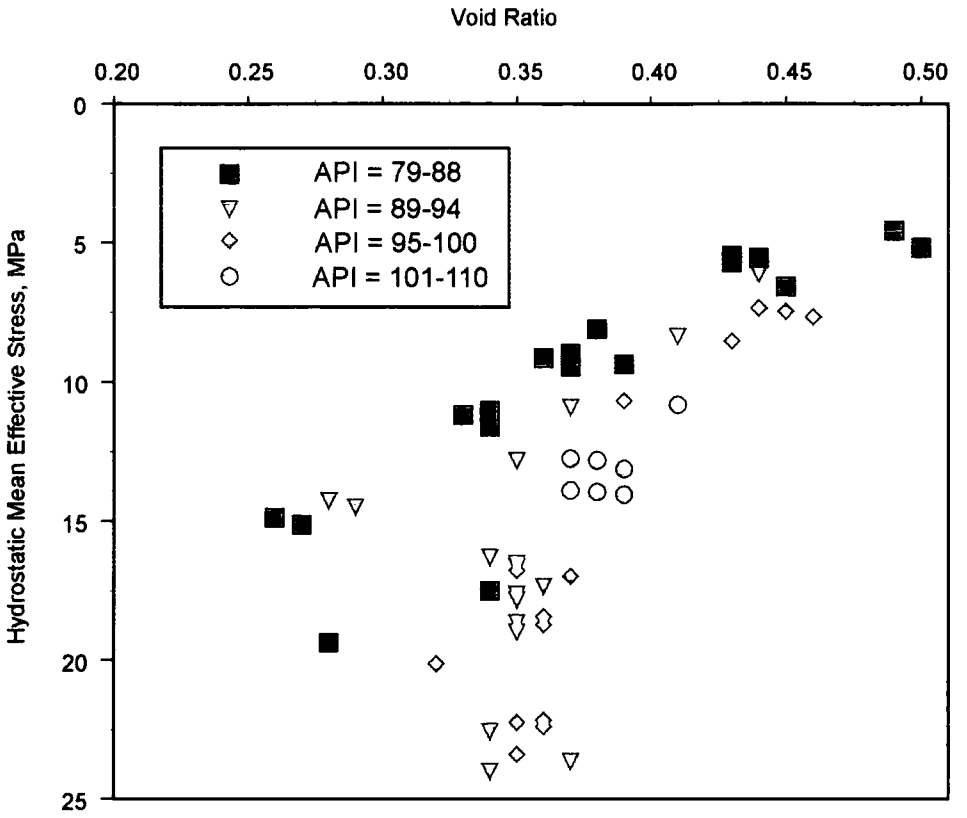

Figure 2.11: Void ratio vs hydrostatic mean effective stress for shales from Well B highlighting a single lithology group.

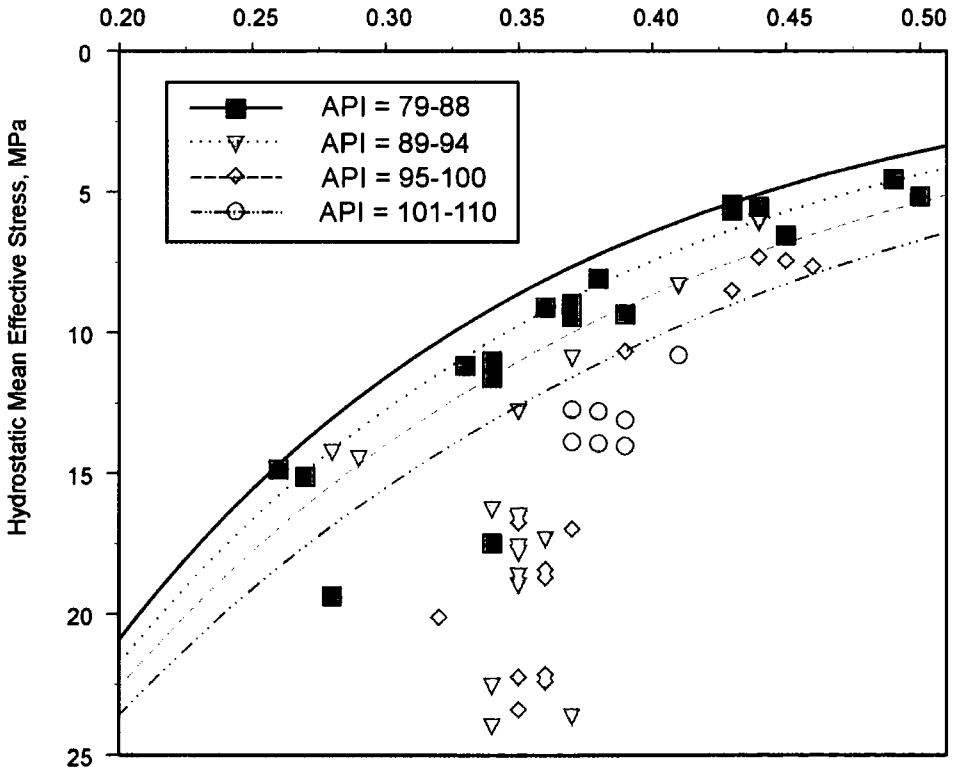

Figure 2.12: Normal compaction curves fitted to bound the void ratio values judged to represent normally compacted shales.

when porosity is related to the mean effective stress instead of to the vertical effective stress. A discussion of the choice of compaction curves is found in section 6.3.2.

As can be seen in Figure 2.12, the curve is fitted to bound the minimum values of void ratio for a given effective stress in the shallow "normally pressured" part of the section. This method of fitting curves implies that the minimum values of porosity are normally pressured, and all values to the right of the curve are overpressured. The method described here was derived from the analysis of Wells A-C (Chapter 3).

Application of the same approach to wells D-G, where there are larger numbers of data, was carried out in the same way but encountered some difficulties introduced by an increase in the amount of scatter as a result of picking a larger data-set. Further discussion of this point is found in section 5.3.4, and in section 6.3.1.

Once the normal compaction curves have been fitted to the porosity values, the effective stress in kilopascals can be derived from values of void ratio computed from the wireline response using [32] (a rearrangement of [7]):

$$\sigma_m = 10^{\left((e_{100}-e)/C_c\right)}.\sigma_{100}, \qquad [32]$$

where, e_{100} and C_c here are sediment mechanical parameters derived for each of the lithological groups and e is the void ratio value derived from the wireline response.

2.3.3 Calculation of pore pressure and mean stress values.

The final step in the pressure analysis involves conversion of the effective stress values derived from [32] into values of pore pressure and mean stress. This procedure is simple if the void ratios have been plotted and curves fitted using vertical hydrostatic effective stress. If this approach is taken, then the pore pressure is simply equal to the lithostatic stress minus the effective stress calculated from the curve fitting. This methodology is applied to Wells A-C simply for comparison with the mean effective stress approach (despite the fact that poroelasticity theory indicates that mean and not vertical stress controls porosity loss (section 1.5)).

Calculation of pore pressure from mean effective stress is somewhat more complicated by the fact that horizontal, and therefore, mean stress is influenced by pore pressure (or vice/versa) and an increase in overpressure is observed to be accompanied by an increase in the horizontal stress (Grauls, 1999; Engelder and Fisher, 1994; Breckels and van Eekelen, 1982). The method presented below

represents the first documented attempt to estimate both pore pressure and mean stress values from porosity and effective stress analysis.

If the pore pressure were simply calculated by subtracting the effective stress from the value of hydrostatic mean stress calculated from [26] and [27], then a circular calculation would ensue where, because the pore pressure was elevated, the mean stress had to be higher which, in turn increases the pore pressure, and therefore the mean stress again.

The new approach proposed in this study instead separates the pore pressure from the horizontal stress in the pressure calculation by assuming $s_h = s_H$ and eliminating s_h between [25], [27] and [30]. The resulting equation may be approximated, without introducing significant error, as

$$p_p = 16.6D^{1.145} + 0.5s_v - 0.5p_{hyd} - 1.5\sigma_m \qquad [33]$$

To calculate the mean stress therefore, the value of pore pressure computed in [33] is added to the value of mean stress computed from the void ratio Vs mean effective stress plot [32].

The normal compaction curves define the maximum possible value of mean (or vertical) effective stress corresponding to each mudrock void ratio value. We should note that if the mudrocks are overpressured in part due to some unloading mechanism, the actual values of mean effective stress will be smaller. The estimates of maximum mean (or vertical) effective stress in the mudrocks are converted to estimates of the minimum pore pressure present, and are compared to the direct measurements of pore pressure in the sands.

Chapter 3: Case study of three wells

"My guide bent down and seized in either fist
a clod of the stinking dirt that festered there
and flung them down the gullet of the beast"
Dante Aligheri

3.1 Introduction

This chapter presents the results of pressure analysis of three wells from different basins in SE Asia. The wireline log data for all three of the wells were supplied in paper format only. Pore pressures calculated for the three wells from void ratio and hydrostatic mean effective stress analysis are compared with the results of hydrostatic vertical effective stress, to test the validity of the two approaches.

3.2 Well A

3.2.1 Data sources

The data used in the pressure analysis of well A are taken from two main sources: the wireline log suite and the well report. Table 3.1 summarises the wireline log data available and shows how the different parameters used in the analysis were derived.

WIRELINE LOG	CALIPER	GAMMA RAY	SONIC	RESISTIVITY (SHALLOW AND DEEP)
Units	inches	API	μs/ft	Ωm
Interval	700-3,599m (2,297-11,808ft)			
Use of Data	Discriminant	Lithology	Porosity	Discriminant
		Overburden		

Table 3.1 Summary of wireline log data used in the pressure analysis of Well A.

3.2.2 Lithology

Analysis of the natural gamma ray profile together with cuttings and core descriptions yielded the simplified lithological column represented in Figure 3.1. The sequence drilled in Well A comprises sands and shales deposited between the Early Oligocene and the present day, and has been subdivided as follows:

1. An Early Miocene to present day section extending down to 1,127m (3,700ft) comprising marine clays with thin interbedded sandstones (up to 30ft thick) deposited at a sedimentation rate of around 50m/My.
2. A thin Early Miocene section of lignite/coal layers interbedded with sand between 1,048 and 1,219m.
3. Early Miocene clays and thin sands between 1,219 and 1,493m (4,000 to 4,900 ft) deposited more rapidly at around 900m/My.

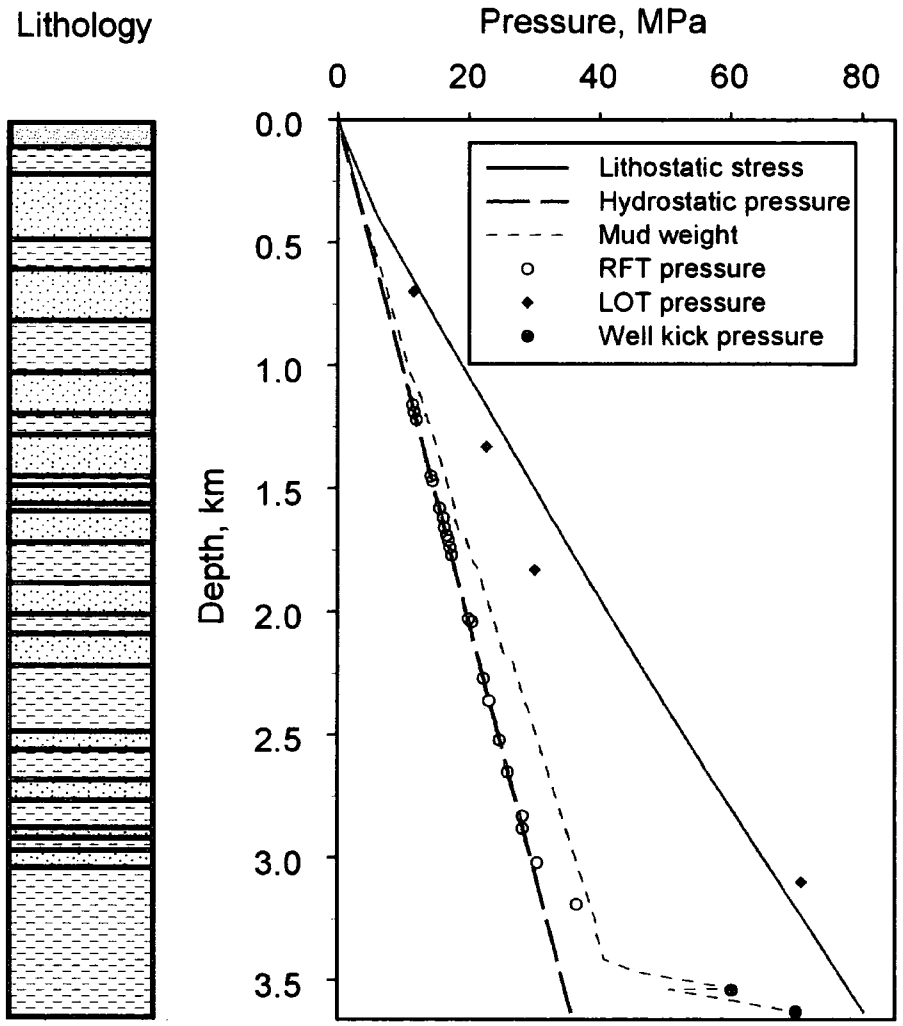

Figure 3.1 Simplified lithological column and pressure data for Well A.

4. A Late Oligocene section extending from 1,493 to 3,136m (4,900 to 10,300ft) deposited at a sedimentation rate of around 700m/My. This interval is dominated by arenaceous units up to 45m (150ft) thick down to 1,965m (6,450ft) with thinner interbedded sands and silty shales over the rest of the interval.
5. Early Oligocene sediments between 3,136 and 3,319m (10,291 and 10,891ft) dominantly argillaceous with many thin sandstone and siltstone intervals. Sands are between 1 and 3m in thickness, described in the report as very well cemented. Sedimentation rates for this unit are lower at around 85m/My.
6. Early Oligocene sediments between 3,319 and TD at 3,636m (10,891 and 11,929ft) deposited at around 50m/My. The sediments comprise very fine grained sands and siltstones with few thin (2m) coal/carbonaceous layers interbedded with shale units varying from 1-10m thick. Drilling was halted in this unit after two well kicks were experienced and increasing the mudweight to 1.99g/cc (16.6lb/gal).

3.2.3 Pressure data

The actual pressure data derived from the well (RFT and LOT pressure measurements, and the mudweights used during drilling) are plotted against depth with the computed values of hydrostatic and lithostatic pressure (Figure 3.1).

The direct measurements of actual pressure taken down the well using the RFT tool show that the pore pressures in the sands are hydrostatic above 3,000m. The profile defined by the RFT measurements represents formation fluids with densities equivalent to 1.0g/cc (~8.4lb/gal), i.e., very low salinity formation waters. Below 3,000m there is a rapid transition into substantial overpressures defined by two RFT measurements and two well kicks before drilling was halted.

The mudweight profile in Figure 3.1 shows that for the upper section despite normal pressures in the sands, slightly higher pressures were used to balance conditions in the mudrocks. Mudweights equivalent to between 1.07 and 1.24g/cc (9 and 10.4lb/gal) were used down to 3,352m (11,000ft). Between 3,352 and 3,517m (11,000 and 11,540ft) mudweights were increased to 1.45g/cc (12lb/gal) in response to increased gas shows in the muds prior to the first of two pressure kicks. The first kick at 3,535m depth required an increase of the mudweight up to 1.73g/cc

(14.5lb/gal), and was followed by a second kick at 3,634m which necessitated a further increase up to 1.99g/cc (16.6lb/gal) prior to drilling being stopped.

Whilst drilling, four leak off tests were performed the results of which are shown in Figure 3.1. The first three points lie below the values of lithostatic stress computed from the sonic and gamma ray logs. The fourth leak off pressure exceeds the lithostatic stress. The interpretation of this final LOT value is that somewhere between 1,800m and 3,000m the minimum horizontal stress has increased from being lower than to at least equal to the vertical stress in the highly overpressured section. It is possible that an elevated LOT pressure could be recorded if the sediments were well consolidated and had a high tensile strength. Shale cutting density measurements and the wireline log responses at the same depth indicate however, that the sediments are high porosity, poorly consolidated sediments (supporting the interpretation of an increase in the minimum horizontal stress relevant to the vertical stress in the overpressured section).

3.2.4 Pressure analysis

For the mudrock pressure analysis, individual mudrock beds were picked on the basis of the caliper, gamma and sonic log responses. Figure 3.2 shows that there is an overall increase with depth in the natural gamma log response. As the gamma ray tool is used to identify shale lithology in this well, the change in response limits the depth intervals for comparison of shales of similar mineralogy to less than 2,000 m.

In Figure 3.3, the void ratios of individual mudrock beds calculated using [20] are plotted against the hydrostatic mean effective stress, calculated using [31].

The sudden nature of the pressure increases together with variable permeability of the drilled formations below 3,000m caused problems with balancing the pressures and resulted in poor borehole conditions for the last logging run. Consequently, for this interval average values for mudrocks over depth intervals of 20-50m are plotted. Also plotted on Figure 3.3 are the normal compaction curves for each class of lithology. These compaction curves were determined empirically by fitting bounding curves to those data points for which the pore pressure is assumed to be hydrostatic. Points which plot to the right of the compaction curves for their respective lithologies indicate overpressure.

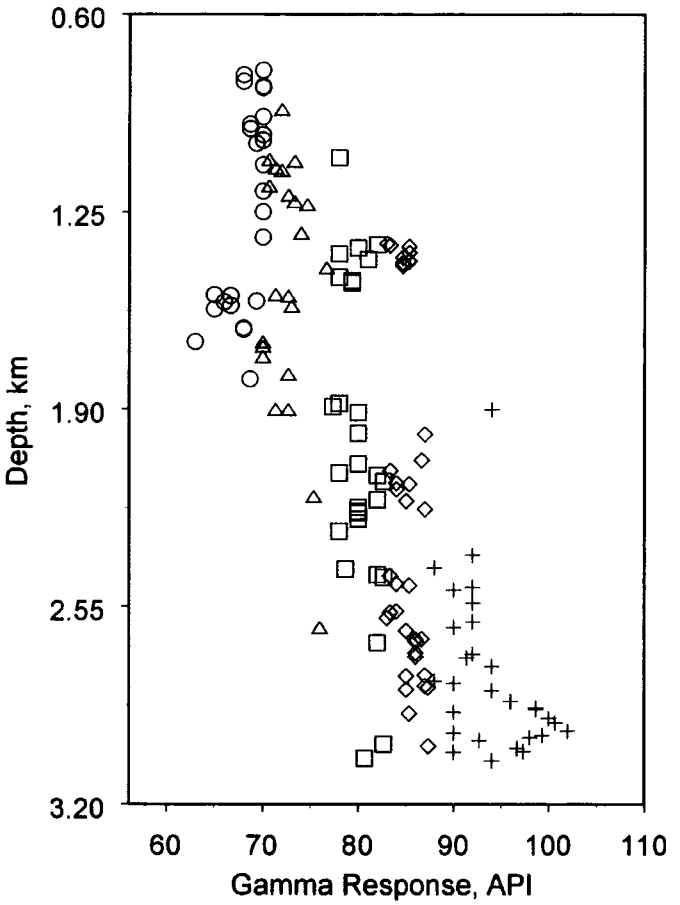

Figure 3.2 Gamma ray values for shales from Well A versus depth in km. The varying symbols represent the subdivision of the shales into different lithological groups based on their API response.

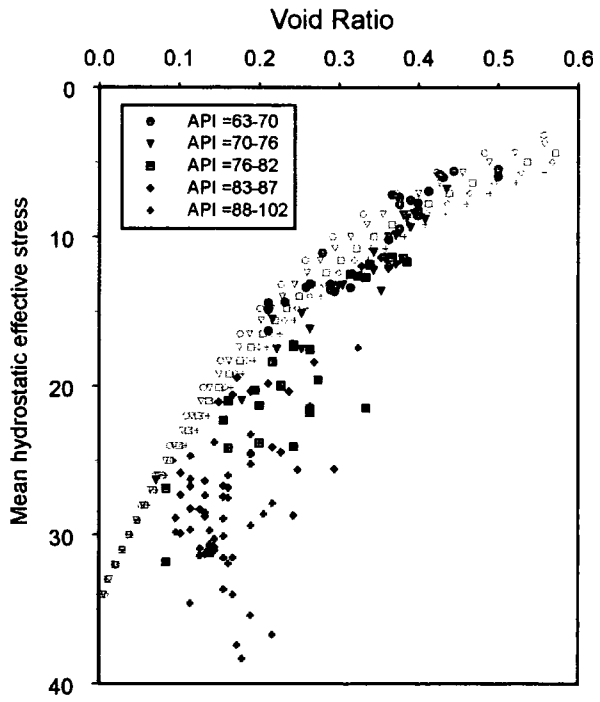

Figure 3.3 Void ratios vs hydrostatic mean effective stress for shales from Well A subdivided on the basis of gamma ray response. Also plotted are the derived normal compaction curves.

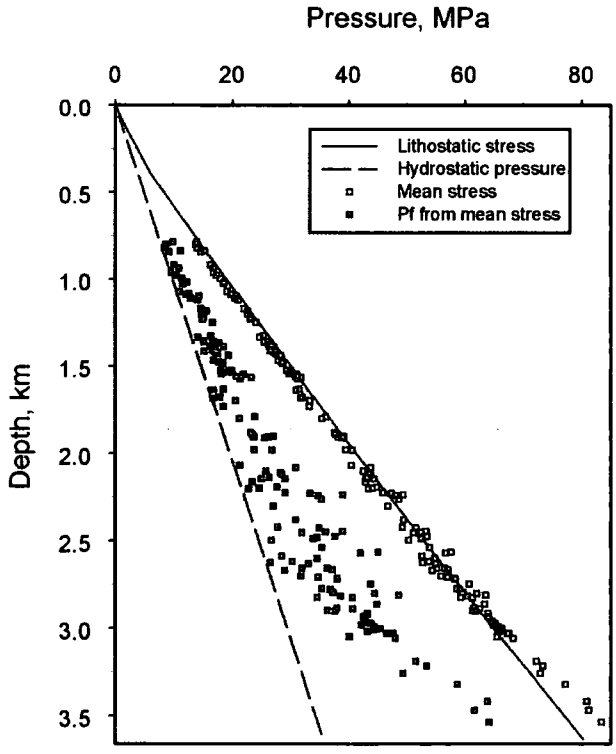

Figure 3.4 Computed pore pressures from mean and vertical effective stress for Well A plotted along with hydrostatic pressure and lithostatic stress profiles as well as direct pore pressure measurements made in the borehole.

The void ratio values were projected vertically on to the respective compaction curves in Figure 3.3 to estimate the values of mean effective stress present in the mudrocks. The mean effective stress values were then converted into estimated pore pressures using [34], and plotted together with the direct measurements of pore pressure in Figure 3.4. The direct measurements of pore pressure above 3,000m indicate that the pore fluid in the sand bodies is hydrostatically pressured. It can now be seen that the less permeable units below 1,000m depth are overpressured. At around 3,500m depth, the two pressure kicks encountered in the sands can now be seen to lie on the trend of pore pressure increase estimated in the mudrocks (Figure 3.4).

The simplest interpretation of the derived pore pressure profile in Figure 3.4 is that overpressure was generated entirely by disequilibrium compaction with a shallow fluid retention depth, consistent with a rapid rate of deposition. Overpressure in the more permeable sand bodies above 3,000m has been allowed to dissipate by lateral and vertical fluid flow. This conclusion is supported by the fact that the formation fluids in the sands appear to have anomalously low salinities considering the majority of sedimentation took place in a marine environment. The implication of the fresh formation fluids is that extensive lateral and vertical connectivity in the sands has allowed communication with a terrestrial fluid source, during which time the pressures were allowed to reach hydrostatic values. The pressure dissipation in the sands has allowed some of the shale porosities to decrease towards normally compacted values, but the less permeable mudrocks not directly adjacent to a sands have not fully de-watered and so are retaining pore pressures greater than hydrostatic. At the base of the section the argillaceous interval between 3,136 and 3,319m appears to be acting as a vertical permeability barrier to the higher overpressures encountered in the sands approaching TD at 3,636m. The thin sands in the argillaceous interval are very well cemented and have very low porosities as shown in Figure 3.5. Below this interval, elevated sand porosities between 13 and 20% are found, implying that disequilibrium compaction has maintained higher porosities in the hydraulically isolated sand bodies as well as the adjacent shales. A more detailed sedimentological study may reveal the link between the depositional environment and the hydraulic isolation of the reservoir units inferred from the elevated pore pressure and porosities

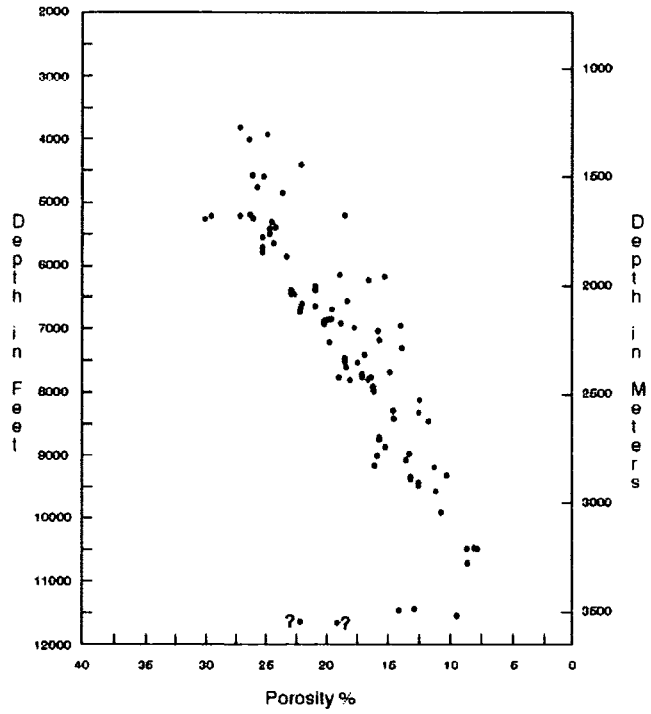

Figure 3.5 Sand porosity plotted against depth for Well A.

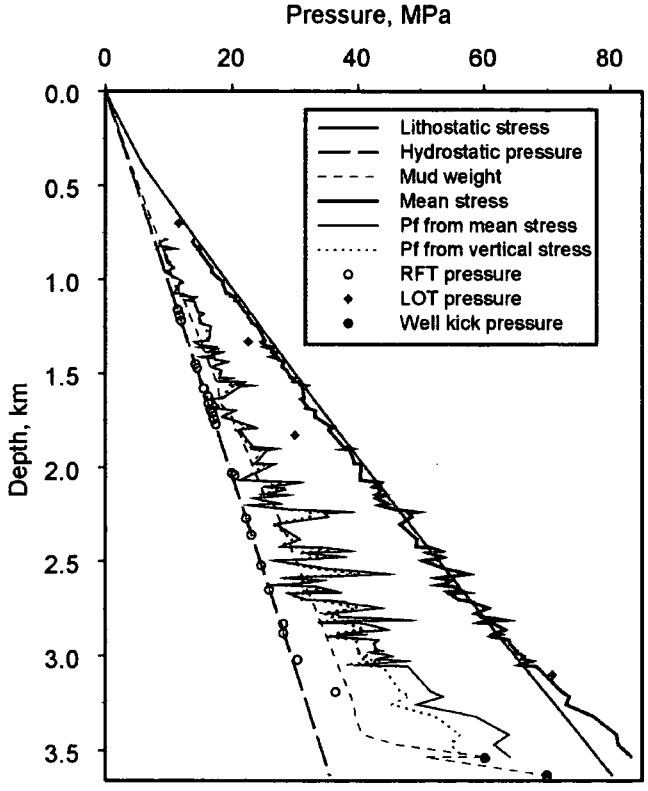

Figure 3.6 Comparison of pressure estimates from mean and vertical effective stress analysis for Well A

in the sands at the base of the well. Due to lack of sedimentological data however, analysis of this type was beyond the scope of the study.

The mudrock void ratio analysis was repeated using the vertical effective stress, and the resulting pore pressure estimates are compared in Figure 3.6. As one would expect, there is no significant difference above 2,500m, where the pore pressures are close to hydrostatic, but they are markedly different in the overpressured section below 3000m. The pore pressures estimated using the vertical effective stress are lower, and significantly less than the two pressure kicks around 3,500 m.

3.3 Well B

3.3.1 Data sources

Data used in the pressure analysis comes from three main sources: the wireline log suite, the well report and previously published studies by Grauls and Cassignol (1993), Bour and Lerche (1994), Grauls (1996) and Grauls (1998). Table 3.2 summarises the wireline log data available and shows how the different parameters used in the analysis were derived.

WIRELINE LOG	CALIPER	GAMMA RAY	SONIC	RESISTIVITY ILD/MSFL	DENSITY	NEUTRON
Units	inches	API	µs/ft	Ωm	g/cc	%
Interval	220-3,210m				645-3,210m	
Use of data	Disc.	Lithology	Porosity	Disc.	Lithology / Porosity	
		Overburden			Overburden	

Table 3.2 Summary of wireline log data used in the pressure analysis of Well B. Disc. = discriminant

3.3.2 Lithology

Analysis of the natural gamma ray profile together cuttings and core descriptions yields a simplified lithological column represented in Figure 3.7. The sequence drilled in Well B comprises sands and shales deposited between the Upper Miocene and the present day. Grauls and Cassignol (1993) subdivide the section into three intervals as follows:

1. An Upper Pliocene section from the seabed down to 1,800m (5,905ft) consisting of sands and shales rapidly deposited at rates exceeding 700m/My.

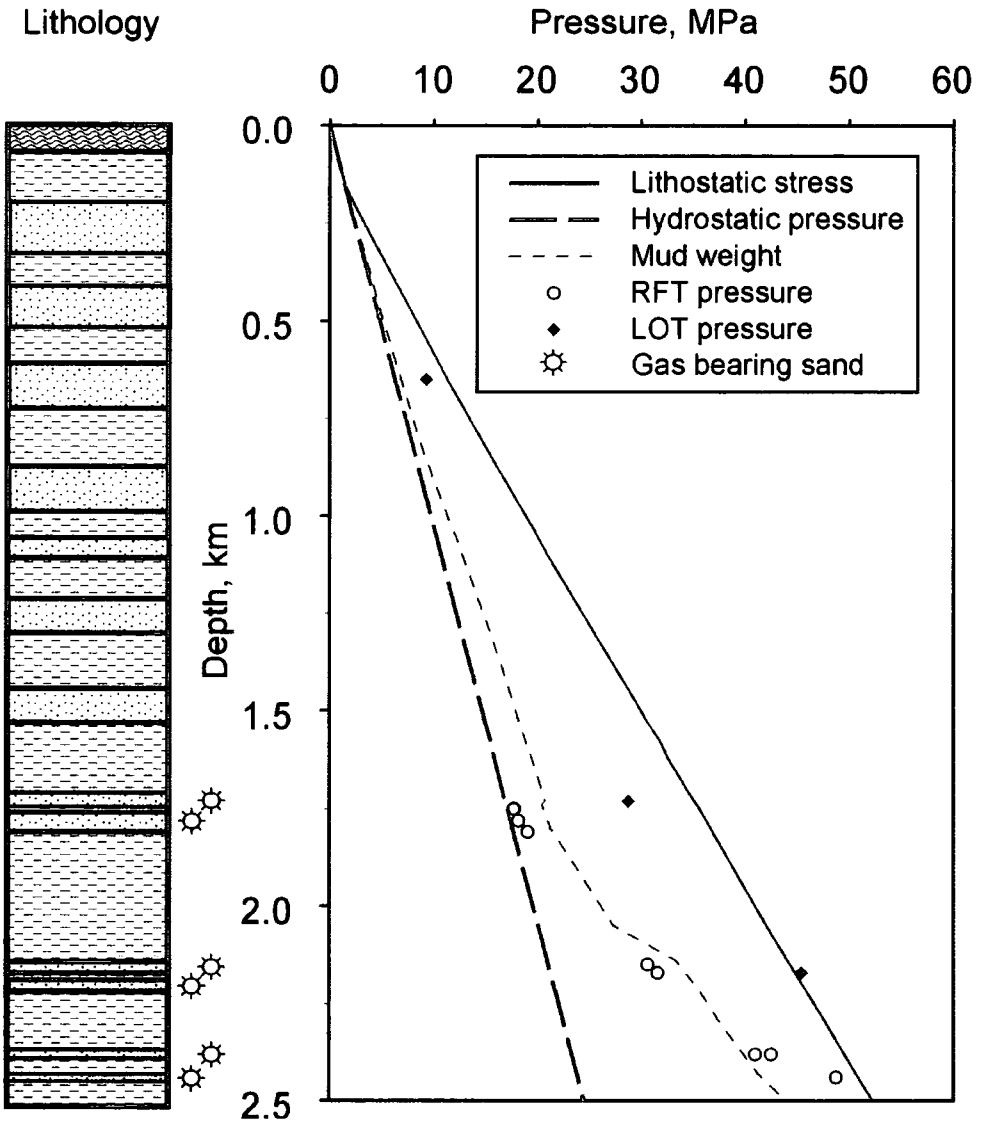

Figure 3.7 Simplified lithological column and pressure data for Well B.

2. A Lower Pliocene section from 1,800 to 2,500m (5,905 and 8,202ft) comprising a thick mudrock section with a few thin sand bodies.
3. An Upper Miocene section from 2,500 to 3,400m (8,202 to 11,154ft) characterised by fissile shales with thin low matrix permeability sand bodies.

Also from the well report, information on the nature of the clay types is available. For the section drilled, sampled clays consisted of 1/3 chlorite, 1/3 illite and 1/3 kaolinite, irrespective of depth. Also, all of the shales appear to have low Total Organic Carbon (TOC) value of less than 5%[1], low smectite and low carbonate content. This observation justifies the use of Issler's (1992) mudrock velocity to porosity transform [16].

3.3.3 Pressure data

The actual pressure data derived from the well (RFT and LOT pressure measurements and the mudweights used during drilling) are plotted against depth with the computed values of hydrostatic and lithostatic pressure (Figure 3.7).

The direct measurements of actual pressure taken down the well using the RFT tool are consistent with the interpretation from the well that pore pressures in the sands above 1,800m are hydrostatic. Below 1,800m the section becomes far more argillaceous and sand bodies where direct measurements can be made are scarcer. The next pressure measurements between 2,150 and 2,170m depth reveal that the amount of overpressure has increased to 10MPa, or an equivalent mudweight value of 1.5g/cc (12.5lb/gal) from its onset at 1,800m.

The next three pressure measurements were not reported in the publication by Grauls and Cassignol (1993) but, after further examination of the well report, they have been included in this study. The first two points, at 2,377.5 and 2,378m, were originally discarded on the grounds of seal failure and described as not stabilised. Swarbrick (pers. comm.) has pointed out that although the pressures are not fully stabilised, the values may still represent minimum estimates of the actual formation pressures assuming the test is not supercharged (the fact that the pressure has not stabilised indicates that the formation has a low permeability and is therefore more likely to be supercharged, Corbett, pers. comm.). The third measurement at 2,440m

[1] TOC values of greater than 5% are considered good source rocks, a prolific source rock such as the Kimmeridge Clay in the North Sea has TOC values averaging around 8% with some intervals with values greater than 20% (Ahmadi, pers. comm.)

was originally discarded on the basis of supercharging (Section 2.1.1.1). The measured value had not stabilised, but still exceeds the pressure exerted by the drilling muds at this depth and therefore must represent a minimum estimate of the pore fluid pressure in the sand body. These three additional points therefore represent a rapid increase in the amount of overpressure up to at least 2.1g/cc (17.6lb/gal) equivalent mud weight, or 25MPa overpressure. The third value is within 2MPa of the computed lithostatic pressure at the same depth and must represent conditions very close to fracture pressure.

The next pressure measurements at 2,900 and 2,980m represent similar values of equivalent mudweight between 2.0 and 2.1g/cc (16.8 and 17.6lb/gal) as the amount of overpressure has increased to 30MPa. No further RFT measurements were made between 2,980m and TD at 3,400m due to the dearth of sands over this interval.

The mudweight profile seen in Figure 3.7 follows approximately the interpolated RFT pressure measurements with the exception of the three originally discarded values. As for well A, the section above 1,800m, where the reservoir units are normally pressured, is drilled with slightly higher pressure muds to balance any overpressure in the shale units. Below 1,800m the mudweight is increased steadily with depth until 2,900m, where values of 2.1g/cc coincide with the measured pressure values. Between 2,900 and TD at 3,400m the mudweight is maintained at between 1.95 and 2.1g/cc.

Four leak off tests were performed during the drilling of well B the three of which are shown in Figure 3.7. As in the case of well A, the estimates of minimum stress in the upper, normally pressured section are lower than the computed lithostatic pressures. Below the transition to overpressure at 1,800m the minimum horizontal stress appears to have increased from less than to equal to or greater than the vertical stress value.

3.3.4 Pressure analysis

The void ratios for individual mudrock beds are plotted against hydrostatic mean effective stress down to 25MPa, equivalent to a depth of 2,540m (Figure 3.8). The plot shows minimum void ratios at around 14MPa effective stress (equivalent to ~1,760m). At this depth the mudrocks are interbedded with sands, which have presumably allowed any overpressure to dissipate by lateral and vertical interconnectivity. All the void ratio values for the mudrock beds were projected up to the normal compaction curves for their respective lithologies to estimate the mean

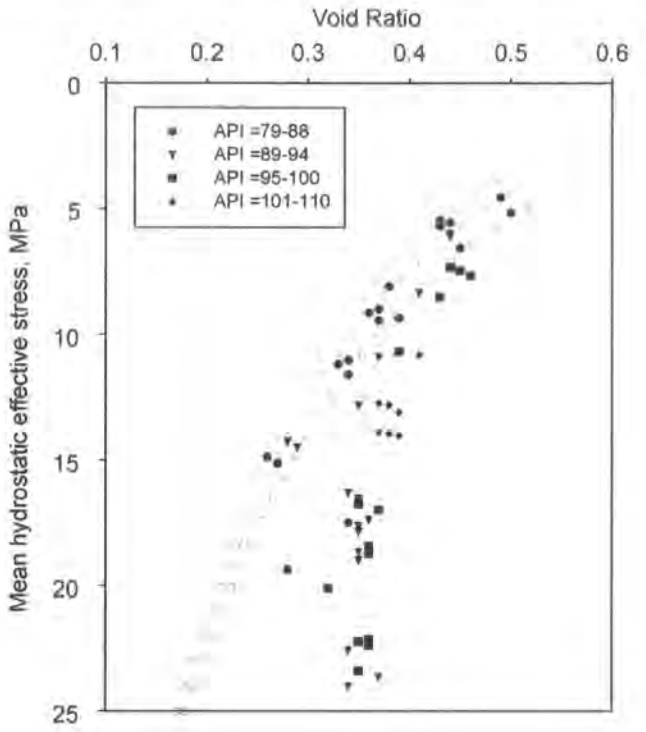

Figure 3.8 Void ratios vs hydrostatic mean effective stress for shales from Well B subdivided on the basis of gamma ray response. Also plotted are the derived normal compaction curves.

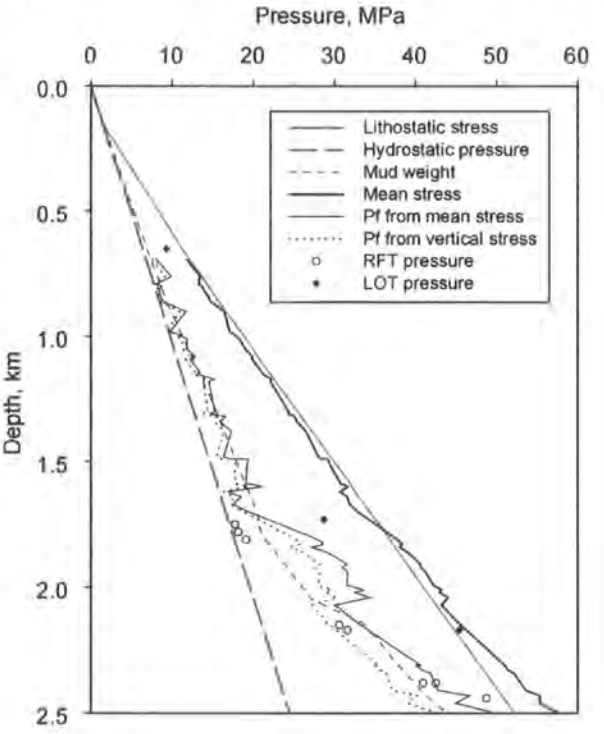

Figure 3.9 Computed pore pressures from mean and vertical effective stress for Well B plotted along with hydrostatic pressure and lithostatic stress profiles as well as direct pore pressure measurements made in the borehole.

effective stress. The corresponding estimates of the pore pressures present are plotted in Figure 3.9 together with the direct measurements of pore pressure taken in the sands and the mudweights used to drill the well.

For the first 1,800m, the shales appear to be overpressured by between 1 and 5MPa. These values agree well with the mudweight pressures used whilst drilling the well. Below 1,800m, as the section changes from more arenaceous units to a thick section of mudrocks, there is a jump in the computed pore pressures to approaching 10MPa overpressure. Pressures continue to increase rapidly below this depth until, at 2,500m, the pressures are within 4MPa of the derived lithostatic pressure. Figure 3.8 indicates that all units in the thick mudrock section stopped compacting at a porosity corresponding to an effective stress of 10MPa or a fluid retention depth of about 1,400m. These results are consistent with the straightforward explanation that principally the process of disequilibrium compaction controls the mudrock porosity profile below 1,800m.

When the analysis was carried out using the vertical effective stress, the estimated pore pressures below 1,800m were lower (Figure 3.9). They are around 10MPa less than the RFT measurements in sands around 2,400m depth, which would appear to imply that unloading has taken place in these sands after compaction. Grauls (1998) reports similar results and suggests that the extra pressure has come from "over-charging" of the reservoir units with higher pressure gas and condensate from deeper in the section. This conclusion implies that formation fluids deeper in the section (here hydrocarbons) have exceeded the pressure required to allow a fault system to be conductive permitting fluids to migrate along the fault plane and into shallower, lower pressure reservoir units. Providing there is a considerable enough volume of fluid available to migrate into the shallower reservoirs, the amount of overpressure will either increase up to the pressure value required to hold the fault system open, or increase until the fracture pressure of the sealing lithology is exceeded. If the volume of fluid deeper in section is not great enough, then the amount of fluid available to migrate along the fracture system may not be enough to maintain pressures in the shallower reservoirs at or near to the fracture pressure. The pressure will instead be controlled by the rate of fluid supply and the rate of fluid escape through the sealing lithology.

Evidence for Grauls' conclusion is taken from analysis of the hydrocarbons in the sand bodies and the maturity of the encasing mudrocks, which at 2,500m depth are not mature enough to have produced the encountered condensates.

The results of the mean effective stress analysis show that all of the pressures above 2,500m are due to the combination of rapid burial and extremely low permeability. There is no need to invoke extra pressure due to hydrocarbon migration as proposed by Grauls (1998).

The explanation for the difference between the calculated values of mean stress, and the LOT value at ~1,750m can be explained by the fact that the LOT was performed in a normally-pressured silty interval. The mean stress calculations are derived from overpressured shales separated by at least 30m from the LOT interval. It is to be expected that the lower horizontal stress values will be encountered in the normally pressured interval (Engelder and Fischer, 1994; Breckels and van Eekelen, 1982).

Below 2,500m the log character changes considerably as the well encounters what is interpreted as a zone of open fractures (Grauls and Cassignol, 1993)). Figure 3.10 shows the mudrock porosities calculated from the sonic, density and neutron logs for the interval from 690-3,200m. As previously described, the section from 690 to 1,800m shows decreasing void ratios with depth for all the logs representing the normally pressured section. Between 1,800 and 2,500m the sonic-derived void ratio remains roughly constant whilst the neutron-and-density derived porosities show an initial increase corresponding to the change to more clay rich mudrocks and a slight decrease across the interval. Below 2,500m the sonic interval transit times (ITT) increase rapidly to 190μs/ft (values supported by the check shot survey and the seismic velocity analysis (Grauls and Cassignol, 1993). The sonic interval transit times are extremely high for shales at this depth and are outside the range of values used by Issler (1992) to derive the sonic ITT to porosity transform. Nevertheless, the sonic-computed porosities are plotted in Figure 3.10 for graphical correlation with the responses of the other logs, even though it is unlikely that the values plotted represent the actual porosities of the mudrocks.

The same data as Figure 3.10 for the interval between 2,500 and 3,200m are plotted in Figure 3.11. The plot reveals a series of porosity "spikes". The sonic

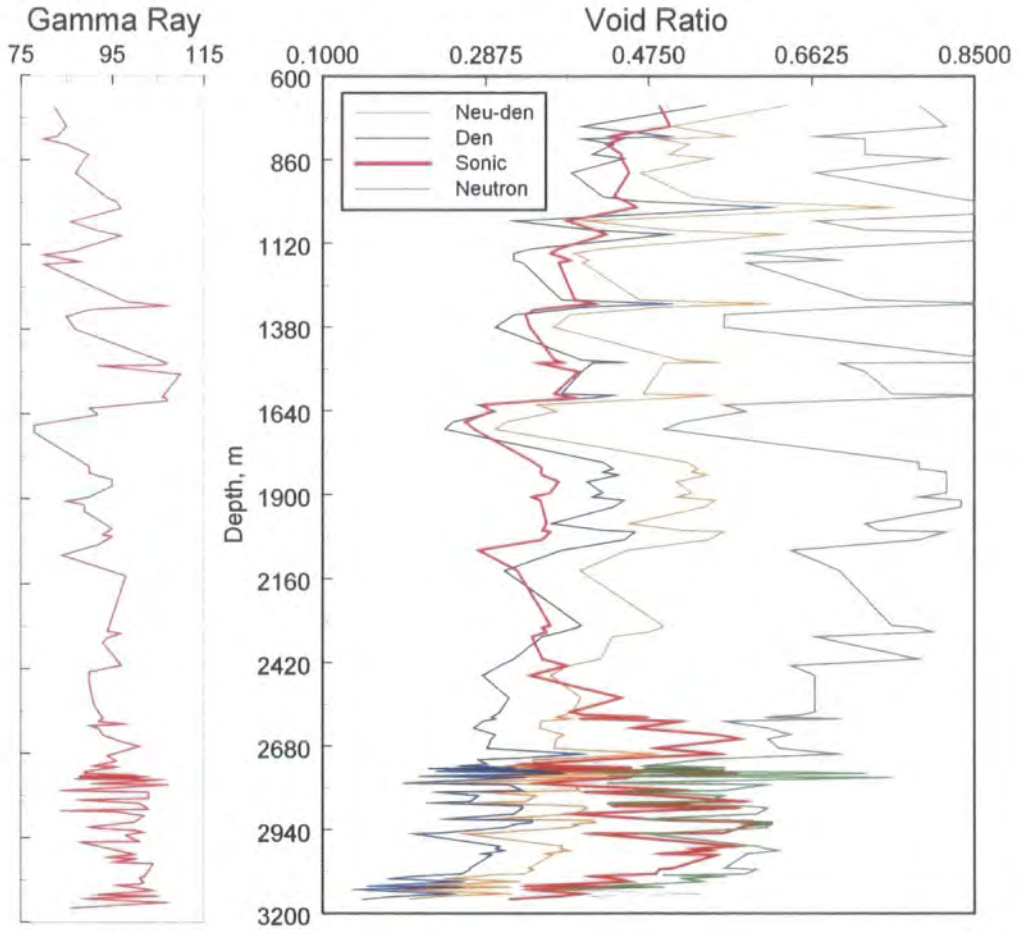

Figure 3.10 Mudrock void ratio values for Well B calculated from sonic, density and neutron log responses, plotted against depth in metres.

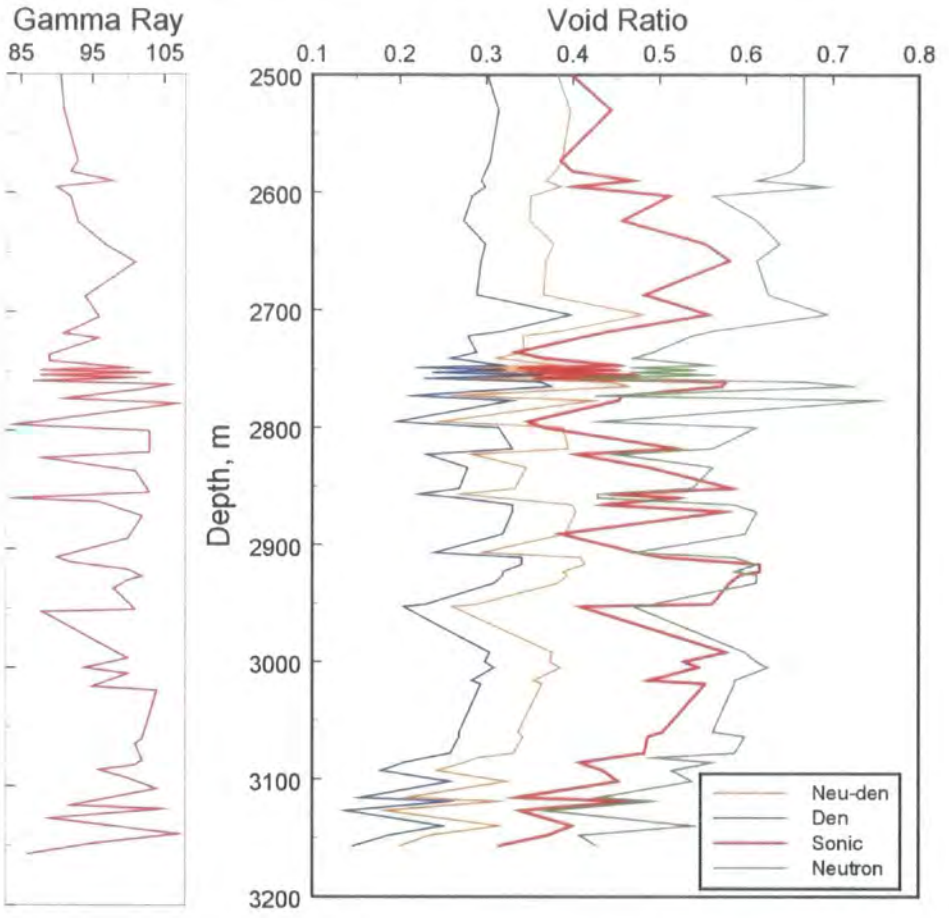

Figure 3.11 Mudrock porosity values for Well B calculated from sonic, density and neutron log responses, plotted against depth for the interval between 2,500-3200m

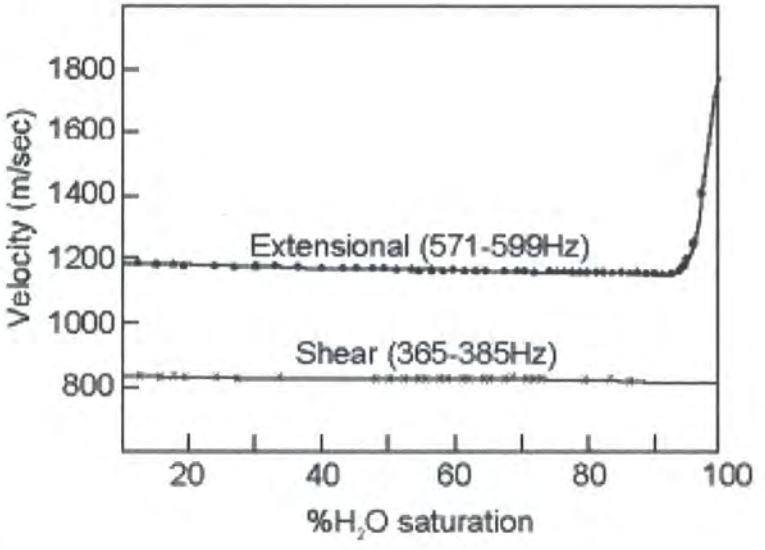

Figure 3.12 Influence of the presence of gas in the pore spaces on compressional sonic travel time.

derived values across this interval show an average increase up to a maximum porosity of 0.36 at 2,910m before the response decreases to values of around 0.25 at 3,150m. The neutron and density logs show increases corresponding to each of the spikes observed on the sonic logs; however, for both logs there is an overall decrease in the average response across the interval. Each of the spikes corresponds to an increase in the gamma ray response and clay fraction interpreted from the neutron and density logs.

The interpretation of the response is that the well bore encountered a zone of sub-horizontal hydraulic micro-cracks / fractures generated by the extremely high fluid pressures filled with between 5 and 10% gas. The nature of these fractures is as proposed for the following reasons:

- The sonic log response below 2,500m records values of interval transit time up to a maximum of 265μs/ft at 2,970m depth. High values may sometimes be due to cycle skipping where the sonic tool fails to pick the first arrival (due to weak signal) and instead picks a later arrival. However, there is a consistent response across the interval between 2,820 and 3,000m where interval transit times are around 190μs/ft. These very high long transit times represent velocities around 5,000ft/s, similar to the velocity of seismic waves in water alone.
- The fact that the neutron and density logs do not show responses of the same order of magnitude as the sonic logs implies that very large open fractures do not exist. Instead, the small observed increase in porosity accompanying each of the sonic peaks represents a zone of open micro-fractures.

This hypothesis still does not explain the extremely high sonic interval transit times. If the fractures are filled with 5-10% gas, however, then the pore fluid will be far more compressible, resulting in a significant increase in the sonic transit time compared to 100% water saturation (Figure 3.12). Only 5-10% gas in the fractures is proposed because larger amounts would result in a greater increase in the density-derived porosity, a decrease in the neutron porosity (not shown from Figure 3.12) and an increase in the resistivity.

The fractures are proposed to be sub-horizontal for three reasons:

1. The sonic log measures interval transit time parallel to the borehole axis, if fractures are sub-horizontal the transit time will be increased as sonic waves are forced to travel through the fractures (Figure 3.13). If the fractures were

sub-vertical then the sonic waves would be able to follow a faster path, which avoids the fractures (Figure 3.13).

2. The caliper log response shows no evidence of caving of the borehole associated with each of the interpreted fractures. If the fractures were aligned parallel to the borehole axis (i.e., sub vertically) then it would be more likely that sediment would be lost into the borehole than if the fractures were perpendicular to the borehole axis (Traugott, pers. comm.). Breakout and FMS data proposed by Grauls and Cassignol (1993) may help resolve this issue.
3. The single LOT value at ~2,200m and the computed values of mean stress for the undercompacted section above 2,500m (where the log response is normal) indicate that the minimum (and therefore the maximum) horizontal stress is equal to, if not greater than, the vertical stress. This observation is consistent with the presence of strike slip and thrust faults at depth in the region of the well (Grauls and Cassignol, 1993). Fractures will open normal to the orientation of the minimum stress, so they will be sub-horizontal if the minimum stress is vertical.

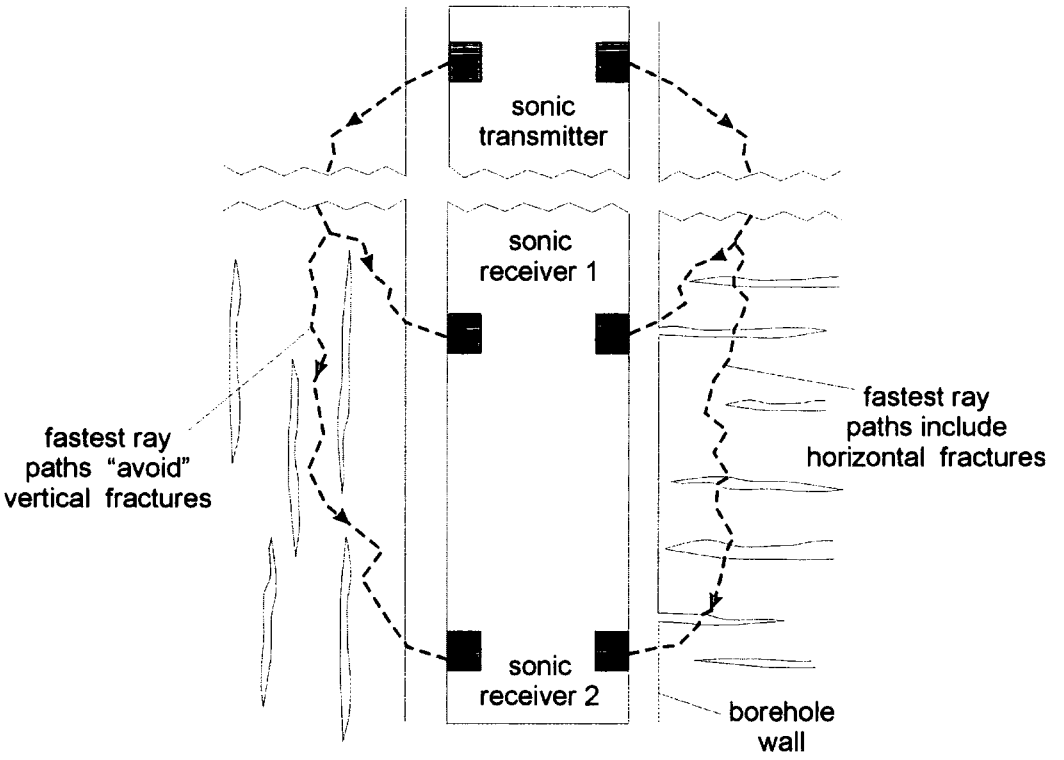

Figure 3.13 Influence of fracture orientation on sonic travel time

The conclusion of the analysis of Well B is that from the seabed down to 1,800m the pore pressures are near hydrostatic, as would be expected given the presence of numerous permeable reservoir units. Below 1,800m the pore pressure is dominantly controlled by disequilibrium compaction in the thick mudrock section. Fluid pressures increase very rapidly up to values within 1-2MPa of the lithostatic pressure at 2,500m and 7-10MPa below the calculated mean stress values. Below this depth the borehole is interpreted as encountering a zone of sub-horizontal hydraulic fractures. The origin of the extremely high pressures is probably principally due to disequilibrium compaction.

The origin of the microfractures below 2,500m can be explained if it assumed that it is valid to have minimum horizontal stress values up to 7MPa greater than the vertical stress (LOTs at 2,200 and 3,180m both exceed the corresponding values of vertical stress). Directly above the zone of fractures at 2,430m, the mean effective stress from the porosity is ~8MPa (s_m =55.3, s_h =57.6MPa), the pore pressure calculated using [33] is 46.5MPa giving a vertical effective stress of <5MPa (s_v=50.6MPa). A differential stress of around 7MPa (possibly greater as the well is drilled on a compressional anticline associated with a strike slip fault, so s_H will be greater than s_h) may be enough to induce sub-horizontal fracture opening in the mudrocks, without the pore pressure having to reach lithostatic stress values (Engelder, 1997). The microfractures may represent ephemeral migration pathways for hydrocarbons to travel vertically to the shallower reservoirs (Figure 3.7), alternatively if the fractures are continuously open, together with the sands, they may represent part of one reservoir system.

If horizontal stresses in excess of lithostatic required for fracture opening are not viable, another process which could explain the extra pressure required to fracture the formation is hydrocarbon generation/cracking (section 1.8.2.1). Gas is present in the reservoirs below 1.8km, and appears to be migrating along faults/fractures in the sediments (Grauls, 1999). If up to 5MPa overpressure is being generated by this process which is possible under realistic basin conditions (Swarbrick and Osborne, 1999), it could explain the presence of the fractures.

3.4 Well C

3.4.1 Data sources

The majority of the data used in the pressure analysis of Well C comes from the wireline log suite with some extra information taken from Yussof (1995). Table 3.3 summarises the wireline log data available and shows how the different parameters used in the analysis were derived.

WIRELINE LOG	GAMMA RAY	SONIC	SP	CONDUCTIVITY	DEEP INDUCTION
Units	API	μs/ft	mV	$\Omega m^2 m$	
Interval	300-2,626m (985-8,617ft)				
Parameter	Lithology	Porosity	Lithology / Discriminant		
	Overburden				

Table 3.3 Summary of wireline log data used in the pressure analysis of Well C.

3.4.2 Lithology

Analysis of the natural gamma ray profile together cuttings and core descriptions yields a simplified lithological column represented in Figure 3.14. The sequence drilled in Well C comprises sands and shales deposited between the Mid Oligocene and the present day and has been subdivided into six sections as follows:

1. A section of Plio-Pleistocene marine clays with scattered thin sandstones (averaging 15ft thick) from the seabed down to 694m (2,278ft) deposited at around 130m/My.
2. An unconformity representing a 6Ma period of uplift and erosion of the crest of the developing structure between the Middle Miocene and the Pliocene is encountered at 694m.
3. A section of Middle Miocene shales with interbedded sands averaging around 20ft thick and numerous coal intervals encountered between 694 and 1,443m (2,278 and 4,735ft). These sediments were deposited at around 115m/My.
4. More argillaceous sediments of Lower Miocene age from 1,443 to 1,672m (4,735 to 5,486ft). The sediments comprise mudrocks with scattered sand and siltstone units towards the top of the interval overlying a thick interval of lacustrine shales down to 2,025m (6,645ft).

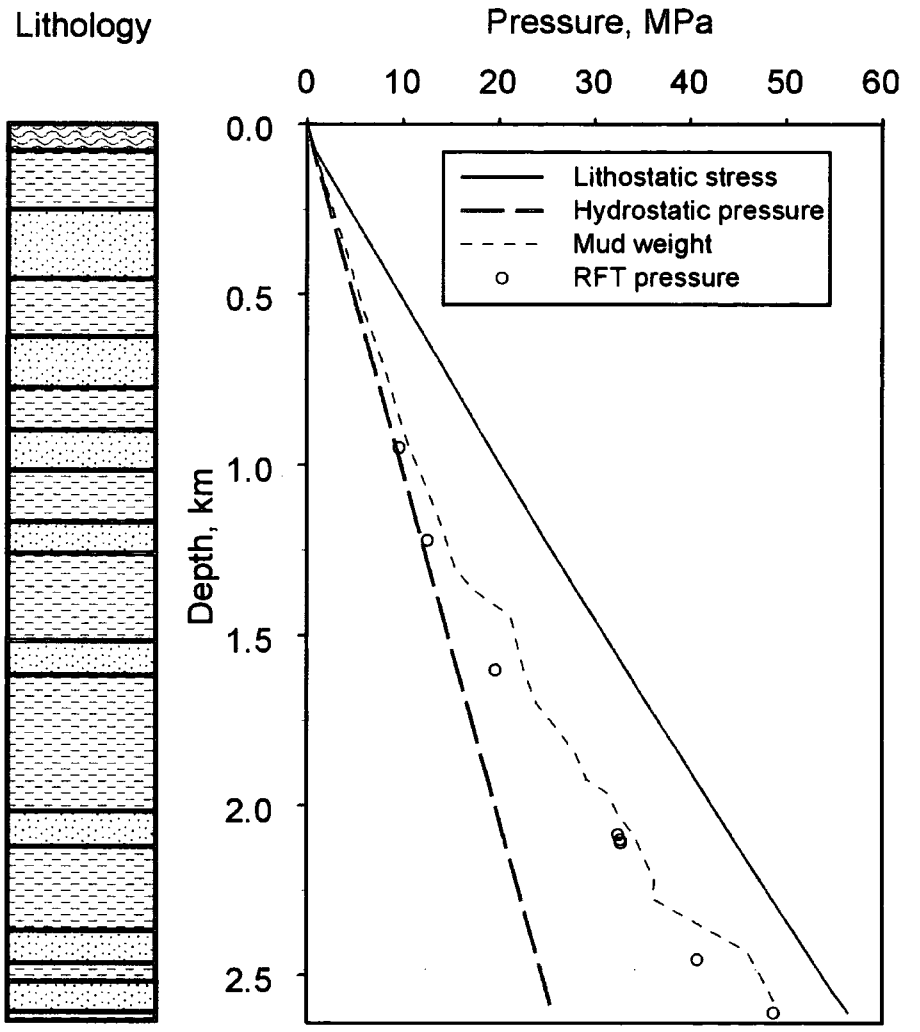

Figure 3.14 Simplified lithological column and pressure data for Well C.

5. A section of Lower Miocene sands between 2,025 and 2,273m. The sand units are up to 60ft thick, separated by thinner interbedded shales. Sedimentation rates average 50m/My for the last two intervals.
6. The final section penetrated comprises an Upper Oligocene section between 2,273 and TD at 2,626m (7,460 and 8,617ft). The sediments are argillaceous with scattered sand and silt horizons averaging 15ft, and up to a maximum of 50ft, in thickness. The bottom of this interval is not encountered so burial rates are not as well constrained as the previous units: a minimum estimate is 175m/My.

3.4.3 Pressure data

The actual pressure data derived from the well (FIT pressure measurements and the mudweights used during drilling) plotted against depth with the computed values of hydrostatic and lithostatic pressure, is shown in Figure 3.14. The direct measurements of actual pressure taken down the well using the Formation Interval Tester (FIT) tool (section 2.1.1.2) show that the pore pressures in the sands are hydrostatic above 1,200m. Below 1,200m measured overpressures steadily increase at a rate slightly greater than the rate of lithostatic increase until, at 2,610m, the overpressure reaches 23MPa equivalent to a mudweight of ~1.9g/cc (16lb/gal). Samples of the pore fluid taken from the well show the presence of gas and that the formation fluids are extremely fresh, as for Well A. Titration results show that the fluids have an average salinity of around 500ppm chloride, whereas a value of around 20,000ppm would be expected for seawater.

The mudweight profile seen Figure 3.14 shows that the pressures used whilst drilling the well follow the same trend as the formation pressure measurements detailed above. For the upper section, down to 1,200m, the mudweights used were slightly higher than the hydrostatic pressures measured in the reservoir intervals. Below 1,300m the mudweight was increased up to values of 1.5g/cc (12.5lb/gal) and the profile approximately follows the rate of lithostatic pressure increase down to 2,270km. The pressure below 2,270m is increased rapidly to 1.8g/cc (15lb/gal) at 2,350m; the remainder of the section down to TD at 2,610m was drilled with muds between 1.8 and 1.9g/cc (15 and 16lb/gal), the pressures used at the base coinciding with the final FIT test value.

Unfortunately, as no LOT pressure values were available for this well, relationship [25] derived from Breckels and van Eekelen (1982) had to be assumed in calculations of values of mean stress and could not be tested for validity. The good agreement found between the LOT pressure data from the other wells in this study and relationship [25] justifies its use in the calculation of pore pressures in this well.

3.4.4 Pressure analysis

The plot of void ratio against hydrostatic mean effective stress is shown in Figure 3.15. The pore pressures present in the mudrocks shown in Figure 3.16 were again estimated by projecting the void ratios up to the compaction curves for their respective lithologies. The computed pressure values exceed the mudweights used to drill the well by between 1 and 5MPa for the upper section down to 2,000m. The low permeability of the mudrocks allowed the well to be drilled with slightly underbalanced muds. The lower pressure FIT measurements in the upper section are explained by pore pressure dissipating via vertical and lateral connectivity in the more permeable sands.

Below 2,000m the difference between the computed pressures and the actual measurements is lower and it appears that the mudrocks and sands are in pressure equilibrium. The good agreement between the pressure measurements and the values computed from mean effective stress analysis indicates that disequilibrium compaction is responsible for the high pressures encountered. Log data was not available at the TD of the well where the final FIT measurement was taken so it was not possible to assess if the shales which bound the deepest penetrated reservoir were in pressure equilibrium as with the interpreted results at ~2.4km depth (Figure 3.16).

When compared to the pressure values calculated using vertical effective stress (Figure 3.16) the FIT measurements at the base of the section are significantly higher. This pressure difference was interpreted initially as evidence for fluid expansion generating mechanisms (Harrold et al., 1996): lateral transfer was invoked to explain the extra pressure because of rapid differential subsidence associated with the well's location over a structure with considerable relief.

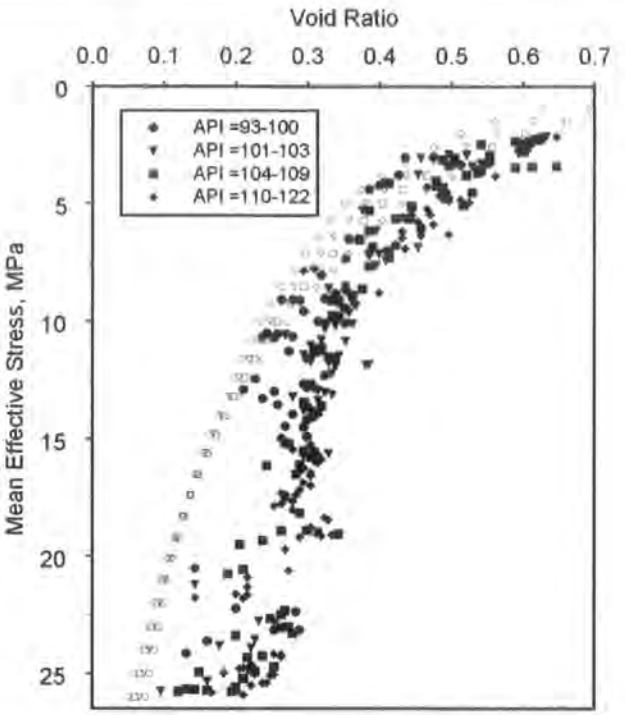

Figure 3.15 Void ratios vs hydrostatic mean effective stress for shales from Well B subdivided on the basis of gamma ray response. Normal compaction curves have been fitted to bound those points considered to be hydrostatically pressured.

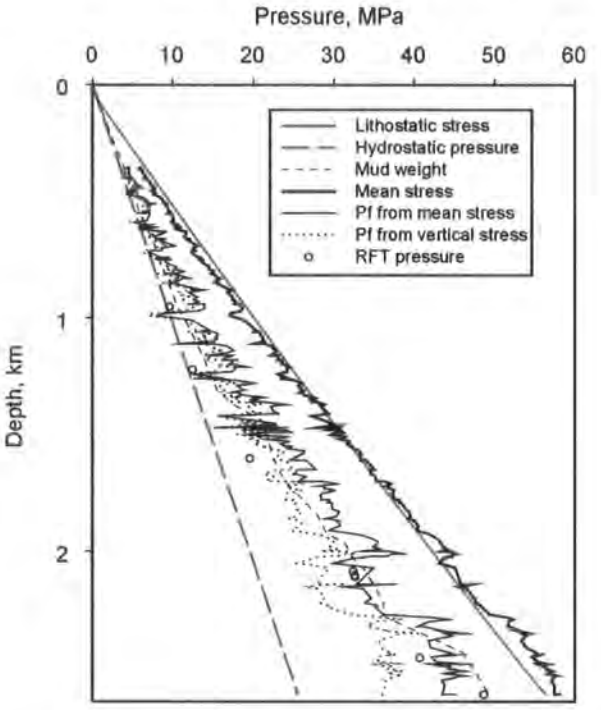

Figure 3.16 Computed pore pressures from mean and vertical effective stress for Well B plotted along with hydrostatic pressure and lithostatic stress profiles as well as direct pore pressure measurements made in the borehole.

Now that the pore pressures have been calculated using mean effective stress the conclusion of this study is that the encountered overpressure is due to disequilibrium compaction associated with rapid burial and low permeability mudrock intervals.

The pressures may have been enhanced through time by the process of lateral transfer, although data from more wells distributed across the structure would be required to support this hypothesis. Further discussion of this issue is postponed until Chapter 7.

3.5 Summary

The results of the analysis for all three of the wells give rise to broadly similar conclusions:

1. For the shallow depths where the pressures defined by direct measurements in the aquifer bodies are hydrostatic, the computed pressures in the mudrocks may be overpressured by up to 5MPa. This situation has arisen by lateral and vertical connectivity in the sand bodies allowing any overpressure to bleed off whilst the lower permeability shales remain overpressured.
2. Below the transition to overpressure defined by pressure measurements in the sand bodies, the mudrock pressures computed using mean effective stress are within 5% of the direct pressure measurements at depth where the highest overpressures are encountered. This agreement contrasts with the pressure values calculated using vertical effective stress, which are consistently lower (up to 15%) than the highest measured pressures.
3. The good correlation between computed and measured pressures implies that disequilibrium compaction produced by rapid burial and low permeability mudrocks could be responsible for all the observed overpressure.
4. No unloading from gas generation or lateral transfer of overpressured fluids is required to account for the high pressures at the base of the sections.

Chapter 4: Integrated analysis of pore pressure in Well D from SE Asia

"Thus we descended the dark scarp of Hell
to which all the evil of the Universe
comes home at last, into the Fourth Great Circle"
Dante Aligheri

4.1 Introduction

Well D was drilled by ARCO; the location of the well in SE Asia is confidential. In contrast with the Wells A, B and C in Chapter 3, which terminated between 2.5-3.5km depth, Well D was drilled down to 5.7km depth in a high pressure/high temperature (HPHT) environment. The high temperatures in excess of 220°C caused problems for the collection of data from the borehole and therefore made the task of understanding the nature and origin of the overpressure more difficult. The main problems stem from a lack of direct pressure measurements in the well which were prevented for two main reasons: firstly, the lack of permeable units in the upper 4km where measurements could be taken; secondly, the extreme pressures and temperatures below 4km depth affected the chemical properties of the highly weighted drilling muds which became more viscous and dense preventing use of the RFT tool. The extreme conditions also affected the wireline logging tools and prevented the final run between 5.08 and 5.7km for all but the gamma ray and caliper tools. The result is that the best estimates of the actual pressure in the well come from the mudweight data which are notoriously inaccurate, particularly in mudrock sections.

As part of an initial study carried out by ARCO, 1D modelling and seismic velocity analysis were performed to try and identify the mechanisms which had generated the encountered pressures. From these results, an initial interpretation was made that lateral transfer had generated a substantial component of the extreme pressures encountered at the base of Well D.

For this study, the results of ARCO's study were re-evaluated and integrated with porosity vs. mean effective stress analysis to produce a new hypothesis as to the origin of the overpressures. The new conclusions were then compared with pressure estimates from 2D basin models to yield final conclusions.

4.2 Data sources

The data used in the pressure analysis of Well D are derived from five main sources: the wireline log suite and mudweights from the well report, coupled with

pressure analysis from seismic velocity data, 1D and 2D modelling results. Table 4.1 summarises the wireline log data available and shows how the different parameters used in the analysis were derived.

WIRELINE LOG	CALIPER	GAMMA RAY	SONIC	RESISTIVITY ILD / MSFL	DENSITY	NEUTRON
Units	Inches	API	μs/ft	Ωm	g/cc	%
Interval	0.942-5.7km		0.942-5.08km		2.61-5.08km	
Use of data	Disc.	Lithology	Porosity	Disc.	Lithology / Porosity	
		Overburden				

Table 4.1 Summary of wireline log data used in the pressure analysis of Well D. Disc. = discriminant of data quality

4.3 Lithology

A simplified lithological column was created by analysis of the natural gamma ray profile, the lithology interpreted from the neutron and density logs and cuttings / core descriptions (Figure 4.1). The section encountered by the well comprises shales, silts and sands deposited between Late Oligocene times and the present day. A schematic diagram of the relationship between sediments and structure is overlain onto a seismic section through the well location (Figure 4.2). The sequence encountered at the borehole has been subdivided into three intervals with a fourth section unpenetrated in this part of the basin:

1. A 3.5km thick section of mudrocks very rapidly deposited between 4Ma and the present day. There is a gradual increase in the silt fraction of the section towards the top of the section
2. Around 0.7km of "post-rift" mudrocks and silts deposited more slowly between 15 and 5Ma.
3. A tilted fault block containing ~1.5km (~800m penetrated by the well bore) of sand and shale "syn-rift" sediments laid down between 35 and 17Ma. Sedimentation rates derived from biostratigraphy from the well cuttings, and stratigraphic models for

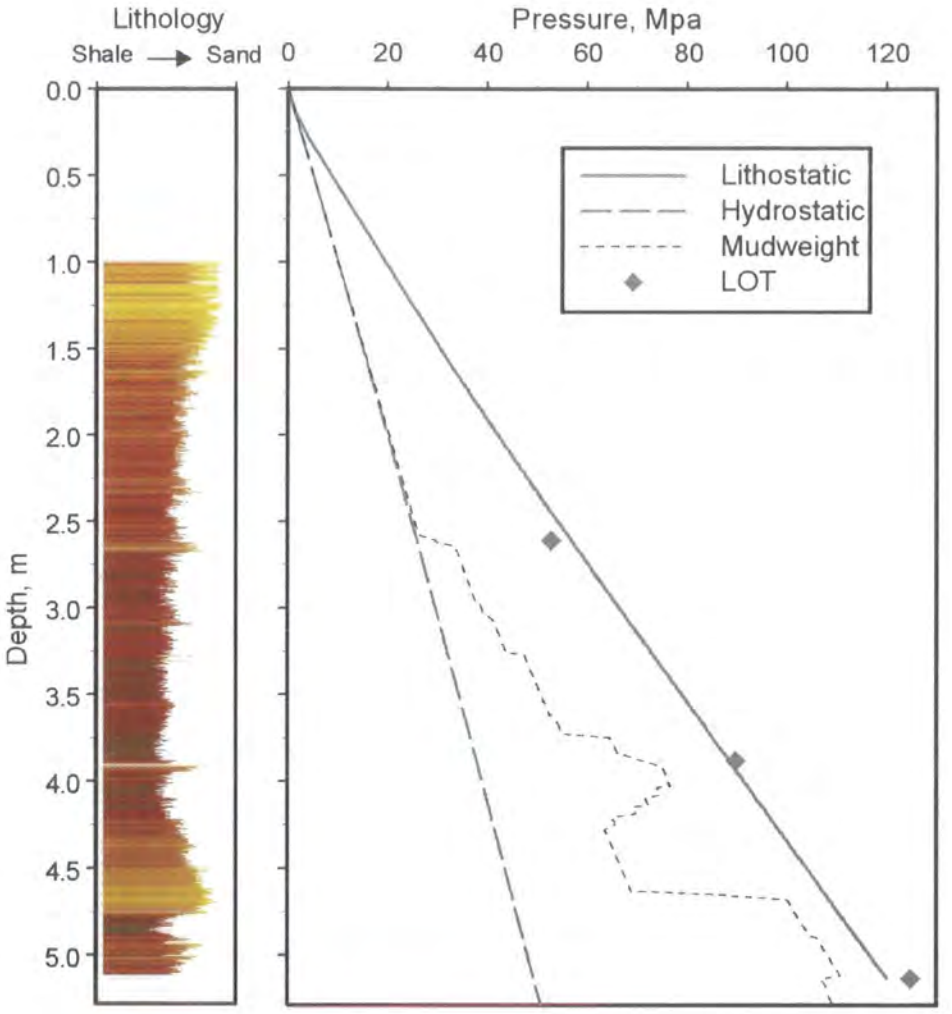

Figure 4.1 Simplified lithological column and pressure data for Well D. Shading in the lithology column represents clay fraction derived from the gamma ray log.

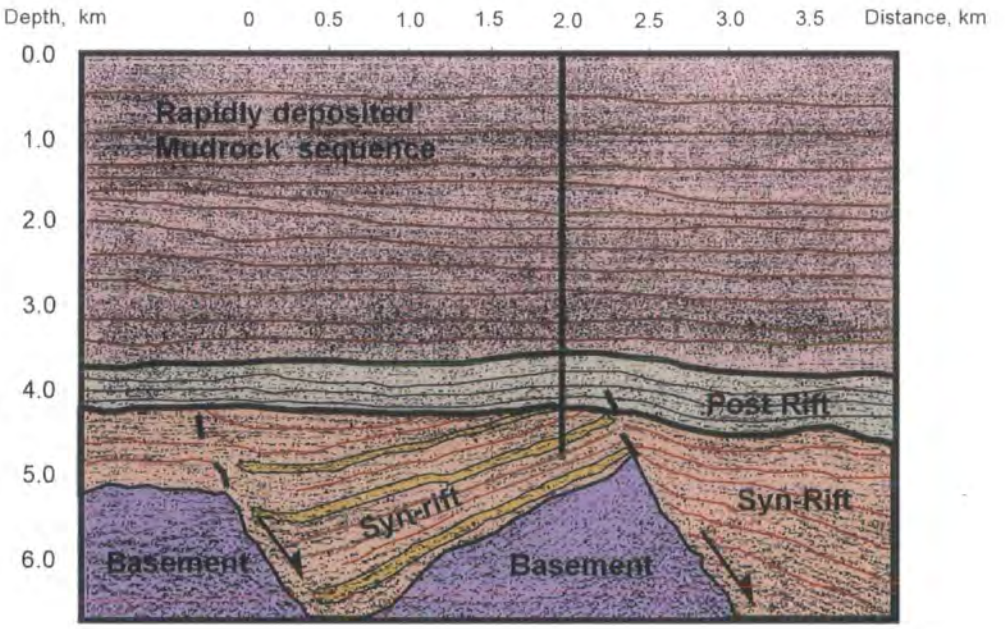

Figure 4.2 Simplified relationship between sediments and structure overlain onto a seismic section through the location of Well D.

the unpenetrated section (A. Brown, pers. comm.), initially were very high at ~1000m/My, before slowing to around 150km/My. Between17 and 15Ma around 0.4km of sediment were eroded from the crest of the structure.

4. A basement section of unknown nature (possibly igneous, or Mesozoic carbonates).

4.4 Pressure data

The pressure data from the well (LOT pressure measurements and the mudweights used during drilling) are plotted along with a simplified lithological column against depth in Figure 4.1. Also plotted are the values of hydrostatic pressure which were computed assuming a brine of 1.03g/cc and the lithostatic stress calculated by integrating the density log, and sonic derived porosities for the shallow section.

Direct measurements of the pore pressure using the RFT tool were not taken for two reasons. Firstly, for the upper 4km, the lithology of the section consists almost entirely of mudrock units and therefore presented few permeable units where measurements could be taken. Secondly, when the borehole encountered the syn-rift section containing more permeable, arenaceous units below 4km, formation pressures of 2.2g/cc (18.6lb/gal) equivalent mudweight and temperature conditions in excess of 220°C (440°F) affected the properties of the drilling muds which became more viscous and dense and prevented use of the RFT tool.

The mudweight profile (Figure 4.1) shows that the well was drilled down to 3.5km with muds weighted between 1.0 and 1.15g/cc (8.6 and 10lb/gal). Between 3.5 and 4.5km the mudweights were increased steadily to balance increasing amounts of gas detected in the drilling muds. Below 4.5km the mudweight was reduced down to a minimum of 1.5g/cc (12.5lb/gal) in response to fluid losses from the borehole. Mudweights were kept at 1.5g/cc until 4.65km depth where the pressures increased rapidly to ~2.16g/cc (18lb/gal) within 200m, and was increased to a maximum value of 2.23g/cc (18.6lb/gal) at 4.8km depth. Because these values of mudweight were used to balance pressures whilst drilling into permeable units, it is likely that they represent fairly accurate estimates of the actual pore pressures in the sands plus a small component of excess mudweight for well control/safe drilling. The mudweights were maintained between 2.16 and 2.23g/cc (17.8 -18.6lb/gal) down to TD at 5.7km,

(18,600ft). The extreme conditions prevented any data collection other than the gamma ray below 5.08km.

Whilst drilling well D, three leak off tests were performed (Figure 4.1). The first point lies below the values of lithostatic stress computed from the sonic and gamma ray logs (Section 2.2.3.2). The second leak off pressure slightly exceeds the computed lithostatic stress value, indicating that somewhere between 2.5 and 3.75km the minimum principal stress has changed from being horizontal in the shallower section to vertical for the highly overpressured section. An even higher minimum stress (presumably vertical) is indicated by the third point.

4.4 Pressure analysis

Because of the lack of actual pressure measurements in this well, a number of different types of pressure analysis were carried out to estimate the magnitude and causes of the overpressures in the mudrocks.

4.4.1 Seismic velocity analysis

4.4.1.1 ARCO in-house pressure estimates.

Initially, 2D seismic data were acquired to establish the nature and extent of the structure prior to drilling,. The seismic data were processed and the velocities used for pre-stack depth migration employed to estimate fluid pressure for points in the seismic volume using ARCO's Pore Pressure/Fracture Gradient (PPFG) software package. To calculate the pressures, a velocity/depth trend was generated by the program user to describe a normally pressured profile, and at each CDP gather the actual velocities were compared against the trend (Figure 4.3). Where actual values diverged from the normal trend, a regionally derived velocity-to-pressure transform was applied to compute the pressure values shown in Figure 4.4. The velocity-to-pressure transform is calculated by calibrating pressure measurements from other wells in the area with their known seismic velocities. The results are estimates of fluid pressure magnitude and distribution in relation to structure, and were used to assist in the planning of the well.

When the well was drilled, the pressures encountered below 4.65km in the syn-rift section were around 20MPa higher than the pre-drill estimates. The discrepancy

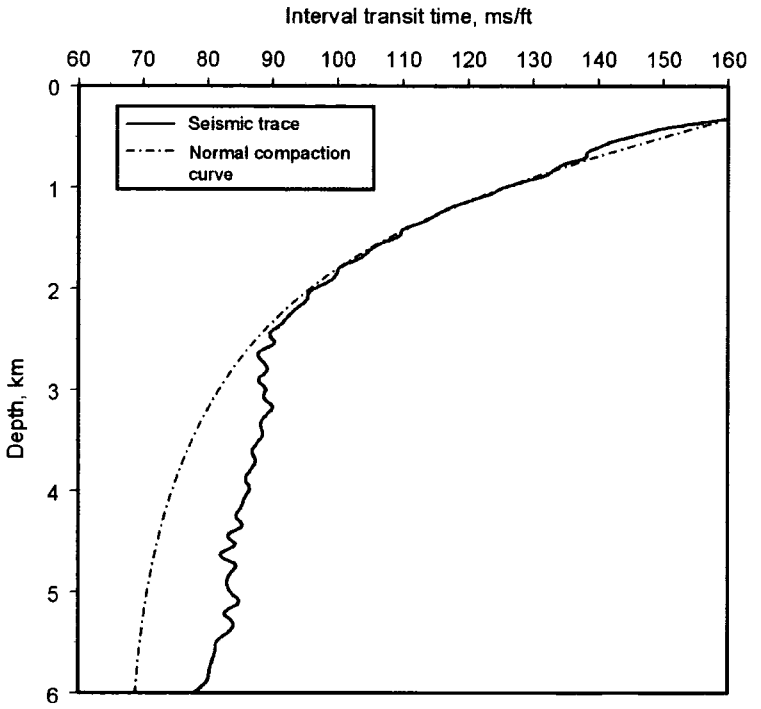

Figure 4.3 Seismic velocity for a single shot point plotted against depth along with a velocity profile used to represent the normal compaction curve.

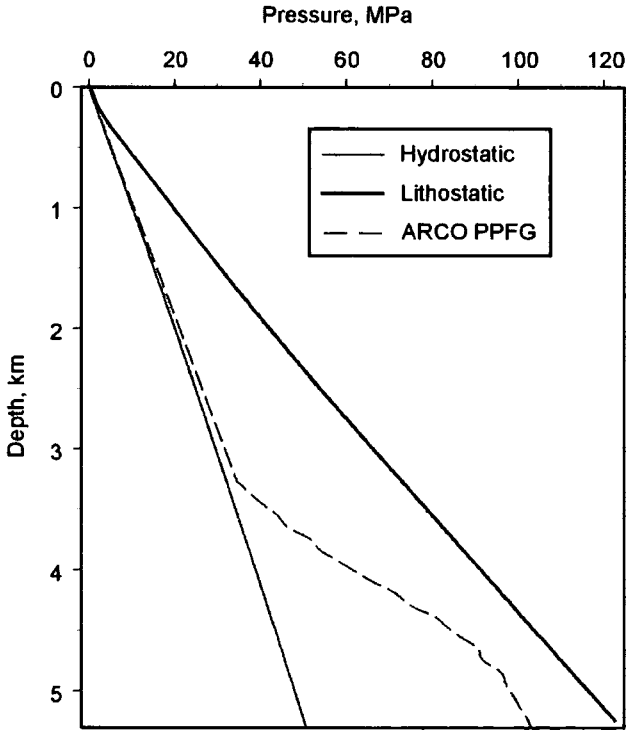

Figure 4.4 Pore pressure computed from seismic velocity values using ARCO's PPFG software package.

between the actual pressures and the pre-drill pressure estimates stemmed initially from an incomplete understanding of the origin of the overpressure in the region.

The seismic data were re-evaluated "post-drill" using calibrations from the well to get an improved picture of the fluid pressure distribution (implications of the seismic calibrations are discussed with the porosity effective stress analysis, Section 4.4.4). The pressures calculated using the PPFG software produce a distinct trend in the equivalent mudweight pressure distribution (Figure 4.5). This plot was generated by computing pressure values at ~25ft depth intervals (velocities would originally have been generated at a much coarser depth interval corresponding to the position of strong reflecting horizons, the values used here would have are interpolated between these values) from over 50 CDP gathers, and shows the following features:

1. The section from the surface down to approximately 3.25km is normally pressured (1g/cc (8.6lb/gal) equivalent mudweight).
2. Between 3.5 and 4.5km the pressures increase to 1.9g/cc (16lb/gal) uniformly across the section.
3. Below 4.5km, the distribution becomes more complicated: at the left and right end of the section, pressure continues to increase with depth up to 2.15g/cc (18lb/gal); over the structure. However, a zone of lower mudweight extends deeper in the section, following the dip of the syn-rift sediments. (Values from below the basement reflector or from areas of poorly constrained velocity have been assigned null values).

The zone of lower pressures seen in Figure 4.5 is described as a "drawdown" and is attributed to lateral transfer (Figure 1.12). When this happens, the fluid drawn out of the shales at the base of the structure produces more compacted shales and this would be likely to show up as a zone of higher velocity on seismic. No correlative pressure increase is observed on seismic over the crest of the structure. An early in-house conclusion (T.K. Kan and B. Kilsdonk, pers. comm.) was that unloading due to lateral transfer could explain the unexpectedly high pressures encountered in the well in the syn-rift section. Further discussion of this point is found in section 7.3.3.

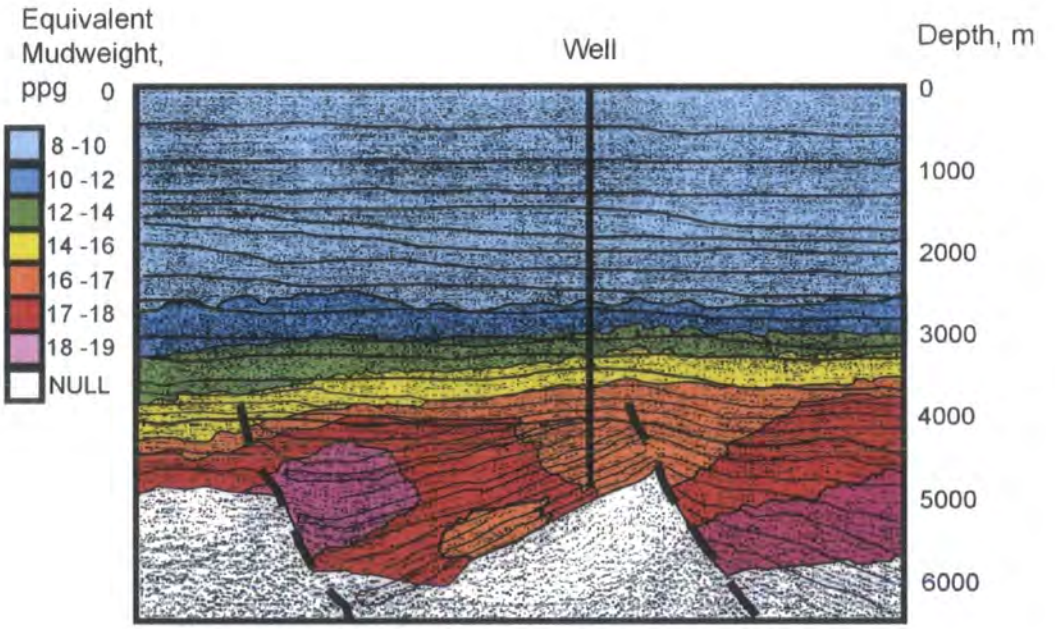

Figure 4.5 Pore pressure distribution computed using ARCO's PPFG software package. The pore pressure values in equivalent mudweight (lb/gal) are overlain onto the 2D seismic stack.

4.4.1.2 Mean effective stress pressure estimates

Estimates of pore pressure calculated using the PPFG software package are designed to link actual pore pressures encountered in wells with seismic velocities used for pre-stack depth migration, such that pressure prediction can be made when planning new wells, as well as for carrying out further analysis of drilled structures. Further analysis was carried out to assess the pore pressures using void ratio vs. mean effective stress analysis on a smaller data set. To this end, computed velocity, density and PPFG-estimated pore pressure profiles for eight CDP gathers at ~2km spacing over the structure were supplied by ARCO for this study.

To check the validity of working on a greatly reduced number of data points, first the PPFG-computed equivalent mudweights contoured for the eight CDP gathers, overlain onto the seismic section were plotted (Figure 4.6). The mudweight distribution in Figure 4.6 is almost identical to the distribution in Figure 4.5. This observation indicates that re-sampling the data set has not significantly affected the pressure distribution interpreted from seismic, and that contouring of this sample data set faithfully reproduces the pressure distribution generated by the full data set.

The same PPFG-estimated pore pressure values shown in Figure 4.6 were re-plotted in Figure 4.7 in terms of overpressure, so that directions of potential fluid flow could be determined. The pattern of overpressure distribution is very similar to the mudweight distribution in Figure 4.6, with the exception of the area over the syn-rift sediments. Whereas the mudweight distribution (Figure 4.6) shows a decrease in equivalent density towards the base of the structure, which might be interpreted as a "drawdown", the overpressure distribution (Figure 4.7) shows that the amount of overpressure still increases with depth along the tilted structure.

To estimate the pore pressures from a void ratio vs. mean effective stress approach for each of the CDP gathers, the parameters used were calculated as follows:

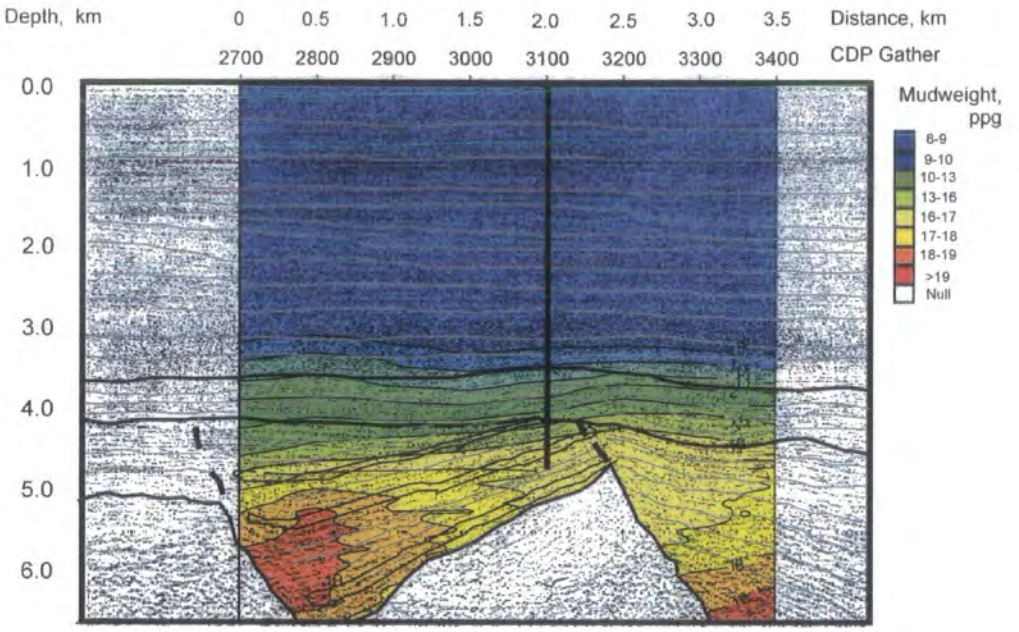

Figure 4.6 Pore pressure distribution overlain onto the 2D seismic stack as for Figure 4.5. The pressure distribution was calculated from a smaller data set to the values used to plot Figure 4.5.

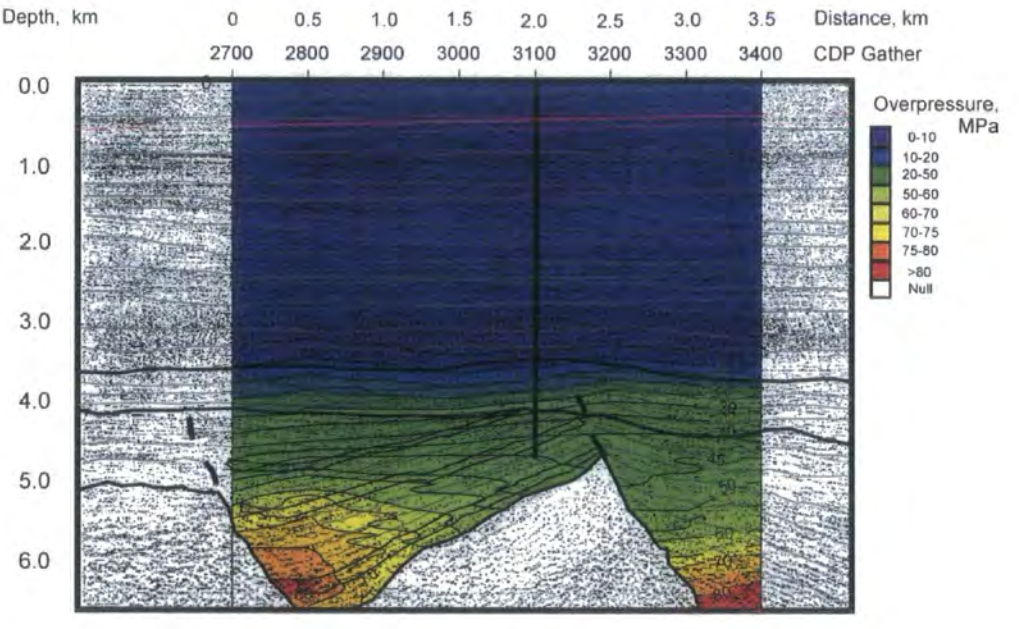

Figure 4.7 Pore pressure values from Figure 4.6 plotted in terms of overpressure (MPa).

1. hydrostatic pressures were calculated using a brine density of 1.03g/cc;
2. lithostatic pressures were calculated by integrating the synthetic density log derived from migration analysis;
3. void ratios were calculated using Issler's (1992) correlation between velocity and porosity [16] on the assumption that the lithology was shale of uniform mineralogy.

The void ratios were plotted against hydrostatic mean effective stress derived using [31] and a bounding normal compaction curve was generated as shown in Figure 4.8. Estimates of pore pressures and values of mean stress were calculated using [33] and plotted in Figure 4.9 along with the computed hydrostatic and lithostatic pressures. The profile shows normal pressures down to around 2km with steadily increasing overpressures below this depth.

The estimated pore pressures were converted to values of overpressure and plotted against depth in Figure 4.10 for comparison with Figure 4.7, (the PPFG software estimated overpressures). The distribution of overpressure is similar for both plots; however, the magnitude of the overpressures is significantly greater for the PPFG derived values which were calibrated to more closely match the encountered pressures.

The pattern of overpressure distribution over the syn-rift sediments indicates that there is a 2D component of fluid flow associated with the structure. At the present day, fluid will be flowing up the dipping aquifer units towards the crest of the structure, thereby enhancing the pressures in the profile cut by the well.

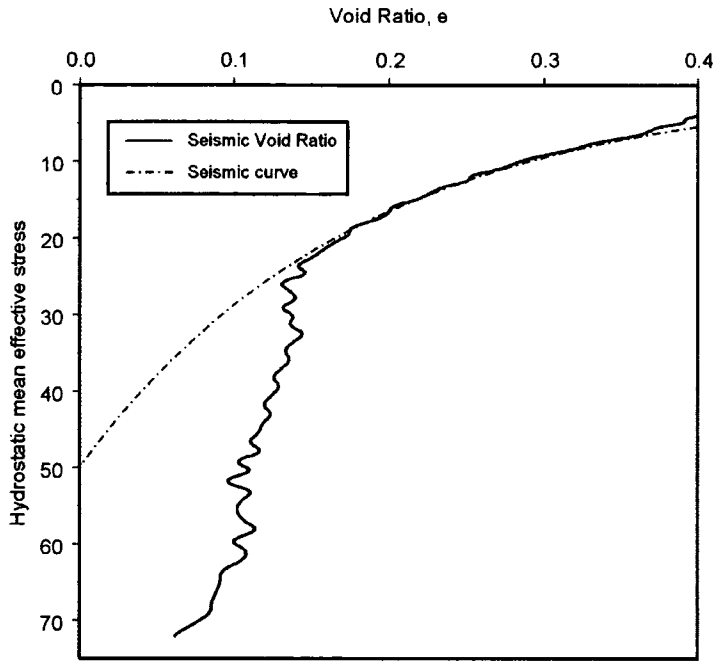

Figure 4.8 Void ratios calculated from seismic velocity values plotted against mean hydrostatic effective stress along with a bounding normal compaction curve.

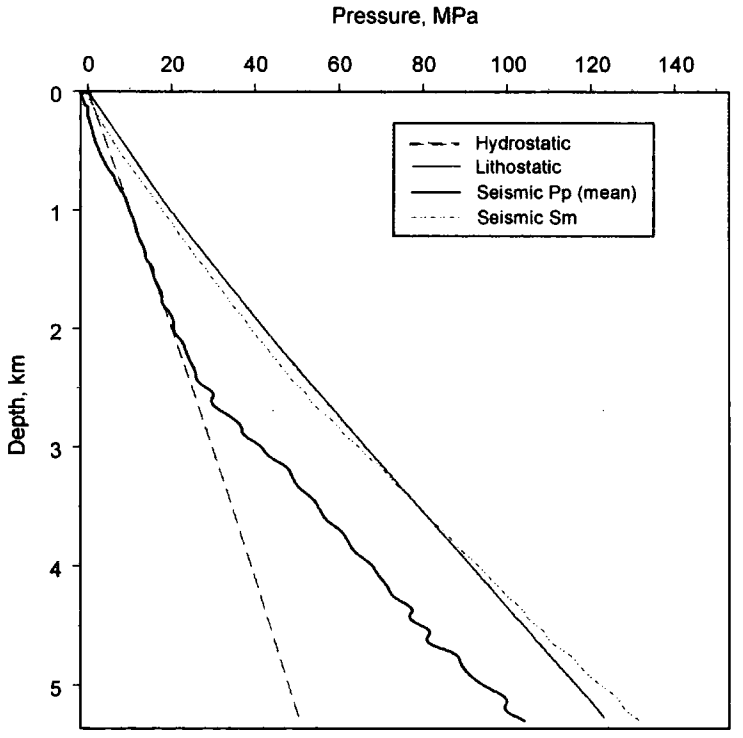

Figure 4.9 Pore pressure and mean stress values calculated from the void ratios in Figure 4.8. Values are plotted against depth along with hydrostatic and lithostatic stress profiles

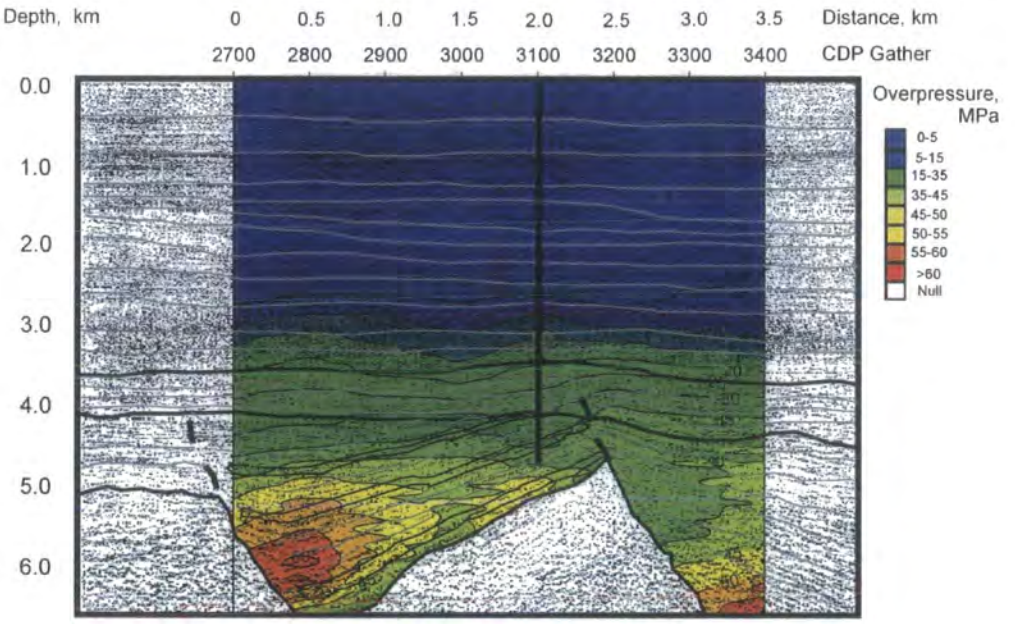

Figure 4.10. Overpressure distribution calculated using a mean effective stress approach and overlain onto the 2D seismic stack as for Figure 4.5.

4.4.2 1D modelling analysis

To reconstruct the temperature and pressure at the well location, a 1D basin model was constructed using ARCO's in-house software, "Genesis 1D". The resulting pressure profile from this model is compared to the mudweights used to drill the well in Figure 4.11. The values of pore pressures generated by the 1D model show hydrostatic values in the mudrocks down to 2.2km before the onset of overpressure due to disequilibrium compaction. Below 2.2km, the pore pressures from the model increase parallel to the rate of lithostatic pressure increase. Comparison of the model-derived pressure profile with the mudweights used shows that the pressures match for the upper section, but below around 4km the model fails to predict the decrease in pressure encountered in the well, or the significant increase to very close to lithostatic pressure at around 4.6km. The fact that the pressure distribution and magnitude could not be simulated using 1D models led to the initial conclusion that 2D and 3D components of fluid flow are important for this well.

One other possible reason why the model failed to predict the very high pore pressures at the base of the section is that the Genesis model computes pore pressures from a porosity versus vertical effective stress relationship. This approach restricts the rate of pore pressure increase due to disequilibrium compaction to the rate of load addition at the top of the section, producing the profile seen in Figure 4.11. If increasing horizontal stresses with depth are included in the model, the pore pressure due to disequilibrium compaction would track the rate of mean stress increase. As the mean stress would increase at a rate greater than the rate of lithostatic stress increase (section 1.8.1), the pore pressures would move to values closer to the lithostatic stress than those observed in Figure 4.11. For further discussion of this point see section 7.6.

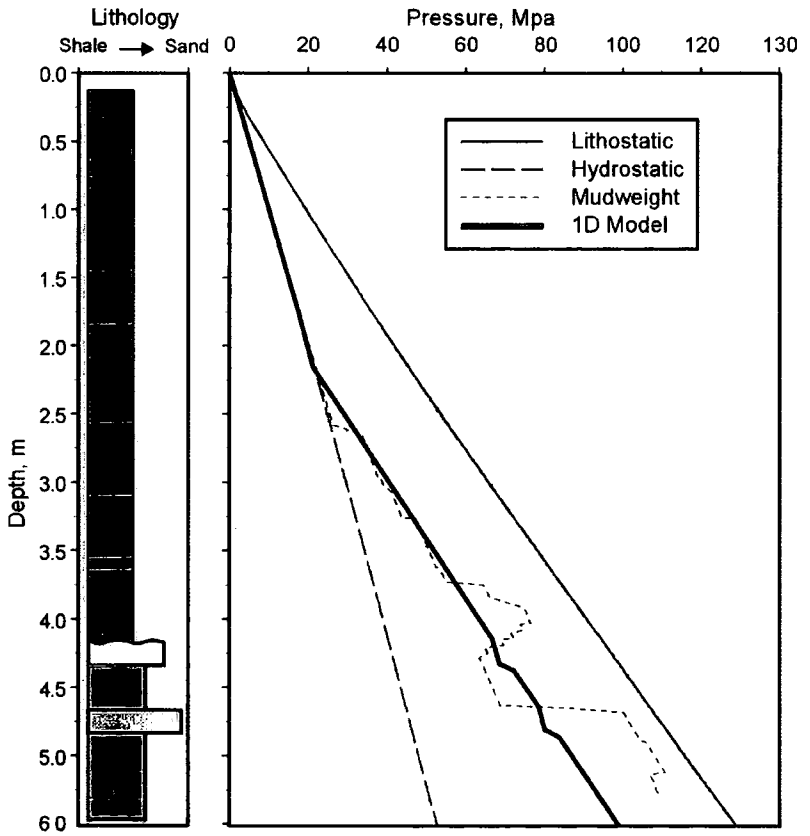

Figure 4.11. Comparison between the pore pressure values calculated using Genesis 1D modelling package and the actual mudweights used to drill the well plotted along with the simplified lithological column used in the model.

4.4.3 Mudrock void ratio versus effective stress analysis

The void ratios calculated from the sonic log using [16] for individual mudrocks are plotted against hydrostatic mean effective stress calculated using [31] in Figure 4.12. The void ratios computed from the sonic log decrease across the interval between 8 and 35MPa (equivalent to 1-3.5km depth). Bounding curves were fitted to the values across this interval to describe the normal compaction behaviour of the mudrocks (Figure 4.12). The corresponding estimates of pore pressure calculated from mean and vertical effective stress approaches are shown in Figure 4.13 and show considerable scatter between 1-3km depth. The scatter could be explained by the presence of overpressured pore fluids in some of the shales whilst others are still normally pressured.

Between 3.2km and 4km depth the void ratios increase to a maximum value of 0.25 at 43MPa hydrostatic mean effective stress. This increase is accompanied by an increase in the clay fraction interpreted from the gamma ray, neutron and density logs. The estimated pore pressures increase steadily to values within 5MPa of the calculated lithostatic stress across this interval, correlating with the increased mudweight used to drill the well.

Below 4.2km the porosity and clay fraction decrease down to a minimum at 53MPa (4.6km). The low porosities at this depth correspond to the low estimates of pore pressure seen in Figure 4.13. Mudweights were reduced across this interval to 1.5g/cc (12.5lb/gal) before the sudden increase in pressure at 4.65km depth. The void ratios increase to values around 0.2 below 4.65km (55MPa) and the derived pressures correspond to the pressures equal to the mudweight values required to drill the well (Figure 4.13). Void ratios remain between 0.1 and 0.2 down to 5.01km depth and the corresponding estimated pore pressures stay within 5MPa of the mudweights used.

The interpretation of the pressure values derived from mean effective stress analysis in Figure 4.13 is that for the shallow section down to 3km some of the sediments are normally pressured whilst the lower permeability mudrock units are overpressured by up to 5MPa. Below 3km pressures increase uniformly to within 5MPa of the lithostatic stress values as a function of the low permeability of the clay rich section and the extremely rapid burial. The pressure decrease below 4.2 km is associated with a shift to a more silty section (Figure 4.1) and could either represent

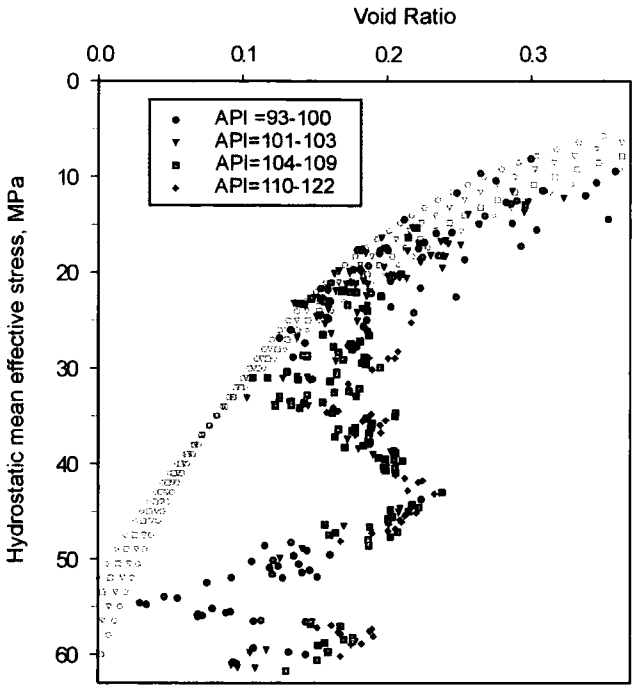

Figure 4.12 Void ratios vs hydrostatic mean effective stress for shales from Well D subdivided on the basis of gamma ray response. Normal compaction curves have been fitted to the porosity values interpreted as normally pressured.

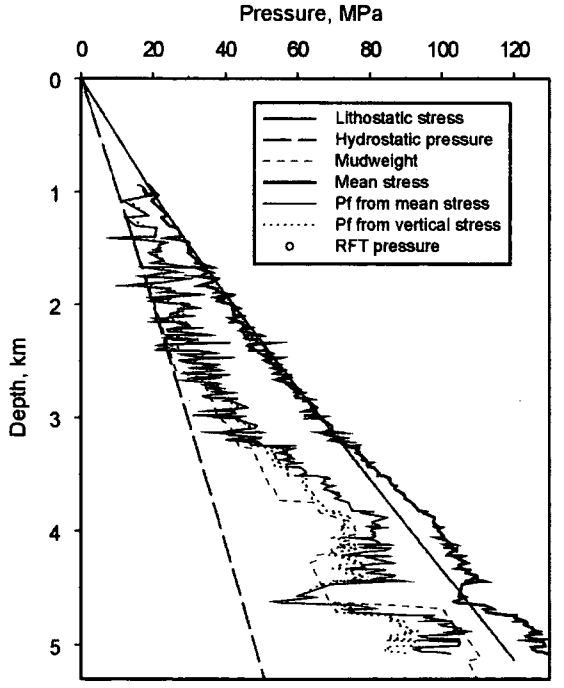

Figure 4.13 Computed pore pressures from mean and vertical effective stress for Well D plotted along with hydrostatic pressure and lithostatic stress profiles as well as direct pore pressure measurements made in the borehole .

sediments which have experienced a deeper onset of overpressure as a function of their higher permeability, or that pressure is escaping laterally. Some evidence to support this latter hypothesis comes from the 3D seismic survey: the stratigraphic units in which the lower pressures were encountered thicken laterally towards the sedimentation source where the sequence is believed to comprise a coarser, more sand rich sequence (M. Cucci, pers. comm.) that might allow some of the pressure to dissipate. Below 4.65km the lithology becomes slightly more mud-rich again. The low porosity units between 4.5 and 4.7km are acting as the pressure seal to the extreme pressures in the syn-rift sediments below 4.7km.

One reason why the pore pressures estimated from the mean effective stress approach between 3.5 and 4.15km are higher than the actual mudweights follows from the decision to calibrate the mudweights for this section with the sonic tool response (i.e., increase the mudweight with increasing interval transit time, Wydrinski, pers. comm.). To derive the pressures, the sonic values would have been compared against depth, a situation which is similar to comparison with vertical effective stress (a function of depth). Comparison of the pressures estimated from vertical and mean effective stress analysis together with the mudweights used are shown in Figure 4.13. Between 3.75 and 4.35km depth, the interval calibrated with the sonic log, the mudweights and the vertical effective stress derived pressures are in good agreement. Below 4.65km the vertical effective stress estimated pore pressures are lower than the required mudweights by up to 15MPa. This discrepancy led to the initial hypothesis that fluid expansion processes were responsible for a significant component of the high pore pressures at the base of the section (Harrold, 1998).

4.4.4 Comparison between seismic and well derived pressures

A comparison between the seismic-derived pressures at CDP 3100 (the gather nearest to the location of the well), the pressures computed from the wireline log response and the required mudweight pressures is shown in Figure 4.14. The plot shows that the calibrated PPFG pressure values are within 10MPa of the very high overpressures encountered at 4.65km depth, whilst the pressures calculated from the seismic velocities using the mean effective stress approach are around 18MPa lower than the pressures from below 4.65km. The reason for the difference between the

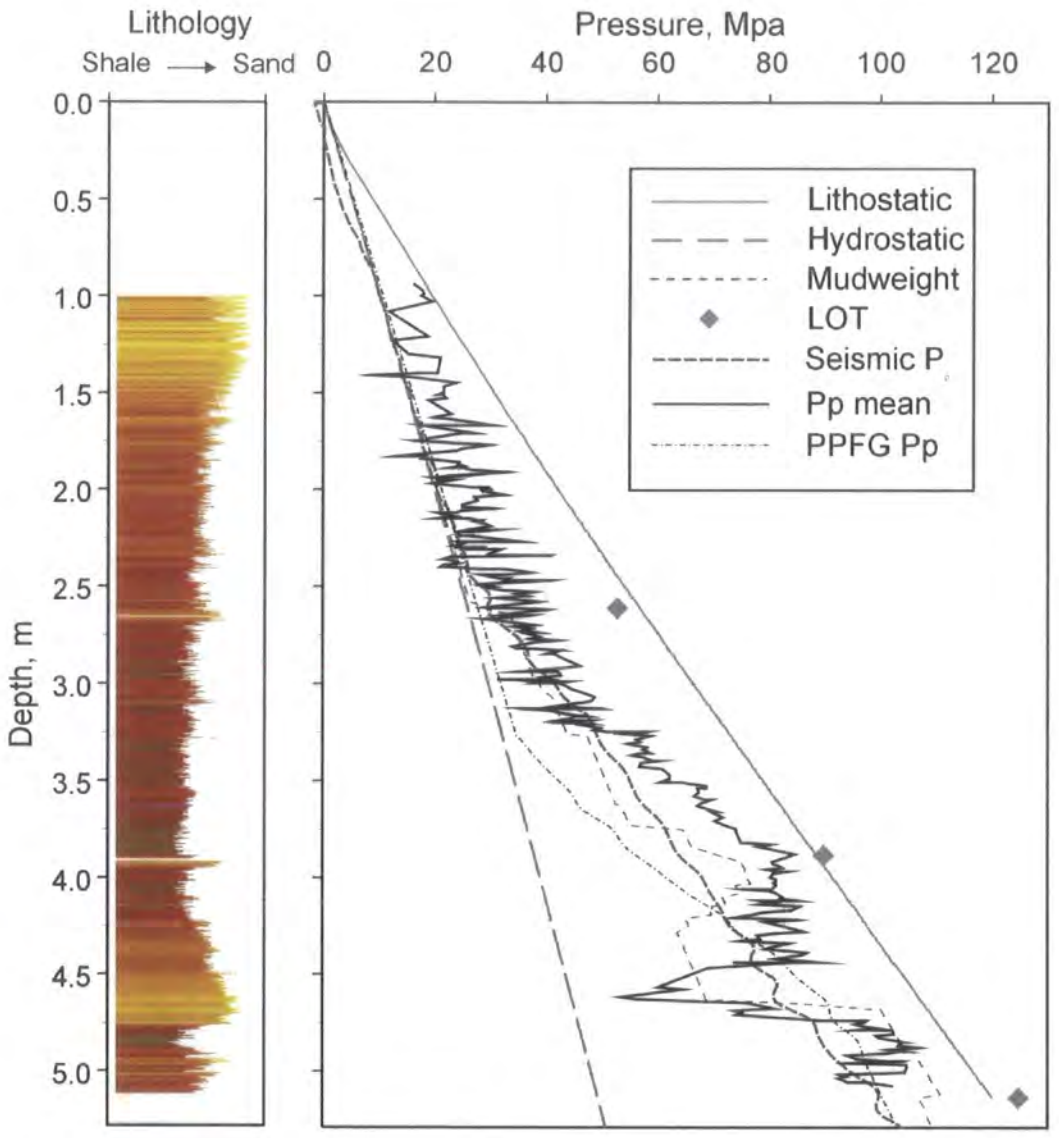

Figure 4.14 comparison of the pore pressure estimates derived from seismic PPFG and mean effective stress approaches with mudweights used to drill Well D.

pressures calculated from the wireline log response and from the seismic velocities originates from the discrepancy between the sonic log and the velocity structure derived from the seismic section (Figure 4.15). For the first 2.5km Figure 4.15 shows the seismic velocities approximately match the normally compacted velocities of the mudrocks from the sonic log. However, for the shaley interval between 3.15 and 4.2km depth the VSP survey and sonic logs were slower than the seismic velocities by a total of 150ms (T.K. Kan, pers. comm.). Assuming that the data is good enough and that the seismic computed values were correctly derived, the difference in velocity was proposed to have arisen due to seismic anisotropy of the clay rich mudrocks. The clays from the interval 2.5-3.5km may have a highly aligned fabric (K. Katahara, pers. comm.) causing a decrease in the velocities measured in the vertical plane by the VSP survey and the sonic logs as seen in Figure 4.16. The seismic wavelets are measuring more of a horizontal component of the velocity than the sonic and VSP survey and are not as strongly affected by the fabric change (Figure 4.16). Horizontal, stress-induced microfractures of the type described in well B (section 3.3.4) could also produce a significant velocity anisotropy (Corbett, pers. comm.) but were not believed to be responsible for the observed difference in this section (Katahara, pers. comm.). Another possible origin of the discrepancy between the calculated sonic and seismic velocities is dispersion (Taylor, pers. comm.), where the difference in measurement frequency used by the two methods means that the lower frequency (seismic) signal does not identify the slower velocity intervals. This phenomenon is generally invoked for individual beds where seismic appears to overestimate the velocity. In this example, however, the velocity differences between the sonic and seismic approaches are much greater and span a much thicker interval than could be accounted for by dispersion alone.

The proposed anisotropy in the shales has two implications. Firstly, as the methodology is almost identical to the analysis of the well log data (which yielded the same pressures as the encountered conditions), if the correct velocities from seismic are derived, it means that the mean effective stress approach will produce the correct pressures. Secondly, it means that an assumption has to be made that the difference between the two velocities remains relatively constant away from the borehole for the pressure distribution to be reliable. Further discussion of these two points is made in section 7.5.

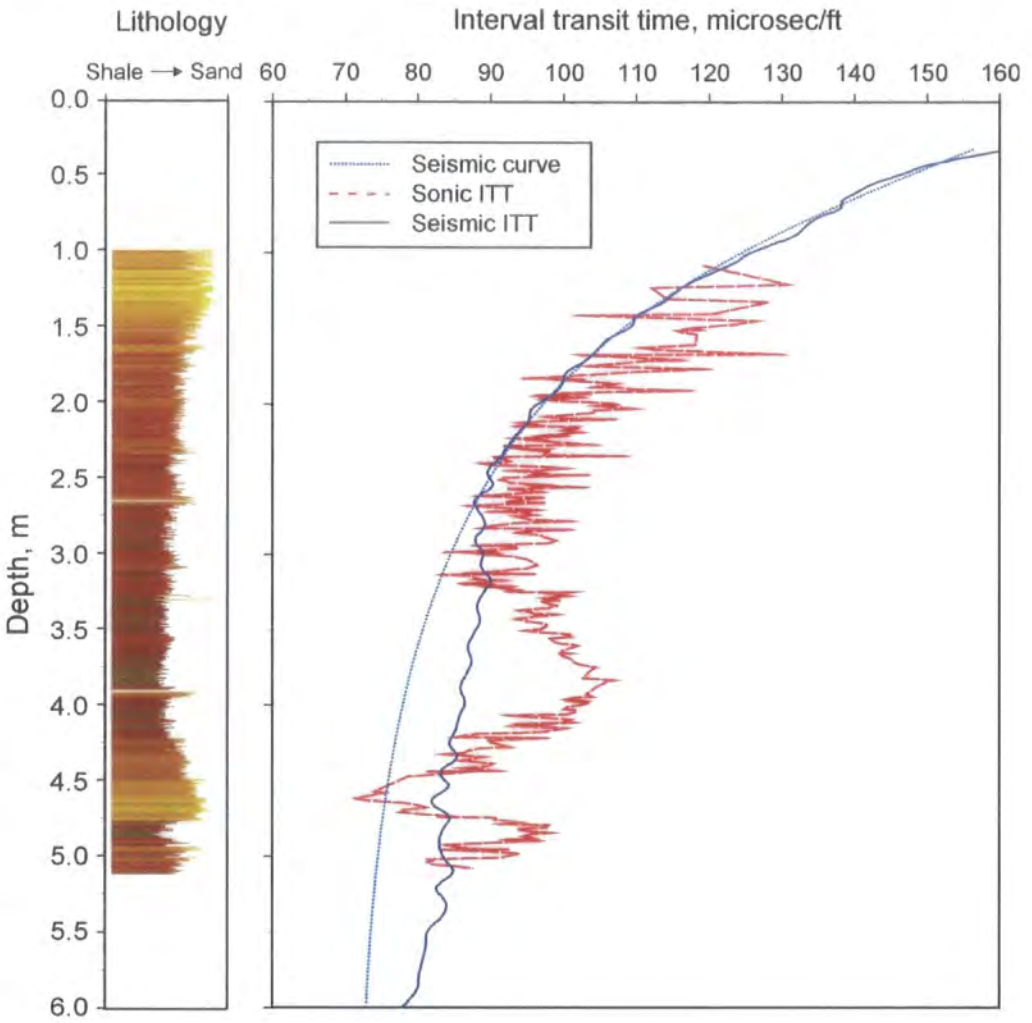

Figure 4.15 comparison of the interval transit times derived from the seismic cross section and the sonic log for Well D.

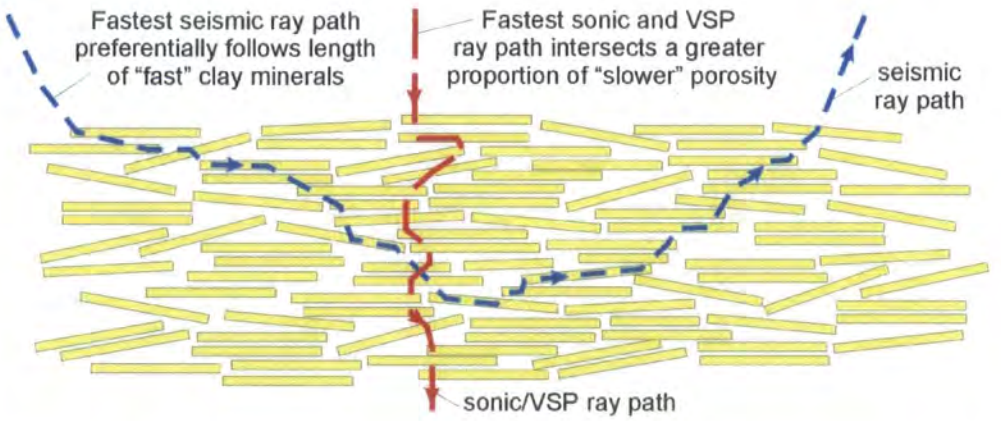

Figure 4.16 Possible origin of the discrepancy between the seismic and sonic log derived velocities through clay rich intervals.

4.5 Initial conclusion

The interpretation of the pore pressures estimated by the mean effective stress method from the wireline log suite is that disequilibrium compaction is responsible for the overpressures encountered at the base of the section. The results of the seismic pore pressure and 1D modelling analysis point to a more complicated pore pressure distribution associated with the lateral and vertical reorganisation of overpressure within the dipping syn-rift aquifer units.

4.6 2D Modelling analysis

This section is subdivided into five parts, to show how models were constructed and used to address the different issues raised by the seismic and mean effective stress analysis.

Section 4.6.1 describes the models used in the analysis and the way in which the modelling parameters are calculated

Section 4.6.2 presents the results of analysis testing whether the drawdown effect observed on the seismic velocity field for pre-stack depth migration of the seismic data was reproducible.

Section 4.6.3 illustrates results from the models testing whether an unloading response due to lateral transfer could be produced at the crest of the structure.

Section 4.6.4 details attempts to quantify the amount of present day overpressure attributable to lateral transfer.

Section 4.6.5 list the conclusions of the 2D modelling analysis.

4.6.1 Construction of models

Prior to the construction of 2D models, 1D profiles through the structure were created using Genesis 1D basin modelling software package. These profiles mimicked the stratigraphy and sediments of the structure illustrated in Figure 4.2.

From the input data defining the 1D models, a 2D cross section of the structure was constructed using Genesis 2D basin modelling software package. This initial 2D model contained a high degree of lithological complexity.

In order to test the influence of varying the parameters describing the sediment, the 2D model was simplified to a single syn-rift sand body encased by shales of uniform

properties. Once a more simple model had been constructed, the properties of the shale and sand were varied to assess their influence on the amount of pressure reorganisation. For each of the parameters, a number of simulations were carried out so that the effect of varying each parameter could be ascertained in isolation from the other parameters. Table 4.2 shows the parameters for which sensitivities were run and the range of values assigned to them, (the values chosen cover the minimum and maximum limits for each of the parameters which could be used to describe normal sediment behaviour, He, pers. comm.).

PARAMETER	POROSITY AT DEPTH Z, ϕ_Z	SURFACE POROSITY, ϕ_0	SURFACE PERMEABILITY, K_0,		PERMEABILITY FACTOR, α	PERMEABILITY, K_0, SAND, M^2	
DEFAULT VALUE	0.1	0.65	m^2	mD	4	m^2	mD
			10^{-11}	10^2		$2*10^{-7}$	$2*10^6$
MIN. VALUE	0.04	0.5	10^{-9}	10^4	3	$2*10^{-6}$	$2*10^7$
MAX. VALUE	0.14	0.8	10^{-19}	10^{-4}	7	$2*10^{-9}$	$2*10^4$

Table 4.2: sedimentary parameters modified for "Genesis 2D" modelling simulations.

Genesis 2D uses two key equations to describe sediment porosity and permeability properties. Firstly the compaction curve of the lithologies used in a model is defined by:

$$\phi = \phi_0 e^{-cz} \qquad [34]$$

where ϕ is the porosity, ϕ_0 is the surface porosity, c is a constant and z is the depth in metres. To adjust the compaction curves for the sediments, Genesis 2D has two input parameters: ϕ_0 the surface porosity of the sediment, and ϕ_z which affects the value of c in [34] to control the porosity of the mudrock at 3km depth (an arbitrary depth kept constant for all the models) under hydrostatic pressure conditions. Thus a low value of ϕ_z dictates a steeper compaction slope and a more compressible sediment.

Note that as the surface porosity ϕ_0 controls the initial porosity of the mudrocks at the time of deposition, it also influences the compaction slope of the sediment (increasing ϕ_0 without changing ϕ_z would cause an increase in the compressibility of the sediment). Therefore, in order to examine the effect of this parameter in isolation, it was necessary to systematically adjust the compaction slope at the same time.

The second of the two equations relates permeability to void ratio as follows:

$$k = k_0\left(\frac{e}{e_0}\right)^{\alpha} \qquad [35]$$

where k is the permeability in metres squared, k_0 is the initial permeability at the surface, e is the void ratio of the sediment, e_0 is the void ratio at the surface and α is the "permeability factor" which controls the rate of permeability decrease with decreasing porosity.

As well as the previous parameters controlling the shale characteristics, the sand body too was changed to identify its impact on the models: for some simulations, the surface permeability k_0 was varied and for others the sand thickness was changed.

4.6.2 Origin of the drawdown inferred from the seismic data

In order to identify the origin of the drawdown initially observed in Figure 4.6, a comparison was made between the pore pressure profiles derived from the 1D and simplified 2D models.

The 1D model pore pressure profiles from the base (CDP 2800, Figure 4.2) and crest (CDP 3100, Figure 4.2) of the structure are shown in Figure 4.17. For both profiles, as for Figure 4.11 the pore pressures generated by the model are hydrostatic for the first 2.5 km. Below this depth, the section is overpressured and the pore pressure profile runs parallel to the rate of lithostatic stress increase.

Similar pore pressure profiles from the simplified 2D models are presented in Figure 4.18. The plot was constructed using data at the 4.9Ma time step as the syn-rift thickness then represented a larger proportion of the total thickness of the section than at the present day, thus enhancing the visual impact of the pressure reorganisation. According to the model at 4.9Ma, the pressure is lower in the sand at the base of the structure than in the encasing shales, so fluid is being drawn out of the mudrocks. At the crest, however, there is no significant increase in the fluid pressure, and certainly no evidence of sands at significantly higher pressures than the encasing shales. This result corresponds to the pressure derived from the seismic velocity field with the anomalously low pressure along the base of the syn-rift section (Figures 4.7 and 4.10).

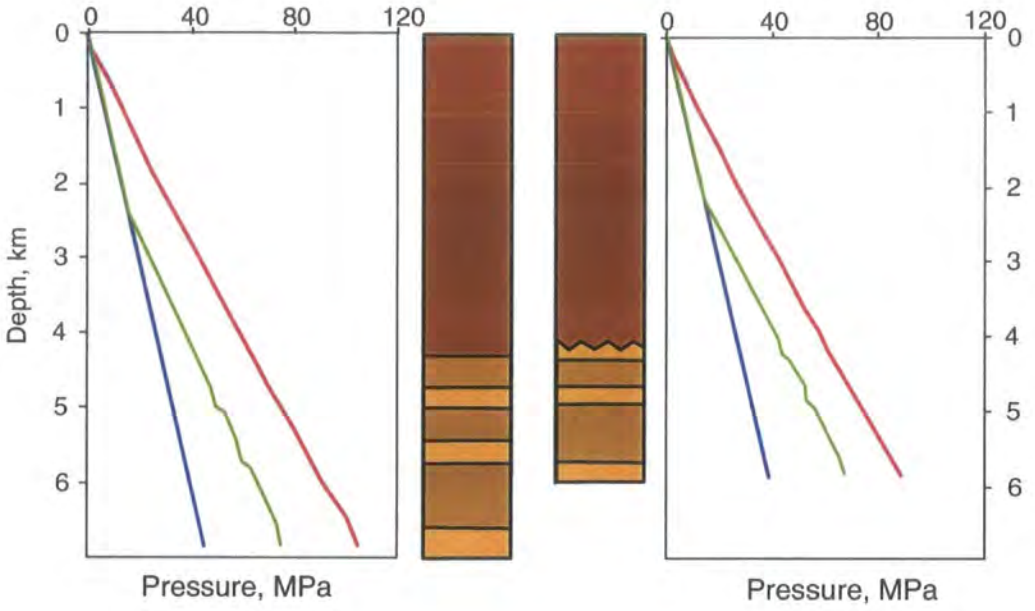

Figure 4.17 pore pressure profiles calculated using Genesis 1D for reconstructions of the stratigraphy at CDP 2800 and CDP 3100 over the base and crest of the structure respectively.

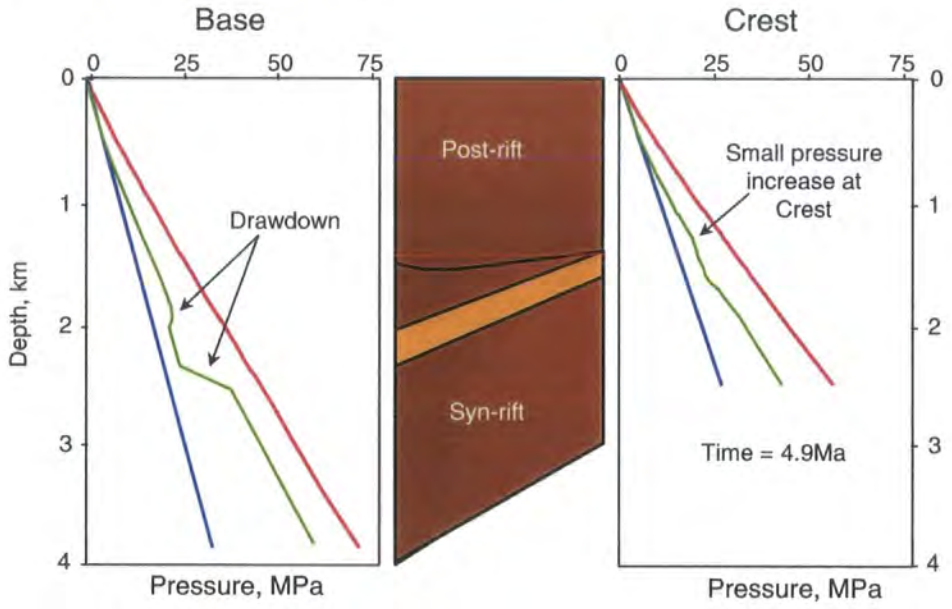

Figure 4.18 pore pressure profiles computed using Genesis 2D for reconstructions of the stratigraphy at CDP 2800 and CDP 3100 over the base and crest of the structure respectively at 4.9Ma.

The pressure reduction at the base of the structure seen in Figure 4.18 is of comparable magnitude for all time steps following the tilting and unconformity event. This observation implies that the "drawdown" observed on seismic was produced by lateral transfer during the period of syn-rift sedimentation and the unconformity event, and that the effect seen has persisted during post-rift sedimentation.

A plot of overpressure difference between the shale directly above the sand body at the crest and the base of the structure plotted against time is shown by Figure 4.19. This diagram shows that the pressure difference is very small (max 0.025Mpa) up to 17Ma at the start of the unconformity period. Between 17 and 13Ma, the overpressure difference increases to a maximum value of 0.15MPa before decreasing again during the post-rift sedimentation phase. During the rapid phase of burial between 5Ma and the present day, the overpressure difference grows again this time to a maximum of 0.35MPa however, this difference is insignificant compared to the total amount of overpressure at the crest of the structure.

The reason for the more significant pressure difference at the end of the syn-rift period is due to the fact that sediment is being eroded from the crest of the structure between 17 and 15Ma, allowing excess fluid pressure to dissipate by virtue of a decreasing overburden. The fluid pressure reduction in the shales encasing the aquifer unit at the base of the structure is limited by their low permeability as well as by the fact that the sediments are still experiencing burial which is generating more overpressure. Consequently, the amount of overpressure in the shales is slightly greater at the base of the section than at the crest in spite of the modelled high permeability of the aquifer unit which could act as an efficient drain. The present day difference between the base and the crest of the structure shows that the system has not fully equilibrated and that flow is still directed along the dipping aquifer units towards the crest of the structure. This result agrees with the results of the mean effective stress analysis of the seismic velocity data (section 4.4.1.2, Figure 4.10).

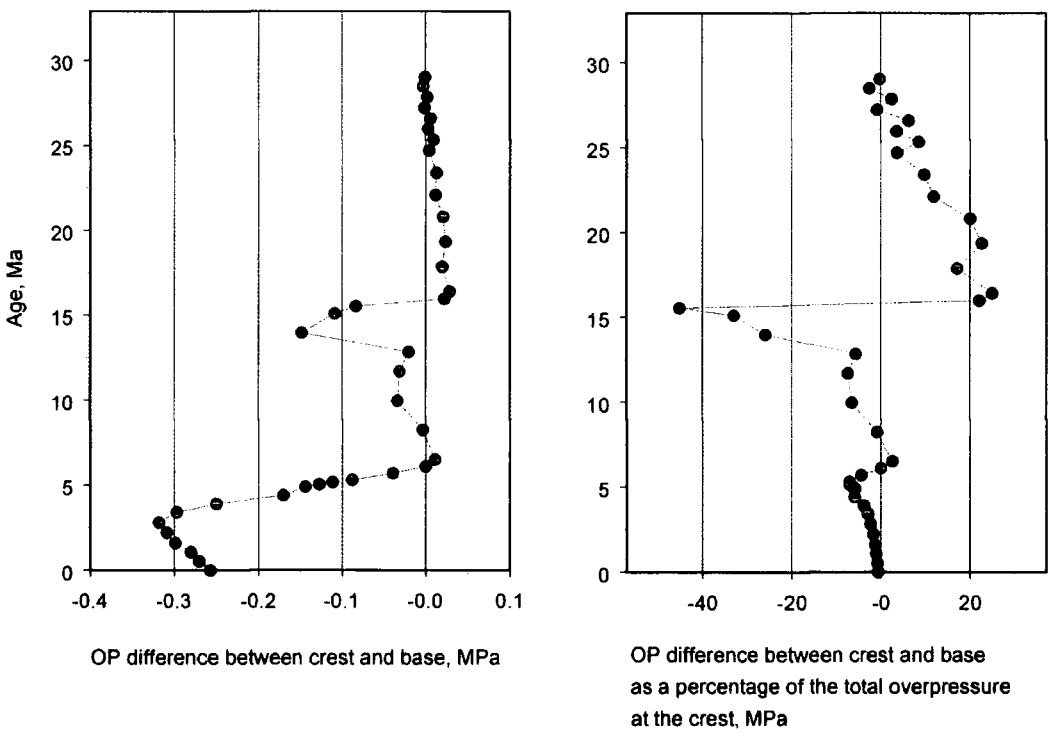

Figure 4.19 Difference in modelled overpressures between the base and crest of the structure plotted against time.

4.6.3 Testing the validity of lateral transfer-induced unloading

The results of all the simulations were examined qualitatively to see if lateral transfer produced unloading in the shales at the crest of the structure. For all the model parameter combinations, the pressure profile seen at the crest was very similar to the profile in Figure 4.18, with the sand being almost the same pressure as the encasing shales. No evidence was found for a significant pressure increase in excess of the pressure generated in the shales by 1D consolidation. Certainly, none of the models produced unloading of comparable magnitude to the 12MPa difference between the encountered pore pressures and the values estimated using the vertical effective stress / porosity relationship (Figure 4.13).

4.6.4 Quantitative assessment of the contribution from lateral transfer

In order to quantitatively assess the effect of lateral transfer, a comparison of the 2D and 1D model generated pressure values is required (cf. Yardley et al., 1998). Due to time constraints, however, it was not possible to generate the required 1D models. Instead comparison was made between pressure values from the 2D model at the crest of the structure and points at the same burial depth over the base of the structure.

The amount of enhancement is calculated by taking the value of overpressure in the shale directly above the sand body at the crest of the structure (marked X in Figure 4.20) , and subtracting the overpressure value from a point at the same burial depth over the base of the structure (Marked X' in Figure 4.20.

Figure 4.21a represents the amount of pressure enhancement due to lateral transfer at the present day plotted for all of the models. Points that represent the maximum and minimum values for each of the parameters listed in Table 4.2 are identified. In this plot, the difference in pressure between the crest and the base of the structure is plotted as a percentage of the total overpressure at the crest of the structure on the x-axis against the total overpressure at the crest of the structure on the y-axis.

For all the models, there seems to be a fairly simple relationship between the amount of enhancement by lateral transfer and the total overpressure at the crest of the structure, emphasised by the linear regression of all the data points also shown in

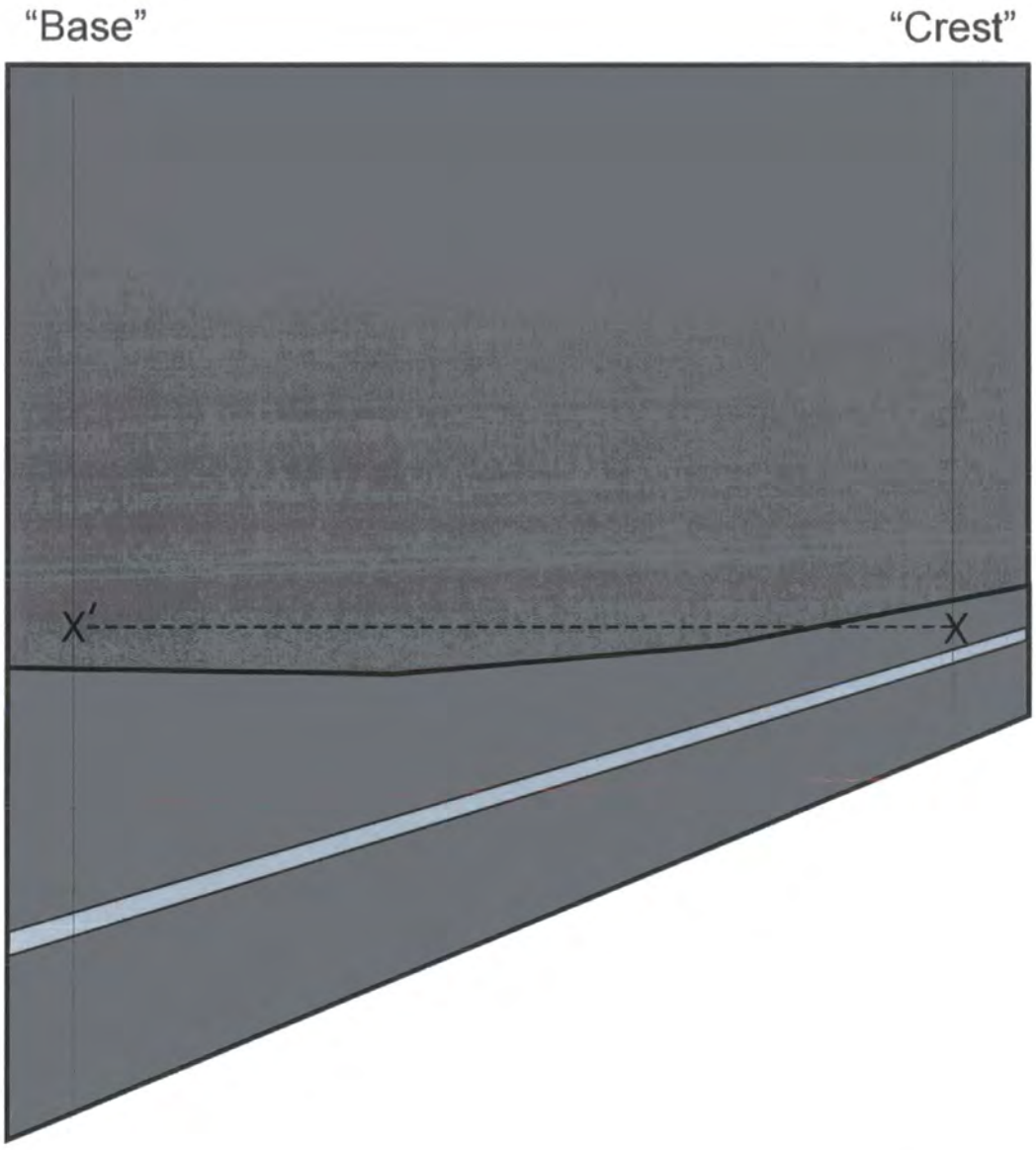

Figure 4.20 Schematic diagram showing the location of points within the 2D model, where pore pressures were extracted to calculate the amount of lateral transfer generated overpressure.

Figure 4.21a. The regression indicates that, if the amount of overpressure is high, the percentage contribution from lateral transfer is lower.

Figure 4.21b shows the same data as Figure 4.21a but with the points on the x-axis representing the actual difference in pressure between the crest of the structure and points at the same depth over the base of the structure (Figure 4.20). The conclusion drawn from Figure 4.21b is that the observed lateral transfer decrease with total overpressure increase (Figure 4.21a) is real, and does not result from the method of calculation. The simplest explanation for the trend seen in Figure 4.21a is that lateral transfer appears to be responding to the permeability through time of the system. All of the models that produce the greatest amount of overpressure represent combinations of parameters that produce shales of the lowest permeability. Consequently, although the overpressures are higher, less fluid is transferred from the base to the crest of the structure than the models which have higher permeability, lower overpressure shales.

More fluid arriving at the crest of the structure through time requires more fluid to be lost before the shales can achieve hydrostatic pressures, and results in a greater pressure enhancement by lateral transfer relative to the total amount of overpressure.

The evolution of lateral transfer can be seen in Figure 4.22, where the amount of lateral transfer is plotted against total overpressure for each of the time steps for five different models. For each of the models, the ϕ_z parameter, which controls the compressibility of the shale, has been adjusted whilst all the other parameters have been kept constant. Figure 4.22 shows that the amount of lateral transfer is roughly equal for all of the models for the time period from 20-5Ma. During this initial period of slower burial, the points are clustered together as the amounts of overpressure remain low. The profiles separate during the period of rapid burial from 5Ma to the present day when the maximum amount of overpressure is generated. For a higher compressibility shales (lower ϕ_z), a given increase in effective stress will produce a greater porosity reduction. The greater amount of compaction has two main consequences: it results in a lower porosity and permeability shale, and yields a greater amount of fluid which has to be lost before normal pressures can be achieved. Thus models with the greatest compressibility produce the largest amounts of overpressure. However, the lower permeabilities associated with these shales result in

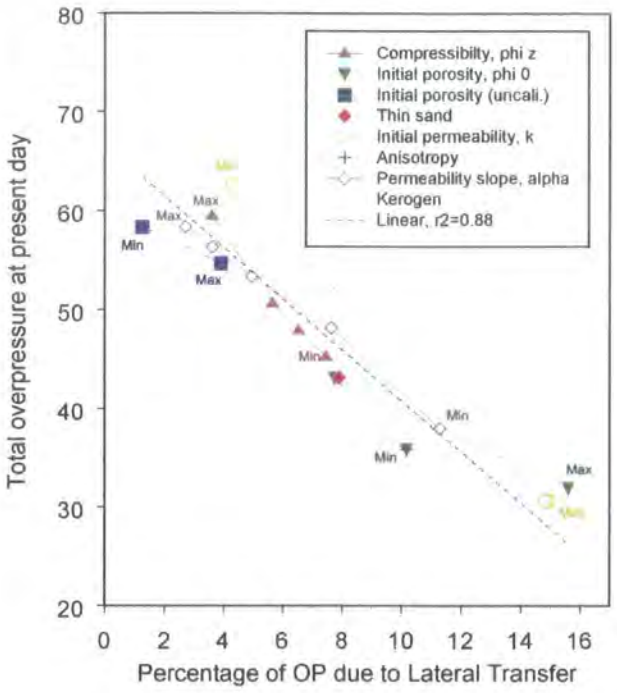

Figure 4.21a Amount of lateral transfer as a percentage of total overpressure at the crest of the structure plotted against the total overpressure at the crest of the structure for all of the models in the study.

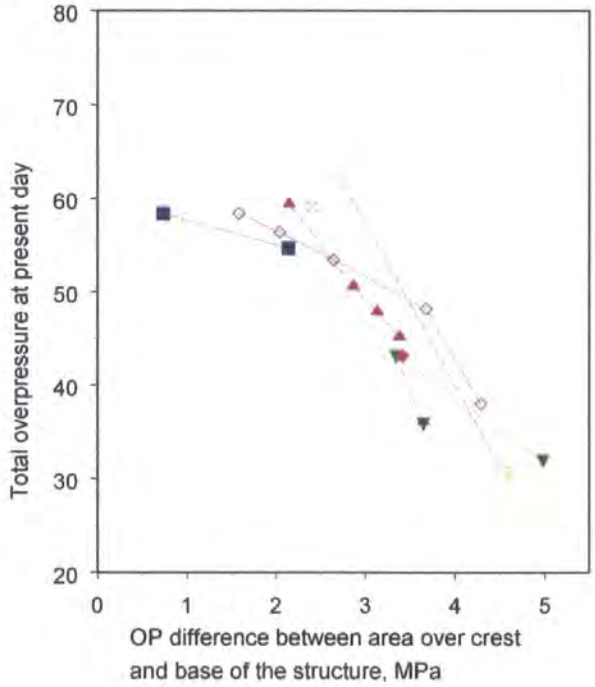

Figure 4.21b. Amount of lateral transfer at the crest of the structure plotted against the total overpressure at the crest of the structure for all of the models in the study

less flow-through-time along the aquifer units and, therefore, less pressure enhancement by lateral transfer relative to models with lower compressibility shales.

A direct comparison between the linear regression in Figure 4.21a and the 60MPa overpressure encountered below 4.65km in the well would lead to the conclusion that only ~2% or 1.2MPa of the overpressure could be attributed to lateral transfer. When making such a comparison it has to be taken into account that the models presented here were originally constructed to qualitatively simulate the overpressure generating mechanisms, and not to replicate exactly the actual stratigraphy. There will obviously be some error in the 2% value assigned to lateral transfer: scatter in the models indicates values may be anywhere between 1-8%. This scatter still does not change the conclusion that 2D basin modelling indicates that lateral transfer has not produced a significant proportion of the total overpressure.

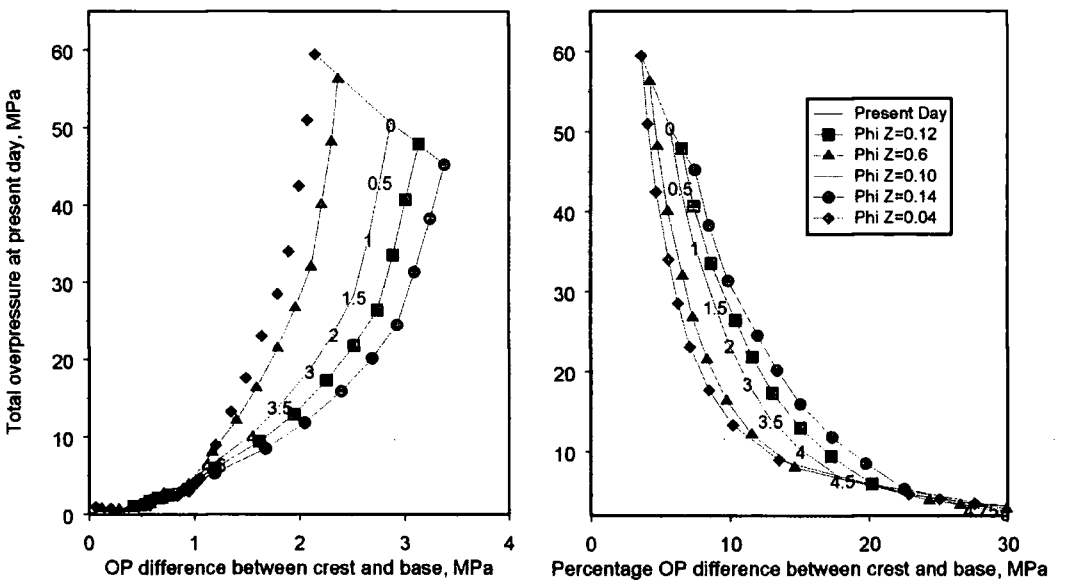

Figure 4.22 Amount of lateral transfer plotted against total overpressure at the crest of the structure for each time step in five different models. In these models, Phi Z is the normally compacted shale porosity at 3km depth.

4.6.5 Conclusions of 2D modelling analysis

- The pressure drawdown (high velocity zone) seen at the base on the structure on seismic appears to have been produced by lateral flow updip and accompanying compaction. It would appear that the higher velocity zone identified on the seismic is real and not an artefact of bad data.
- The drawdown developed during the unconformity period when fluids could escape from the top of the structure. Since the onset of post-rift sedimentation (13Ma), the porosity distribution around the dipping aquifer unit has remained roughly constant, as most of the potential for fluid flow was lost during the tilting and unconformity event.
- Lateral transfer does not appear to have produced any unloading in the sediments at the crest of the structure. Instead, fluid flow along the structure appears to have enhanced the pore pressures over the crest of the structure. This conclusion is in agreement with the results of modelling similar stratigraphy presented by Yardley (1999).
- The exact amount of enhancement is not certain, but it would appear from the models that it is less than 8% of the total overpressure above the crest of the structure (<4.5MPa). The main reason why the pressure may not been further enhanced lies in the escape of a large amount of fluid during the unconformity period. This escape reduced the potential for further flow and therefore enhancement during the post rift sedimentation.

4.7 Final conclusions

1. The overpressures encountered in Well D were produced by disequilibrium compaction as a function of very rapid burial and the high proportion of low permeability mudrocks in the succession.
2. Pressure analysis of seismic velocity data and the results of 1D basin modelling indicate that the pressure distribution around the dipping syn-rift sediments has a significant two/three dimensional component.
3. The results of 2D basin modelling simulations indicate that although flow has been focused along the dipping aquifer units throughout most of the burial history of the structure, it has not resulted in a significant pressure enhancement around the crest of the structure due to lateral transfer. The main reason why the pressures have not been enhanced more by lateral transfer stem from the mode of sedimentation during the syn-rift period (the time of maximum differential sedimentation on the structure). At this time, sediment was being eroded over the crest of the structure with the consequence that the reservoir units were only shallowly buried, and much of the extra fluid from the base of the section was able to escape. The fluid escape had the effect of reducing the overpressure at the crest of the structure before the onset of rapid post-rift sedimentation. Also, the fluid escape lowered the pressure in the shales at the base of the section, reducing the potential for further pressure reorganisation and enhancement at the crest.

Chapter 5: Case studies of three wells from the same basin in SE Asia

"Reader, Judge for yourself, how each black word
fell on my ears to sink into my heart:
I lost hope of returning to the world"
Dante Aligheri

5.1 Introduction

Wells E, F and G were all drilled within 50km of each other in the same delta in SE Asia; the locations of the wells are confidential. The objective of this part of the study was to test the validity of using a single methodology on multiple wells. The approach taken was to use one method of subdividing the shales on the basis of lithology and then apply a common set of compaction curves for use in the pressure analysis. For each of the wells, in addition to the sonic, gamma ray, caliper and resistivity logs, neutron and density logs were supplied for more detailed lithological analysis (section 2.2.1.3). In contrast with Wells A, B and C (Chapter 3), the data for these case studies was supplied in digital format, allowing analysis using Terra Station well log analysis software.

5.1.1 Data problems

One of the initial goals of this part of the study was to use the digital format data to attempt more detailed lithological analysis using the neutron and density log crossplot method (section 2.2.1.3) as well as the gamma ray approach (section 2.2.1.2). Using two approaches would allow the relative merits of each to be assessed and, if the results were similar, add weight to the conclusions drawn from using just the gamma ray approach.

Unfortunately, the planned neutron and density log analysis was limited by bad borehole conditions in Wells E and G, and by a lack of data in the shallow section of Well F. The density log seems to have been most strongly affected by the borehole conditions as illustrated for Well E (Figure 5.1) showing the caliper, gamma ray, sonic, neutron, density and resistivity log responses plotted against depth. For the interval chosen, the plot shows that there are a significant number of spikes on the density log (compared to the response of the sonic neutron and resistivity logs) where the caliper log is indicating some degree of caving. The reason for the spiked response can be attributed to the design of the density tool. The density log tool (as described in section 2.1.1.5) requires contact of the sensor pad, where the source and detectors are located, with the borehole wall to take accurate readings. Where the borehole is enlarged by caving, the sensor cannot be pressed against the sidewall, and the readings are strongly influenced by the density of the mud in the hole.

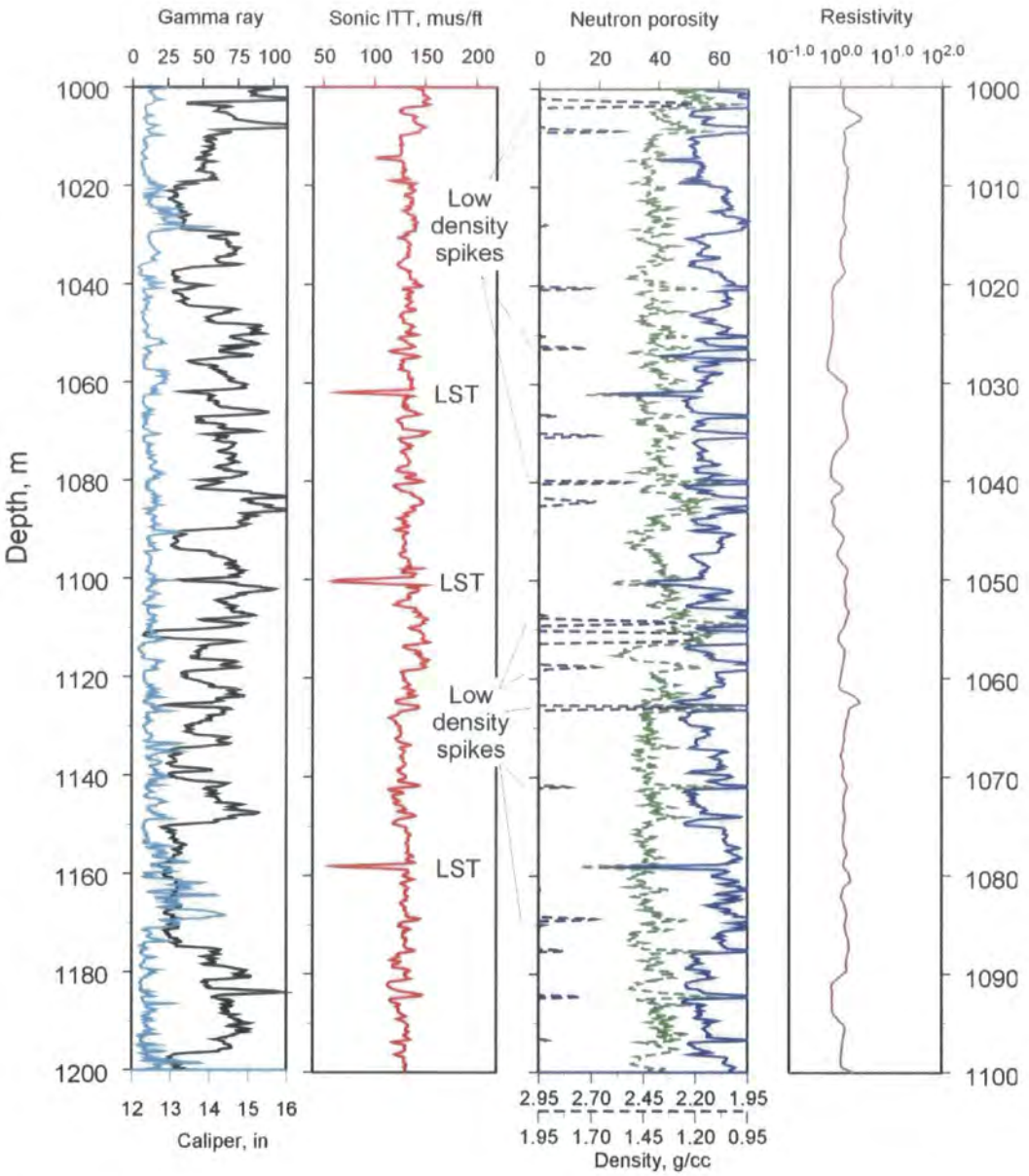

Figure 5.1 Caliper, gamma ray, sonic, neutron, density and resistivity log responses plotted against depth for Well E. LST = limestone beds.

To try and remove this effect, density values were plotted against the caliper size (Figure 5.2a) and against the roughness or rugosity of the borehole (Figure 5.2b) of Well E. The rugosity was calculated by measuring the rate of change of the borehole size on three different scales (0.15, 0.30 and 0.45m). Although the caliper logs indicate high borehole rugosity in places, no clear linkage between the density log response and borehole damage which could be used as a discriminant was identifiable (Figure 5.2). The possibility of coals affecting the density response in Well E was ruled out by Poix (pers. comm.). Consequently, it was decided that the density and neutron logs should not be used for calculation of porosity or lithology in these wells. To emphasise this point Figure 5.3 shows a neutron-density cross-plot for each of the wells together with a triangle representing the responses of the tools for pure water, sand and shale matrix components (water density = 1g/cc, neutron response = 100%; sand matrix density = 2.65, neutron response ~= 0%; shale matrix density = 2.75, neutron response = 45%). A large number of data points for wells E and G lie below the sand / water mixing line where anomalously low densities are found. In order to fit the data to calculate lithology from neutron and density log responses for Well E (Figure 5.3), it would be necessary to change the expected neutron values of water and sand to 70% and -5% respectively. As the raw logs were not available and it is not known what changes have already been made to the log response values, such a change was not justifiable, and lithology was calculated from the gamma ray tool instead.

Because of the problems with the density log, it was not possible to integrate the tool response values to calculate the overburden. Instead, the overburden was computed as described in section 2.2.3.2, by plotting all the density data against depth and visually fitting a curve over the density values as shown in Figure 2.6 for Well G. The computed curve was then integrated to calculate the overburden.

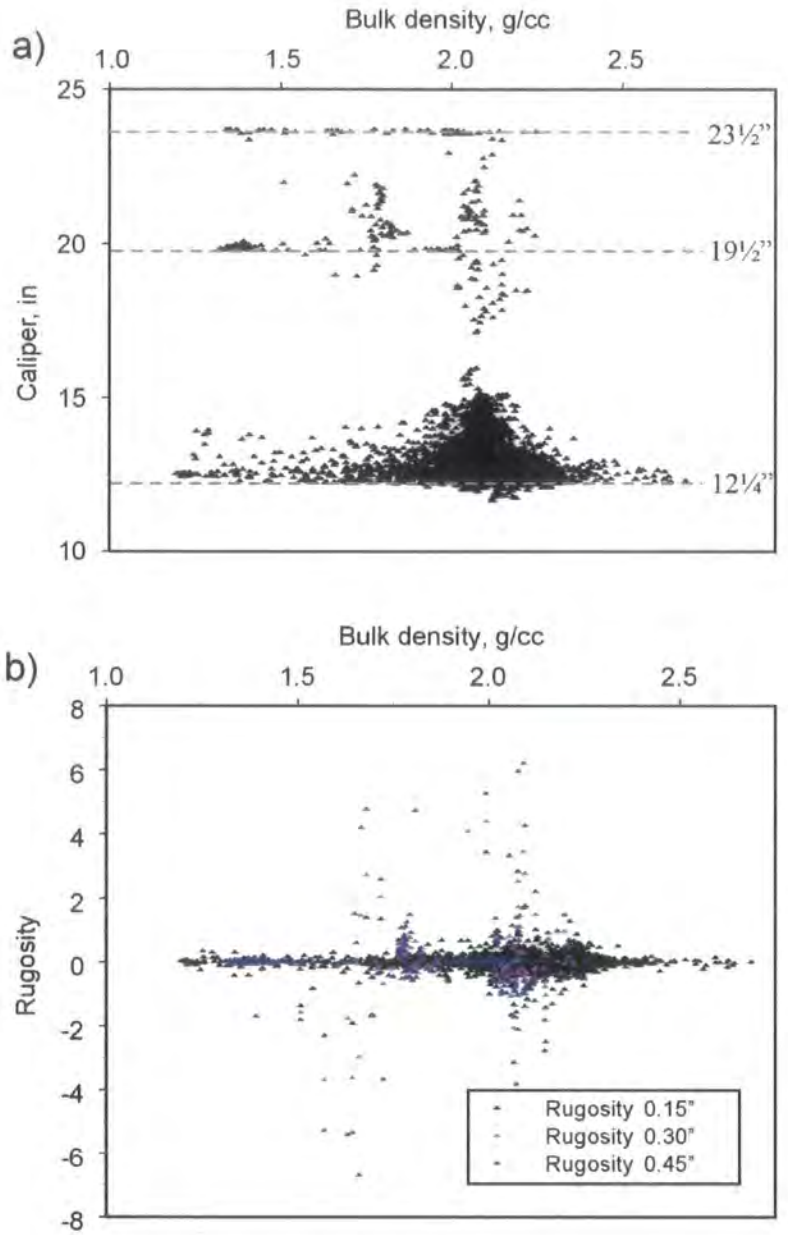

Figure 5.2 Bulk density values for Well E plotted against (a) caliper size and (b) rugosity.

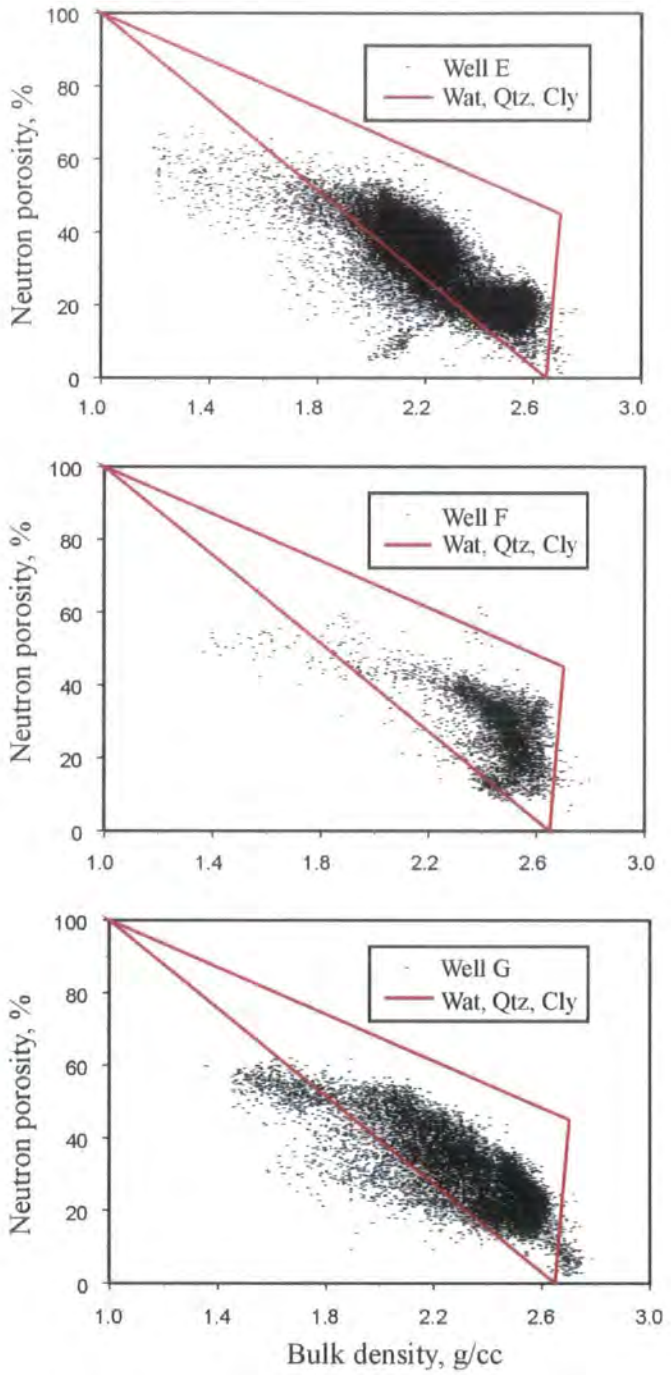

Figure 5.3 Neutron -density crossplots for Wells E, F and G.

5.1.2 Lithological analysis

As mentioned at the start of this chapter, the approach taken for the lithological analysis was to group all the shales from the three wells and subdivide each of the wells into lithology groups of the same API response. The previous approach for wells A-D has been to make separate subdivisions for each of the wells. The advantage of this approach is that it allows comparison of shales between wells. The main assumptions for using this methodology are described in section 2.2.1.2:

1. The varying API values in the mudrock units were not a function of changing clay mineralogy but simply of varying abundance of quartz and clay of near constant properties.
2. The gamma ray tools for each of the wells are responding in the same way, i.e., the tools are properly calibrated to read the correct API values.
3. There are no significant differences in mud chemistry between the wells which could affect the gamma ray response.

All the shale data for Wells E-G are plotted in Figure 5.4. The plot shows two histograms for each of the three wells. The first histogram shows the distribution of API values for the entire well (around 25,000 values), whilst the second shows the distribution of API values of the mudrock units picked for the pressure analysis (between 250-850 values). There are clear differences between the three wells in terms of the distribution of gamma responses seen in Figure 5.4.

The explanation of these differences is attributed to depositional setting within the delta. Well F is located closest to the shoreline/depositional source and has a higher fraction of clean sands (API 20-30) when compared to Well E which is located more distally in the delta and has a higher fraction of pure clays (API >70). The section encountered by Well G is located between Wells E and F and has a rather atypical gamma ray distribution for deltaic sections, comprising dominantly silty shales (API 40-60) with few "clean" sands or pure shales.

Based on the assumption that the clay mineralogies are near constant between the wells and the varying API response is due to variation in the quartz-clay ratio, the data were subdivided into groups of API values as shown by the overlain histogram in Figure 5.4.

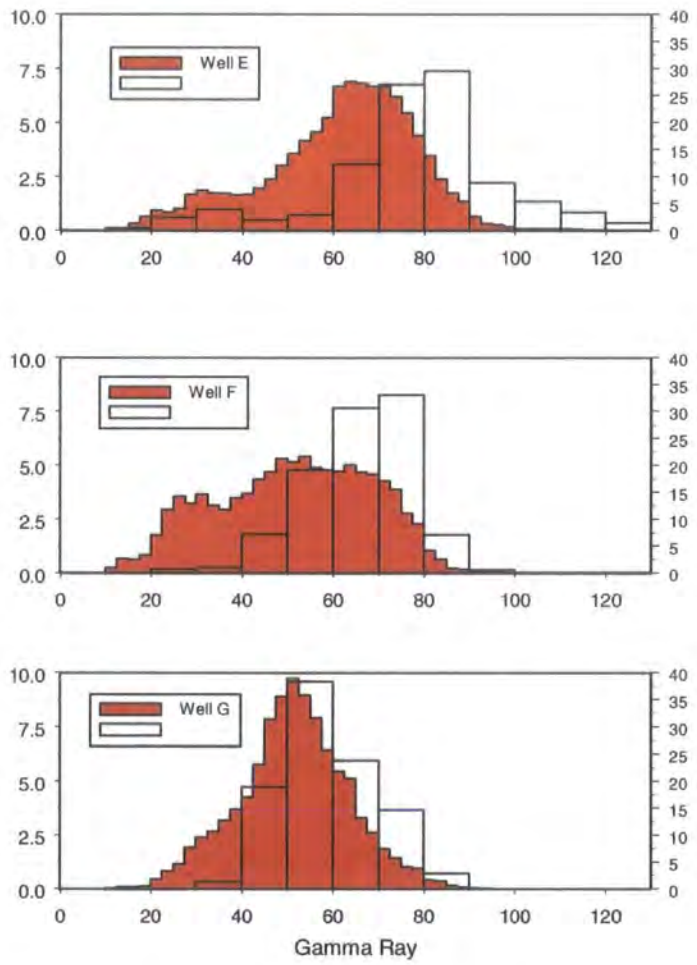

Figure 5.4: Histograms of gamma ray response for Wells E-G. Shaded area indicates inclusion of all gamma ray values from the wells. Transparent columns indicate histograms constructed from the gamma ray values of the shales selected for analysis only.

5.1.3 Compaction analysis

Following on from using the same criteria for the subdivision of the shale lithologies (section 5.1.3), it was decided to use a single suite of compaction curves to describe the compaction behaviour of the mudrocks in these wells. Justification for choosing one set of curves is taken from a plot of sonic ITT vs. depth for wells E, F and G (Figure 5.5), which shows a high degree of overlap between the three profiles down to 3km.

The plot of void ratio vs. mean hydrostatic effective stress (Figure 5.6), shows all the mudrock porosity data from the wells subdivided on the basis of gamma response (section 5.1.3), plotted along with the set of curves used to define the normal compaction profile. Because there are a far greater number of data points, individual curves were derived from a separate plot of void ratio vs effective stress for each of the lithology groups (Figure 5.7).

Implicit in fitting compaction curves, to bound the mudrock values with the lowest void ratios for a given hydrostatic mean effective stress, is the assumption that these values represent the normally compacted void ratios of the shales. Where this approach is applied to Wells A-C (Chapter 3) the number of data points is smaller, and it is to be expected that there will be less scatter compared to the larger data sets picked from Wells E-G. Any scatter which results in the selection of shales with anomalously low porosities (due to cementation etc) will have a strong influence on the form of the bounding compaction curve and, therefore, subsequent pressure calculations. Further discussion of this point is located at the end of this chapter (section 5.5).

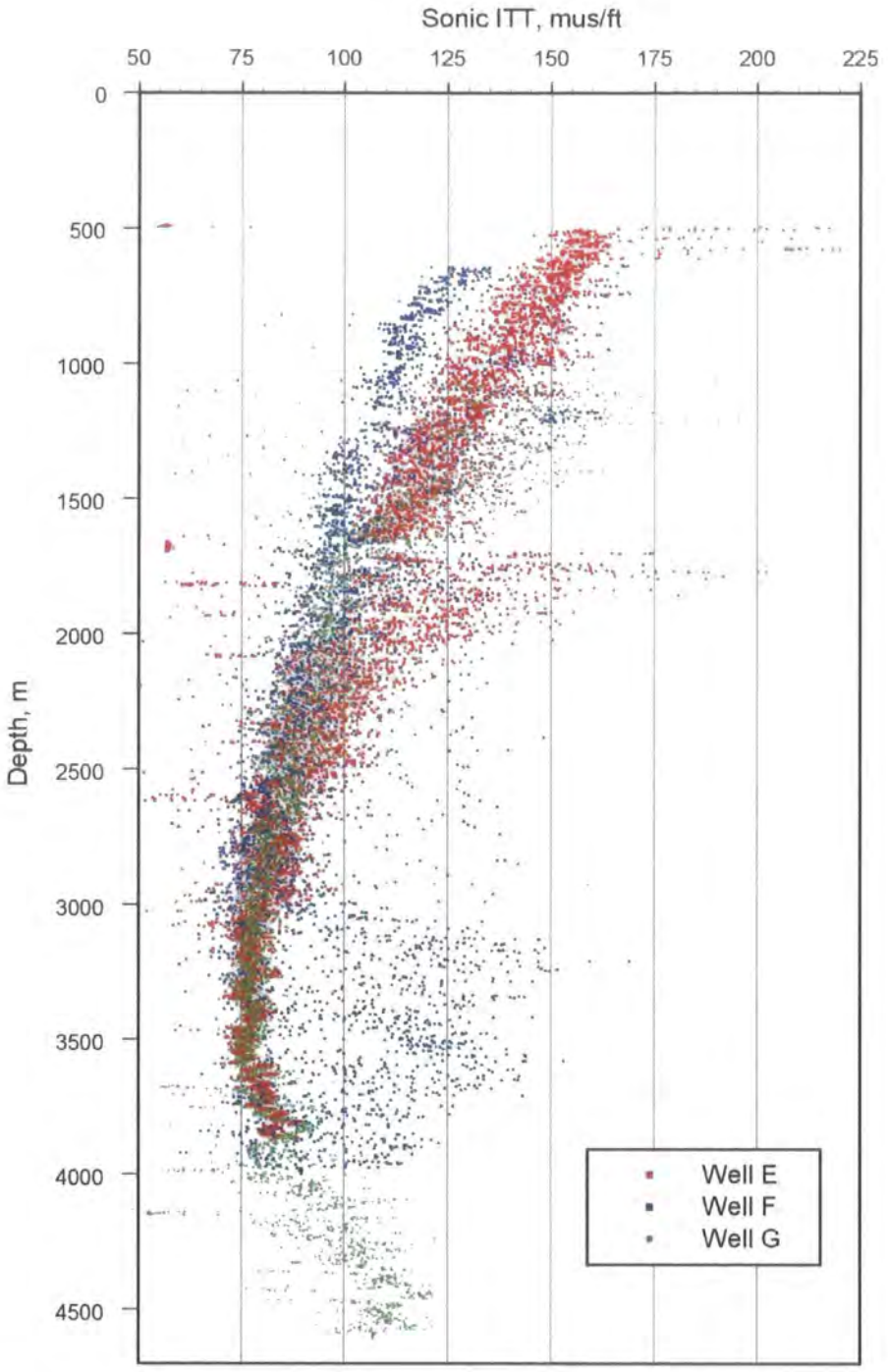

Figure 5.5 Sonic interval transit time vs depth for Wells E, F and G

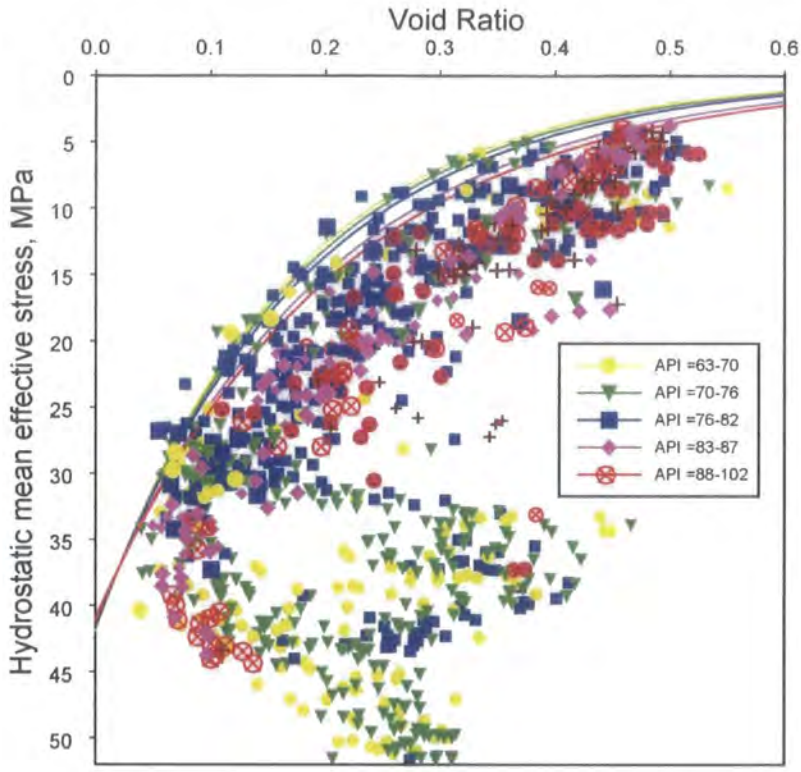

Figure 5.6 Void ratio vs mean hydrostatic effective stress for all shales from Wells E, F and G. Shales are subdivided into lithology on the basis of gamma ray response.

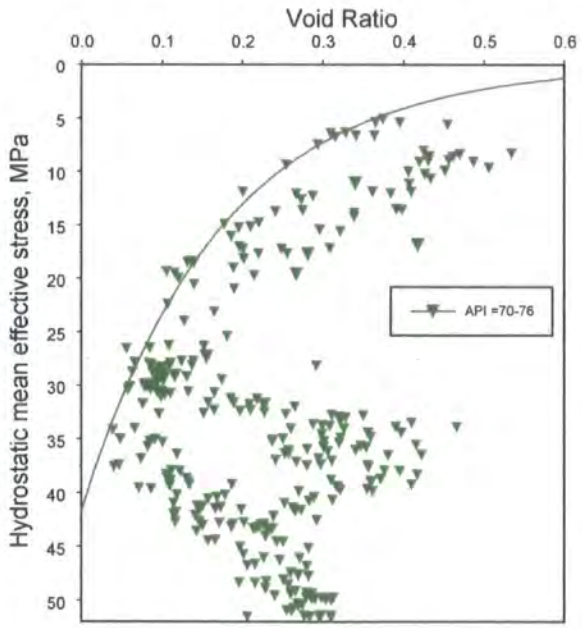

Figure 5.7 Void ratio vs mean hydrostatic effective stress a single lithology group of shales from Wells E, F and G.

5.2 Well E

5.2.1 Data sources

Data used in the pressure analysis of Well E comes from the wireline log suite. Table 5.1 summarises the wireline log data available and shows how the different parameters used in the analysis were derived.

WIRELINE LOG	CALIPER	GAMMA RAY	SONIC	RESISTIVITY ILD / MSFL	DENSITY	NEUTRON
UNITS	Inches	API	µs/ft	Ωm	g/cc	%
INTERVAL	487-3,883m					
USE OF DATA	Discrim.	Lithology	Porosity	Discrim.	Lithology Overburden	
		Overburden				

Table 5.1 Summary of wireline log data used in the pressure analysis of Well E

5.2.2 Lithology

Analysis of the natural gamma ray profile yields a simplified lithological column represented in Figure 5.8. The sequence drilled in Well E comprises very rapidly deposited sands and shales deposited in a deltaic environment between 8 Ma and the present day. The section has been subdivided into seven lithostratigraphic intervals as follows:

1. From the seabed down to 0.96km the sediments comprise interbedded shales and silts with an average bed thickness of 10m.
2. Between 0.96-1.24km the section becomes more arenaceous with sand units up to 30m thick interbedded with thinner shales and numerous coal horizons.
3. The section from 1.24-1.44km is characterised by an increase in the thickness of the shale units which are interbedded with thin silt horizons and occasional coals.
4. From 1.44-1.70km, sands and silts dominate the section with far fewer shale horizons. Burial rates for the first four intervals average around 500m/Ma.
5. Between 1.70-2.80km, there are far fewer coal horizons, and the section comprises shales interbedded with sand bodies up to 20m in thickness which constitute around 25% of the interval.

6. Between 2.80-3.35km, the number of sand bodies is further reduced to less than 5% of the section. The interval consists of shales interbedded with thin silt horizons. The section becomes slightly siltier between 3.2-3.35km.
7. The interval encountered between 3.35 and the base of the well at 3.87km shows a further increase in the clay fraction with very few, isolated sand bodies. The gamma ray response of the mudrocks across this interval is higher than for the rest of the section, corresponding to higher clay fraction, pro-delta sediments. Sedimentation rates for the last three intervals are extremely high and average around 1000m/Ma.

5.2.3 Pressure data

The actual pressure data derived from the well (RFT and DST pressure measurements and the mudweights used during drilling) are shown in Figure 5.8 plotted against depth, with hydrostatic and lithostatic pressure gradients. Hydrostatic pressure was computed assuming a brine density of 1.03g/cc.

During drilling, a total of 22 successful RFT measurements and 6 DSTs were performed between 1.21 and 3.28km, all of which show near hydrostatic pressure conditions (the maximum recorded pressure was 0.79MPa overpressure at 3.26km depth). No successful tests were carried out below 3.28km depth due to the poor porosity/permeability characteristics of the reservoirs.

The mudweight profile (Figure 5.8) shows the well was drilled using mudweights around 1.1g/cc down to 2.2km depth. Mudweights were increased slowly to 1.17g/cc at 3.42km and further increased to 1.23g/cc by 3.8km, implying only minor amounts of overpressure in the permeable units encountered in the section.

For Well E, a total of 23 LOT values were supplied for the pressure analysis. However, the values presented appear to be unusually low: from the surface down to 3.45km depth the maximum reported value is equivalent to 1.43g/cc, with many values nearer to 1.1g/cc. The lowest value from the other wells in this study is 1.65g/cc. For this reason it is proposed that these very low values are either formation integrity tests (section 2.1.1.5) or that they represent pressure values where mud is lost into the formation at values below the fracture pressure of the sediment. The proposed mechanism for the apparent loss of mud into the formation is that the increasing mudweight during the LOT induces deformation of poorly consolidated

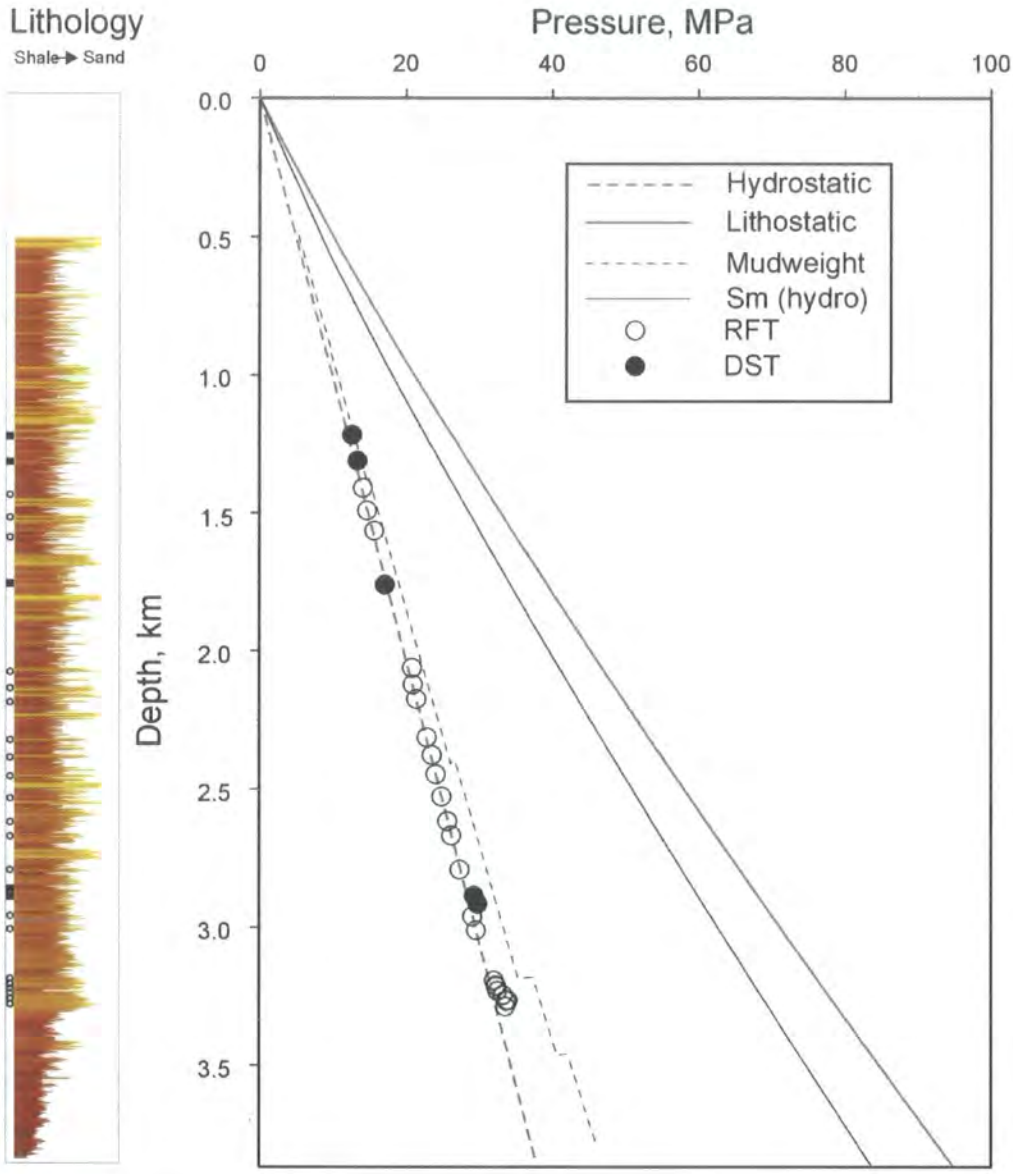

Figure 5.8: RFT, DST and mudweight pressure values for Well E plotted together with the hydrostatic, lithostatic and mean hydrostatic pressure profiles and a schematic lithological column.

sediments, in particular sand bodies, a process often referred to as "ballooning". As the interpretation of this data was that the values presented are significantly lower than the actual minimum stress values, they are not used in the pressure analysis.

5.2.4 Pressure analysis

Void ratios for individual mudrock beds were plotted against mean hydrostatic effective stress as seen in Figure 5.9. The plot shows that with the exception of the interval between 15 and 20MPa effective stress, the void ratios decrease with increasing effective stress down to around 35MPa effective stress (equivalent to ~3.4km). Below this depth the void ratios increase slightly to values approaching 0.12 at 3.86km. The bounding curves shown in Figure 5.9 are derived from the data from all three wells, as described in section 5.1.

The void ratio values for the mudrock beds in Figure 5.9 were projected up to the normal compaction curves for their respective lithologies to estimate the mean effective stress. The resulting estimates of the pore pressures present are plotted in Figure 5.10 together with the direct measurements of pore pressure taken in the sands and the mudweights used to drill the well.

The pore pressures estimates in Figure 5.10 show that between 0.5 and 1.7km the pore pressure increases in the mudrocks at a rate slightly less than the rate of lithostatic stress increase. Below 1.7km depth, the computed pore pressures increase considerably as the sonic porosities are up to 10% higher than for the overlying units. The caliper log for this part of the well indicates caving may have affected the sonic responses (some of the peaks on the sonic transit time reach values of 170μs/ft which are approaching the transit time for the mud in the borehole). Values where the borehole was damaged were not included in the analysis, which is why there are fewer data points between 1.8 and 3.5km depth. The remaining data points still indicate that the porosities and pore pressures are high in the shales. The caving may therefore be a result of drilling through this section with mudweights considerably below the formation pressures.

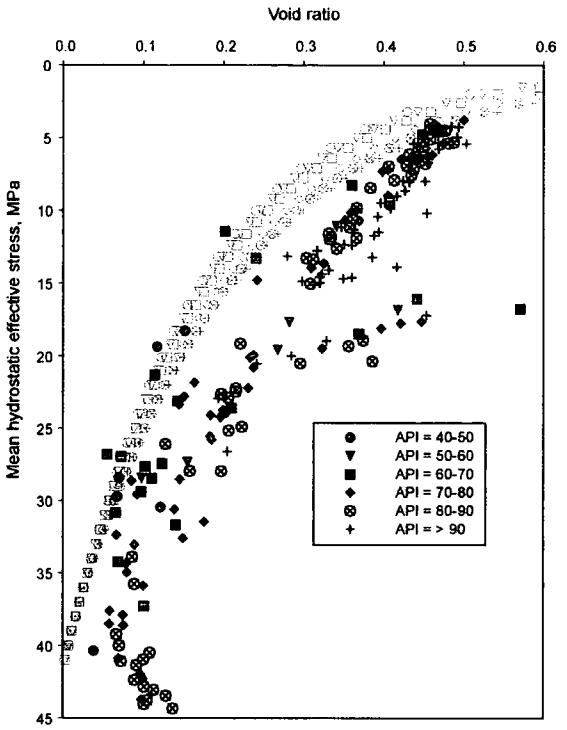

Figure 5.9: Void ratio vs mean hydrostatic stress for shales from Well E subdivided on the basis of gamma ray response, plotted together with their derived normal compaction curves.

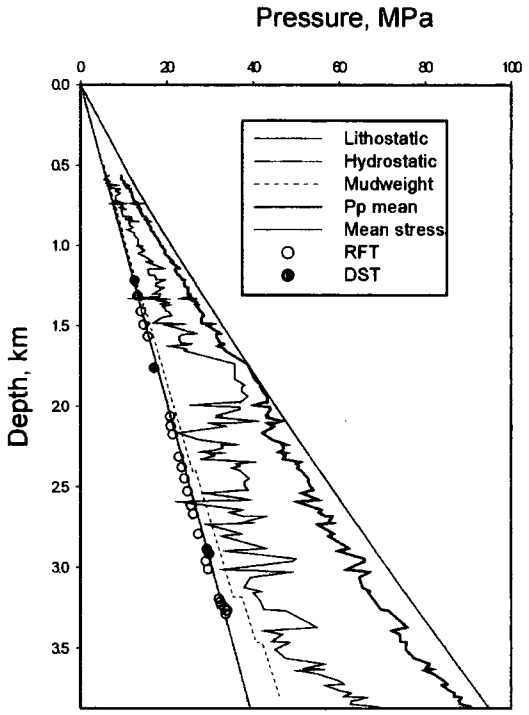

Figure 5.10: Estimates of mudrock pore pressure and mean stress values for Well E plotted against depth together with RFT, DST and mudweight pressures in the borehole.

Between 2.2km-3.5km the overpressure estimates from the sonic vary between 5 and 20MPa, with maximum values continuing the same trend of increasing pore pressure as the interval between 0.5 and 1.5km.

Between 3.5 and TD at 3.87km, the pore pressure estimates are seen in to increase linearly to ~35MPa overpressure where there are fewer sand bodies. The driller's comments accompanying the RFT and DST measurements all indicate that the sands are across this interval "tight" i.e., they have very low permeabilities, preventing any direct pressure measurements.

The interpretation of the pore pressure analysis in the shallow section between 0.5-1.7km is that rapid burial of mudrocks has resulted in the shallow onset of overpressure. The higher pressure estimates between 1.8 and 2.2km coincide with a decrease in the amount of sand in the section (only one DST was performed across this interval compared with five measurements between 1.2-1.8km). The pore pressures through this interval may represent the maximum amount of overpressure generated by the rapid burial rates, where there are fewer permeable aquifer units which could otherwise allow a fraction of the overpressure to dissipate.

Considerable scatter in the values is seen over the interval from 2.2 to 3.5km where shales are interbedded with sand bodies. All pressure measurements across this interval indicate hydrostatically pressured sands, where overpressure has bled off from some of the adjacent shales, whilst others remain more highly overpressured, presumably on account of their of lower permeability. Evidence to support the existence of highly overpressured shales interbedded with normally pressured sands was gathered in a nearby well where the mudweight was finely adjusted to balance the connection gas values measured during drilling (Grosjean pers. comm.). At ~3km depth, mudweights as high as 1.9g/cc were required to balance connection gas values (an indicator of pore pressure) in shales separated by less than 5m from normally pressured sands.

Below 3km, the driller's comments accompanying approximately 50 attempted RFT measurements strongly suggest tight reservoirs; there are no direct measurements below 3.28km. This inferred reduction in reservoir permeability precedes the estimated pressure increase to approximately 35MPa overpressure in the mudrocks below 3.5km (Figure 5.10). Although all the direct pressure measurements in Well E indicate near hydrostatic conditions, in one well drilled within 5km of Well E an RFT

test measured 20MPa overpressure at 3.45km depth, and in another nearby well, a severe kick was experienced at ~3.93km depth which represented 31MPa overpressure. These pressures may represent sands which were isolated hydraulically from the surface during burial and have kept the same pressure the encasing shales.

5.2.5 Conclusion

1. The results of pressure analysis indicate that shales in Well E between 0.5-3.5km are overpressured by disequilibrium compaction. Direct measurements of pore pressure across the same interval indicate that lateral and vertical connectivity in the sands maintains near normal pore pressures.
2. The amount of overpressure present in the shales appears to be strongly influenced by the degree of separation from a normally pressured sand unit which can allow some of the overpressure to dissipate.
3. Below 3.5km depth the pore pressure estimates indicate that there is a transition zone to higher overpressures generated by disequilibrium compaction. The base of the transition zone is not encountered in this well.
4. Although no direct measurements of pore pressure were made below 3.28km, measurements taken in nearby wells indicate that the pressure in the sands is above hydrostatic, and due to isolation may be in equilibrium with the shales.
5. There are strong similarities between the results of the analysis of Well E and the conclusions drawn from Well A (section 3.2.4, section 7.1).

5.3 Well F

For the pressure analysis of Well F, a slightly different picking strategy was undertaken (discussed in Chapter 2.3.1.2), i.e., all shale points were picked as long as the caliper and resistivity logs were indicating that the hole was in good condition and that the log values could be relied upon as shown in Figure 2.9. The result is a total of over 850 data points where, in other wells, borehole conditions have restricted the amount of data to between 100-400 points. This change in strategy has implications for the pressure estimation, which is discussed in section 6.3.1, as well as within this section.

5.3.1 Data sources

Data used in the pressure analysis of Well F comes from the wireline log suite. Table 5.2 summarises the wireline log data available and shows how the different parameters used in the analysis were derived.

WIRELINE LOG	CALIPER	GAMMA RAY	SONIC	RESISTIVITY ILD / MSFL	DENSITY	NEUTRON
UNITS	Inches	API	µs/ft	Ωm	g/cc	%
INTERVAL	635-3,998m				2,700-3,998m	
USE OF DATA	Discrim.	Lithology	Porosity	Discrim.	Lithology Overburden	
		Overburden				

Table 5.2 Summary of wireline log data used in the pressure analysis of Well F

5.3.2 Lithology

Analysis of the natural gamma ray profile yields a simplified lithological column represented in Figure 5.11. The sequence drilled in Well F comprises sands and shales deposited between ~14Ma and the present day at an average rate of 285m/My, the section has been subdivided into eleven intervals as follows:

1. From the surface down to 602m, the section is dominated by sands interbedded with shales deposited between 0 and 7Ma, burial rates average less than 100m/Ma for the interval, with burial rates for the last 3Ma no greater than 25m/Ma.
2. The section between 602-1160 is dominated by sandbodies up to 30m thick, interbedded with slightly thinner shale intervals deposited at rates between 200-400m/Ma.

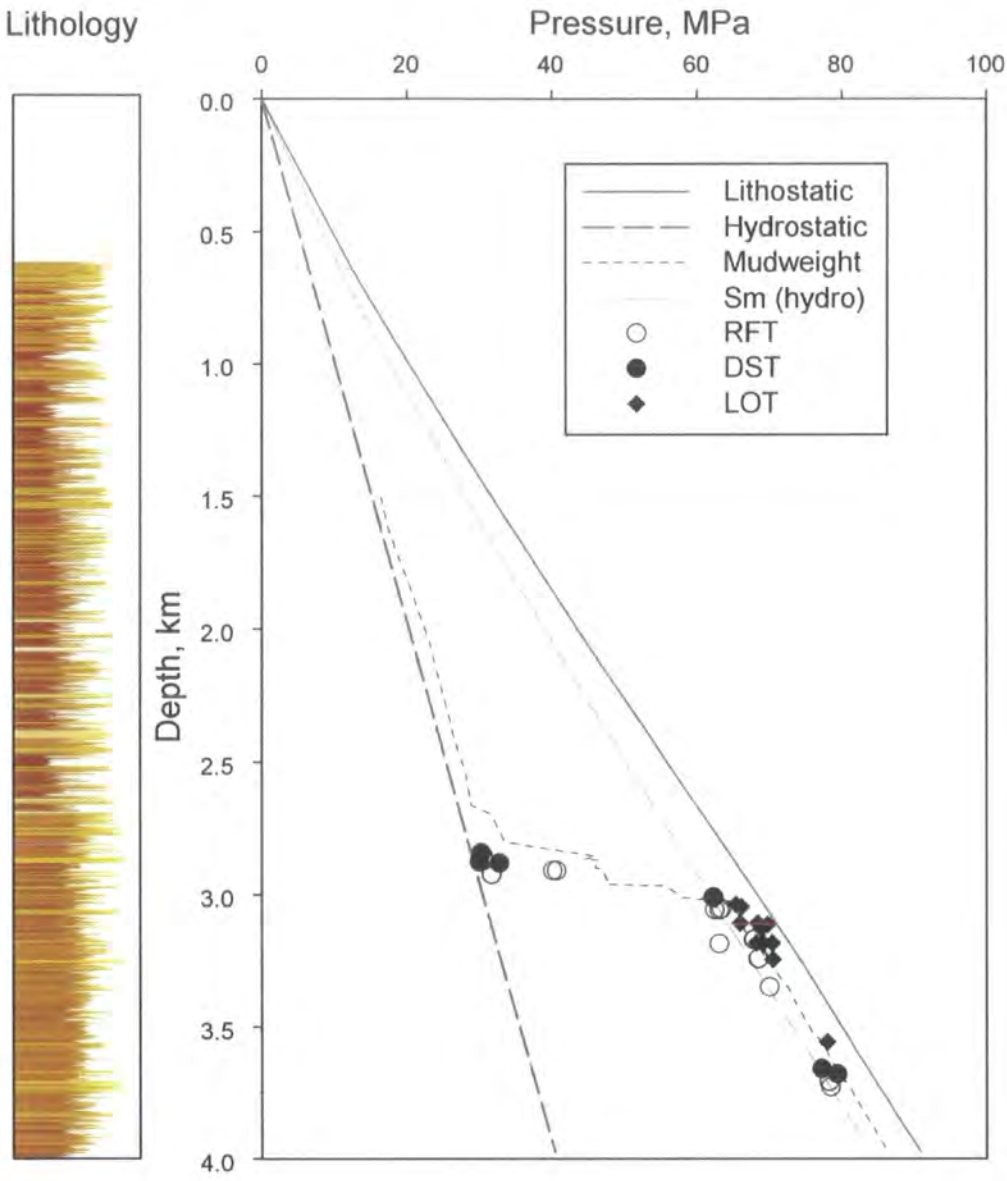

Figure 5.11: RFT, DST, formation integrity test and mudweight pressure values for Well F plotted together with the hydrostatic, lithostatic and mean hydrostatic pressure profiles and a schematic lithological column.

3. Between 1160-1480m the section becomes more argillaceous with thicker shale units deposited more rapidly at up to 2000m/Ma. There is a slight decrease in the API response of the shales towards the base of the section.
4. The interval from 1480-1560m consists of 80m of sand bodies between 10-30m thick separated by thin shale beds; the burial rates for this interval exceed 1500m/Ma.
5. Shale units interbedded with sands and occasional thin silty intervals are found between 1560-1830m, deposition rates average around 800m/Ma.
6. The section from 1840-2140m contains four 20m thick sand bodies separated by thinner interbeds of shale and silt deposited at around 800m/Ma.
7. The section from 2140-2700m comprises a 120m section of thin clay and sand interbeds followed by a 240m interval of sands (averaging over 20m thick) separated by thin clay and silt interbeds. The base of this interval is more argillaceous consisting of 200m of thin shales and silts with only one 20m thick sand body present at 2640m. Burial rates for this interval average around 1000m/Ma.
8. Below 2700m, the log character changes and the section is dominated by thinner more silty shales. Between 2700-2900m thin silts are interbedded with sands for the first 100m followed by a section comprising largely silt with a single 20m thick sand body at the base of the interval. This interval was deposited at around 1500m/Ma.
9. From 2900-3100m, 40m thick sections of silt/silty-shale interbeds are separated by thinner sand bodies.
10. Thin beds of silt dominate the section between 3100-3590m with occasional thin sands and shales.
11. Between 3590 and the base of the well at 3,987m there is an increase in the number of sand bodies separating the interbedded silts and sands. There is a slight increase in the API response of the silty shales accompanying an increase in the bed thickness towards the base of the section. Burial rates for the last three intervals average at around 500m/Ma.

5.3.3 Pressure data

The actual pressure data derived from the well (RFT and DST pressure measurements, LOT values and the mudweights used during drilling) are plotted in Figure 5.11 against depth, with the hydrostatic and lithostatic pressure gradients. Hydrostatic pressure was computed assuming a brine density of 1.03g/cc.

DST and RFT measurements were taken between 2.85 and 3.87km. The first six measurements between 2.85 and 2.87km show near hydrostatic pressures before a rapid transition to values within 4MPa of lithostatic stress values at 3km. Measurements below this depth remain within 5MPa of the lithostatic stress down to 3.87km.

As Well F is one of a number of wells drilled on the same structure, the increases in mudweight below 2.6km depth (Figure 5.11) represent the pressure profile planned in anticipation of actual formation pressure increases. This observation explains why the mudweights are increased ~200m before the measured onset of overpressure interpreted from the RFT and DST data. Between 2.65-3.0km the mudweights are between 5-15MPa greater than the direct pressure measurements which would have been chosen to allow safe control of any unexpected pressure increases (Swarbrick, pers. comm.). For this reason the mudweight values below 2.6km are not considered an important source of pressure information in the pressure analysis. The near normal mudweights above 2.6km may underestimate the pore pressures in the mudrocks; however, it is likely that they are close to the actual pressures in any of the permeable units in the shallow section.

Between 3.0-3.5km a total of 14 LOT values are reported, all of which are within 1-3MPa of the direct measurements of the pore pressure and the mudweights used to drill the overpressured section. In contrast with the data from the other wells in this study, all of the LOT measurements in the overpressured section lie below the computed values of lithostatic pressure. If these represent the actual minimum stress values, then the interpretation is that the minimum principal stress in the highly overpressured section is horizontal. Another interpretation of these data stems again from the fact that a number of wells had already been drilled on this structure. LOT values from these earlier wells would have been used to define the values of minimum stress around the structure. When it came to drilling Well F, rather than induce fracturing of the formation which could result in permanent damage to the formation

and an unstable drilling environment, it is likely that the values represent formation integrity tests (section 2.1.1.5). In this way, the pressures would have been increased to a defined maximum pressure, without mud loss, considered high enough to continue drilling ahead safely. For the analysis of this well, both interpretations of the LOT values have been considered and are discussed in sections 5.3.4 and 6.3.3.2

5.3.4 Pressure analysis

The void ratios calculated from the sonic log using [5] for individual mudrock beds are plotted against mean hydrostatic effective stress together with the normal compaction curves described in section 5.1 (Figure 5.12). Between 5-30MPa effective stress (equivalent to 0.75-2.65km depth) the majority of the void ratios decrease parallel to the normal compaction curves. Between 19.5-28MPa some of the mudrocks have void ratios up to 0.25 greater than the average values for that depth.

At around 29MPa (equivalent to 2.7km depth) there is change in the lithology of the mudrocks to lower gamma ray API values, indicative of siltier formations. The void ratios of the shales between 29-30 MPa show less scatter than the overlying interval with nearly all the void ratios between 0.1-0.2.

Below 31MPa, the void ratios increase rapidly to values which average around 0.35 between 32-40MPa (3.1-3.6km), before decreasing again down to values of 0.2 at 43MPa (3.95km).

The estimates of pore pressure computed from the void ratios (Figure 5.13) indicate that between 0.5-1.8km depth the majority of the mudrocks are overpressured by between 5-12MPa, with a large number of the data points within 5MPa of the computed values of lithostatic stress. There is considerably more variation in the pressure estimates between 1.8-2.7km, with some values still within 5MPa of lithostatic (~30MPa overpressure), whilst a larger number of points are overpressured by between 0-15MPa. The mudweights used for this section indicate that the well was drilled with near normally weighted muds (section 5.3.3). I infer that the sands in this section are in hydraulic communication with the surface, and therefore normally pressured. As in the shallow section of Well E, these sands are allowing some of the

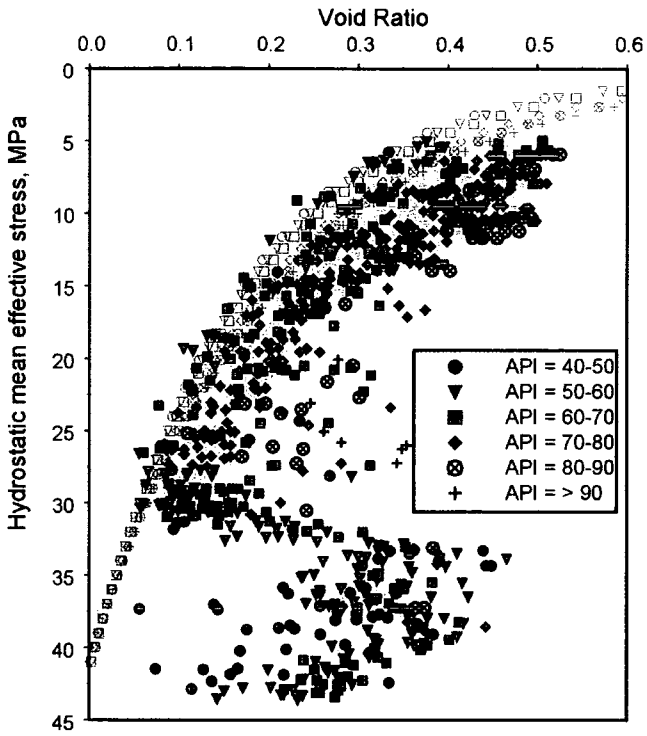

Figure 5.12: Void ratio vs mean hydrostatic stress for shales from Well F, subdivided on the basis of gamma ray response, plotted together with their derived normal compaction curves.

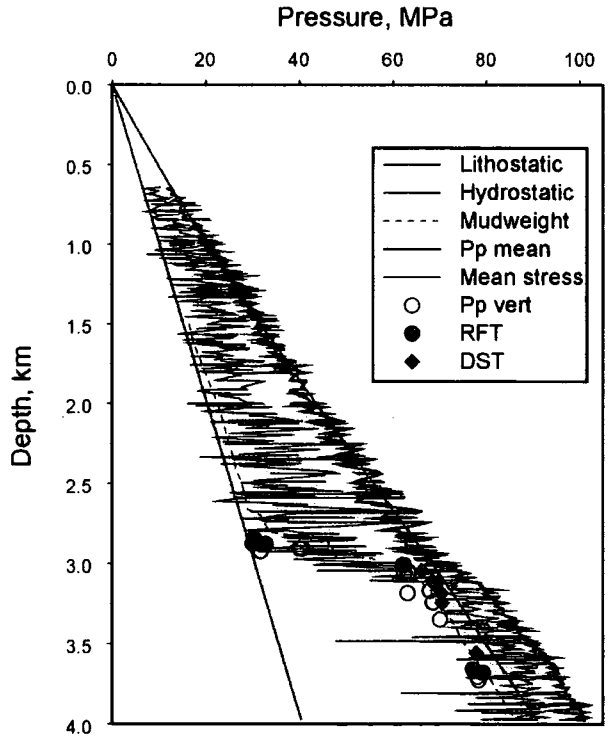

Figure 5.13: Estimates of mudrock pore pressure and mean stress values for Well F plotted against depth together with RFT, DST, LOT and mudweight pressures in the borehole.

overpressure to bleed off from the mudrocks whilst other shales remain more highly overpressured.

At around 2.75km depth, there is a decrease in the maximum estimates of pressure and the degree of variability of the pressure estimates compared with the overlying section (1.8-2.7km). This decrease coincides closely with the six near-normally pressured RFT and DST measurements (2.85-2.87 km depth) and precedes the narrow transition zone to very high overpressure detected in the sands (between 2.87-3km). The pressure estimates in the mudrocks across the interval from 2.7-3km increase rapidly, following the profile defined by the direct measurements of pore pressure.

Below 3.1km the estimates of overpressure from the mudrock void ratios reach maximum values between 2-8MPa greater than the derived lithostatic stress values. Between 3.1 and TD at ~4km, the majority of the estimates remain between 0-8MPa greater than the lithostatic stress values, running parallel to the rate of increase of pressure defined by RFT and DST measurements below 3.1km. The corresponding estimates of mean stress across this interval indicate that the mean stress averages around 10MPa greater than the estimates of vertical stress.

5.3.5 Problems with pressure estimates

The estimates of overpressure in the mudrocks below 3.1km (Figure 5.13) appear unreasonably high for three reasons:

1. Pore pressures in excess of lithostatic stress are uncommon in sedimentary basins and tend to be confined to active compressional regions such as accretionary prisms (Moore, 1992; Westbrook, 1992) or thrust belts (Traugott, pers. comm.). Although some compression has accompanied sedimentation in this region, no pressures in excess of lithostatic stress have been reported.
2. If the LOT/FIT values are accurate estimates of the minimum stress magnitude, then the pore pressure estimates are ~12MPa in excess of fracture pressure (slightly lower if the LOT values represent formation integrity tests and underestimate the actual stress values). For pore pressures to remain significantly higher than minimum stress would require the sediments to have very high tensile strengths. Evidence from the wireline logs suggests that the sediments are poorly consolidated shales and silts with high porosities (Figure

5.12). It is highly unlikely that these sediments could sustain pore pressures in excess of fracture pressure for any geologically significant period of time.

3. The computed pore pressures are around 15MPa greater than the direct measurements of pore pressure in the sand bodies across this interval. Significant differences such as this one are uncommon in highly overpressured environments (Swarbrick, pers. comm.).

5.3.6 Origin of pressure overestimation

Following on from the conclusion that the pore pressure estimates are too high, one of three reasons could explain why the analysis produced these results.

1) The first of these factors is the form of normal compaction curves chosen. As with all the wells in this study, compaction curves have been derived by fitting a bounding curve to the lowest void ratios for a given mean hydrostatic stress. This approach has produced seemingly reasonable results for the other wells in this study, where it was applied to smaller datasets. For Well F, a total of 806 data points were picked from the wireline logs as described in section 2.3.1.2, which has produced a void ratio vs mean hydrostatic effective stress plot (Figure 5.12) that looks significantly different from the plots for the other wells in this study (e.g., Figures 3.3, 3.8 and 3.15).

Normal compaction curves for Well F were fitted in the same way as for all the other wells in this study. As well as the consistent trend in the minimum porosity values in Figure 5.12, it is possible to discern another suite of normal compaction curves lying to the right of the first set. Fitting curves to these data instead of the bounding solution, would mean that for a given mudrock void ratio, its computed effective stress values would be higher and therefore the corresponding pore pressure and mean stress estimates would be lower.

For this explanation to be valid would imply that some of the sediments in the shallow section have anomalously low porosity values for their effective stress. One possible reason for such behaviour could originate from the selection of greater numbers of data points from the well log and the inclusion of data points close to aquifer units which have become cemented. Alternatively some normally pressured mudrocks may have lost extra porosity by the process of creep compaction during the last 2Ma whilst the sediments have been at almost constant effective stress.

2) The second possible reason for the overestimation relates to the use of the Breckels and van Eekelen (1982) equation for estimating horizontal stress magnitude from depth and overpressure, in which leakoff and pore pressure data were taken from a number of wells in offshore Brunei with horizontal stresses equalling ~0.8s_v in the shallow, normally pressured section. A simple extrapolation of the trend of horizontal stress increasing with overpressure yields values of s_h and s_m in excess of s_v (section 6.3.3.1). Whilst this may be the case in other wells where there are compressive forces operating at depth, below 3km in well F the reported leakoff test values indicate that the minimum horizontal stress, s_h, is less than the vertical stress, s_v. Therefore, a simple extrapolation of the Breckels and van Eekelen (1982) relationship is not valid for this well.

To accurately compute the pore pressures in this well from mudrock porosity would require the derivation of a new relationship between pore pressure and horizontal stress for this part of the basin. Unfortunately, not enough well data were available to allow a new relationship to be made. A further discussion of this point is made in section 6.3.3.1.

3) A third possible reason for the pressure overestimation is that the calculations depend upon void ratio values calculated from the sonic log. To check that the void ratios calculated from the sonic log response below 2.7km (Figure 5.12) are indeed representative of very high porosity values and not the presence of gas or fractures, Figure 5.14 shows a plot of the sonic, density and neutron log responses together with values from the resistivity and gamma ray logs between 2.5-3.4km depth. The plot shows that there is a significant increase in response from all three logs, while at the same time no significant change in the resistivity or gamma ray response. As the magnitude of porosity increase is the same for all three logs, it is proposed that the sonic response represents a genuine increase in porosity. The lack of response from the resistivity logs indicates that neither gas nor fractures are responsible for the increased sonic log response. (Neither of these two effects would be expected to increase the porosities inferred from the neutron and density logs as much, (cf. Well B below 2.6km, section 3.6)).

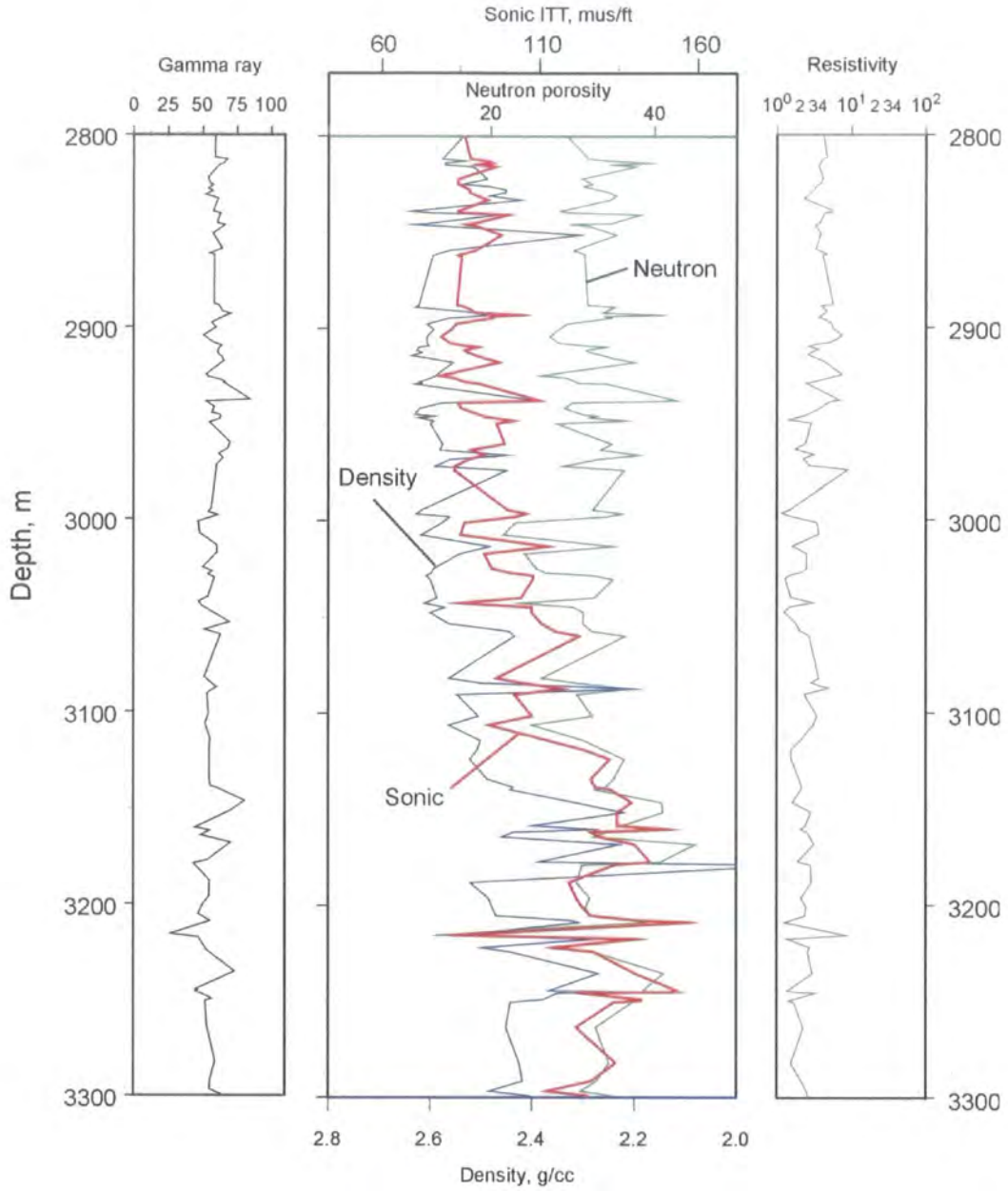

Figure 5.14 Sonic, density and neutron log responses vs depth for shales from Well F plotted along with their gamma ray and resistivity log responses.

5.3.7 Pore pressure calculation from leakoff test data:

Another approach to understanding the pore pressure below 3km depth in Well F is to work backwards from the direct measurements of minimum stress (s_h), and pore pressure (p_p). At 3.245km depth a leakoff test estimated a minimum stress, (s_h) of 70.5MPa, the corresponding estimate of vertical stress, (s_v) is 75MPa and the RFT fluid pressure measurement taken in the adjacent reservoir unit is 68MPa (Figure 5.11). The horizontal effective stress (σ_h) in the sediments is therefore 2.5MPa ($\sigma_h = s_h - p_p$). Assuming that the maximum horizontal stress (s_H) is only slightly greater than the minimum horizontal stress (s_h), say 3MPa, then the mean stress (s_m) is ~72MPa and the mean effective stress (σ_m) is 4MPa.

If all of the overpressure encountered at 3.25km was produced by disequilibrium compaction alone, then the shales would be expected to have a very high porosity corresponding to 4MPa mean effective stress. The shale unit closest to the depth where the leakoff test and RFT measurements were performed has a porosity value of 0.28 (void ratio 0.39). This value corresponds to a mean effective stress of 4.15MPa on the curve for shales of API 50-60 (Figure 5.12) and is therefore within 0.5MPa of the predicted mean effective stress derived from the LOT and RFT results. Within 10-15m of the direct measurements of stress and pore pressure, all other shales units have porosities differing by less than 5% of the value for the mudrock unit described above, indicating that all or nearly all of the encountered overpressure was generated by disequilibrium compaction. At 3.57km depth, a leakoff test indicates that the minimum stress is 76MPa, the lithostatic stress is 81MPa and the mudweight used is within 1MPa of the leakoff value (mudweights below 3km depth agree very well with the direct measurements of pore pressure as seen in Figure 5.11). The porosities in the mudrocks are only slightly lower than in the units around 3.25km, and the corresponding estimates of mean effective stress vary from 4-11MPa. Whilst the difference between the measured effective stress and the values computed from the porosity is small, the measured effective stress values implies that some unloading mechanism has contributed to the pore pressure.

There is a possibility that the mean stress is slightly higher in the highly overpressured than the values reported above as mentioned in section 5.3.3. If the LOT values reported are in fact representative of formation integrity tests, then the

values of minimum, and therefore mean stress, are slightly higher than the values reported. If the LOT values reported are slightly less than the actual minimum stress, then the implication is that the mean stress, and therefore the mean effective stress in the sand bodies where pressure measurements are taken are higher than the values reported earlier in this section.

To take the example of the pressure measurement at 3.245km, the RFT measurement was 68MPa, the LOT value was 70.5MPa and the computed mean stress was 72MPa, resulting in a mean effective stress of 4MPa. If the actual minimum stress is slightly higher than the reported value (say for example it, and the maximum horizontal stress, is equal to the value of lithostatic stress at 75MPa, then the mean effective stress will be 7MPa. As the effective stress estimated from the porosity of the mudrocks is only 4.5MPa, then the implication is that the pore pressure due to disequilibrium compaction in the shales is slightly higher (~2.5MPa) than the pressure measurement in the sand body. Actual mean stress values greater than 75MPa would imply that the shales have still higher pressures than the sands.

5.3.8 Conclusion

The interpretation of Well F is that from the surface down to 2.7km disequilibrium compaction has produced overpressure in many of the shales as a function of low permeability and rapid burial rates. Sands in this shallow section are normally pressured and have allowed overpressure to escape from some of the mudrocks. Below 2.7km, following a reduction in sand fraction in the section, there is a rapid transition to very high overpressures. The rapid burial rates and high porosities of the sediments indicate that disequilibrium compaction is the most likely cause of the overpressure. These very high porosity values are consistent a shallow onset of overpressure. Estimates of the pore pressure using the leakoff test data combined with porosity vs. mean effective stress analysis indicate that all of the overpressure encountered in the highly overpressured zone below 3km could have been produced by disequilibrium compaction, with the possibility that the pore pressures in the shales are slightly higher than in the sand bodies where direct pressure measurements were taken.

5.4 Well G

5.4.1 Data Sources

Data used in the pressure analysis of Well G come from the wireline log suite. Table 5.3 summarises the wireline log data available and shows how the different parameters used in the analysis were derived.

WIRELINE LOG	RESISTIVITY ILD / MSFL	CALIPER	GAMMA RAY	SONIC	DENSITY	NEUTRON
UNITS	Ωm	Inches	API	μs/ft	g/cc	%
INTERVAL	346-4,601m			1,061-4,601m		
USE OF DATA	Discrim.	Discrim.	Lithology	Porosity	Overburden	
			Overburden			

Table 5.3 Summary of wireline log data used in the pressure analysis of Well G Disc. = discriminant

5.4.2 Lithology

Analysis of the natural gamma ray profile yields a simplified lithological column represented in Figure 5.15. The sequence drilled in Well G comprises sands and shales deposited between ~13Ma and the present day. Limited stratigraphic information was available for this well, but the average sedimentation rate is moderately high at approximately 350m/Ma (similar to the average rate for the sediments in Well F). The section has been subdivided into eleven intervals as follows:

1. The interval from the seabed down to 875m comprises interbedded clays and silts averaging ~10m in thickness with occasional sands between 5-15m thick.
2. Between 875-1150m shales are interbedded with sand bodies averaging around 10m thick, the shale units become siltier towards the base of the section.
3. Between 1150-1290 sand bodies up to 30m thick are interbedded with thinner silty intervals.
4. There is a decrease in the average bed thickness to less than 5m between 1290-1560; the interval comprises thin silty sands, silts and shales. There is an initial decrease in API of the shales between 1290-1340m before the clay

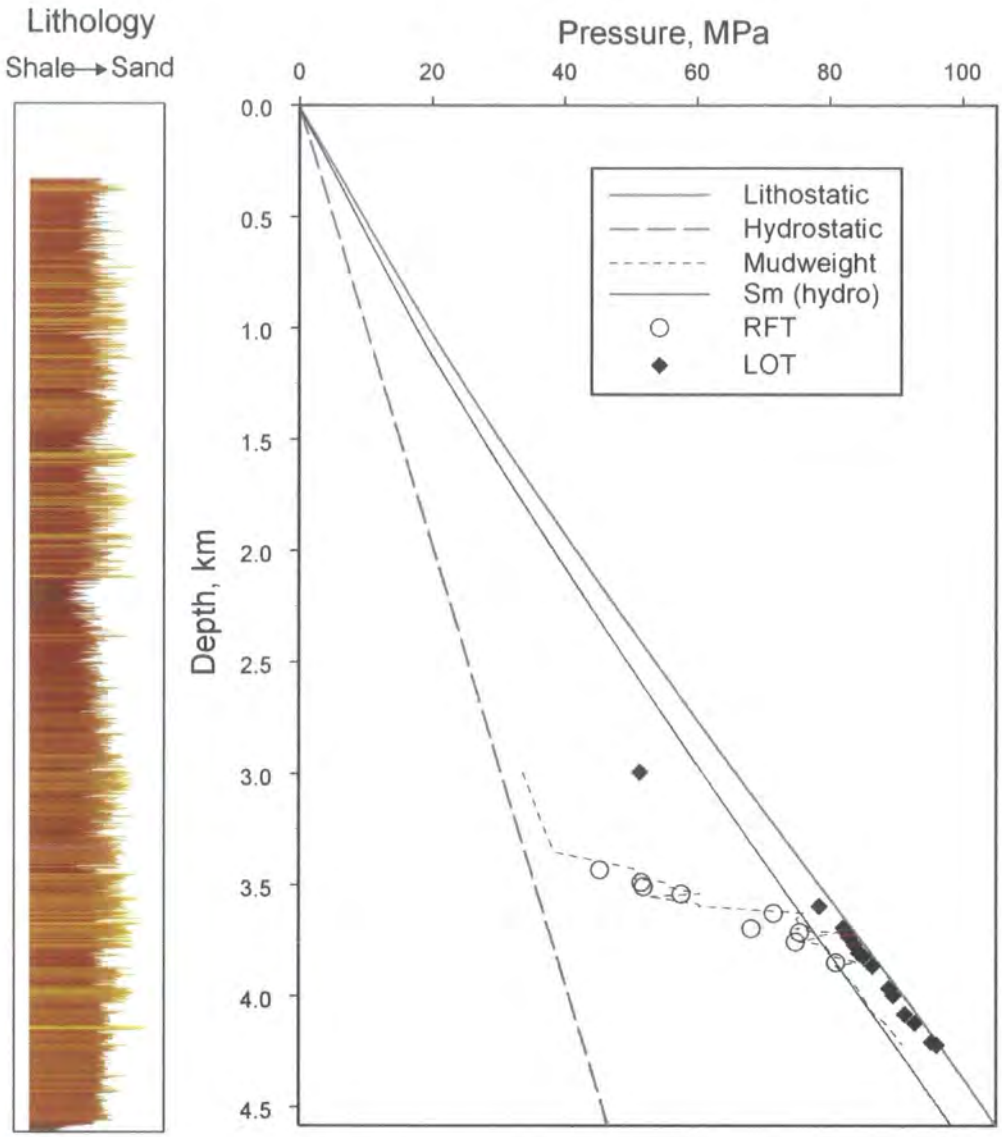

Figure 5.15: RFT, DST, formation integrity test and mudweight pressure values for Well G plotted together with the hydrostatic, lithostatic and mean hydrostatic pressure profiles and a schematic lithological column.

5. fraction increases gradually between 1340-1560. The sand units have almost constant properties across this section.
6. Shales are interbedded with numerous sand bodies, up to 30m thick, between 1560-2130m.
7. Between 2130-3000m, a decrease in the average bed thickness is accompanied by a reduction in the proportion of sand in the section. There is a gradual decrease in the average API response of the shales with increasing depth across this interval.
8. The section from 3000-3280m is characterised by thin sands and shales interbedded with silts.
9. Between 3280-3800m there is a further reduction in the API responses of the shales and the section comprises thin silty shales and sands.
10. The interval from 3800-4030m comprises a 70m section of mudrock followed by a 100m section of silts and shales and a 60m section of sands interbedded with silts.
11. The interval between 4030-4500m shows little variation, consisting largely of silts with a 20m thick, fairly clean sand body at 4140 and very few other sands, all less than 5m thick.
12. The final 101m drilled between 4500-4601m the consists entirely of mudrocks

5.4.3 Pressure data

The actual pressure data derived from the well (RFT and DST pressure measurements, LOT values and the mudweights used during drilling) are plotted against depth along with hydrostatic pressure, lithostatic and mean hydrostatic effective stress pressure profiles in Figure 5.15. Hydrostatic pressure was computed assuming a brine density of 1.03g/cc.

Direct measurements of actual pore pressure derived from the well using the RFT tool were taken between 3.43 and 3.75km. The first four measurements between 3.43 and 3.53km represent pressure measurements taken within a narrow transition zone to much higher overpressures, unlike the pressure profile in Well F, there is no distinct change in lithology associated with the transition to overpressure. The remaining four pressure measurements below 3.62km are all between 7-12MPa of the computed lithostatic stress profile.

The mudweight profile seen in Figure 5.15 indicates that the pressures in the permeable units are near hydrostatic for the shallow part of the between 3-3.35km depth. Below 3.35km, the mudweights were increased rapidly and follow closely the trend of the RFT pressure measurements down to 3.62km. Below this depth, the average values for the mudweights are slightly higher than the measurements in the permeable units and remain within 5MPa of the computed values of lithostatic stress. As with the mudweight data from Well F, it is believed that the profile seen in Figure 5.15 is largely a function of planning before drilling, as a number of wells were drilled on this structure prior to this one. Mudweights appear very close to the measured pressures in the highly overpressured section compared to exploration wells which will generally be drilled more overbalanced, this is likely to be for one of two reasons:

1) The pressure environment was well understood from previous wells

2) The operations were trying to limit formation damage by drilling close to balance in the reservoir sections

The estimates of the minimum stress from leak-off tests are also plotted in Figure 5.15; the first of these points at 3.0km depth is around 13MPa less than the corresponding value of lithostatic stress. Below 3.6km the reported values of minimum stress are still lower than the lithostatic stress values, but the separation between the two values is between 0.5 and 2MPa. The close spacing of these data points, the consistent trend defined by them and the fact that a number of other wells have already been drilled on this structure leads to the conclusion that the values, more than likely, represent the results of formation integrity tests and therefore underestimate the actual minimum stress values. As with Well F, the impact of using a range of values for the minimum stress on the pore pressure calculation are considered in the pressure analysis.

5.4.4 Pressure analysis

The void ratios calculated from the sonic log using [16] for individual mudrock beds are plotted against hydrostatic mean effective stress together with the normal compaction curves described in section 5.1 (Figure 5.16). Between 9-35MPa effective stress (equivalent to 1.1-3.3km depth), the void ratios decrease in much the same way as the data for Well E (Figure 5.9) and Well F (Figure 5.12). Below 35MPa effective stress (3.3km) the void ratios begin to increase again. In common with Well F, there

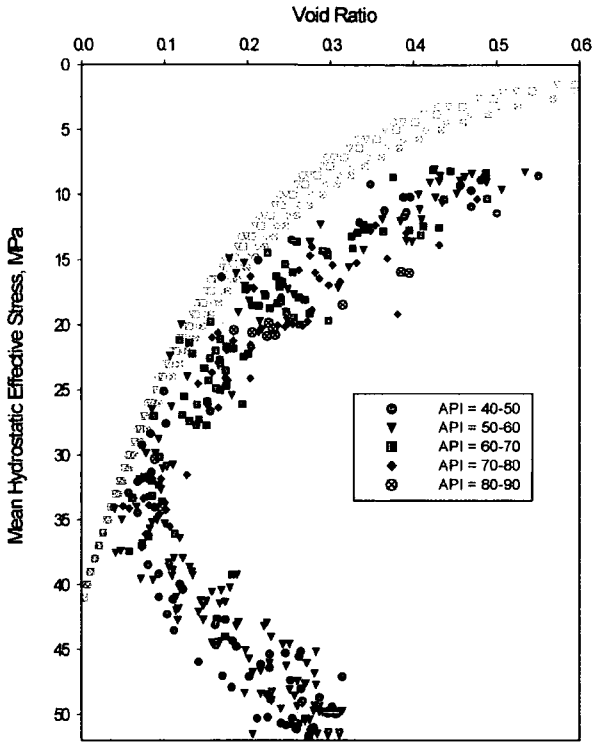

Figure 5.26: Void ratio vs mean hydrostatic stress for shales from Well G, subdivided on the basis of gamma ray response, plotted together with their derived normal compaction curves.

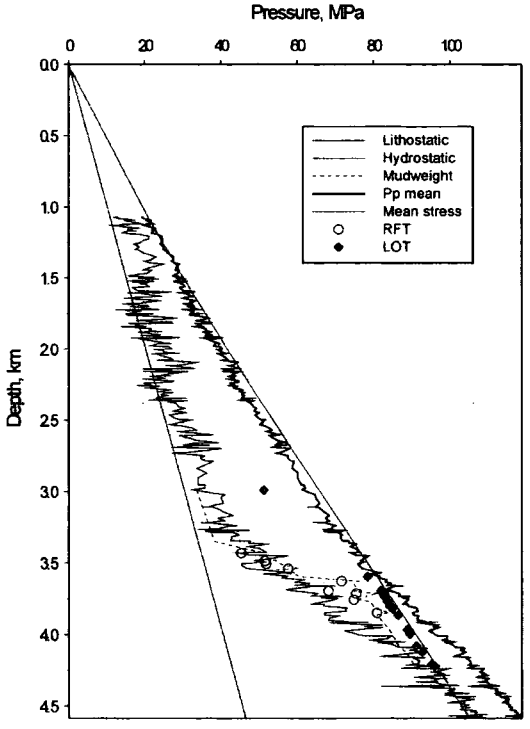

Figure 5.17: Estimates of mudrock pore pressure and mean stress values for Well G plotted against depth together with RFT, DST, formation integrity test and mudweight pressures in the borehole.

is a change to lower API shales below 38MPa (3.55km) accompanying the increase in void ratio values which continue to increase down to the base of the well at ~51MPa (4.57km) where they attain values around 0.27.

The estimates of pore pressure and mean stress calculated from the void ratios are plotted in Figure 5.17 along with the RFT, LOT and mudweight data. For the first 3.25km, the pressure estimates in most of the shales are within 7MPa of hydrostatic pressure with only a few points overpressured by more than 10MPa. Below 3.34km depth, the estimated pore pressures begin to increase linearly with depth approaching the values of lithostatic stress at 4.5km.

The interpretation of the pressure profile in Figure 5.17 is that the pore pressures in the shales are near normally pressured for the first 3.25km where they encase interconnected, normally pressured sand units. Below this depth, the porosity and the pore pressure due to disequilibrium compaction begin to increase across a broad transition zone, the base of which is not encountered in this well. The reason for the transition zone being so broad is not clear, but may be a function of drainage via interconnected sand bodies in the upper section and a slightly higher permeability section below 3.25km depth which cannot sustain a narrow pressure transition zone. Consistent with the proposed higher permeabilities is the fact that the sediments below 3.25km are far more silty than the shallow section (Figure 5.15).

Comparison of the pressure estimates with the measured pore pressure values shows that below 3.25km the rate of pressure increase interpreted in the shales is significantly slower than the rate of pressure increase defined by the direct measurements in the reservoir intervals between 3.43-3.62km. The result is that the measured pore pressures are between 4-14MPa greater than the estimates of pore pressure in the mudrocks from 3.62-3.75km.

The interpretation of these results is that disequilibrium compaction has produced overpressure in the some of the shales above 3.35km as a function of rapid burial and low permeability of the mudrocks. The pore pressure interpreted from the limited mudweight data across the shallow section indicates that the pore pressures in the sands are hydrostatic due to lateral and vertical interconnectivity. This observation is consistent with the results of Wells E and F in the same basin.

Below 3.35km the pressure transition zone in the sands appears to be controlled by another generating mechanism which is producing pore pressures very close to fracture pressure.

The reason another process is implicated is that the mean effective stress determined from porosity in the mudrocks at 3.59km (the top of the highly overpressured section) is around 22MPa, whilst the estimates of actual effective stress (derived from an LOT measurement of 78MPa, the lithostatic stress of 80MPa and an RFT measurement of 71MPa) are ~8MPa. This means that the pore pressure due to disequilibrium compaction in the shales is 14MPa lower (slightly less if the LOT values are underestimating the actual minimum stress values) than the actual pressures measured in the sand bodies. This mismatch of the pressure can be explained if an unloading process is responsible for the extra pressure in addition to the amount produced by disequilibrium compaction. For all of the encountered overpressure to be produced by disequilibrium compaction would require mean stress values at least 7MPa greater than the values of lithostatic stress. This situation cannot be the case, as, at 4.5km depth, the effective stress derived from mudrock porosity is 4MPa. If the mean stress was 7MPa greater than lithostatic, then the pore pressure in the shales would be 3MPa greater than s_v.

The two candidate fluid expansion processes that could account for the 14MPa shortfall in pore pressure calculated from σ_m (Figure 5.17) are lateral transfer and gas generation.

For lateral transfer to be effective would require extensive sand bodies with good connectivity and considerable structural relief as well as rapid growth on the structure (Yardley, 1998). A number of points indicate that this process is not responsible for the 14MPa encountered in excess of the pressures calculated from mean effective stress (Figure 5.17):

1. Modelling based studies of lateral transfer (Yardley, 1999, Yardley et al., 1998, Harrold, 1998) indicate that, except under exceptional circumstances, the process produces enhancement rather than unloading at the crest of a developing structure. The structure drilled in Well G was produced during the Miocene time period since when little differential sedimentation across the structure which could have produced lateral transfer has taken place. In this respect the burial history is similar to that of Well D, where extensive

modelling showed that no unloading was produced after the period of differential sedimentation (section 4.7).

2. Grosjean (pers. comm.) has informed me that models involving laterally extensive sand bodies are not viable due to rapid variations in facies away from the structure. This effect will reduce reservoir connectivity.
3. Bates (1996) reports that sands in the highly overpressured sections of this basin have very poor porosity and permeability characteristics which decay very rapidly with pressure reduction. Therefore any drawdown associated with pressure reorganisation would quickly destroy porosity and permeability of the aquifer units in the down-dip position.

The possibility still remains that the extra pressure is due to hydrocarbon generation, either directly from kerogen or by cracking of liquid phase hydrocarbons. The structure drilled contains an oil accumulation indicating the generation of hydrocarbons in the vicinity of the structure. Although the findings of volumetric studies indicate that pressure generation from hydrocarbon generation is more effective for oil-to-gas cracking than for oil production, the results show that a pressure increase could still be produced during light oil generation (Swarbrick and Osborne, 1996). Hydrocarbons do not appear to have been encountered in the sands around 3.65km. If the well was drilled slightly away from the crest of the structure generation of fracture pressures at the crest would allow hydrocarbons to escape from the structure before it filled to the location of the well; meanwhile the pressure effects of the hydrocarbon generation would be seen in the sands.

The final interpretation for Well G is that disequilibrium compaction is responsible for the majority of the overpressure encountered in the borehole, with fluid expansion produced by hydrocarbon generation responsible for enhancing these pressures to within 5MPa of lithostatic stress between 3.6-4.3km depth.

5.5 Conclusions

For wells E, F and G, rapid burial coupled with low permeability sand and shale sequences has produced widespread disequilibrium compaction as well as evidence for fluid expansion processes in Well G.

For all three wells, the upper, "normally" pressured sections are characterised by lateral and vertical connectivity in the aquifer units which is allowing pressure to bleed off whilst some of the encasing shales remain overpressured as a function of their lower permeability.

All three wells appear to have a pressure transition zone (Well E terminates in this section) which in Wells E and F is characterised by increasing mudrock porosity with increasing depth. Well G appears to have a very broad transition zone defined by the increasing porosity below 3.3km; however, the measured pressure increase in the sand bodies indicates a much narrower transition zone around 200m wide where pressures go from near hydrostatic to within 5MPa of the lithostatic stresses.

Pressures in the highly overpressured sections of Wells F and G appear to be controlled by the minimum principal stress. In Well F this control is direct as the actual measurements of pore pressure are equal to, or within 1MPa, of the reported values of minimum stress which appear to be lower than the vertical stress in the highly overpressured section. For Well G the pore pressures remain around 5MPa below the LOT measurements of minimum stress. It is possible that this difference represents the fact that the structure is being breached at the crest of the structure and that Well G was drilled slightly away from the crest of the structure.

Chapter 6: Methodology appraisal / improvements

"...that is the last depth and the darkest lair
and the farthest from heaven which encircles all,
and at that time I came back even from there"
Dante Aligheri

All of the results presented in Chapters 3-5 depend upon the validity of the approaches described in Chapter 2. This section considers the possible errors associated with the methodology used and discusses alternative techniques that were either unavailable or beyond the scope of this study.

6.1 Raw data

Wireline logs were supplied for all the wells in this study. The raw log values were supplied in paper printouts for each of the tools in wells A-C, whilst the data for wells D-G were supplied in digital format. Some of the digital data were supplied in a processed format (e.g., the neutron log for wells E-G were reported in porosity values of 0.0 to 1.0 instead of the conventional output of limestone porosity units of -15 to +45). Because the corrections applied to the raw log values were not supplied with the data, it was not possible to assess the validity of the corrections or apply any further environmental corrections in case these had already been carried out. It therefore had to be assumed that the corrections applied were valid and accurate.

Ideally for a study of this kind, digital copies of the raw log responses should be supplied such that the actual tool responses can be accessed and environmental corrections can be applied as required.

For the pressure data supplied for the analysis, as mentioned in section 2.1.1, only the interpreted values and some drillers comments have been supplied for the analysis such that there is very little opportunity to appraise the quality of the data. As for the wireline log data, the raw RFT, DST, FIT and LOT log charts would be of greater value to this study allowing pressure values plus possible error bars to be used in the pressure analysis.

6.2 Parameter calculation

Mudrock pore pressure is estimated in this study from three key parameters, namely lithology, porosity and hydrostatic mean effective stress. This section details extra information which could better constrain the parameters, and reviews the ways in which the assumptions used could be tested in future studies.

6.2.1 Lithology

Shale lithology, as detailed in section 2.2.1, was derived from three main sources: cuttings descriptions, XRD analysis, and wireline log responses.

Direct analysis of samples from the boreholes obviously yields the most information as to the mineralogy and nature of the shales. More information of this

type would have allowed the testing of the assumption that the mineralogy and diagenetic state of the shales in the study are not significantly variable with depth, along with some of the assumptions implicit in the wireline analysis. More data from sample analysis such as shale cutting density measurements would allow for calibration of the wireline log responses and more effective discrimination of intervals to be included/excluded in the pressure analysis.

Shale lithology calculations from the wireline logs response rely upon three main assumptions:

- The clay mineralogy is constant with depth throughout each of the wells.
- The gamma ray tool is appropriate for subdivision.
- The neutron/density crossplot can be applied to determine lithology in shales as well as sands and carbonates.

To assess these assumptions would require more detailed analysis of rock samples from the well or possibly an outcrop study of the formations encountered in the borehole (Ahmadi 1997).

If the analysis reveals that the relationships used are not as simple as the methodology described in section 2.2.1, the problem could be addressed by using neural networks "trained" with correlations between the actual samples and their corresponding log responses (Brown, 1999).

More information on the shale lithology could be taken from extra wireline logs such as the spectral gamma ray (Rider, 1996) or NMR tools, or from using the resistivity tools with more information as to the borehole environment (Holbrook, 1995).

6.2.2 Porosity

Mudrock porosity is the key term used to calculate pore pressure in this study. Two key methods were used to calculate porosity in this study.

6.2.2.1 Sonic response

Porosity from all the wells was calculated using [14], which incorporates the sonic response into a Raiga-Clemenceau type equation (section 2.2.2.1). This approach has been used in the Beaufort Mackenzie basin (Issler, 1992), Norwegian shelf (Hansen et al., 1996) and Gulf Coast (Audet, 1995). The results produced in this study appear reasonable. Two possible ways in which the assumptions implicit in using [14] could be tested are as follows:

- A more detailed analysis of the lithologies of the shales (section 6.2.1) used in this study would be useful to check that the mineralogies match the assumptions set out in Issler (1992) (from the analysis of the data available, it appears that the approach taken is valid for this study).
- Ideally a larger dataset would be available where the acoustic formation factor and the shale matrix travel time could be derived using the methodology set out in Issler (1992) or Hansen (1996). A larger study involving rock samples from wells coupled with wireline log responses could allow for a more detailed interrogation of the form of the Raiga-Clemenceau relationship and its use in calculating shale porosity.

6.2.2.2 Density/neutron derived porosity

The key to calculating porosity in mudrocks using neutron and density tools is knowledge of the lithology/mineralogy. Variations in the abundance of different clay minerals have significant influence on the matrix density and hydrogen index, which are used to calculate porosity from the density and neutron tool response respectively. Grain densities for mudrocks have been reported at anywhere between 2.45-2.85g/cc (Rider, 1996) and results of XRD analysis reported in Well D (Table 2.1) give density values up to 2.95g/cc. This range of grain densities produces significantly different porosity values from the bulk density log, e.g., a bulk density of 2.0g/cc will give porosity values of 31% or 48% using grain densities of 2.45 and 2.95g/cc respectively. A change in the porosity of 17% will have a very large effect on the corresponding estimation of pore pressure. The magnitude of variation in matrix response for shales is about the same for the neutron log. Consequently, in this study, either constant values had to be assumed for porosity calculation or the log responses were not used quantitatively in the analysis.

6.2.2.3 Alternative methods

The results presented in Chapters 3-5 used sonic, density and neutron porosity values in the pressure analysis. The results appear reasonable; however, the integration of extra methods of porosity calculation would add weight to the conclusions drawn if all the methods were consistent. Any discrepancies between different calculation methods may shed more light on the processes involved in compaction and overpressure generation (e.g., Hermanrud et al., 1998).

Other data sources that would have been of use to this study for porosity information, but which were unavailable, include

- Direct measurements on samples to validate log calculated porosities.
- Full waveform sonic logs could be used to determine shear and stonely wave propagation through the mudrocks which in turn give insights on the porosity and the bulk and elastic moduli of the sediments (Traugott, pers. comm.).
- Porosity determination from NMR logs.
- More detailed information concerning borehole conditions and formation resistivities that would allow porosity calculation from conductivity/resistivity data (Holbrook, 1995).

6.2.3 Hydrostatic mean effective stress

Hydrostatic mean effective stress calculated as described in section 2.2.3.4 requires knowledge of the hydrostatic pressure, lithostatic stress and an estimate of the horizontal stress.

6.2.3.1 Hydrostatic pressure

For this study, the hydrostatic pressure was calculated using measured formation brine densities supplied with the well reports. Significant under/overestimation of the fluid density will result in errors at depth in the well. However, the supply of fluid composition data coupled with very few salinity variations reported from the wells means that, hydrostatic pressure is not considered a significant source of error in this study.

6.2.3.2 Lithostatic stress

The lithostatic stress was calculated as described in section 2.2.3.2 using density or sonic logs depending upon availability. The limitations of using the described approaches are as follows:

- Estimations of vertical stress in the shallow sections involved the extrapolation of density/sonic log trends. Further studies would benefit from shallow wireline log data or measurements of densities from cores/cuttings in the shallow intervals, similar to the approach taken by Audet (1995).
- Poor quality density data in Wells E-G will have affected the accuracy of the overburden calculations. If a number of wells within the same area are available, the density information could be combined to remove the effect of locally bad data.

Ideally, core or density logs for the entire well would be available for the calculation of the overburden. This type of data would not only allow for accurate determination, but the assessment of errors induced by using the approaches described in section 2.2.3.2.

6.2.3.3 Horizontal stress

Horizontal stress information in this study came from two sources: LOT measurements in the wells and the relationship defined by Breckels and van Eekelen (1982). The values were used to calculate mean hydrostatic stress using [26].

A. LOT measurements

LOT data for each of the wells were supplied as interpreted values only, without any extra information that would allow an assessment of these values. There may therefore be errors associated with the estimates of minimum stress used, in particular for Wells E-G where only formation integrity test data were supplied (section 5.1).

B. Breckels and van Eekelen (1982) relationship

In order to calculate the hydrostatic mean effective stress, the horizontal stress for a given depth was calculated using [25] assuming normal pore pressures such that the second term on the right hand side is equal to zero and the relationship is simplified to [26] (section 2.2.3.3).

The form of [25] was derived by fitting a minimum bounding curve to over 300 LOT and FIT values from the Gulf Coast, and was adapted to fit a smaller dataset from Brunei. Access to the raw LOT data would allow the form of this relationship to be assessed. One possible source of error in [25] comes from the fact that it is a bounding solution to fit the lowest values of minimum horizontal stress at any depth. If any of the LOT values are, for some reason, lower than they should be (e.g., due to very poor consolidation) then these data points will influence the form of the curve chosen to a far greater extent than if the LOT value was an overestimation of the actual minimum stress.

No attempt was made in this study to try and relate the horizontal stress to the magnitude of the vertical stress with which it is likely to have a more systematic relationship (e.g., Engelder and Fisher, 1994). Combining a dataset of similar size to that presented by Breckels and van Eekelen (1982) with analysis of lithostatic stress values would be one way of improving the method of horizontal stress calculation in future studies.

6.3 Pore pressure calculation

6.3.1 Data selection

The strategy used to select data points in this study appears to be a valid approach for the analysis of the chosen wells, with the possible exception of Well F where it is possible that too many points adjacent to permeable units were picked. A larger study carried out on a number of wells from the same area would allow the influence of different picking strategies to be tested (re-picking an individual well may reveal the influence of the log character of that well, so more wells would add statistical value to any conclusions drawn). A larger study could also be used to test the feasibility of automating the picking process.

Access to the digital format data removes any errors associated with reading values from a paper copy and also makes it easy to increase the number of data points that can be picked.

6.3.2 Compaction curves

6.3.2.1 Form of curve

The use of [32] (p. 67, derived from Burland, 1990) to define the normal compaction behaviour of the mudrocks was chosen even though it is an exponential relationship and therefore gives negative void ratios at high effective stresses. Negative void ratios are obviously unreasonable, however the form was chosen for four main reasons:

1. For consistency with the soil mechanics approach. Use of e_{100} and C_c means that the calculated values can be compared with results of compression tests on mudrocks from the borehole or the surrounding area.
2. Until high effective stresses are achieved, the normal compaction curve is a straight line when plotted on a semi-log plot of void ratio versus effective stress (Karig and Hou, 1992). None of the data points in this study appear to be at very high effective stresses where the compaction profile becomes non-linear on a semi-log plot. Although some of the mudrocks are buried down to 5km, disequilibrium compaction in the mudrocks means that the maximum effective stress experienced is equivalent to no more than 30MPa (equivalent to ~3km burial where pore pressure is hydrostatic).
3. Burial in all the wells has been rapid, and the oldest sediments encountered are Late Eocene in age. The continuous burial means that the sediments are presently

at their maximum effective stress, except for the interval between 3.75-4.25km in Well G, which is experiencing some unloading due to hydrocarbon generation/cracking (section 5.4.4). Long periods of time at a constant effective stress may allow creep compaction to take place whereby the bulk modulus of the sediment changes through time due to chemical changes (see sections 1.10 and 7.3.5). So although mudrocks are used from depths where chemical compaction would be expected, the rapid continuous burial, young sediments, high overpressure (high porosity) all counteract this process.

4. Undoubtedly, chemical transformations are taking place within the sediments. However, none of the wells studied have high smectite, carbonate or TOC in the mudrocks. These three components are more susceptible to chemical transformation during burial and their absence strengthens the argument for comparing points of the same API/lithology from the top and bottom of the well against the same compaction curve.
5. Burland et al. (1996) report that sediments that have been deposited rapidly (or in shallow tidal conditions) plot with a void ratio versus effective stress line that is very close to the intrinsic compression line (ICL). The ICL is the compaction curve that a clay follows when it has been reconstituted for compression testing. This curve defines the values of the sediment mechanical parameters (e_{100} and C_c) used in [32]. The conclusion drawn, therefore is that it is valid to compare the rapidly deposited shales (same as those used in this study) with the results of compression tests on reconsolidated samples. If the porosity can be accurately determined from the wireline log response and the sediments are currently experiencing their maximum effective stress, then the void ratio versus effective stress plot should be the same as the curve defined by the oedometer.

A plot of all the sediment mechanical parameters (e_{100} versus C_c) used in the analysis of wells A-D is shown in Figure 6.1 along with the values published by Burland (1990). The plot shows good agreement between the values used in this study and those obtained from direct measurement in an oedometer, similar to the results of analysis in the Gulf Coast (Audet, 1995). The sediment compaction parameters shown for wells A-D in Figure 6.1 were derived from the vertical effective stress analysis. The results are not significantly different, however, if the sediment mechanical parameters derived from mean effective stress analysis are used instead.

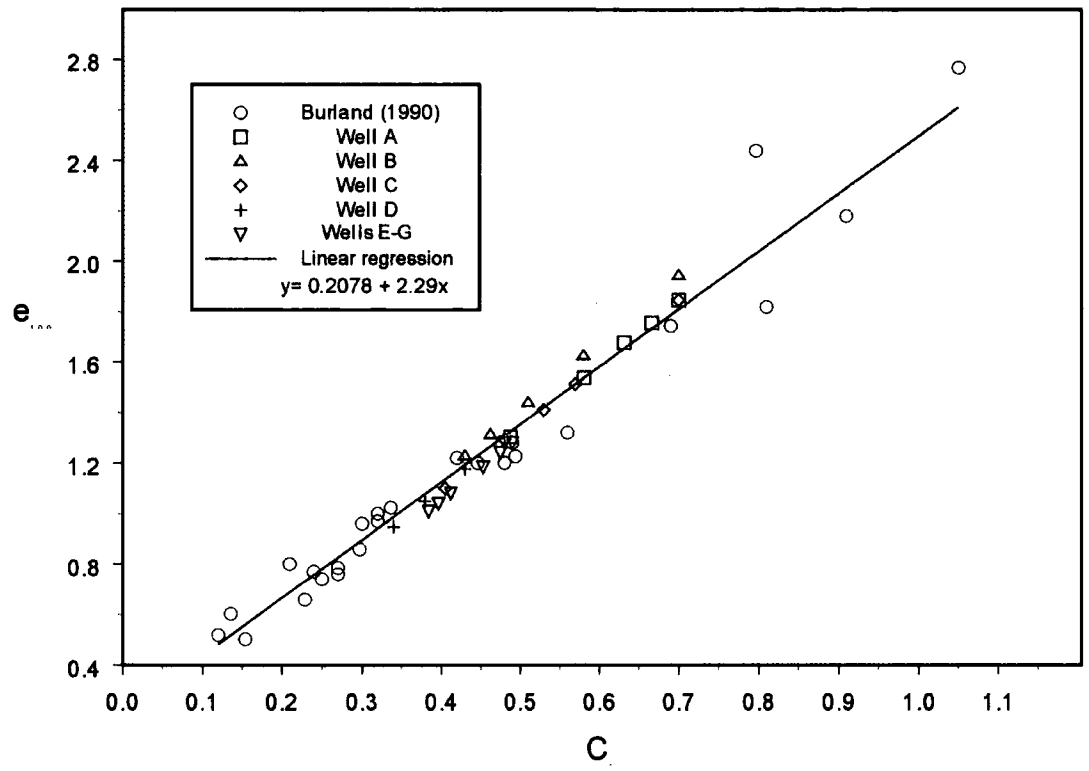

Figure 6.1: Comparison of sediment mechanical parameters e_{100} and C_c derived from direct measurements on samples (Burland, 1990) and fitting of compaction curves to porosity data in this study.

The reason for the similarity between Burland's (1990) vertical effective stress derived results and those calculated from mean effective stress analysis in this study stem from the fact that hydrostatic mean effective stress is calculated using horizontal stresses from [24]. This relationship between horizontal stress and depth assuming normal pressures was defined by fracture tests in Brunei, where Breckels and van Eekelen (1982) report the horizontal stresses s_h to be close to $0.8s_v$. Consequently, the mean hydrostatic effective stress is approximately $0.9s_v$. The difference, therefore, between plotting void ratio against hydrostatic mean or vertical effective stress is not great, so the form of the compaction curves is not significantly different.

For each well in Figure 6.1 there is a systematic relationship between the sediment mechanical parameters and the clay fraction interpreted from gamma ray response. In all the wells in this study, the increasing gamma ray response in the shales is associated with an increase in the e_{100} and C_c values. The magnitude of the increase produces a straight line which runs parallel to the best-fit line through the results of the actual compression test data. This relationship between increasing clay fraction and increasing compressibility and initial porosity agrees with the results presented by Skempton (1970) and Aplin (1995) as shown in Figure 1.6 and strengthens the argument for using the compaction curves chosen (section 1.6).

6.3.2.2 Fitting of curve

Visually fitting the bounding curves chosen seemed to work fine for the smaller datasets taken from the paper log copies (Wells A-C, Chapter 3). However where larger numbers of data points are picked (Wells D-G) there is increased scatter in the void ratios for a given hydrostatic mean effective stress or depth (Figure 5.12, section 5.3.4). More scatter will influence the bounding curve chosen and therefore, the resulting pressure calculations. For this study, a consistent approach was taken to fitting the bounding curves, and the effect on the results of alternative bounding curves was discussed where necessary (e.g., Well F, section 5.3.6)

A plot of all the normal compaction curves derived for mean effective stress analysis of the wells in this study is shown in Figure 6.2. Also included in the diagram is a data point representing a shale bed from well A, which is at 2.519km below sea level (equivalent to 25 MPa hydrostatic mean effective stress), has a void ratio of 0.30 (porosity = 23%) and sedimentary compaction parameters of e_{100}=1.651 and c_c=0.64. Shown in Figure 6.3 is the pore pressure estimate from mean effective stress analysis

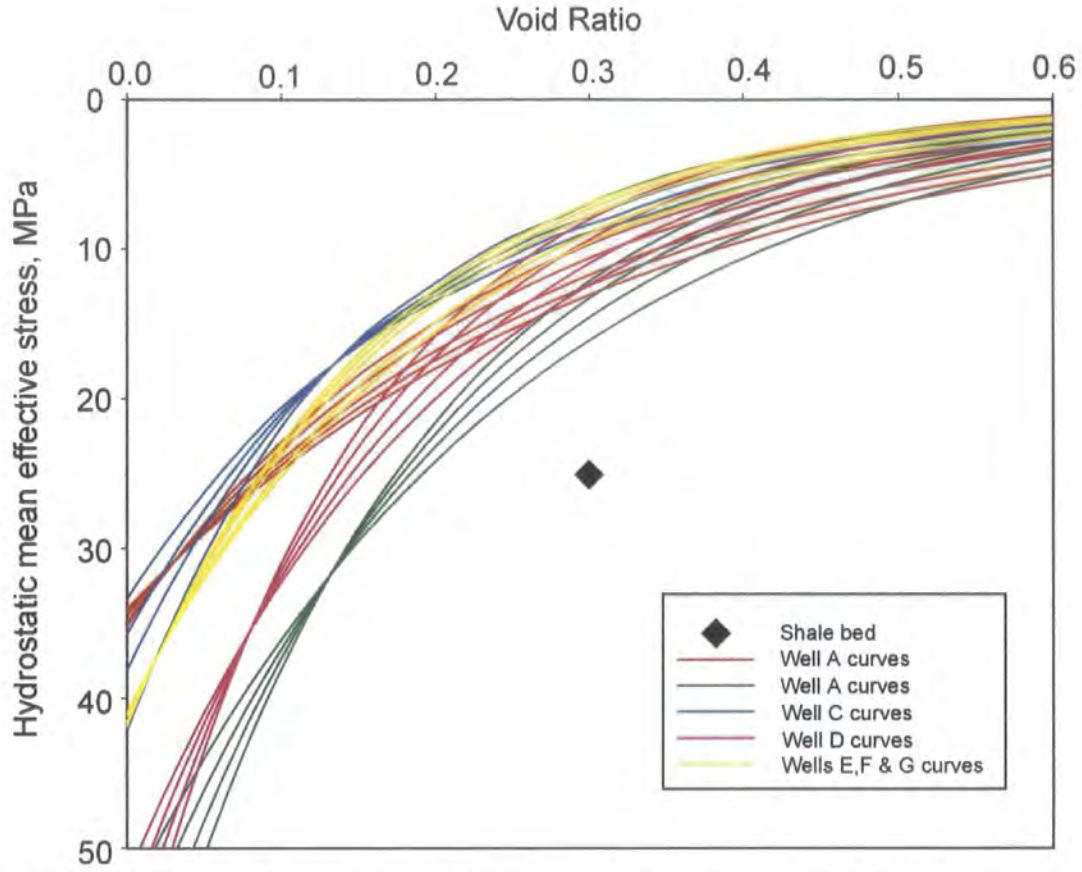

Figure 6.2 Lithology specific compaction curves for all wells in this study, together with a data point representing a shale bed from well A.

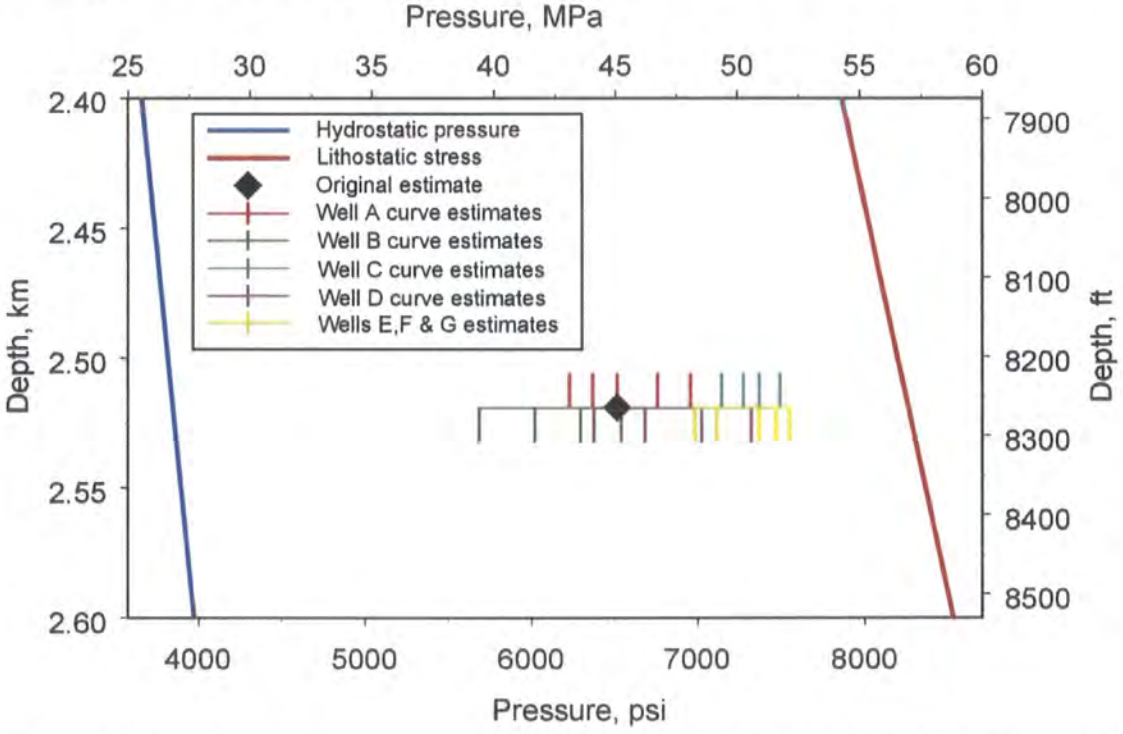

Figure 6.3 Range of pore pressures calculated by comparing the data point in Figure 6.2 against the lithology specific compaction curves shown in Figure 6.2.

for the shale unit shown in Figure 6.2 calculated by comparison to its lithology specific compaction curve. Also shown in Figure 6.3 are pore pressure estimates when the shale is compared to the other compaction curves in Figure 6.2 together with the hydrostatic and lithostatic pressure profiles. It can be seen that, as there is considerable variation in the nature of the compaction curves shown in Figure 6.2, there is a corresponding variation in the range of pressure estimates for the shale unit in Figure 6.3. The significance of the variation in the pore pressure estimates is evident in Figure 6.3: where the original pressure estimate was 8MPa lower than the value of lithostatic stress for that depth, pore pressures estimated from comparison to the other compaction curves vary from 14 to 1.4MPa lower than s_v. The range of pressure estimates represent values that are moderately to very highly overpressured, and have very significant consequences for the interpretation of the pressure environment and the planning of further wells.

This observation strengthens the argument for improving normal compaction curve determination. One way of refining the approach used here could come from collecting data from a number of wells with very similar sediments and burial history. This strategy should allow the compaction curves to be more effectively identified. Fitting curves to individual wells rather than a larger data set will mean that the curves are more strongly influenced by the amount of scatter in the porosity data.

6.3.3 Pressure calculation

So far in this chapter, the data sources and parameters used in the pore pressure estimation have been discussed. This section considers the validity of using [33] derived from Breckels and van Eekelen (1982) to calculate pore pressures.

6.3.3.1 Pore pressure calculation using [33]

Firstly, as previously discussed in section 6.2.3.3, the raw LOT data were not available to this study in order to assess the bounding form of [24] used to define the relationship between horizontal stress, depth and overpressure. It was possible, however, to make some assessment of the pore pressures used in the derivation of [24] (Figure 6.2a). The plot shows the LOT and corresponding pore pressure values from Breckels and van Eekelen (1982) together with hydrostatic pressure and lithostatic stress profiles and the horizontal stress profile calculated using [25]. It can be seen in Figure 6.2a that the horizontal stress data from Brunei only extend to 3km depth, and that only one of the pore pressure values is within 10MPa of the corresponding LOT value.

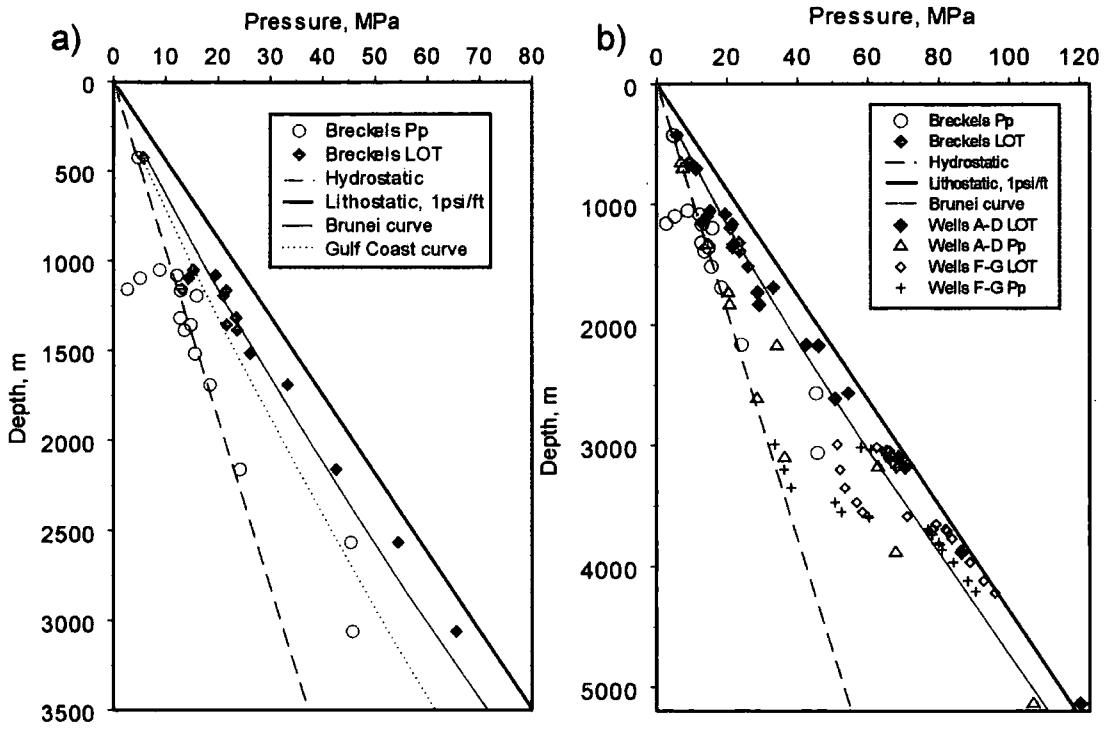

Figure 6.2. (a) LOT and pore pressure measurements from Brunei together with the horizontal stress profiles from Brunei (solid grey line) and the Gulf Coast (dotted line) assuming normal pore pressures (Breckels and van Eekelen, 1982). (b) As for (a), with the addition of LOT and pore pressure values from mudweights and RFTs for wells A, B & D as well as FIT and pore pressure values from mudweights and RFTs for wells F and G. For both plots, hydrostatic pressure and lithostatic stress profiles are represented by a dashed grey line and a solid black line respectively.

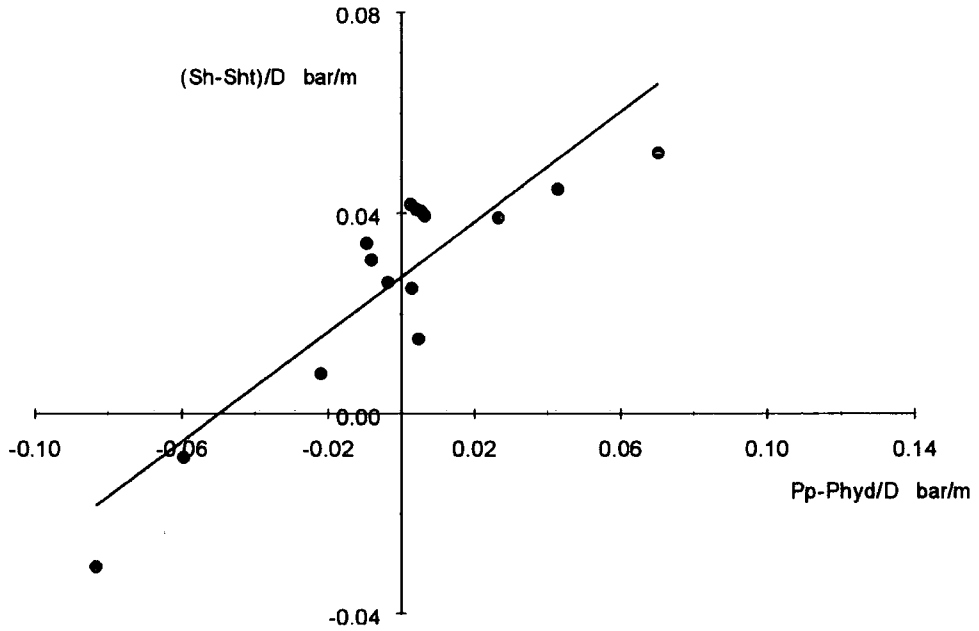

Figures 6.3 influence of overpressure (p_p - p_{hyd}) on the deviation of the minimum horizontal stress (s_h) from a normal trend (s_{h_t}) normalised for depth. Redrawn after Breckels and van Eekelen (1982) for Brunei data.

In contrast, Figure 6.2b shows the same data plotted in Figure 6.2a along with the LOT and corresponding pore pressure values taken from mudweights and RFT tests for the wells used in this study. A distinction is made between the LOT values from wells A, B and D, and the formation integrity tests used in the analysis of Wells F and G (Figure 6.2b). It can be seen from Figure 6.2b that the data used in this study extend down to 5.2km depth (>2km deeper than the values used to derive [24]). It is also evident from the plot that a significant proportion of the pore pressure values are within 10MPa of the corresponding LOT and FIT values. Mudweight values were used as estimates of the formation pressure for comparison with LOT and FIT values in Figure 6.2b where no corresponding RFT value was available at a comparable depth.

A number of significant points arise from Figures 6.2a and 6.2b, which indicate the limitations of using [24] and [33] to calculate pore pressures and mean stress values.

1. For the 15 LOT values from Brunei, only three of the corresponding estimates of pore pressure are moderately overpressured (the remaining values are either near hydrostatic or underpressured). Figure 6.3 shows the plot of minimum horizontal stress (s_h) minus the trendline value of minimum stress assuming normal pressures for the Gulf Coast (s_{h_t}, Figure 6.2a) divided by depth plotted against the amount of overpressure divided by depth for the data from Brunei (Breckels and van Eekelen, 1982). Although the magnitude of the horizontal stress increase attributed to the presence of overpressure interpreted from Figure 6.3 agrees with the results of analysis of the larger dataset from the Gulf Coast (Breckels and van Eekelen, 1982, Figure 4), three data points are not really enough to define the relationship between horizontal stress and overpressure.

2. None of the three overpressured units in Figure 6.3a are close to the fracture pressures in the borehole. Studies by Grauls (1999), Engelder (1984), have indicated that the horizontal stress profile follows a trend similar to the one shown in Figure 6.4a and the maximum rate of horizontal stress increase as a function of pore pressure occurs when the pore pressures are intermediate between normal and fracture pressure (i.e., in transition zones).

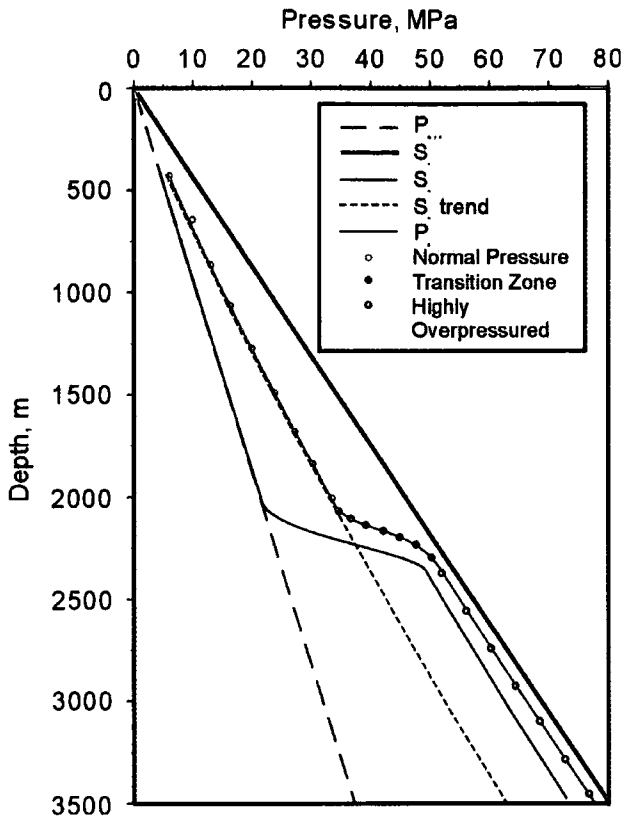

Figure 6.4a Schematic pressure plot illustrating the correlation between pore pressure and horizontal stress increase.

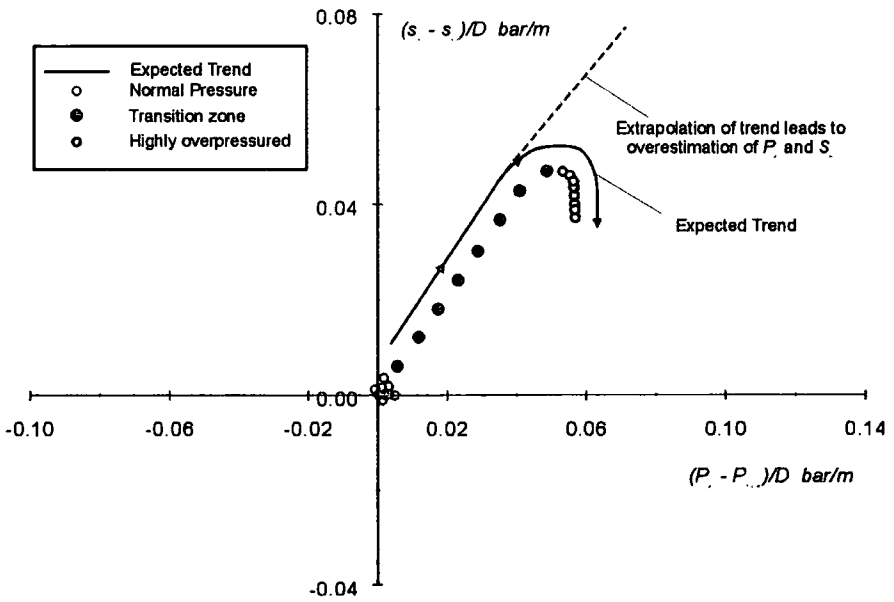

Figure 6.4b Schematic plot illustrating the relationship between horizontal stress and overpressure increase, as well as the potential for horizontal stress overestimation by extrapolation of the transition zone trend.

In normally pressured sequences, the horizontal stress increases with depth along a profile shown in Figure 6.4a and points plotted in the same format as Figure 6.3 will cluster around an area on the y-axis (Figure 6.4b).

At the onset and transition to overpressure, the horizontal stress begins to increase more rapidly until it and the corresponding value of pore pressure approach the value of vertical stress (Figure 6.4a). Data points from the transition zone will form a linear trend of increasing $(s_h - s_{h_t})/D$ with increasing overpressure (Figure 6.4b).

Once the pore pressure approaches the fracture pressure, the maximum rate of overpressure increase is limited to the rate of increase of the fracture pressure with depth (Figure 6.4a). Consequently, below this depth, the overpressure gradient $((p_p - p_h)/D)$ becomes constant with increasing depth. As p_p approaches s_v, the horizontal and therefore mean stresses tend to converge on the vertical stress (Figure 6.4a) as the stress field becomes more isotropic (high differential stresses are hard to maintain in poorly consolidated sediments at such low effective stresses). The result is that $(s_h - s_{ht})/D$ begins to decrease with increasing depth producing the trend seen in Figure 6.4b. It can also be seen from Figure 6.4b that a simple extrapolation of the trend defined by the slope in the transition zone (Figure 6.3) will cause the pore pressure and mean stress values to be overestimated.

To account for the relationship between pore pressure and horizontal stress represented by Figure 6.4a using the approach used by Breckels and van Eekelen (1982) would require a considerably larger dataset from the normal pressured, transition zone and highly overpressured sections.

3. It is not apparent from Breckels and van Eekelen (1982) what source the pore pressure values used to correlate with the horizontal stress data came from. It is unlikely that the LOTs were performed in permeable aquifer units where RFT pressure measurements could be obtained (high permeability would allow fluid to escape into the formation during the performance of the test and affect the ability to identify the leakoff pressure). If the LOT values used originated from units with lower permeability than the intervals where the RFTs were performed, then there exists the possibility of pressure differences between the two formations which will affect the derivation of the horizontal stress equation.

4. Differences in the lithology may also have affected the values of leakoff pressure from LOTs, independent of pore pressure. This effect is caused by variations

in the tensile strength between the lithologies. To take account of the lithology effect requires either analysis of a large dataset so factors can be derived to convert LOTs from one lithology to another or only use LOT data from shales to derive the relationship between horizontal stress and pore pressure.

The data from Figure 6.3 are re-plotted in Figure 6.5a along with the leakoff and pore pressure data from the wells used in this study (actual values are seen in Figure 6.2b). The data from Wells A-G shows a considerable amount of scatter when compared to the values from Brunei, and one simple trend that would reinforce the findings of Breckels and van Eekelen (1982) is not apparent. The same plot annotated to show different factors are influencing the positions of the data points is shown by Figure 6.5b.

What is apparent from Figure 6.5b is that there are little or no data which follow the expected trend described for the transition zone (Figure 6.3) for the reason that there are often significant differences in pressure between formations around the onset of overpressure (as discussed in section 7.1). Pressure differences between units will lead to either underestimation of pore pressures resulting in data that plots to the left of the expected trend (as for the data points from Well A), or the converse, where pore pressures are determined in an overpressured interval and the LOT is performed in a normally pressured formation (as shown for Well B). The amount of scatter in the data meant that it was not possible to derive a single trend of the type shown in Figure 6.4a, the dashed line shown in Figure 6.5b merely highlights the uncertainty in the range of values.

Because it was not possible to define a clear relationship which could be used to calculate pore pressures in this study, [33] derived from Breckels and van Eekelen (1982) was used to compute pore pressures. A consideration of possible overestimation of stress and, therefore, of pore pressure are discussed for wells F and G in sections 5.3.6 and 5.4.4, respectively, and the implications for wells A-D are considered below.

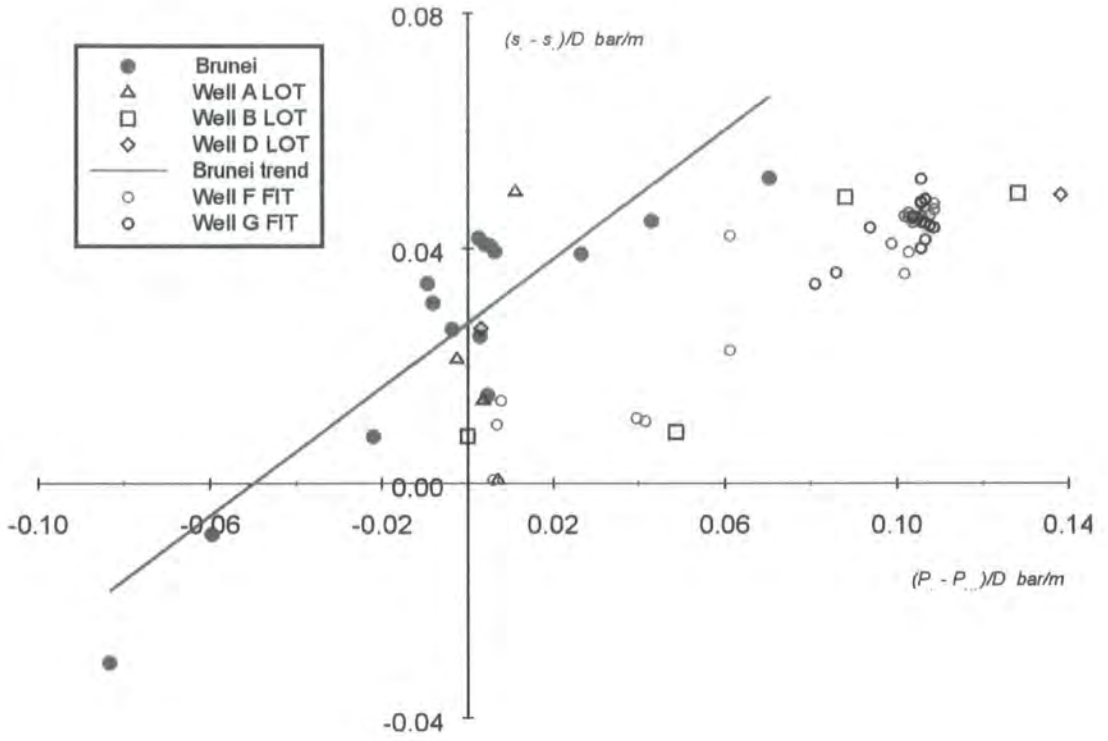

Figure 6.5a Comparison of LOT and pore pressure values from Wells A-G with data from Brunei

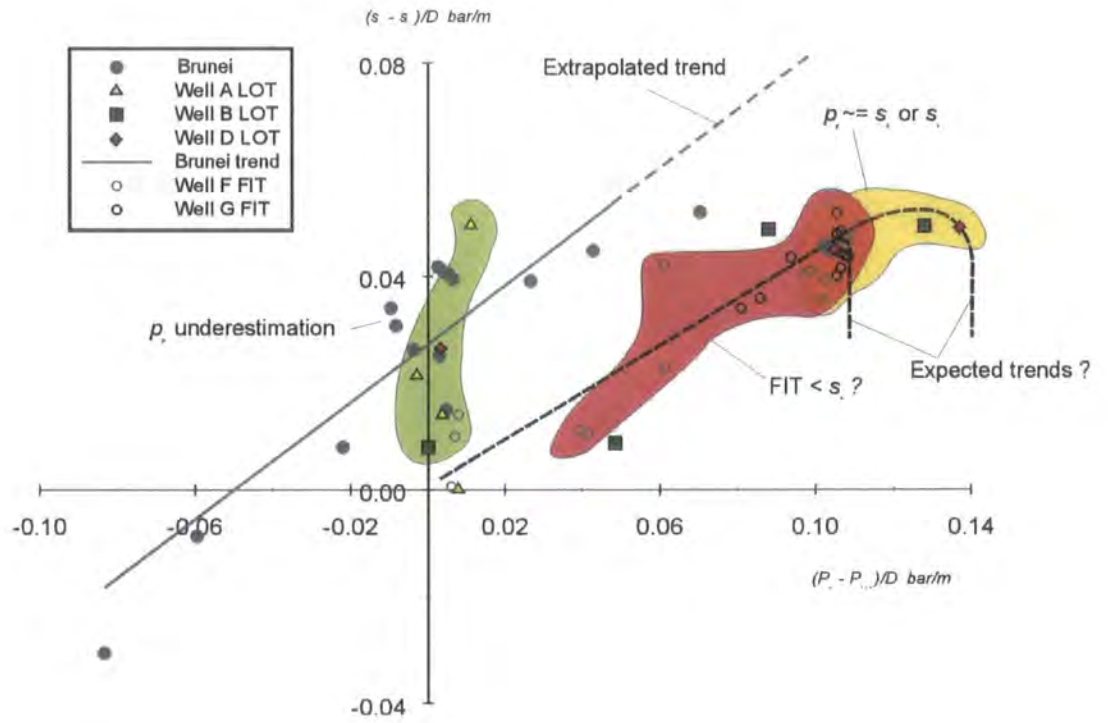

Figure 6.5b As for Figure 6.5a, with annotation to show how underestimation of pore pressure and/or minimum stress influence the distribution of data points.

6.3.3.2 Estimations of minimum stress from wells in this study

For all the wells where LOT values have been used, raw profiles were not supplied so it is not certain whether the values given represent true leakoff values, are poorly picked or are formation integrity tests. The most reliable data points are made when casing is set, as this is generally the only time where the objective is to actually fracture the rock and estimate the minimum stress prior to further drilling (section 2.1.1.5)

The results of pressure estimates using LOT values for Wells F and G (sections 5.3.6 and 5.4.4, respectively) both include a discussion of the implications of what would happen if the LOT values presented are in fact underestimating the minimum stress, and show how this would influence the interpretation of the pressures and the generating mechanisms.

The same discussion has not been applied to Wells A, B and D (no leakoff test data were available for Well C) for the reason that the LOT values performed exceed the computed lithostatic stress in the highly overpressured sections, indicating that the minimum stress is vertical and that the horizontal stresses may be higher still. Under these circumstances, [33] (derived from Breckels and van Eekelen, 1982) was assumed to be valid for computation of pore pressure and mean stress.

It is possible that all the leakoff pressures reported in Wells A, B and D represent only the minimum horizontal stresses in the wells. This could be the case if the computed overburden had been underestimated by between 0.5-4.3MPa. Table 6.1 shows the LOT values for the overpressured sections in Wells A, B and D together with the computed lithostatic stress and the calculated values of mean stress using [26].

WELL	DEPTH KM	LOT MPA	LITHOSTATIC MPA	LOT – SV MPA	CALCULATED SM MPA
A	3.11	70.8	67.5	3.3	68.3 @ 3.05km
B	2.14	45.5	45	0.5	45.26 @ 2.14km
B	3.17	70.4	67.5	2.9	75.23 @ 3.16km
D	3.88	89.5	89	0.5	98.19 @ 3.88km
D	5.14	124.5	120.2	4.3	129 @ 5.08km

Table 6.1: LOT values from wells A, B and D taken in overpressured formations, compared with computed lithostatic and mean stress values at the same depth.

If the lithostatic stresses in these three wells were greater than the recorded leakoff test values then this would imply that the mean stress cannot be significantly greater than s_v. This would have the effect of reducing the amount of calculated pore pressure attributable to disequilibrium compaction in the highly overpressured sections. The results presented in Chapters 3 and 4 show that the mean stress computed from [33] minus the effective stress computed from porosity gives pore pressures comparable to the direct measurements made in the borehole. If these computed pressures are dependent upon a mean stress which has been overestimated, then the pore pressures due to disequilibrium compaction will be lower than the values presented by the same amount as the mean stress has been overestimated.

For Wells A and B, this effect will not be too significant as the computed value of mean stress is slightly lower than the LOT values. However, for Well D both the computed values of mean stress shown in Table 6.1 are significantly greater than s_v and the reported leakoff values. If the LOT values actually equal the lithostatic stress and for the purposes of this discussion, the mean stress, then the pore pressures due to disequilibrium compaction will be 75.6MPa at 3.88km (89MPa mean stress – 13.4MPa mean effective stress computed from a porosity of 18%) instead of the computed pore pressure of 89MPa. This lower value is slightly closer to the mudweight value of 70MPa used to drill the mudrock section. At the base of the well, the computed pore pressure will drop from 102.6MPa down to 93.1MPa (120.2MPa mean stress – 27.1 mean effective stress computed from a porosity of 11%). The mudweight required to balance the pressure in this part of the section which is sand dominated was equal to 108MPa and the implication is that if the leakoff value actually represents the mean stress, then 15MPa of the encountered overpressure is due to an unloading process as only 93MPa can be attributed to disequilibrium compaction.

6.3.3.3 Improving the relationships between pore pressure and mean stress

It was not possible to derive a new relationship between horizontal stress and pore pressure from the data supplied for this study. Further studies are required to focus on this issue. These studies would benefit from either a very large dataset which would allow a more rigorous assessment of the approach taken by Breckels and van Eekelen (1982) or by choosing an alternative method of relating the stresses and pore pressures. Karig and Hou (1992) relate effective vertical and horizontal stresses in

compression tests. This approach may be a more useful and realistic method of calculation. However, it is presently limited by the fact that the data were only gathered during normal compaction with no overpressure because the design of their measuring apparatus precludes any measurements of horizontal stresses whilst the sediments are overpressured. Also, each data point in the study was gained from tests lasting ~24 hours, when the compaction phenomena being considered are taking place on the order of millions of years.

Chapter 7: Summary, implications and discussion.

"So we went down across the shale and slate
of that ruined rock, which often slid and shifted
under me at the touch of living weight."
Dante Aligheri

This chapter summarises the results of the analysis of Wells A-G and discusses the implications of the results for:

Regional origin/distribution of overpressure

a) Global origin/distribution of overpressure
b) Overpressure generating mechanisms
c) Relationships between porosity and mean effective stress,
d) Calculation of pore pressure from seismic velocity
e) Basin modelling
f) Future areas of research in the field

7.1 Summary of results.

Data for this study was supplied from a total of seven wells drilled in five SE Asia basins. Although the wells were drilled to different depths through varying sedimentary columns, they encountered similar pore pressure environments summarised by Table 7.1 and Figure 7.1. The pore pressure profile in Figure 7.1 shows a normally pressured section, a transition zone and a highly overpressured section where the pore pressure is very close to the minimum stress values. Also plotted in Figure 7.1 are data points indicating where, in terms of pore pressure environment, each of the wells terminate.

Well	A	B	C	D	E	F	G
Base of normally pressured section, km	3.01	1.8	1.2	2.58*	3.28	2.9	~3.31
Base of transition zone, km	NP	2.5	NP	4.7	NP	3.05	3.73
Transition zone thickness	>0.62	0.7	>1.42	0.07	>0.6	0.15	0.42
TD, km	3.63	3.4	2.62	5.7	3.88	3.99	4.6

Table 7.1 summary of the pressure distributions in wells in this study. NP = not penetrated. * The base of the normal pressured section in Well D is interpreted from mudweights in the absence of direct pressure measurements

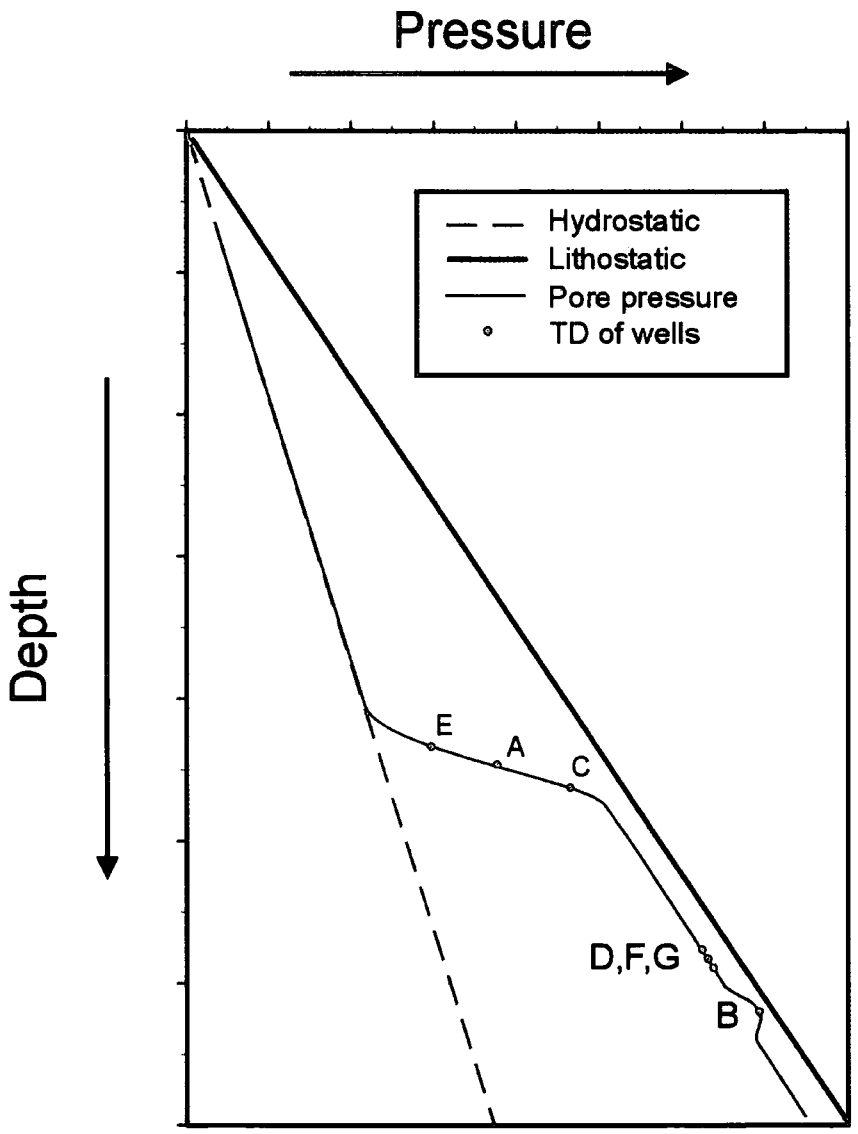

Figure 7.1 Schematic pore pressure plot indicating the location of TD for each of the wells in this study.

It can be seen in Figure 7.1 that:

1. all of the wells drilled through a section where the reservoirs are normally pressured and the shales are overpressured by variable amounts,
2. Wells A, C, and E reached TD in the pressure transition zone,
3. Wells B, D, F and G were all drilled down into the highly overpressured section.

For each of the three pore pressure zones in turn, similarities between the wells are as follows:

1) The normally pressured section

For the shallow sections where the measured pore pressures in the reservoir units are hydrostatic, the calculated pore pressures in the mudrock units are highly variable and often indicate significant amounts of overpressure.

2) The pressure transition zone

The onset of overpressure in the reservoir units and transition to much higher overpressures is generally preceded by a minima in the porosity of the mudrock units and a local increase in the sand fraction of the sediments.

Within the pressure transition zone, with the exception of well G, the pore pressures computed from the mudrock porosity values closely match the direct measurements in the reservoir units (in the case of Well D, computed pressures match the mudweights required to balance the pressures in the permeable reservoir units).

3) The highly overpressured zone

Similarities between the wells are not as clear in this section compared to the normally pressured section and the transition zone. With the exception of Well G, however, computed pore pressure values in the highly overpressured zone indicate that all or nearly all of the pore pressure is generated by disequilibrium compaction and the shale pressures match the measured pressures in the reservoir units.

7.2 Implications of results of well analysis

7.2.1 Regional scale

The five sedimentary basins studied have broadly similar pressure environments as described above. For the three pressure zones the following conclusions can be drawn as to the nature and origin of the encountered overpressure:

1) The normally pressured section.

The shallow section of all of the wells drilled is characterised by normally pressured sands separated by shales which have highly variable amounts of overpressure from 0-17MPa. This conclusion is drawn from the results of porosity effective stress analysis and was not confirmed by direct measurements in any of the wells studied. Grosjean (pers. comm.) has, however, informed me that studies carried out during the drilling of further wells in the vicinity of Well E indicated that shales directly adjacent to normally pressured reservoirs were overpressured by up to 1.8g/cc (15lb/gal) equivalent mudweight. Another well on the same structure took a high pressure (1.7g/cc, 14lb/gal) RFT measurement in a thin sand at ~3.75km depth. This sand is believed to be isolated from the normally pressured sand and to be in equilibrium with the high pressure shales identified from the well logs.

The origin of the pressure differences between the sands and the shales can be explained by rapid burial rates and lateral and vertical connectivity in the reservoir units. The high sedimentation rates produce a shallow onset of overpressure in the sediments due to disequilibrium compaction. This overpressure is allowed to dissipate from the sand bodies, which are connected hydraulically to the surface, leaving the shales overpressured as a function of their lower permeability and isolation from the aquifer units.

From the dataset supplied for this study, it has not been possible to test whether the normally pressured sands were in hydraulic communication with the surface throughout the burial history or whether the connection to the surface and overpressure dissipation is a more recent phenomenon. A larger scale study of the basin or detailed basin models may be able to shed more light on the process.

2) The transition zone

For the wells included in this study, the base of the upper "normally pressured" section seems to be characterised by the observation of a mudrock porosity minimum

and an increase in the sand fraction of the sediments. Compared to the overlying section, there appears to be less variability in mudrock porosity and therefore pore pressure (e.g., Well F at 2.85km depth (Figure 5.12) ~30MPa hydrostatic mean effective stress (Figure 5.13)).

Below the porosity minima, the pore pressures are seen to increase linearly towards maximum overpressures within 2-10MPa of the measured minimum stress values. In all but Well G, the mudrock porosity profiles indicate that the pore pressure due to disequilibrium compaction in the shales across this interval is increasing at the same rate as the pressure in the sands. There seems to be less variability in the shale porosity within the transition zone (e.g., Well F (Figure 5.13) 31-33MPa hydrostatic mean effective stress).

It is proposed that the increase in sand fraction and the porosity minima represents the presence of regional drains which are allowing all or nearly all of the overpressure at that level to bleed off (thus reducing the variability of the shale pore pressure).

At the base of the porosity minima, the permeability of the section is reduced to the point where the aquifer units can retain overpressure, and pressure builds with increasing depth towards fracture pressure. The linear increase in overpressure with depth in both the sand and the shale units implies that the rate of pore pressure increase and width of the transition zone is controlled by the vertical permeability of the section (overpressure escaping laterally from the aquifers would result in pressure differences between the sands and shales as seen in the shallower section).

Two possible factors that may be controlling the formation and shape of the transition zone are the connectivity of the reservoir units (related to sedimentation) and the effect of a regional drain/drainage on the reservoirs.

If the sands below the porosity minima have lower lateral and vertical connectivity than the overlying sediments as a function of a differing depositional environment. Fluid escape from the highly overpressured section would then be controlled by the vertical permeability of the section. It would be possible to test this theory with outcrop or regional studies of the sedimentology.

Alternatively, it is possible that the reservoir units were deposited with good permeability and connectivity that has been damaged by drainage induced compaction during burial. Escape of overpressured fluids from the reservoir units during burial will increase the effective stress on the sands causing a reduction in porosity and permeability. If the sands and the encasing shales experience high enough effective

stresses then the porosity and permeability will be reduced to a level where they can retain overpressure. This process could explain the failure of a large number of RFTs due to poor reservoir permeability below 3.25km (the top of the pressure transition zone) in Well E.

In Well G, the porosity minima at 3.3km overlies a very broad transition zone interpreted from the porosity profile (porosity is still increasing at TD at 4.75km, Figure 5.17). This broad transition zone may have been produced by drainage from the reservoir units inducing porosity loss to a point where some overpressure could be retained, but that drainage or effective stress levels were not sufficient enough to produce a strong seal that could maintain a high overpressure gradient during subsequent burial. At the present day, continued burial and drainage means that the sands at 3.3km are experiencing ~35MPa effective stress and permeability in the sands has been reduced to such an extent that they are able to retain extra overpressure generated by a fluid expansion mechanism. This more recent reduction in permeability is responsible for the producing the narrower pressure transition zone defined by the RFT measurements (Figure 5.19). Continued drainage and reduction of permeability in the sandstones at 3.3km will not significantly affect the porosity profile below this depth, as a large amount of the porosity from the sediments has already been lost.

The porosity and pore pressure profile seen in Well F (as well as in Well D) indicates that the narrow pressure transition zone encountered between 2.9-3.05km (Figure 5.12) has been in part generated by escape of fluid from a regional drain recently rather than throughout the burial history of the section. Porosity values in the mudrocks above and below the drain (Figure 5.13) are high and indicative of a shallow onset of overpressure due to disequilibrium compaction. Recent escape of pressure from the sand bodies between 2.8-2.9km has locally drawn the pressure out of the shales, producing an interval of well compacted sands and mudrocks. This drawdown of pressure and compaction has produced an efficient seal which is able to maintain a high pressure gradient and therefore a narrow pressure transition zone.

If overpressure had escaped from the sandy interval in Well F when the sediments were more shallowly buried, then the drawdown would have resulted in relatively lower effective stresses being applied to the shales and sands. Consequently, porosity reduction and sealing capacity would not be as great, resulting in a broader transition zone and a porosity profile similar to that seen in Well G.

3) The highly overpressured section

The highly overpressured section was only penetrated by four of the seven wells in this study. Limitations of the Breckels and van Eekelen (1982) derived relationship [33] (section 6.3.3.1) mean that pore pressure estimates in this section are less reliable and interpretations of the origin of the overpressure are more qualitative. Each of the four wells have different characteristics in the highly overpressured section as follows:

1) Well B has a zone of constant, high porosity within the transition zone (Figure 3.8) and pore pressures due to disequilibrium compaction which approach the minimum stress values at 2,600m. Below 2,600m porosity determination within the highly overpressured zone is influenced by the presence of gas in micro-fractures held open by differential stresses (section 3.3.4). It would appear that the high overpressure across this interval is controlled principally by disequilibrium compaction (with the data available, it is not possible to tell if any other fluid expansion processes are acting to maintain the high pressures).

2) The increase in porosity values directly above and within the highly overpressured section for Well D indicates that disequilibrium compaction slightly enhanced by lateral transfer is responsible for the encountered pore pressures (section 4.7). It is possible however, that the pore pressure values calculated using [33] are overestimated (as discussed in section 6.3.3.1). The conclusion of section 6.3.3.2 is that it is possible that up to 15MPa of the high overpressures encountered are due to another generating mechanism. Lateral transfer as a producer of unloading, was ruled out by a basin modelling study (section 4.6.5) leaving hydrocarbon generation/cracking or chemical compaction as possible candidates (the latter of the two mechanisms is discussed in section 7.3.5).

3) Well F has a porosity profile (Figure 3.13) that indicates disequilibrium compaction is responsible for all of the pressure encountered in the overpressured section. As with Well B, it is not clear whether any fluid expansion processes are operating to enhance/maintain the pressures.

4) The porosity profile for Well G indicates that the sediments below 3.3km are overpressured by disequilibrium compaction and that the pressures from this mechanism approach the fracture pressure at TD at 4.6km. The top of the highly

overpressured section defined by RFT measurements at 3.73km reveals that another mechanism is responsible for producing and maintaining overpressures close to fracture pressure between 3.73 and >4.0km (Figure 5.19). At present hydrocarbon generation/cracking is proposed as the process responsible, it was not possible to test this hypothesis further with the dataset provided.

7.2.2 Global scale

A number of similarities between the wells included this study have been detailed in the previous section. It is predicted that void ratio vs. mean effective stress analysis of wells in other basins will yield similar conclusions as follows:

- Disequilibrium compaction is likely to be responsible for the majority, if not all, of the encountered overpressures.
- Overpressure generated by unloading mechanisms is not expected to be as significant in terms of magnitude of contribution/frequency of occurrence (Hart et al., 1995; Hunt, 1980).
- Lateral transfer is expected to enhance pressures due to disequilibrium compaction rather than producing unloading.
- With regard to the distribution of overpressures, obviously the pore pressure profiles will vary considerably depending upon the burial history and sediment type. It is likely, however, that where there is interconnectivity between the aquifer units, significant pressure differences will arise between the reservoir units and the encasing shales. The relevance of identifying such pressure differences is seen in the results of a number of the wells in this study, where the magnitudes of the overpressure identified in the shallow sections were representative of high pressures encountered deeper in the wells. For example, in well A, identification of highly overpressured shales during the drilling of the shallow section may have allowed the pressure increase deeper in the section to be predicted and the taking of two pressure kicks prevented.

Although these observations are likely to apply best to wells where the burial history and sediment types most closely match those of the wells studies (e.g., US Gulf Coast, Nile Delta, Trinidad), it is expected that some similarities will be observed in other overpressured environments. A table of the burial rates from the wells in this study together with some representative values from a number of other basins around the world are shown in Table 7.2.

Basin Name	Average Sedimentation Rate (mMy)	Reference
N North Sea	35	Mann & Mackenzie, 1990
Haltenbanken mid-Norway	50	Mann & Mackenzie, 1990
Tertiary, C North Sea	55	Holm, 1998
Well C	**105**	**this study**
Well A	**134**	**this study**
Gulf of Paris, Trinidad	200	Hepperd et al, 1998
Malay Basin	240	Yusoff & Swarbrick, 1994
Well F	**285**	**this study**
Well G	**350**	**this study**
U Tertiary, C North Sea	500	Swarbrick et al, 1998
Flexture Trend, GOM	600	Mann & Mackenzie, 1990
Well B	**700**	**this study**
Nile Delta	810	Mann & Mackenzie, 1990
Well D	**165 (max. >900)**	**this study**
GOM shallow silty	1000	Unpublished
GOM deep water shaley	1000	Unpublished
Well E	**500 (max >1000)**	**this study**
Azerbaijan	1300	Unpublished
GOM deep water shaley	1400	Unpublished
S.E. Trinidad	2000	Hepperd et al, 1998
GOM deep water shaley	2000	Unpublished
GOM deep water shaley	2850	Unpublished
Flexture Trend, GOM	3000	Mann & Mackenzie, 1990

Table 7.2 Average sedimentation rates for the wells in this study and a number of other basins. GOM = Gulf of Mexico; Max = approximate burial rate at the present day. Table reproduced from Swarbrick et al. (in prep) with extra data courtesy of BP.

All the wells described by Table 7.2 were overpressured, the onset of overpressure due to disequilibrium compaction is estimated to have taken place when the sediments were buried by between 0.5km and 1.5km (Swarbrick et al., in prep). The table shows that burial rates of the sediments studied in this thesis are representative of a number of overpressured basins around the world. There are some basins which have even higher sedimentation rates than those encountered in wells D and E, but it is likely that the theory developed in this study will apply equally well to these more rapidly subsiding basins. In these sections, there has been even less opportunity for chemical compaction and significant temperature increases (which may affect the compaction processes) to occur. Obviously differences in mudrock type such as the high smectite content of the Gulf of Mexico shales, will have to be taken into account and will require further study to quantify.

The observations and conclusions presented here may not compare as directly to the more slowly deposited, higher temperature sections such as the Central North Sea where extreme overpressures are encountered in Jurassic sediments (Hermunrud et al., 1998; Holm, 1998). To better understand these sections will require further study of the processes of chemical compaction and fluid expansion generating mechanisms.

7.3 Overpressure generating mechanisms

This section gives a brief review of the overpressure generating mechanisms in light of the results produced by this study.

7.3.1 Disequilibrium compaction

The results of this study indicate that the process of disequilibrium compaction operates in the much same way as is described in most previous studies (e.g., Swarbrick et al., 1999; Mann and Mackenzie, 1990). The only real difference originates from the fact that, as porosity is dependant upon mean effective stress, the maximum rate of pressure increase due to disequilibrium compaction is equal to the rate of mean stress increase. This means that the maximum rate of pore pressure addition during burial due to disequilibrium compaction can exceed the rate of lithostatic stress increase.

The lithostatic-parallel pore pressure profile as described in section 1.8.1 has been attributed to very low permeability conditions during burial resulting in no fluid escape from the sediment pore spaces. Consequently the trapped pore fluid bears the weight of any increase in overburden at the top of the section and the pore pressure increases parallel to s_v. Results from this study incorporating mean effective stress theory, indicate that very low or zero permeability conditions are not necessary to generate a lithostatic parallel pore pressure profile.

Taking the example of Well C, the pore pressure profile defined by RFTs and mudweights below the onset of overpressure (Figure 3.15) is approximately parallel to the rate of lithostatic stress increase. The pore pressures computed from void ratio vs. mean effective stress analysis indicate that the pressure due to disequilibrium compaction matches the profile defined by the RFT measurements (Figure 3.17). If the porosity was dependant upon vertical effective stress then the corresponding porosity profile should be constant with increasing depth. The actual void ratio profile within the overpressured section (Figure 3.16) reveals that the porosity is decreasing with increasing depth.

The implication of such results is that the lithostatic parallel pore pressure profile does not require zero permeability conditions, and that this profile can be maintained by a more dynamic system involving compaction and vertical escape of fluid through the sediments. This conclusion is in agreement with the results of most basin modelling simulations which tend to show enhanced fluid flow when pore pressures (and therefore porosities and permeabilities) are higher.

Another important observation of the occurrence of disequilibrium compaction from the wells studied, is the highly variable nature of the pore pressure profiles which are produced by the interaction of low permeability shales and locally/regionally interconnected reservoir units. In particular, the presence of significantly overpressured shales in the shallow sections where the adjacent reservoir units are normally pressured is an effect that has not been reported in many previous studies. It is likely that the pressure differences described in this study will be encountered in other basins where shales and interconnected sands are rapidly deposited together.

7.3.2 Hydrocarbon generation/cracking

It was beyond the scope of this study to carry out a quantitative assessment of the contribution of hydrocarbon generation as an overpressure generating mechanism. Recent studies of the process (e.g., Swarbrick et al., 1999) have concluded that the process of gas generation from kerogen or from cracking of hydrocarbons involves a significant volumetric increase which could have contributed to high overpressures encountered in the north sea.

In this study hydrocarbon generation was invoked in Well G to account for the shortfall in pressure due to disequilibrium compaction in the absence of any other mechanisms which could be responsible for the extra pressure. A more detailed study involving a larger number of wells as well as volumetric and thermal modelling would be required to test this hypothesis.

The high pressures encountered in the other wells in this study were all accounted for by disequilibrium compaction, enhanced in at least one well by lateral transfer. The possibility remains however, that gas generation could have contributed to maintain the high overpressures in the sediments. For example, the shales from Well F at 3.1km have void ratios between 0.3-0.45 and mean effective stresses between 4-12MPa (Figure 5.13). Normally compacted shales at this depth should have void ratios and mean effective stress values of <0.1 and >30MPa respectively. These high porosities imply that almost no fluid has escaped from the pore spaces during the last 2.5km of burial (the void ratios correspond to a fluid isolation depth of less than 500m). This inferred lack of fluid escape is in spite of the fact that for the last 3Ma, the sediments have undergone almost no further burial. If however, 1MPa of overpressure was being generated by gas generation and the sediments were being unloaded, then any fluid escape from the sediments (as long as it does not induce a pressure loss of greater than 1MPa) would not affect the high porosities of the shales.

7.3.3 Lateral Transfer

Lateral transfer as described in section 1.8.2.3 has been invoked recently to account for shortfalls in pore pressures computed from vertical effective stress. Correct calculation of pore pressures from mean effective stress in this study revealed that the pore pressures in the sands and shales are equal and lateral transfer induced-unloading was therefore not proposed.

Basin modelling and seismic velocity analysis were carried out to assess the contribution of lateral transfer to the total overpressure encountered in Well D (Chapter 4). The conclusions of this study are in agreement with a more detailed basin modelling based study reported by Yardley et al., 1998, which are that lateral transfer operated to enhance the amount of overpressure produced by disequilibrium compaction rather than produce unloading. The basin models revealed that as soon as extra overpressure was generated at the base of the structure it was transferred to the crest and no significant pressure differences developed during the evolution of a structure. The results of mean effective stress analysis agreed with this conclusion, indicating that disequilibrium compaction in the shales was responsible for the encountered overpressures.

7.3.4 Aquathermal pressuring

As described in section 1.8.2.1 it is not believed that aquathermal pressuring represents a generating mechanism that can produce more than 1MPa overpressure. However, as for hydrocarbon generation/cracking (section 7.3.2), the possibility remains that aquathermal pressuring is contributing a minor amount to the total encountered overpressures (to maintain high pressures generated by disequilibrium compaction).

7.3.5 Chemical /secondary compaction

As described in section 1.8.2.2, chemical compaction is proposed to generate pressure by reducing the strength of the sediment such that unless porosity is lost, part of the load borne by the sediment is transferred to the pore fluid. The factors which will increase the effectiveness of the mechanism are temperature, mineralogy and age.

The theory and methodology described in Chapters 1 and 2 is designed to identify overpressure generated by primary disequilibrium compaction, assuming that the sediment retains it's sediment compaction parameters from deposition at the sea bed. This assumption implies that it is valid to derive normal compaction curves in the shallow section, and compare porosity values of shales from deeper in the section against the curves to derive pressures. If however, chemical compaction has increased the compressibility of an individual shale, then, for a given porosity, the effective stress derived from the actual compaction curve will be lower than from comparison against the curve derived from shallow compaction behaviour.

Taking the example of Well D (which experiences high temperatures below 4.5km). Shale pore pressures from mean effective stress analysis matched the encountered pressures (section 4.4.3). However, discussion in section 6.3.3.2 reveals that if the mean stresses are overestimated, then up to 15MPa of the encountered overpressure at 3.8km is due to unloading. Shale porosity at 5.1km was 15% and by comparison against the derived normal compaction curve (e_{100} and C_c values of 1.3 and 0.48 respectively) the mean effective stress values are ~27MPa. The measured mean effective stress at the same depth is 12.2MPa (section 6.3.3.2). One explanation for this is that the shortfall in pressure is due to unloading from gas generation. If, however, the compressibility C_c, was increased to 0.50 (Figure 7.2) then the effective stress estimates would be reduced to around 12MPa. Compression tests on samples from the wells could be used to try and confirm this hypothesis, however, none were available for this study, so the approach described in Chapter 2 was used instead.

It was not possible to identify whether or not the sediments included in this study have been affected by chemical compaction and therefore the study was performed on young sediments with mineralogies and temperatures which would make them less susceptible to chemical compaction.

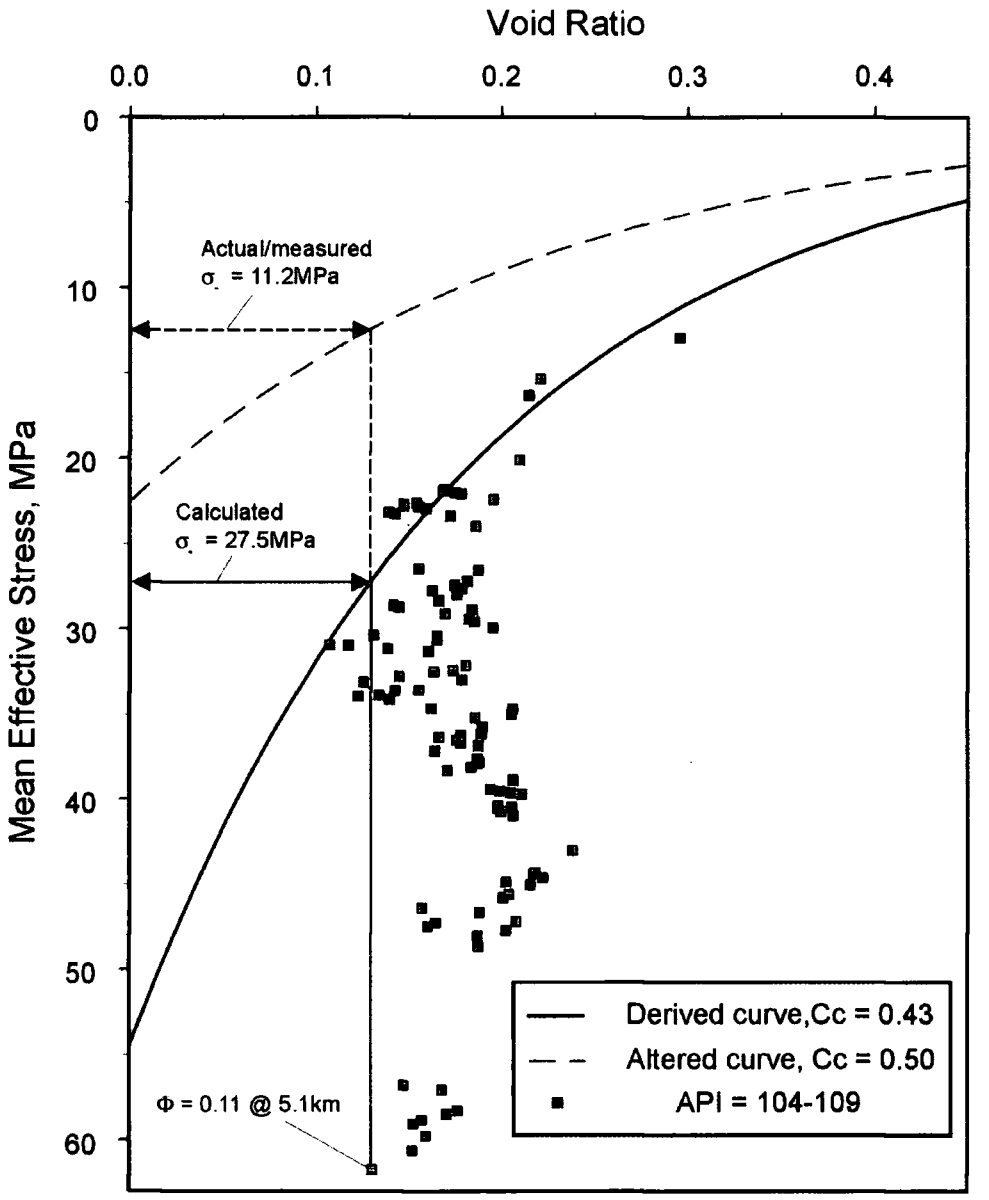

Figure 7.2 Influence of increasing shale compressibility due to chemical compaction on the estimation of mean effective stress values from porosity at the base of Well D.

7.3.6 Generating mechanisms conclusions

Disequilibrium compaction is the major source of overpressure in all the wells studied. Rapid burial and the abundance of low permeability shale horizons have produced large amounts of overpressure. The overpressure distribution is complicated by the presence of interconnected aquifer units that are allowing some of the fluid to escape to the surface.

The process of lateral transfer (in line with basin modelling based studies) acts to enhance disequilibrium compaction generated overpressures at the crest of structures. This conclusion is in contrast with vertical effective stress based studies which invoke lateral transfer as an unloading mechanism (e.g., Stump et al., 1998).

Hydrocarbon generation/cracking was proposed as contributing to the total overpressure in one of the wells in this study, with the possibility remaining that the process could be producing/maintaining some of the very high overpressures at the base of the other wells. A more detailed case study involving analysis of rock samples and constraint on the volumes involved would be required to confirm the validity of this process.

Aquathermal pressure is not proposed as a significant overpressure generating mechanism, however, as with hydrocarbon generation, it may produce a small amount of the total overpressure in the base of some of the wells.

The final mechanism considered in this study is chemical compaction, which operates as described in sections 1.8.2.2 and 7.3.5. It is possible that this process has contributed to the extreme pressures encountered in some of the wells, but without rock samples and compression tests results, it has not been possible to test whether or not the rock compressibility has changed through time.

7.4 Significance of mean vs. vertical effective stress analysis

Goulty (1998) has demonstrated that mudrock porosity during normal compaction is a function of mean rather than vertical effective stress. The significance of this observation is exemplified by the results presented in Chapter 3, where pore pressures for Wells A-C were computed from vertical, as well as, mean effective stress. The results show that shale pore pressures calculated from vertical effective stress are, on the whole, significantly lower than the RFT measurements taken in the sands. The

logical conclusion of such results is that disequilibrium compaction generated some of the overpressure and that the rest was due to an unloading mechanism. Similar conclusions were drawn by other studies based on porosity vs. depth or vertical effective stress (e.g., Hart et al, 1995; Harrold et al., 1996; Stump et al., 1998).

Results presented in this study show that shale pressures computed from mean effective stress analysis are not significantly lower than the RFT measurements taken in the sands in all but one of the wells. The conclusion of these results therefore is that the majority of the overpressure was generated by disequilibrium compaction, and that unloading processes are far less common in the subsurface.

The second conclusion drawn from the results of mean effective stress analysis is that the generation of a lithostatic parallel pore pressure profile does not require the presence of zero permeability seals/zero flow in the subsurface (section 7.3.1).

The limitations of calculating pore pressures from mean effective stress using [24] are discussed in section 6.3.3. It is apparent that extrapolation of the Breckels and van Eekelen (1982) derived relationship leads to unreasonably high mean stress values in the highly overpressured sections. However, at this moment in time [24] represents the best available solution, and an improvement on calculating pore pressures from vertical effective stress only. Shown in Figure 7.3 is a plot of the amount of overpressure calculated from Figure 6.2 (comparison of a single shale point against all of the lithology specific compaction curves used in this study) plotted against the difference between mean and vertical effective stress pressure estimates. The plot shows that, as the amount of pore pressure estimated from mean effective stress analysis increases, the difference between mean and vertical effective stress analysis increases (mean effective stress values increase relative to the vertical effective stress estimates). The plot shows that, for individual wells, there are linear relationships linking increasing overpressure and the difference between pressure estimates, however there is not one simple relationship that links all lithologies. A number of other ways of representing this data were tried, but none revealed a simple relationship that would allow one to estimate pore pressure due to mean effective stress from pressure values computed using vertical effective stress analysis. The reason for this is that there are a number of interacting components that affect the relative magnitudes of pressures calculated from mean and vertical effective stress analysis. For example changing the clay fraction of a shale by 5% will involve changing both e_{100} and c_c, adjusting one of these parameters in isolation will reveal its

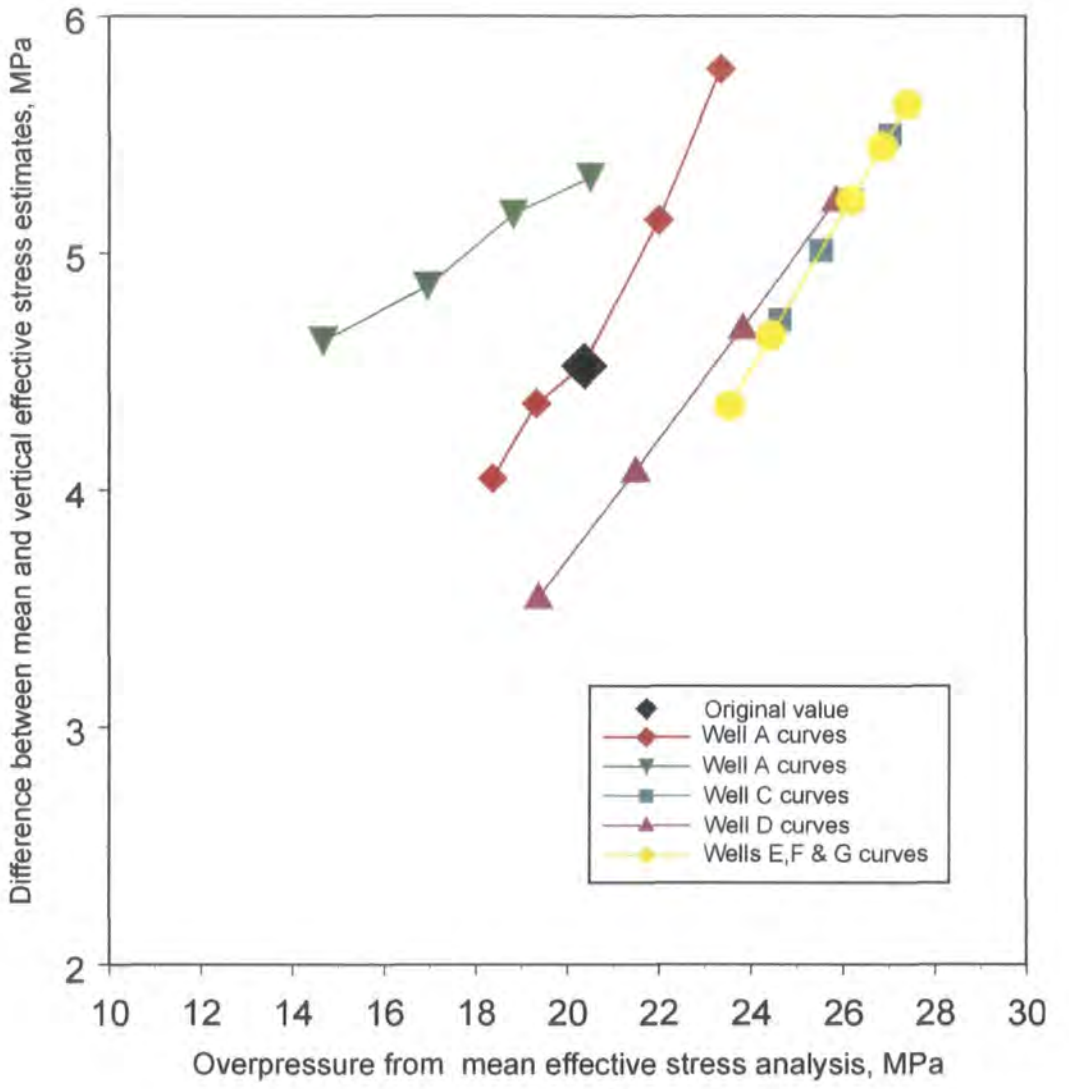

Figure 7.3 amount of overpressure calculated from Figure 6.2 for a single shale unit plotted against the difference between mean and vertical effective stress pressure estimates.

influence on the relative magnitudes of mean and vertical effective stress analysis, but the results do not represent natural variations of lithology, and will not be useful for comparison with a real dataset. Given the limitations of the mean effective stress analysis (section 6.3.3), it is proposed that would be better to refine and simplify the methodology used to estimate pore pressure from mean effective stress than it would be to try and identify a method of calculating the mean effective stress estimates presented here from vertical effective stress pressure estimates.

For this study, knowledge of the limitations discussed in section 6.3.3 allows the results of pressure calculations to be tempered, and the approach described in section 6.3.3.2 can be used as an alternative method of pore pressure assessment where LOT data are available.

Derivation of a new relationship between horizontal and vertical effective stresses is required in order to improve on [24], as discussed in section 6.3.3.3.

7.5 Implications for seismic pore pressure prediction

The results of Chapter 4 show that it is possible to treat seismic velocity data in the same way as sonic log derived velocities for pore pressure and mean stress calculation. The conclusion of the analysis is that if the correct seismic velocities are derived, then the resulting pore pressures will match those from the wireline log analysis. The reason for mismatches between seismic and sonic log-derived pore pressures stems from the fact that, although the velocity trends from the two data sources are similar, the actual values are often different. This discrepancy is due to the fact that the velocities used for pre-stack depth migration are not as high resolution and will represent average velocities over an interval. Consequently, much of the fine scale effects such as narrow zones of highly overpressured shales seen from the sonic log (e.g., Well F, Figure 5.13) are not resolvable.

Significant differences between the seismic and sonic log velocities may also arise where either the seismic data is poor quality; the seismic velocity model is inaccurate or that different velocities are detected as a function of the angle to bedding that the velocity is measured (section 4.4.4). Under these circumstances, seismic pore pressure estimates may not even be valid as a qualitative estimate of the pressure magnitude and distribution.

Calibration of the seismic velocity field with VSP and sonic log values from boreholes in the seismic section can be used to reduce the mismatch between the seismic and sonic data. It must be assumed however, that the differences between the two sources remain constant away from the boreholes. As for the analysis carried out in Chapter 4, the results of such seismic analysis should only be treated qualitatively, and if possible, tested using 2D or 3D basin modelling studies.

7.6 Implications for basin modelling

As part of the integrated study of Well D in Chapter 4, 1D and 2D basin models were constructed to test hypotheses as to the origins of the high overpressures. One of the conclusions of the simulations was that neither the magnitudes nor the profile of the actual pore pressures were reproducible. One of the reasons why the model results failed to match the encountered pressures was the fact that the models related porosity to vertical rather than mean effective stress (section 4.4.2).

Incorporation of porosity and mean effective stress relationships into basin models would mean that the rate of pore pressure increase would not be limited to the rate of overburden increase. This change may have allowed the extremely high pore pressures at the base of Well D to be simulated by the 1D models, but it would not affect the models inability to reproduce the pressure regression between 4.3 and 4.6km depth which is essentially a 3D effect.

Although, inclusion of mean effective stress theory would affect the magnitude of the pore pressures, as long as the increase in mean stress is not due to a tectonic component, the distribution of overpressure zones would remain the same.

7.6 Summary of future work

In this thesis I have proposed a new methodology of analysis and drawn a number of conclusions as to the origin and quantification of overpressure in seven wells in SE Asia. In order to refine the mode of analysis employed and validate some of the proposed hypotheses, further study of a number of topics is suggested:

1) Probably the most important issue that needs further investigation is the relationship between the magnitudes of pore pressure and the vertical and horizontal stresses. To address this issue, a more detailed analysis of leakoff test data from a large number of wells where there are many RFT measurements and gauge hole conditions (so effective stress can be estimated from the log responses of the shales) is proposed. This analysis should yield an improved empirical relationship between

overpressure and the magnitude of the principal stresses. If the results were coupled with further studies on rock properties of the type proposed by Karig and Hou (1992) this could lead to much greater understanding of the interrelationships between pore pressure and the principal stresses.

2) More detailed analysis of other wells drilled near those described in this study should allow the proposed hypotheses as to the origin of the overpressure to be tested. Availability of more complete datasets including more stratigraphic and lithological information coupled with good log data would greatly aid this process.

3) Study of wells where shale compression test data is available would allow:

a) study / refinement of the log-derived lithological analysis

b) examination of the validity of the fitted compaction curves

c) testing of the assumption that it is valid to compare shales with the same log response from the shallow and deep sections to a single compaction curve

d) quantification of chemical compaction as a generating mechanism were it demonstrated that the compressibility of shales increases with increasing time, depth or temperature.

4) Continued study of fluid expansion mechanisms to quantify how much they can contribute to the total overpressure in basins. Studies of this nature could also be used to test the hypothesis proposed here that fluid expansion mechanisms may be operating to maintain disequilibrium compaction-generated pressures in highly overpressured environments.

5) Incorporation of mean effective stress theory into seismic velocity analysis and basin models.

"...and beauteous shining of the heavenly cars.
And we walked out once more beneath the stars"
Dante Aligheri

References

"You do not question what souls these are that suffer here before you?
I wish you to know before you travel on that these were sinless"
Dante Aligheri

Ahmadi, Z.M., 1997, Sequence stratigraphy of the Upper Jurassic, derived from wireline logs, PhD thesis, Dept. of Geological Sciences, University of Durham.

Aplin, A.C., Y. Yang and S. Hansen, 1995, Assessment of Beta, the compression coefficient of mudstones and its relationship with detailed lithology: Marine and Petroleum Geology, v. 12, p. 955-963.

Appe, H., 1998, Drilling through transition zones : TOTAL experience in Indonesia (Tunu field) : Mitchell, A. and Grauls, D.(eds) Overpressures in Petroleum Exploration, Proc. Workshop Pau, Bull. Centre Rech. Elf Explor. Prod., Mem. 22, 248 pp. 215 fig., 8 tab.

Athy, L.F., 1930, Density, porosity, and compaction of sedimentary rocks : Bull. Amer. Assoc. Petroleum Geol., v. 14, 1, p. 1-22.

Audet, D.M., 1995, Compaction and overpressuring in Pleistocene sediments on the Louisiana Shelf, Gulf of Mexico: Marine and Petroleum Geology, v. 13, p. 467-474.

Audet, D.M., and J.D.C. McConnell, 1992, Forward modelling of porosity and pore pressure evolution in sedimentary basins: Basin Research, v. 4, p. 147-162.

Bachu, S., and Underschultz, J.R., 1995, Large-scale underpressuring in the Mississippian-Cretaceous succession, southwestern Alberta Basin : AAPG Bulletin, v. 79, p. 989-1004.

Baldwin B., and C.O. Butler, 1985, Compaction Curves, AAPG Bulletin, v. 69, p. 622-628.

Barker, C., 1972, Aquathermal pressuring – the role of temperature in the development of abnormal pressure zone: AAPG Bulletin, v. 56, p. 2068-2071.

Batzle, M., and Wang, Z.J., 1992, Seismic properties of pore fluids: Geophysics, v. 57, p.1396-1408

Berg, R.R., and A.H.Avery, 1995, Sealing properties of Tertiary growth faults, Texas Gulf Coast, AAPG Bulletin, v. 79, p 375-393.

Bjørlykke, K., 1993, Fluid flow in sedimentary basins: Sedimentary Geology, v. 86, p. 137-158.

Bour, O., I. Lerche and D. Grauls, 1995, Quantitative models of very high fluid pressure: the possible role of lateral stresses: Terra Nova, v. 1, p. 49-68.

Bowers, G.L., 1994, Pore pressure estimation from velocity data: accounting for overpressure mechanisms besides undercompaction: Proceedings of the 1994 IADC/SPE Drilling Conference, Dallas, Texas, p. 515-530.

Breckels, I.M., and H.A.M. van Eekelen, 1982, Relationship between horizontal stress and depth in sedimentary basins: Journal of Petroleum Technology, v. 34, p. 2191-2198.

Brown, M.P., 2000, Shale porosity and clay fraction in clastic sedimentary basins: PhD Thesis, University of Durham.

Burland, J.B., 1990, On the compressibility and shear strength of natural clays: Géotechnique, v. 40, p. 329-378.

Burrus, J., Brosse, E., Choppin, Grossjean, J., 1994, Interactions between tectonism, thermal history, and paleohydrology in the Mahakam Delta, Indonesia : Model results, petroleum consequences (Abs): AAPG Bulletin, v. 78, p. 1136-1142.

Burrus, J.E., Brosse, G.C. de Janvry and Oudin, J., 1992, Basin Modelling in the Mahakam delta based on the integrated 2D model TEMISPACK, Proc. Indonesian Petroleum Association, 21st Annual Convention, p. 23-43.

Colton-Bradley, V.A.C., 1987, Role of pressure in smectite dehydration – effects on geopressure and smectite to illite transition : AAPG Bulletin, v. 71, p. 1414-1427.

Dutta, N.C., 1988, Fluid flow in low permeable porous media, Rev. Inst. Francais du Petrol., v. 43, p.165-180.

Eaton, B.A., 1975, The equation for geopressure prediction from well logs: Society of Petroleum Engineers, Paper 5544.

Engelder, T., Fischer, M.P., 1994, Influence of poroelastic behaviour on the magnitude of minimum horizontal stress, s_h, in overpressures parts of sedimentary basins, Geology, v. 22/10, p. 949-952.

Etnyre, L.M., 1989, Finding oil and gas from well logs, Van Nostrand Reinhold publications, 305 pp.

Freed, R.L., and Peacor, D.R., 1989, Geopressured shale and sealing effect of smectite to illite transition: AAPG Bulletin, v.73, p. 1223-1232.

Gaarenstroom, L., R.A.J. Tromp, M.C. de Jong and A.M. Brandberg, Overpressures in the Central North Sea: implications for trap integrity and drilling safety, *from* Pteroleum Geology of Northwest Europe: Proceedings of the 4th Conference (Edited by J.R. Parker) The Geological Society, London pp. 1305-1313.

Goulty, N.R., 1998, Relationships between porosity and effective stress in shales: First Break, v. 16, p.413-419.

Grauls, D., and C. Cassignol, 1993, Identification of a zone of fluid pressure-induced fractures from log and seismic data - a case history: First Break, v. 11, p. 59-68.

Hansen, S., 1996, Quantification of sediment compaction with emphasis on shales : PhD dissertation, Dept. of Geology, Univ. of Arhus, Denmark.

Harrold, T.W.D., R.E. Swarbrick, N.R. Goulty, 1996, Estimating pore pressure from wireline logs in wells from SE Asia, Proc. Indonesian Petroleum Assoc. p., 867-872.

Harrold, T.W.D., 1998, Integrated pressure analysis : A case study from SE Asia, in Overpressures in petroleum exploration, Proc. Workshop, Pau, Bull. Centre Rech. Elf Explor. Prod. Mem, v. 22, p. 99-102.

Harrold, T.W.D., R.E. Swarbrick, N.R. Goulty, 1999, Pore pressure estimation from mudrock porosities in Tertiary basins, SE Asia, AAPG v. 83, no. 7, p. 1057-1067.

Hart, B.S., Flemings, P.B., and Deshpande, 1995, Porosity and pressure : Role of compaction disequilibrium in the development of geopressures in a Gulf Coast Pleistocene basin : Geology, 23, p. 45-48.

Heppard, P.D., and Traugott, M., 1999, Use of seal, structural, and centroid information in pore pressure prediction, in Proc. AADE, Pressure regimes in sedimentary basins and their prediction, Lake Conroe, Texas.

Heppard, P.D., H.S. Cander, and E.B. Eggertson, 1998, Abnormal pressure and the occurrence of hydrocarbons in offshore eastern Trinidad, West Indies: In Law, B.E., G.F. Ulmishek, and V.I. Slavin eds., Abnormal pressures in hydrocarbon environments: AAPG Memoir 70, p. 215-246.

Hermanrud, C., Wensas, L., Teige, G.M.G., Vik, E. Bolas, H.M.N and Hansen, S., 1998, Shale porosities from well logs on Haltenbanken (offshore mid-Norway) show no influence of overpressures in hydrocarbon environments : Mem. Amer. Assoc. Petroleum Geol., 70, p. 65-85.

Holbrook, P., D.A. Maggiori and R. Hensley, 1995, Real time pore pressure and fracture pressure determination in all sedimentary lithologies: SPE Formation Evaluation, December 1995, p. 215-222.

Holm, G.M., 1998, Distribution and origin of overpressure in the Central Graben of the North Sea. In: Law, B.E., G.F. Ulmishek and V.I. Slavin (eds), Abnormal pressures in hydrocarbon environments. AAPG Memoir 70, p. 123-144.

Hubbert, M.K., 1940, The theory of groundwater motion, Journal of Geology, v. 48, p. 785-944.

Issler, D.R., 1992, A new approach to shale compaction and stratigraphic restoration, Beaufort-Mackenzie Basin and Beaufort Corridor, Northern Canada: AAPG Bulletin, v. 76, p. 1170-1189.

Jev, B.I., C.H. Kaars-Sijpesten, M.P.A.M. Peters, N.L. Watts, and J.T. Wilkie, 1993, Akaso field, Nigeria: use of integrated 3-D seismic, fault slicing, clay smearing, and RFT pressure data on fault trapping and dynamic leakage, AAPG Bulletin, v. 77, p. 1389-1404.

Jones, M.E., 1994, Mechanical principles of sediment deformation, *in* Alex Maltman, *ed.*, The Geological deformation of sediments, Chapman and Hall, p. 37-71.

Kan, T.K. and Kilsdonk, B., 1998, Geopressure prediction from 3D seismic data : case studies from the Gulf of Mexico, Overpressures in petroleum exploration, Proc. Workshop, Pau, Bull. Centre Rech. Elf Explor. Prod. Mem., v. 22, p. 157-167.

Karig, D.E., and Hou, G., 1992, High-stress consolidation experiments and their geologic implications : Journal of Geophysical Research, v. 97, p. 289-300.

Lahann, R., 1998, Impact of smectite diagenesis on compaction profiles and compaction equilibrium, in Pressure Regimes in Sedimentary Basins, proc. AADE Industry Forum, West Lake Park, Houston

Lakagawa, K., 1991, Diagenetic effects on the density of argillaceous sediments during compaction: Journal of Geosciences, Osaka City University, v. 34, p. 85-102.

Luo, M., and Vasseur, G., 1995, Modelling of pore pressure evolution associated with sedimentation and uplift of sedimentary basins : Basin Research, 7, p. 35-52.

Mann, D.M., and MacKenzie, A.S., 1990, Prediction of pore fluid pressures in sedimentary basins : Marine and Petroleum Geology, 7, p. 55-65

Meissner, F.F., 1978, Petroleum geology of the Bakken Formation, Williston basin, North Dakota and Montana, in D. Rehrig, ed., Willistin Basin Symposium Guidebook: Montana Geological Society, p. 207-227.

Mello, U.T., Karner, G.D. and Anderson, R.N., 1994, A physical explanation for the positioning of the depth to the top of overpressure in shale-dominated sequences in the Gulf Coast basin, United States, J.Geophys. Res., 99, B2, p. 2775-2789.

Moore, J.C. and P. Vrolijk, 1992, Fluids in accretionary prisms, Rev. Geophys., v. 30, p. 113-135.

Mouchet, J.P. and Mitchell, A., 1989, Abnormal Pressures While Drilling. Manuels Techniques 2 , Elf Aquitaine pp. 287

Osborne, M., and R.E. Swarbrick, 1997. Mechanisms for generating overpressure in sedimentary basins: a reevaluation: AAPG Bulletin, v. 81, p. 1023-1041.

Raiga Clemenceau, J, Martin, J.P., and Nicoletis, S., 1988, The concept of acoustic formation factor for more accurate porosity determination from sonic transit time data, The Log Analyst, 29, p. 54-60.

Raymer, L.L., Hunt, E.R. and Gardiner, J.S., 1980, An improved sonic transit time to porosity transform. SPWLA 21st Ann. Symp. Trans., Paper P, p. 1-12.

Rider, M.H., 1986, The Geological Interpretation Of Wireline Logs. 2nd Edition, Whittles Publishing, pp. 212

Roberts, S. and J.A. Nunn, 1995, Episodic fluid expulsion from geopressured sediments, Marine and Petroleum Geology, v. 12, p. 195-204.

Schlumberger, 1989, Log Interpretation Charts, pp. 151

Schlumberger, 1996, Wireline formation testing and sampling, pp. 158

Schneider, F., J. Burrus, and S. Wolf, 1993, Modelling overpressures by effective-stress/porosity relationships in low-permeability rocks: empirical artifice or physical reality? *in* A.G. Doré et al., eds, Basin modelling: advances and applications: Elsevier, p. 333-341.

Sclater, J.G., and Christie, P.A.F., 1980, Continental stretching : an explanation of the post-Mid-Cretaceous subsidence of the Central North Sea Basin: Journal of Geophysical Research, v. 85, p. 3711-3739.

Skempton, A.W., 1970, The consolidation of clays by gravitational compaction : Quarterly J. Geol. Soc. London, 125, p. 373-411.

Stump, B.B., P.B. Flemings, T. Finkbeiner, M.D.Zoback, 1998, Pressure differences between overpressured sands and bounding shales of the Eugene Island 330 field (offshore Louisiana, U.S.A.) with implications for fluid flow induced by sediment loading: Mitchell, A. and Grauls, D.(eds) Overpressures in Petroleum Exploration, Proc. Workshop Pau, Bull. Centre Rech. Elf Explor. Prod., Mem. 22, pp. 248

Swarbrick, R.E., M.J. Osborne, and G.S. Yardley, in prep., Comparison of overpressure magnitude resulting from the main generating mechanisms, AAPG Bulletin.

Swarbrick, R.E., 1999, Understanding Pore Pressure : Japec Course Notes, pp. 162

Swarbrick, R.E., and M. Osborne, 1998, Mechanisms which generate abnormal pressures: an overview: *in* B.E. Law, G.F. Ulmishek and V.I. Slavin, eds, Abnormal pressures in hydrocarbon environments: Memoir 70, AAPG, Tulsa, p. 13-34.

Swarbrick, R.E., M.J. Osborne, and G.S. Yardley, 1998, The magnitude of overpressure from generating mechanisms under realistic basin conditions. American Association of Drilling Engineers Forum. Del Lago, Houston, September 1998.

Terzaghi, K., 1936, The shearing resistance of saturated soil and the angles between the planes of shear: Proceedings of the 1st International SMFE Conference, Harvard, Mass., v. 1, p. 54-56.

Traugott, M.O., 1996 The pore pressure centroid concept: reducing drilling risks, Compaction and Overpressure Workshop, Paris.

Ungerer, P., Behar, E., and Discamps, D., 1983, Tentative calculation of the overall volume expansion of organic matter during hydrocarbon genesis from geochemistry data. Implications for primary migration, in Advances in Organic Geochemistry, John Wiley, p. 129-135

Ward, C.D., K. Coghill, and M.D. Broussard, 1994, Pore-pressure and fracture pressure determinations - effective stress approach: Journal of Petroleum Technology, v. 47, p. 123-124

Wyllie, M.R.J., Gregory, A.R., and Gardiner, LW., 1956, Elastic wave velocities in heterogeneous and porous media : Geophysics, 21, p. 41-70

Yardley, G.S., A. Aplin, G. Macleod, M.J.Osborne, R.E.Swarbrick, 1998, Pore pressure enhancement at structural crests by lateral transfer, proc. AADE Industry Forum, West Lake Park, Houston.

Yusoff, W.I., and R.E. Swarbrick, 1994, Thermal and pressure histories of the Malay Basin, offshore Malaysia (Abs): AAPG Bulletin, v. 78, p. 1171-1189